INFLUENCE OF FLOOR SLAB ON SEISMIC DESIGN OF RECTANGULAR STRUCTURAL WALL IN RC FRAME-WALL BUILDINGS

by

Snehal Kaushik

DEPARTMENT OF CIVIL ENGINEERING
INDIAN INSTITUTE OF TECHNOLOGY GUWAHATI
GUWAHATI-781039, INDIA

September 2017

INFLUENCE OF FLOOR SLAB ON SEISMIC DESIGN OF RECTANGULAR STRUCTURAL WALL IN RC FRAME-WALL BUILDINGS

A Thesis Submitted
in Partial Fulfillment of the Requirements
for the Degree of
DOCTOR OF PHILOSOPHY

by

Snehal Kaushik

DEPARTMENT OF CIVIL ENGINEERING
INDIAN INSTITUTE OF TECHNOLOGY GUWAHATI
GUWAHATI-781039, INDIA

September 2017

CERTIFICATE

It is certified that the work contained in this thesis titled "*Influence of Floor Slab on Seismic Design of Rectangular Structural Wall in RC Frame-Wall Buildings*" by Mrs. Snehal Kaushik (Roll no.: 10610414), has been carried out under my supervision, and this work has not submitted elsewhere for a degree.

Dr. Kaustubh Dasgupta
Assistant Professor
Department of Civil Engineering
Indian Institute of Technology Guwahati

Date: 20 September 2017

ABSTRACT

Reinforced Concrete (RC) structural wall, also commonly known as shear wall, has large in-plane lateral strength and lateral stiffness by virtue of its large in-plane dimensions. So, these members are widely used in the lateral load resisting system of multistoried buildings in region with the possibility of strong earthquake shaking. In such frame-wall buildings, the walls are connected to floor slabs at different levels. Consequently, the junction region of shear wall and floor slab constitutes an important link in the load path from slab to wall in a highrise building. Due to the presence of slab, there is a local increase in the stiffness at the wall-slab junction which leads to stress concentration at that location. During strong earthquake shaking, the wall-slab junction may undergo significant inelastic action with the spread of damage in the adjacent floor slab and the wall panel. The same has been observed during the 1985 Chile and 2010 Chile earthquakes. Although the behaviour of shear wall with the effect of coupling beams and coupling slabs has been investigated in the past studies, none of them has focused on detailed investigation of shear wall with the possibility of damage in the wall-slab junction and the adjacent floor slab. The possible influence of inelastic wall-slab junction response on the seismic design of shear walls also has not been studied.

In the present study, a wall-slab assemblage is first proposed to represent the behaviour of shear walls, with connected floor slabs, in multistoried buildings. Based on displacement-controlled nonlinear static analysis, finite element model is validated with the experimental results of a previous study on behaviour of squat wall-slab assemblage under lateral loading. In the wall-slab assemblage, the concrete and the steel reinforcement are modelled using 8-noded solid elements and 2-noded truss elements respectively. For material characteristics, the Concrete Damaged Plasticity (CDP) model is used for concrete and bilinear strain hardening constitutive model is assigned to steel reinforcement. The same modelling details are used for further studies.

From the inelastic behaviour of the wall-slab assemblage, it is observed that the slender wall gets partitioned into a number of smaller panels between successive floor slabs. Each such panel behaves as a squat wall with the formation of diagonal strut between two successive slab-wall junctions. This effect needs to be considered to design a slender shear wall in multistoried building. The formation of strut leads to the propagation of damage in the slab which is not expected during strong earthquake shaking. The portion of slab connected to wall undergoes significant damage at higher level of lateral displacement. The finite element analysis shows the formation of damage at the base of the shear wall first and then the damage is incurred at the wall-slab junction region. Detailed

parametric study shows the requirement of seismic design methodology to avoid damage at the wall-slab junction region.

Parametric study is carried out using the proposed exterior wall-slab assemblage to understand the behaviour of wall-slab junction and to address the shortcomings of the current design requirements. Influence of two parameters on the behaviour of wall-slab junction namely (a) aspect ratio of wall panel and (b) vertical reinforcement ratio of shear wall are studied using the finite element model of the assemblage. It is observed that higher aspect ratio and lower reinforcement ratio result in maximum damage at lower values of lateral drift.

Conventionally, in seismic design of shear walls, the region of inelastic behaviour is considered at the base of the wall which represents the response of an isolated slender shear wall. However, for walls connected to floor slabs at different levels, the wall-slab junction shows extensive inelastic behaviour. In the present study, the extent of the zone of inelastic behaviour, i.e., plastic hinge length is obtained at the wall-slab junction region by carrying out nonlinear static analysis of the wall-slab assemblage. Based on curvature distribution and variation of tensile damage along the height of wall, analytical expressions for plastic hinge length are proposed. A parametric study is carried out by varying axial compression on wall and wall panel aspect ratio. It is observed that unlike the concentration of inelasticity at the base of a wall without slabs, the curvature demand increases significantly at the wall-slab junction, leading to the development of nonlinearity and damages at those locations.

Finally, nonlinear static analysis of wall-slab assemblage is also carried out to study the estimate the lateral drift limit of RC frame-wall buildings with rectangular structural walls. A drift limit in the range of 0.08% - 0.15% is recommended to avoid the damage at the junction region of shear wall and floor slab under strong earthquake shaking. In order to achieve the objective, the recommended length of wall should not exceed 3 m along with minimum wall panel aspect ratio of 1.0. Based on these, a drift-based design strategy for shear walls connected with floor slabs is proposed. The proposed lateral drift limit and the design method need to be validated by carrying out further experimental studies.

ACKNOWLEDGEMENTS

I would like to express my sincere gratitude to my thesis supervisor Professor *Kaustubh Dasgupta* for the continuous support of my doctoral research, for his patience, motivation, and guidance. I could not have imagined having a better advisor and mentor for my Ph.D.

Besides my advisor, I would also like to thank the rest of my doctoral committee members: Professor *S. K. Deb*, Professor *Anjan Dutta*, and Professor *Debabrata Chakraborty*, not only for their insightful comments and encouragement but also for the numerous questions that helped me widen my research from various perspectives. I am indebted to all my teachers at IIT Guwahati for teaching me what structural engineering is all about. Interactions with faculty members at IIT Guwahati has played an important role in developing my overall personality. Also, I extend my deep appreciation to the Head, Department of Civil Engineering, for providing an excellent working atmosphere to carry out the research work. Financial assistance provided by the Ministry of Human Resource Development, Government of India, is gratefully acknowledged.

I am also thankful to all my friends for their support, encouragement, and invaluable help extended during the tenure of my research work. I will always cherish the moments I spent with them. I am grateful to my parents, siblings, and family members for their support, patience, and understanding during my doctoral work. None of this would have been possible without the unconditional support and encouragement of my husband. Special thanks are due to my lovely kids, *Palak* and *Aryan*, who have shown immense understanding and patience during all these years, and have never complained! I would like to dedicate my PhD thesis to my kids.

Snehal Kaushik

TABLE OF CONTENTS

LIST OF TABLES

LIST OF FIGURES

LIST OF SYMBOLS

A_h = Area of horizontal shear reinforcement

A_{st} = Area of uniformly distributed vertical reinforcement

A_{strt} = Cross-sectional area of the inclined strut

A_w = Cross-sectional area of the concrete

C_d = Compressive force in the boundary elements

CM = Compressive meridian

D_0^{el} = Undamaged elastic stiffness

D_c = Compression force in the inclined strut

D^{el} = Degraded elastic stiffness

E = Young's modulus

E_0 = Initial elasticity modulus of the material

E_c = Modulus of elasticity of concrete

E_s = Elastic modulus of steel

G = Flow potential represents the Drucker-Praguer hyperbolic function

H_w = Total height of shear wall

K_c = Ratio of the second stress invariant on the tensile meridian to that on the compressive meridian

$L.C.$ = Line of contraflexure in slab

L_p = Plastic hinge length

$L_{p,cy}$ = Plastic hinge length for cyclic loading

$L_{p,mon}$ = Plastic hinge length for monotonic loading

L_s = Distance from the section of maximum moment to the section of zero moment

L_w = Length of wall

M/V = Moment-to-shear ratio

M_{max} = Maximum moment in the length of the member

M_u = Ultimate moment as per American code ACI 318-08

M_{uv} = Moment of resistance as per Indian standards IS 13920:2016

M_y = Yield moment

N_u = Factored shear force

P = Axial load

P_u, P_f = Axial compression on wall

R_m = Moment ratio

R_ε = Strain ratio

$\bar{S}$ = Deviatoric stress

S_L = Strut width

S_v = Vertical spacing

T = Temperature

T_d = Tensile force in the boundary elements

TM = Tensile meridian

V_c = Nominal shear strength provided by concrete

V_d = Shear force carried by the squat wall

V_f = Factored shear force

V_n = Nominal shear strength

V_s = Steel shear resistance

V_u = Factored shear force

V_{us} = Shear force to be resisted by the horizontal reinforcement

$\bar{p}$ = Effective hydrostatic pressure

$\bar{q}$ = Mises equivalent effective stress

a_s = Horizontal length of the compression zone at the wall base

a_{si} = Zero-one variable

c = Distance from extreme compression fiber to neutral axis

d = *D*amage variable

d_b = Diameter of bar

d_c = Damage parameter for concrete in compression

d_h = Horizontal length between the tensile and compressive forces in the boundary elements

d_t = Damage parameter for concrete in tension

d_v = Effective shear depth of the wall

d_w = Effective depth of the member

e = *E*ccentricity

f_c = Average value of axial compressive strength

f_c' = Cylindrical compressive strength of the concrete

f_{cc} = Concrete cube strength

f_{cd} = Compressive strength along the axis of the strut

f_{ck} = Characteristic compressive strength of concrete

f_i = Predefined field variables

f_t = Average value of axial tensile strength

f_y = Yield strength of reinforcement

h_s = Height of wall panel

k_1 = Factor that considers the influence of the tension reinforcement

k_2 = Factor that considers the influence of axial load

k_3 = Factor that considers the influence of concrete strength

l_d = Development length of wall

l_s = Standard length equal to 1 m, inserted to make the model parameters dimensionless

p = Pressure invariant

s_t, s_c = Functions of the stress state that represents the stiffness recovery for reversal loads

t_s = Thickness of slab

t_w = Thickness of wall

w_c = Stiffness recovery parameter in compression

w_t = Stiffness recovery parameter in tension

x_u, x_u^* = Depth of neutral axis from extreme compression fibre

α = Dimensionless material constants

α_1, α_2 = Model parameters, and equal to 0.427 and 0.077 respectively

α_l = Dimensionless parameter on length of wall

α_s = Angle of inclination

β_h = Dimensionless parameter on height of wall

β = Factor accounting for the shear resistance of cracked concrete

γ = Dimensionless material constants

Δ = Relative displacement of floors

Δ_p = Plastic displacement

Δ_y = Yield displacement

ε = Total strain

$\dot{\varepsilon}^{el}$ = Elastic strain rate

$\varepsilon_0^{'}$ = Strain related to the peak stress

ε_c = Compressive strain corresponding to f_c

$\varepsilon_c^{\sim pl}$ = Compressive equivalent plastic strain

$\tilde{\dot{\varepsilon}}_c^{pl}$ = Equivalent plastic strain rates in compression

ε_{ce} = Concrete strain in the extreme compression fiber at yield curvature

ε_{cu} = Concrete strain in the extreme compression fiber at ultimate curvature

ε_{ln}^{pl} = Logarithmic plastic strain

ε_{nom} = Nominal strain

ε^{pl} = Plastic strain

$\dot{\varepsilon}^{pl}$ = Plastic strain rate

ε_t = Tensile strain corresponding to f_t

$\varepsilon_t^{\sim pl}$ = Tensile equivalent plastic strain

$\tilde{\dot{\varepsilon}}_t^{pl}$ = Equivalent plastic strain rates in tension

ε_u = Crushing failure at an ultimate strain

θ = Angle between the diagonal tension crack and the longitudinal wall axis

θ_p = Plastic rotation

θ_x = Rotation in X-direction

θ_z = Rotation in Z-direction

λ = Modification factor for concrete

$\dot{\lambda}$ = Nonnegative plastic multiplier

μ_Δ = Displacement ductility

μ_ϕ = Curvature ductility

ξ_L = Model error term

ρ = Vertical reinforcement ratio = $A_{st}/t_w L_w$

ρ_{sh} = Ratio of vertical web reinforcement of wall

ρ_t = Ratio of horizontal shear reinforcement area to gross concrete area of vertical section

σ_{b0} = Initial equibiaxial compressive yield stress

σ_{b0}/σ_{c0} = Stress ratio

$\bar{\sigma}$ = Effective stress

$\bar{\sigma}_c$ = Effective compressive cohesion stress

σ_{c0} = Initial uniaxial compressive yield stress

σ_{cu} = Ultimate stress

σ_{nom} = Nominal stress

$\hat{\bar{\sigma}}_{\max}$ = Maximum principal effective stress

$\bar{\sigma}_t$ = Effective tensile cohesion stress

σ_{t0} = Failure stress

σ_{t0} = Uniaxial tensile stress at failure

σ_{true} = True stress

τ_c = Design shear strength

τ_v = Nominal shear stress

ϕ_r = Strength reduction factor

ϕ = Total curvature

ϕ_c = Resistance factor for concrete,

ϕ_s = Resistance factor for steel

ϕ_y = Yield curvature

ψ = Dilatation angle

$\acute{\omega}$ = Compression reinforcement index

ω = Tension reinforcement index

Chapter 1
INTRODUCTION

1.0 OVERVIEW

Reinforced Concrete (RC) structural wall is widely used in the lateral force resisting system for multistoried buildings located in the earthquake-prone regions. By virtue of its large in-plane dimension, the wall provides large strength and stiffness to the lateral load resisting system of the building. In the multistoried buildings, the wall is connected to the RC floor slab at every floor level. The junction region of shear wall and floor slab constitutes an important link in the load path from slab to wall during earthquake shaking, thereby influencing the pattern of lateral load distribution in the various structural members of the system. Consequently, the behaviour of the lateral load resisting element affects the seismic performance of the overall building. During Chile earthquake of March 3, 1985, many moderate-rise RC buildings got severely damaged. Most of them were designed with structural walls to resist both gravity and seismic loads. Walls and slab-wall connections sustained extensive cracking during that earthquake (Riddell, 1992). Also during 27 February 2010 Chile earthquake, extensive cracking of RC walls and floor slabs were observed in many highrise buildings which caused significant building distortions. Damage caused to the buildings was also due to the compression failure of thin shear walls in the lower levels of the buildings (Sherstobitoff et al., 2012). Thus, damages in the shear wall, connected floor slab and the wall-slab junction have been observed in past earthquakes. Although observed in several past earthquakes, investigation of the combined behaviour of wall, floor slab and slab-wall junction has not been carried out in detail in the past.

From the past experimental research on a single storey slab-wall assemblage, it was observed that the shear wall-slab junction experienced large stress concentration under combined axial and cyclic lateral loading (Pantazopoulou and Imran, 1992). The shear wall considered for analysis was squat in nature, and no study has been carried out on slender shear walls with connected floor slabs. Although various studies have been carried out on coupling action of beam and floor slab in building with shear walls, the failure modes of shear wall-floor slab junction and their possible implications on seismic design of walls have not been studied extensively. Using finite element modelling and experimental studies, the bending stiffness of floor slab and its effects on the distribution of bending moments and stresses in slab have been investigated (Coull and Wong, 1985; Qadeer and Smith, 1969; Schwaighofer and Collins, 1977; Paulay and Taylor, 1981). Howerver, none of the past

studies has focused on detailed investigation of the behavior of floor slab and shear wall junction under earthquake shaking.

In view of the mentioned background, the main objectives of the current study are:

(a) Investigation of tensile and compressive damage pattern in the shear wall- slab assemblage under lateral loads.
(b) Investigation of failure modes of wall, connected floor slab and wall-slab junction.
(c) Possible change in seismic design methodology of RC wall considering the influence of connected floor slab.

1.1 Major Concern And Need of the Study

In RC building, the junctions of the floor slabs and walls play a major role in determining the transfer of forces into the walls and finally to the foundation. Although, past studies have been carried out separately on isolated shear wall and floor slab-column junctions, the shear wall-floor slab junction has not been studied extensively. The bending stiffness of floor slab and its effects on the distribution of bending moments and stresses in slab have been investigated using finite element modelling and experiments (Qadeer and Smith, 1969; Schwaighofer and Collins, 1977; Paulay and Taylor, 1981; Coull and Chee, 1983; Coull and Chee, 1984; Coull and Wong, 1985). All these studies were carried out for coupled RC wall structures. However, cracking in floor slab tends to reduce the coupling action under large lateral displacement (Coull and Chee, 1990). Like coupled wall structures, interaction of slab and core wall in tall buildings tends to reduce the torsional deformation in core wall (Coull and Chee, 1986). None of the past studies has focused on detailed investigation of inelastic coupling of floor slab and RC wall under earthquake shaking.

In tall buildings with RC walls, wall-slab junctions play a very important role in transferring forces from each floor level to the wall during earthquake shaking. Finite element analysis of RC wall-slab junction showed the theoretical strains, deflections and failure loads to be in good agreement with the experimental values (Bari, 1996; Bari, 1987; Mahmood, 1984). Some researchers have also carried out modelling of composite beam-RC wall junction (Henriques et al, 2013). Apart from monolithic wall-slab junctions, behavior of precast wall-slab junction has also been investigated experimentally. The mathematical models, strut and tie model and modified stiffness matrix method are proposed in order to analyze both monolithic and precast type of connections (Zenunovic and Folic, 2012). Experiments have been carried out on RC slab-squat wall panel under monotonic and cyclic lateral forces to obtain the inelastic behavior in the members (Pantazopoulou and Imran, 1992). It was observed that RC slab can undergo significant damage which gets initiated from wall-slab junction. Based on theoretical and experimental research, methods to estimate the strength of

wall-slab junction have been proposed using different types of walls. It was proposed that special care needs to be taken while choosing the central strip of slab, since the concentration of stresses near the wall edge is high (Mahmood, 1984). Research has been carried out using vertical stirrups as shear reinforcement in the coupling slabs along the periphery of wall to enhance the strength of the slab (Bari, 1987). It was proposed that the design of wall-slab connection must be done considering the stress concentration to avoid redistribution of forces from walls to other elements not necessarily designed for lateral load resistance. Greeshma and Jaya (2013) have done experimental and analytical studies of the floor slab-shear wall connection by considering different details of reinforcement at the joint region. It was observed that the specimens detailed with 90° bent slab bars with slab shear reinforcement exhibited higher ultimate strength as compared to the other specimens. However, seismic design of wall-slab junction, in light of damages in slab and wall, has not been considered in any of the past studies. Also, the effect of possible earthquake ground motions on wall-slab junction behaviour has not been investigated.

Considering the limited research on seismic behaviour of shear wall-slab junction, the main aim of this study is to investigate the damage pattern at the wall-slab junction region under in-plane loading and possible implication on the seismic design of wall and slab members. More specifically, the study aims to investigate different slender shear wall-floor slab specimens to study the effects of amount of vertical reinforcement and slab length to wall length ratio on damage process in wall-slab junction region. The main objective is to obtain the possible tensile and compressive damage, load carrying capacity, and failure mode of shear wall - floor slab junction under seismic loading. Finite element modelling of the specimens is carried out using the computer program ABAQUS (2011). Stresses and damage pattern are monitored in wall, slab and at the shear wall-slab junction to see the possible failure modes in both wall and slab. The results highlight the requirement of changes in seismic design methodology of RC wall connected with floor slabs.

1.2 ORGANISATION OF THE RESEARCH STUDY

The work accomplished in this study is mainly divided into five parts, namely: (a) Validation of material properties with the experiments on slab-wall connection carried out by Pantazopoulou and Imran (1992); (b) behaviour of one five storied and another ten storied building and their comparison with the behaviour of an isolated slender wall and a typical wall-slab assemblage; (c) evaluation of damage at the RC wall-slab junction by varying salient structural parameters; (d) development of plastic hinge length for the wall-slab junction region; and (e) proposal of improved design methodology based on lateral drift limit to reduce the damage in the floor slab region.

Apart from the introductory chapter, which introduces the subject matter of this research, the study performed is presented in seven relatively independent chapters. Recent developments on nonlinear behaviour of shear walls during earthquake are presented in Chapter 2. A comprehensive review of behavior and design of RC structural walls is discussed in this chapter. A brief summary of various analytical models used for slender and squat RC shear walls is also presented. Chapter 2 ends by defining the gap areas and scope of present study.

In Chapter 3, details of RC wall-slab assemblage for further analysis in Chapters 4 and 5 are obtained for a multistoried RC frame-wall building with symmetry in plan. To carry out the nonlinear static analysis, Concrete Damage Plasticity (CDP) model is discussed in details and is validated with the experiments carried out on slab-wall junction from the previous work. In addition, mesh convergence study is also carried out.

Conventionally, slender shear wall in multi-storied buildings is designed in the same way as isolated shear walls. However, due to the presence of slabs, lateral stiffness of wall tends to increase at each slab-wall junction. Thus, the slender wall tends to gets partitioned into a number of smaller panels between successive floor slabs. Chapter 4 presents a detailed numerical study on the nonlinear static behaviour of shear wall-slab junction under lateral loading for the assessment of tensile damage. The study is carried out on one five storied and another ten-storied building with and without embedded reinforcement. In addition, the behaviour of an exterior wall-slab assemblage and an isolated slender shear wall is compared with the behaviour of multistoried buildings under seismic action.

To understand the behavior of wall-slab junction and address the shortcomings of the current design requirements, the influence of two major parameters, namely (a) aspect ratio and (b) longitudinal reinforcement ratio on the behavior is studied. Chapter 5 explores in details the influence of floor slab on behaviour of the shear wall with variation in those line parameters. An exterior shear wall-slab assemblage from a multistoried building is considered for carrying out nonlinear static analysis. The damage pattern and the variation of stresses at the junction region of the shear wall and floor slab are observed under lateral loading applied in the plane of the shear wall.

Chapter 6 presents the results of the pushover analysis carried out considering both monotonic as well as cyclic lateral loading on an exterior wall-slab assemblage from a five storied shear wall building. The effects of axial load ratio, length of wall as well as wall aspect ratio on plastic hinge length (L_p) are investigated. Based on the results of nonlinear static analysis, an expression for L_p as a function of length and height of wall panel is proposed for shear wall at the wall-slab junction region considering the effect of floor slab.

In case of multistoried building, the maximum elastic drift is estimated by carrying out linear static analysis for different load combinations as recommended by the Indian Seismic Code (BIS, 2016b). However, during strong earthquake shaking, the lateral load resisting members in a building are expected to exhibit inelastic behaviour upto different extents. Hence, the inelastic lateral drift levels also need to be monitored and correlated with the extent of damage in those members. The monotonic displacement controlled nonlinear static analysis of a shear wall-slab assemblage is carried out by varying thickness of wall, thickness of slab and aspect ratio of shear wall panel. The results of the same are presented in Chapter 7. Further, lateral drift criteria are proposed based on the observed damage at the wall-slab junction region of the specimens.

The findings of the entire study are summarized in Chapter 8; the conclusions are drawn from the present study, along with the discussions on limitations, and the future scope of work.

Chapter 2
REVIEW OF LITERATURE

2.0 OVERVIEW

RC structural walls are very effective in providing lateral load resistance and lateral stiffness to multistoried buildings by virtue of their large sectional dimensions. Buildings braced by structural walls are stiffer than framed structures, reducing the possibility of excessive deformations during strong earthquake shaking. The walls also participate in transmitting gravity loads from different floor levels to the foundation level at the bottom. They are usually provided between column lines, in stair wells, lift wells and in shafts that house other utilities. The use of structural walls is also a popular and effective means of strengthening deficient existing construction. In this chapter, past experimental and numerical studies on behaviour of structural walls in multistoried buildings are reviewed. Based on the review, the gap areas are identified and objectives of the present study are mentioned.

2.1 CLASSIFICATION OF RC STRUCTURAL WALLS

Based on cross-sectional shape, structural walls are mainly classified into three groups, namely (a) rectangular, (b) barbell and (c) flanged walls (Figure 2.1). Barbell shape results when the wall is provided monolithically between two columns. The end columns of the barbell-shaped wall are termed as boundary elements, which increase the strength of the wall in flexure and shear. Intersection of two walls results in flanged wall sections. Based on the geometry, RC structural wall is classified into three categories, namely (a) slender walls, (b) intermediate walls and (c) squat walls (Figure 2.2) (BIS, 2016a). When the height (H_w) to length (L_w) ratio is greater than 2, then it becomes a slender wall, and the behaviour is similar to that of a vertical cantilever beam. For intermediate shear wall, the height to length ratio (H_w/L_w) lies between 1 and 2. The height to length ratio is less than 1 for squat walls. The behavior of slender wall is mainly controlled by flexural deformation with small and negligible shear deformations. The squat walls usually have height to length ratio less than one with more dominant shear deformation. The squat walls can be elastic walls, rocking walls and ductile walls based on their response characteristics. When the overall height to length ratio is greater than one but less than two, then the wall can be categorized as intermediate wall. As per Indian seismic code (BIS, 2016b), the shear wall is classified into two types, namely (a) ordinary RC structural wall and (b) ductile RC structural wall. Ordinary RC structural wall are designed

without considering the effect of lateral forces, while the ductile RC structural wall are designed to resist the designed lateral force.

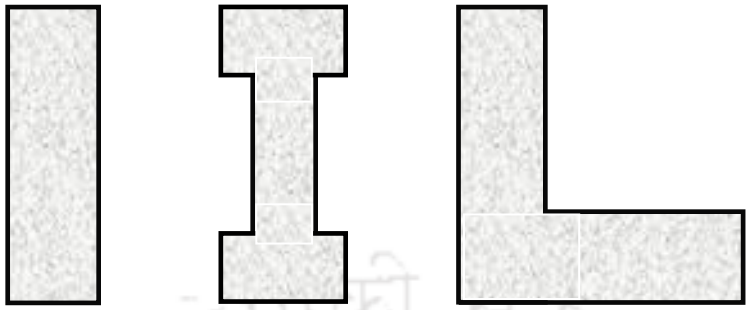

Figure 2.1: Classification of RC structural walls based on shapes: (a) rectangular wall, (b) barbell wall and (c) flanged wall.

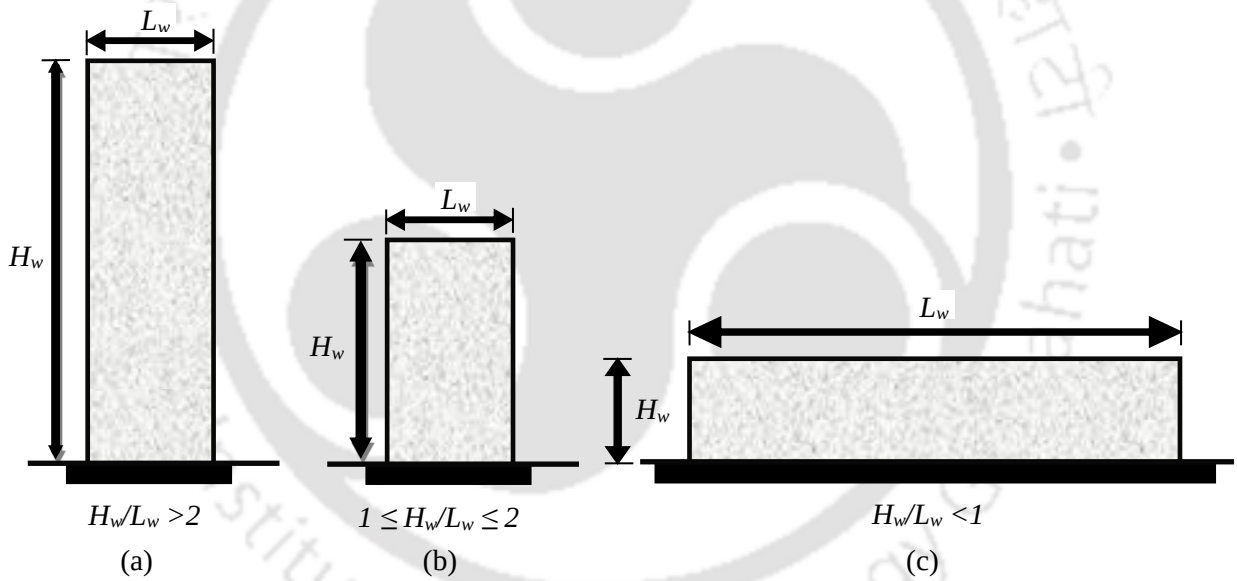

Figure 2.2: Classification of RC structural walls based on aspect ratio: (a) slender wall (b)intermediate wall, and (c) squat wall.

2.2 FAILURE MODES OF STRUCTURAL WALL

In this section, the possible failure modes of an RC structural wall are discussed. Although, the RC structural walls are commonly referred to as shear walls because of their large lateral shear capacity, the failure modes of the structural walls are not necessarily dominated by shear alone. Both flexure-dominant and shear-dominant behaviours are possible for the walls. The occurrence of possible failure modes depends on the aspect ratio of the wall.

2.2.1 Slender Walls

As mentioned earlier, slender walls exhibit flexure-dominant response during strong earthquake shaking. The various possible failure modes for slender walls are discussed below.

(a) *Flexural tension failure*: It is the principal source of energy dissipation in laterally loaded cantilever walls, characterized by the yielding of the flexural reinforcement in the plastic hinge region (Paulay and Priestley, 1992). The flexural cracks get concentrated at the base of the wall with the occurrence of maximum bending moment. Walls with boundary elements show extensive cracking and yielding of longitudinal steel in the bottom portion of boundary elements. This leads to higher overstrength flexural capacity with higher concentration of steel in boundary region (Elnashai et al., 1990).

(b) *Flexural Compression Failure*: This brittle mode of failure is characterized by crushing of concrete at the compression toe of wall bottom (Figure 2.3a). For walls with or without boundary elements, compression demand may exceed compression capacity due to inadequate dimensioning of wall base or inadequate detailing of boundary element steel or due to both; in any of these cases, the concrete at the bottom can get crushed. Generally, under increased direct and/or flexural compression demand, crushing of toe concrete takes place if out-of-plane failure modes are suppressed. Confinement of concrete is required at the bottom of the wall in order to avoid such brittle failure.

(c) *Diagonal Tension Failure:* For a slender wall behaving like a vertical cantilever member, the bottom portion of the wall adjacent to the foundation shows the characteristics behaviour of D-region. This can lead to diagonal tension failure or shear cracking of concrete even under moderate level of earthquake shaking (Figure 2.3b). Web shear cracks and flexure shear cracks occur in the web and at the bottom of the wall respectively. The flexural shear cracks originate at the wall edge and propagate into the web under increased deformation demand. To prevent this mode of failure, web reinforcement consists of smaller diameter bars placed with smaller spacing (Paulay and Priestly, 1992).

(d) *Diagonal Compression Failure:* In the bottom D-region of a slender RC structural wall, the diagonal compression failure take place at the plastic hinge region with high web shear stress, even when excess shear reinforcement is provided (Figure 2.3c). It has been observed that increasing shear reinforcement beyond the required amount does not improve the post-yield deformational characteristics of such walls (Elnashai et al., 1990). Under reversal of loading, web crushing in the plastic hinge region occurs due to rapid strength degradation of cracked concrete (Paulay and Priestley, 1992).

(e) *Sliding Failure:* Sliding failure of slender RC wall may occur at the potential plane of weakness which may be generated due to merging of deep flexural cracks under reversal of loading (Figure 2.3d). The planes where excessive sliding displacement can occur, may also be represented by construction joints. Provision of diagonal reinforcement across the potential sliding planes of the plastic hinge zone can prevent this type of failure. A much closer spacing of the vertical reinforcement across sliding planes region is preferable. Barbell-shaped walls have greater resistance against sliding due to dowel action of vertical bars in boundary elements.

(f) *Direct Compression Failure:* Failure due to concrete crushing can occur towards the bottom of the wall when the direct compression strain in concrete exceeds the failure strain in the compression. Such a failure can occur in slender rectangular walls that have a large percentage of vertical reinforcement and subjected to large axial load. Walls with unsymmetrical cross sections are particularly vulnerable to this failure mode (Medhekar and Jain, 1993). This mode of failure can be avoided by using diagonal web reinforcement. Web crushing usually limits the shear capacity of flanged shaped walls. The compression boundary element in such walls tends to shear through after web crushing.

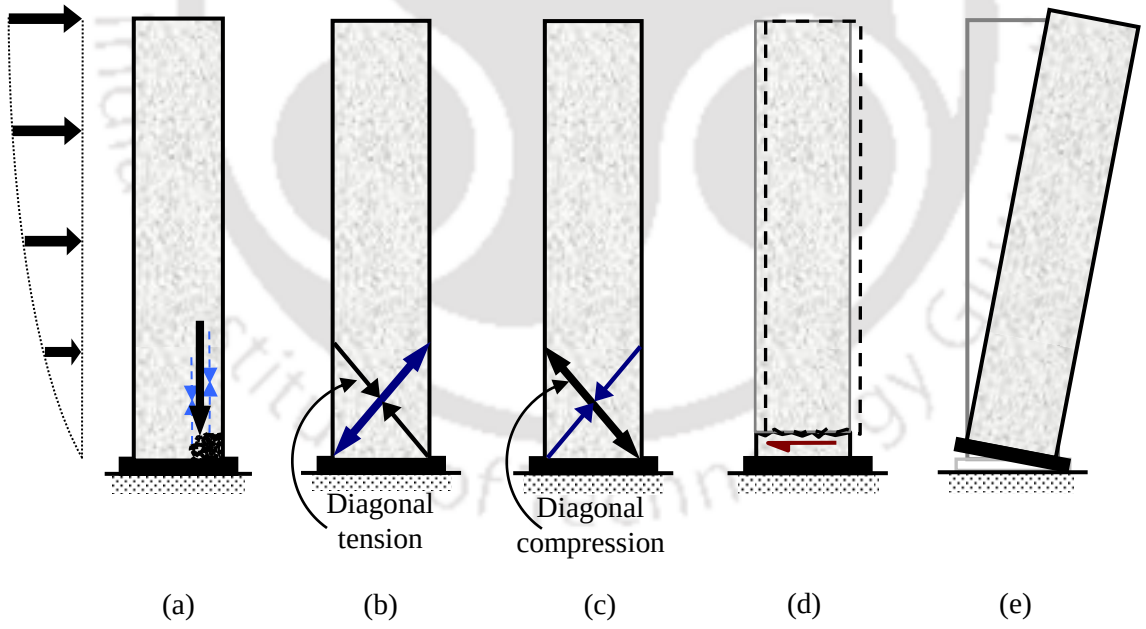

Figure 2.3: Failure modes in slender walls: (a) flexural compression, (b) diagonal tension, (c) diagonal compression, (d) sliding and (e) rocking. (Dasgupta, 2008).

(g) *Out-of-plane Instability:* This mode of failure occurs when a thin wall section in plastic hinge region is subjected to high vertical compressive force. During repeated reversals of loading, the modulus of elasticity and the section modulus get reduced. This leads to the possibility of

regions of instability between the cracks in concrete, and can cause buckling of vertical steel occur under heavy vertical compression.

(h) *Rocking Failure:* During reversal of loading, slender walls with isolated shallow footing may get partially uplifted (Figure 2.3e). This also depends on the type of soil and any lateral restraint along the height of the wall. Rocking failure of structural walls is observed during the 1994 Northridge earthquake (EERI, 1996).

2.2.2 Squat Walls

Under lateral loads, the behaviour of squat walls is governed by shear deformation under large shear stresses, diagonal strut-and-tie system develops in the web of the wall (Figure 2.4a). The possible failure modes of such walls are discussed below.

(a) *Diagonal Tension Failure:* In absence of sufficient reinforcement, a squat wall may fail due to large and extensive diagonal cracks in concrete. Depending on the nature of loading and aspect ratio of the wall, the tension failure plane may be oriented in the exactly diagonal direction or with a steeper angle (Figures 2.4b and 2.4c). A tie beam at the top of the wall can transfer the shear force to the rest of the wall avoiding such type of failure (Paulay and Priestley, 1992).

(b) *Diagonal Compression Failure:* Under the combined action of vertical and lateral loads, squat walls may also fail due to diagonal compression or web crushing. With high shear demand and adequate horizontal shear reinforcement, the crushing of concrete can rapidly spread over the entire length of the wall (Figure 2.4d). Under reversal of loading, the diagonal compression failure may occur at a level of lower lateral shear force. Some extent of ductile behaviour can be achieved by designing the web reinforcement to yield before the crushing of the web.

(c) *Sliding Shear Failure:* Under reversed cyclic loading, developed cracks may join to form a continuous horizontal shear path causing sliding shear failure of squat RC walls (Figure 2.4e). The tendency to fail in sliding shear increases with an increase in the applied shear stress and with a reduction in axial compression and aspect ratio of the wall. Providing diagonal reinforcement in the web of the wall tends to resist the sliding shear failure mode. Also, the provision of well confined boundary elements along the wall edges can prevent this type of failure (Paulay et al., 1982).

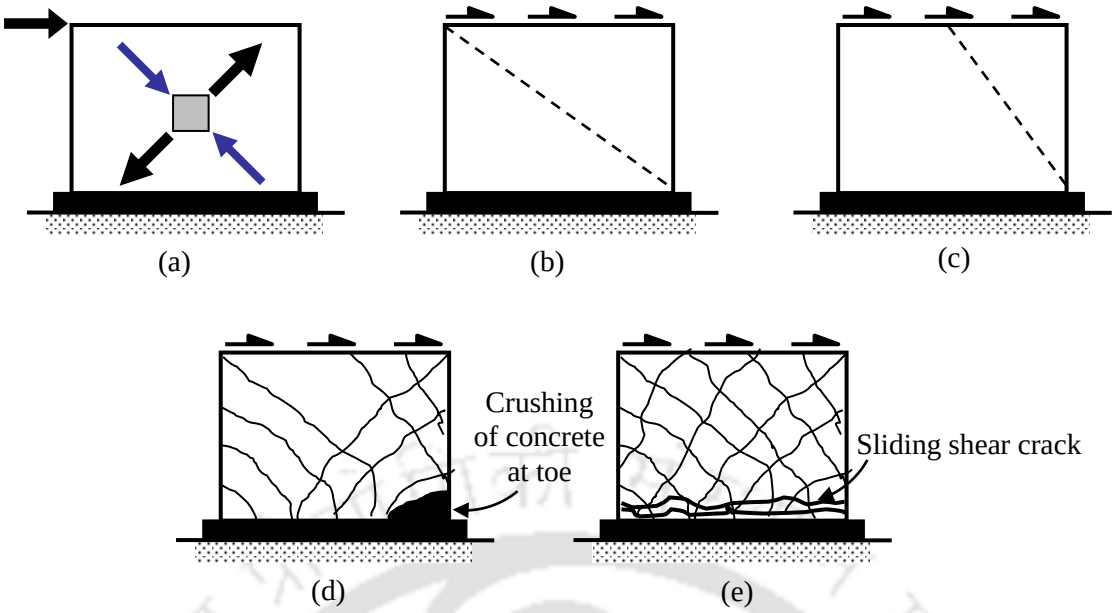

Figure 2.4: Failure modes in squat walls: (a) strut action, (b) predominant diagonal tension failure plane, (c) steeper tension failure plane, (d) diagonal compression, and (d) sliding shear.

In all the past studies, failure modes of isolated slender and squat walls have been discussed. However, investigation of failure modes of a shear wall connected to floor slabs in a multistoried building has not been carried out.

2.3 Modelling And Analysis of RC Structural Wall

In the past, various analytical and numerical models have been proposed for the analysis of isolated shear walls as well as for shear walls connected to floor slabs in multistoried buildings. The proposed models fall primarily into three categories, namely (1) equivalent frame models, (2) multispring models, and (3) finite element models. The salient aspects of these different categories of models are discussed in the following sub-sections.

2.3.1 Equivalent Frame Models

In equivalent frame models, the finite width of the wall is generally represented using rigid elements, while wall behaviour is modeled using an equivalent beam-column element placed along the center-line of the wall (Figure 2.5). This method of modelling reduces the computational effort required for a finite element model. However, since the location of the wall neutral axis changes substantially during a nonlinear analysis, beam-column elements placed at the wall centroids can be inaccurate unless they account for the effects of axial-flexural interaction. When equivalent frame models are employed, special attention should be paid to ensure that shear behavior is either adequately

considered in the model or that its effect can be conservatively ignored. Figure 2.5b shows the model of beam-column elements for the coupling beams and walls. A rigid link is used to represent the physical size of the walls, and a rigid connection is assumed between the connecting beam and the rigid link (El-Tawil et al., 2010).

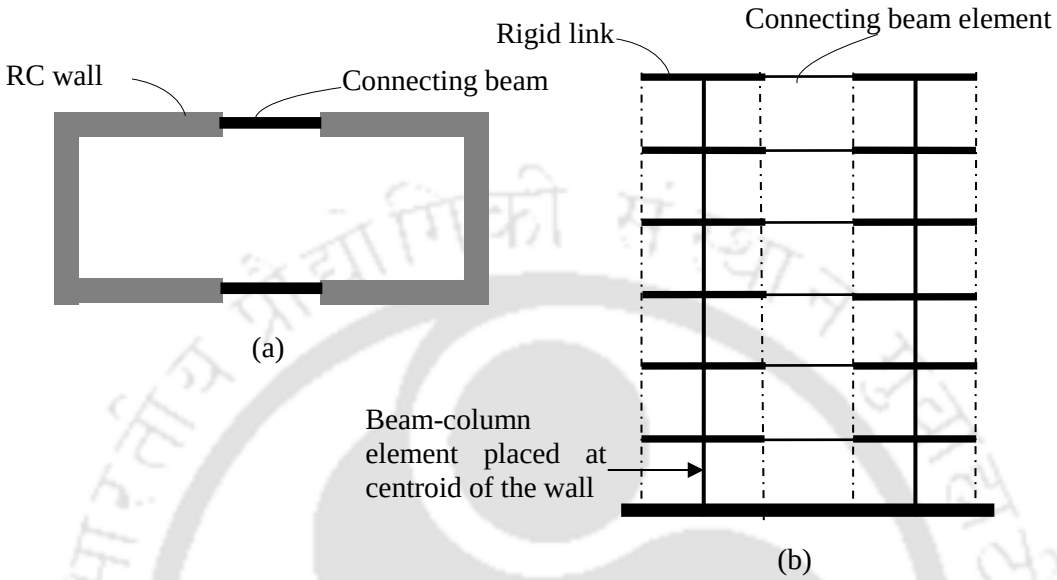

Figure 2.5: Equivalent frame model in walls: (a) plan of RC frame wall system and (b) equivalent frame model.

2.3.2 Multisprings Models

In the multispring method of modelling, different springs are proposed to represent the axial, flexural and shear stiffness of the RC wall. Kabeyasawa et al. (1983) proposed a Three Vertical Line Element Model (TVLEM) to simulate the inelastic response of RC structural walls. The TVLEM was modified by incorporation of an Axial Stiffness Hysteresis Model (ASHM) consisting of two axial elements in series. On the basis of the original TVLEM model, other researchers proposed a more refined model in which a number of springs in series or parallel configuration were used while rigid elements are used to represent the physical dimension of the wall (Colotti, 1993; Vulcano et al., 1988; Orakcal and Wallace, 2006). The refined model was known as Multiple Vertical Line Element Model (MVLEM) (Figure 2.6a). In MVLEM model a horizontal spring with stiffness K_H is placed at the element center of rotation to simulate the shear response of the wall panel. Flexural and shear modes of deformation of the wall element are considered to be uncoupled, i.e., flexural deformations do not affect the shear strength or shear deformation of the wall panel (Orakcal and Wallace, 2006). The flexural response is stimulated by a multi uniaxial element in parallel model with infinitely rigid beams at the top and bottom floor levels. The two external elements represent

the axial stiffness (K_1 and K_2) of the boundary columns, while the interior elements (K_3,….,K_n) represents the axial and flexural stiffness of the central panel (Vulcano et al., 1988).

More recent modifications of the MVLEM (Fischinger et al., 1990; Fajfar and Fischinger, 1990; Fischinger et al., 1991, 1992) have included implementing simplified force-deformation rules for the model sub-elements to capture the behavior observed in experimental results; however, the resulting models are tied to somewhat arbitrary force-deformation parameters, the selection of which was based on engineering judgment. An alternative approach is adopted by Orakcal et al., (2006), where up-to-date and state-of-the-art cyclic constitutive relations for concrete and reinforcing steel are adopted to track the nonlinear response at both the global and local levels instead of the use of simplified force-deformation rules as done in prior studies. Therefore, the MVLEM implemented relates the predicted response directly to material behavior without incorporating any additional empirical relations.

The MVLEM was further modified by assigning a shear spring to each microfiber (Figure 2.6c) of the element (Massone et al., 2009). Each macrofiber is then treated as an RC panel element subjected to membrane actions, namely the in-plane uniform normal and shear stresses. Thus the flexure-shear interaction got incorporated at the fiber level. It was shown that the mentioned modeling approach adequately captured the overall load-deformation response for walls having aspect ratio of 3.

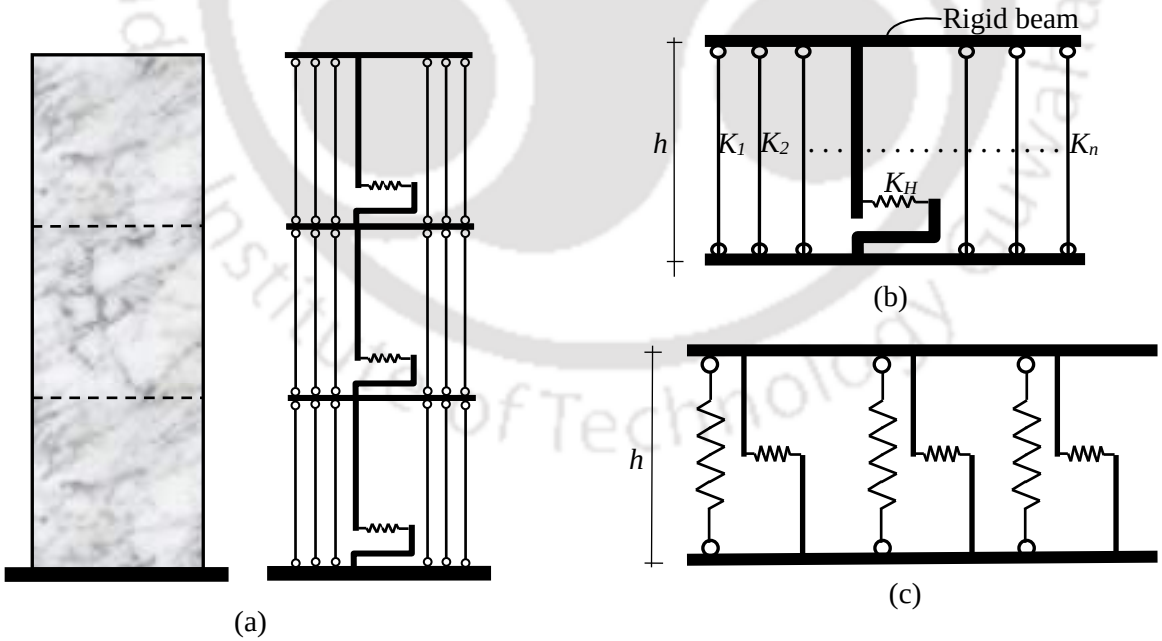

Figure 2.6: Multiple vertical line element model: (a) Representation of wall in multistoried building using MVLEM, (b) MVLEM element (Orakcal and Wallace, 2006), and (c) coupled model element (Massone et al., 2009).

2.3.3 Finite Element Models

Although equivalent frame method of modelling provides a computationally less expensive method for obtaining behaviour of structural walls, it may be difficult to obtain the response of walls with openings and complex boundary conditions using that method. In such cases finite element modelling of wall is resorted to for obtaining the response of the walls. In this section, the past studies covering the different aspects of finite element modelling have been reviewed.

The nonlinear element models of shear walls ranged from three dimensional nonlinear solid elements, two dimensional nonlinear shell elements to simplified models using frame elements (Fahjan et al., 2010). The RC shear wall without boundary element can be modeled using four-noded plane elements considering the top slab to be rigid (Kwak and Kim, 2004). Kim et al. (2005) developed a three dimensional super element for shear walls and floor slabs and a substructure was formed by assembling the super elements to reduce the time required for the modeling and analysis. The plane stress element used by Lee (1987) for the development of 2D super elements for the analysis of a shear wall structure with openings was the Lee element with 12 DOFs, as shown in Figure 2.7a. A shell element with 6 DOFs per node was introduced by combining the Lee element and a plate bending element (Figure 2.7c). For this purpose, 12 DOFs plate bending element with a rectangular shape was selected because of the convenience in the combination of stiffness matrices. The RC shear walls can be modeled either with Mid-Pier frame element or with shell element. The nonlinear material for the Mid-Pier frame element was assumed to be plastic hinge, while a multilayer model considering the concrete and reinforcement as a layered shells. The advantage of using shell elements is the ability to model very long, interacting and complex shear walls within the 3-D model.

8-noded isoparametric solid elements were also recommended for modeling RC walls because of their desired behaviour under non-uniform strain distribution (Mulas et al., 2007). Kwan and He (2001) developed a finite element model that takes into account the effect of concrete confinement for non-linear analysis of RC structures. Using this model, a finite element (FE) procedure based on secant stiffness formulation is developed. They carried out a parametric study on the effect of concrete confinement on the behaviour of RC shear walls using the FE procedure developed. It was revealed that the confinement of the concrete in the compression zone can significantly increase the lateral strength and ductility of wall. Khatri and Anderson (1995) analysed a shear wall building using plane stress isoparametric elements. Steel reinforcing was modeled using nonlinear truss element. Combination of linear and nonlinear shell elements with embedded reinforcement are also used in finite element modelling of wall piers (Bignell et al., 2005).

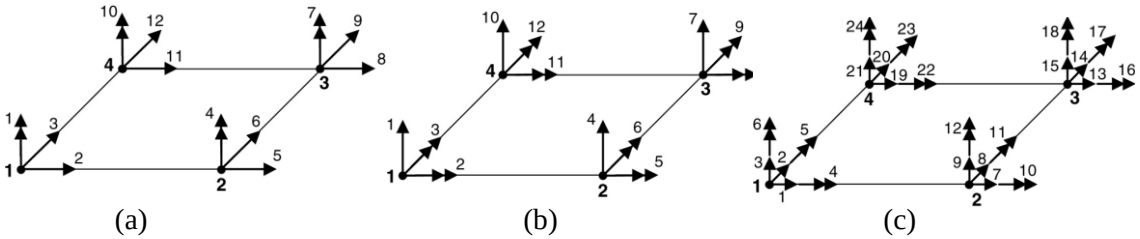

Figure 2.7: Finite elements for shear wall: (a) 12 DOFs plane stress element (Lee element) (Lee, 1987), (b) 12 DOFs plate bending element (MZC element) (Zienkiewicz and Cheung, 1964), (c) 24 DOFs shell element (Kim et al., 2005).

For micromodelling of shear wall, generally 8 noded solid elements are used to model the concrete part and 2 noded truss elements are embedded as a reinforcement in the concrete (Ile and Reynouard, 2004; Kazaz, 2010; Bohl and Adebar, 2011; Greeshma and Jaya, 2013). Separate constitutive models are used to obtain the behaviour of confined concrete and unconfined concrete, respectively (Figure 2.8). This type of modelling approach is able to provide detailed structural response in terms of local effects along with global force distribution. The major difficulty in carrying out analysis using micromodelling technique is the sensitivity of the model to the material constitutive laws, definition of the interface connections and their calibration. In addition, analyses of the large buildings require high computational effort which may not be feasible from the aspect of engineering practice.

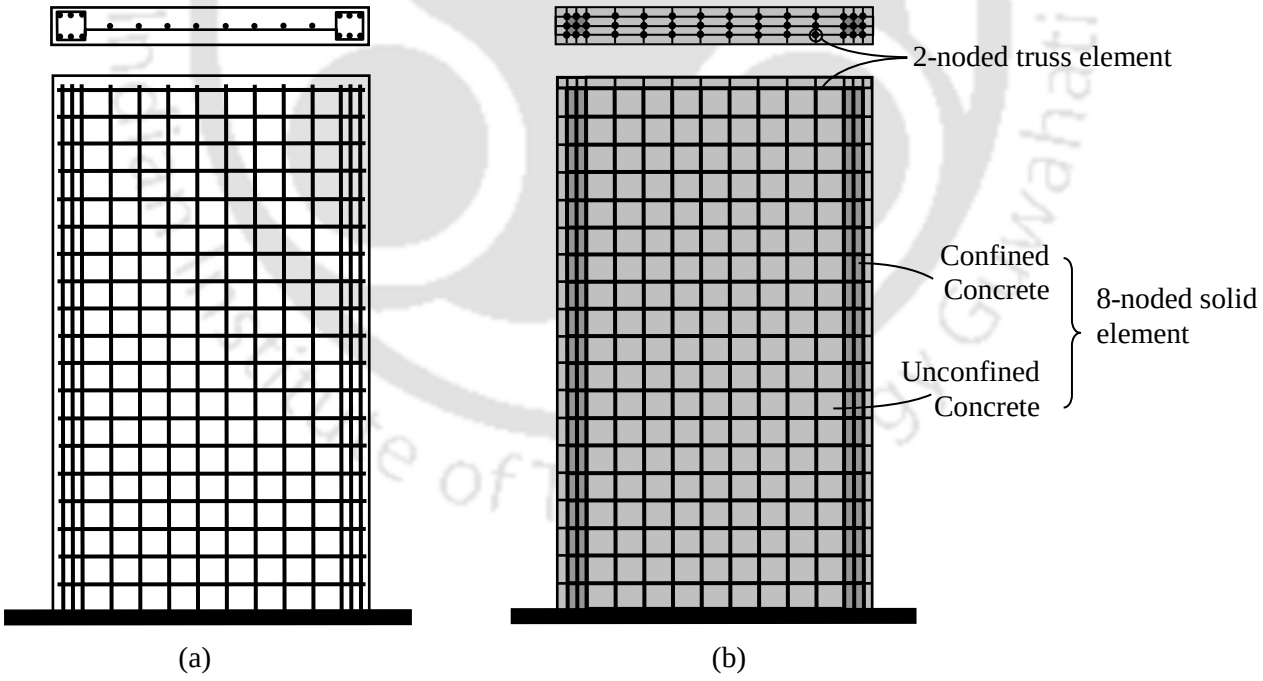

Figure 2.8: Finite element modeling of RC wall: (a) slender wall with concentrated vertical steel at the ends, and (b) finite element discretisation using solid elements and truss elements (Khatri and Anderson, 1995).

Selection of proper mesh size is an important aspect of finite element modeling of RC walls for obtaining proper behaviour. A refined mesh may be employed in the regions of high stress gradient or particularly complex geometry, and a much coarser mesh in regions of low or uniform stress. It is also possible to model a structure by combination of finite element meshing in the region involving detailed local response and an equivalent frame in the remaining region of the member. When constructing a mesh for a finite element analysis, rectangular elements should be close to the square shape as possible, triangular elements should be as close to the equilateral shape as possible and quadrilateral element should be as close to a parallelogram with equal sides as possible, to achieve most accurate results (Smith and Coull, 2011).

2.3.4 Strut and Tie models

The strut-and-tie model is a hypothetical truss system used to represent the force transfer mechanism in a structural member. It consists of (a) struts which carry compressive forces in concrete, (b) ties which represent one or several layers of reinforcement for carrying tensile forces, (c) nodes which are idealised pinned joints at the intersections of struts and ties, and (d) nodal zones which are areas of concrete around the nodes. The system of forces in struts and ties remains in equilibrium with the given set of loads, and the factored member forces at every section in the region of strut-and-tie model do not exceed the corresponding member capacities at the same sections (MacGregor and Wight, 2005). The structure also requires sufficient ductility to make the transition from elastic to plastic behaviour with the redistributed internal forces satisfying force equilibrium and limiting member capacity criteria. This ensures mobilization of lower-bound strength of structural member based on the assumed strut-and-tie model. Although the strut-and-tie configuration is based on elastic analysis (Schlaich and Schafer, 1993), redistribution of stresses in cracked RC sections tends to alter the flow of forces (ASCE-ACI, 1998).

Kassem (2015) adopted a rational approach based on the strut-and-tie model to develop a closed-form expression for shear strength estimation of RC squat walls. The proposed analysis method consists of the application of the strut-and-tie model and accounts for shear strength contributions provided by concrete strut and web reinforcement. In squat RC walls with boundary elements (Hwang et al., 2001; Hwang and Lee, 2002; Kassem, 2015), the proposed strut-and-tie model consists of three mechanisms, namely (a) diagonal mechanism which consists of a single diagonal strut with angle of inclination with the horizontal (Figure 2.9a) given *as*,

$$\alpha_s = tan^{-1}(H_w / d_h) \tag{2.1}$$

where H_w is the distance from point of application of V_d to base, and d_h is the horizontal length between the tensile and compressive forces in the boundary element, (b) horizontal mechanism

which consists of a horizontal tie and two flat struts (Figure 2.9b), and (c) vertical mechanism which consists of a vertical tie and two steep struts (Figure 2.9c).

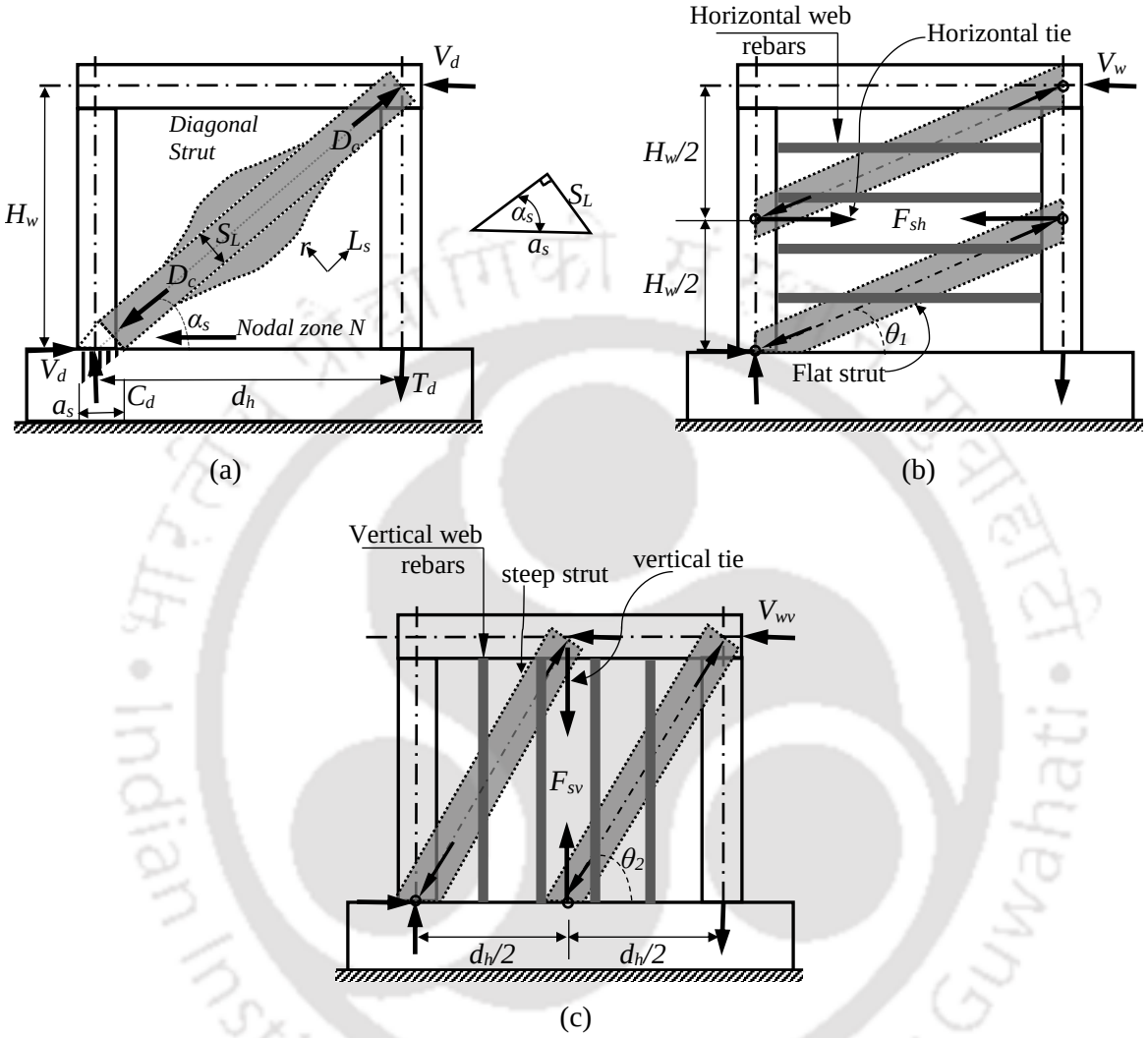

Figure 2.9: Shear resistance of squat wall through: (a) diagonal, (b) horizontal and (c) vertical mechanism (Kassem, 2015).

The diagonal mechanism comprises a single diagonal compression strut running from the point of load application to the opposite corner. The selection of this mechanism is based on the observed inclined cracking patterns in squat wall. At peak shear strength level or beyond, this mechanism represents the diagonal tension, diagonal compression and possible sliding shear failure modes.

For the diagonal mechanism, Kassem (2015) has proposed that d_h be calculated as $d_h = L_s - \left(\frac{a_s}{3}\right)$, where L_s is the distance from extreme compression fibre to location of resultant of forces in vertical

reinforcement in tension, and a_s is the horizontal length of the compression zone at the wall base (Figure 2.9a).

Considering the equilibrium of the forces at nodal zone N, the tensile (T_d) and compressive (C_d) forces in the boundary elements can be obtained as,

$$T_d = C_d = D_c \sin(\alpha_s) \tag{2.2}$$

$$V_d = D_c \cos(\alpha_s) \tag{2.3}$$

where, D_c is the compression force in the inclined strut and V_d is the shear force carried by the squat wall without considering the web reinforcement effect. The strut width, S_L, can be estimated as,

$$S_L = a_s \sin(\alpha_s) \tag{2.4}$$

As proposed by Park and Paulay (1975), the simplified equation for a_s is given by,

$$a_s = \left(0.25 + 0.85\frac{P}{A_w f_c^{'}}\right) L_w \tag{2.5}$$

where, A_w is the cross-sectional area of the concrete section bounded by the web thickness (t_w)and the length of the section in the direction of the shear force (L_w), and $f_c^{'}$ is the cylindrical compressive strength of the concrete. From Eq. 2.5, it can be observed that the axial load enlarges the cross-sectional area of the compression strut and thus increases the shear resistance. Using Eqs. 2.4 and 2.5, the cross-sectional area of the inclined strut, A_{strt}, is given by,

$$A_{strt} = t_w a_s \sin(\alpha_s) \tag{2.6}$$

Thus, the compression force in the inclined strut (D_c), can be calculated considering the cross-sectional area of the inclined strut (A_{strt}), and the effective concrete compressive strength along the axis of the strut (f_{cd}), according to the following expression:

$$D_c = A_{strt} f_{cd} \tag{2.7}$$

The force D_c can be further compared with the strut capacity of the wall panel. The proposed strut-and-tie model by Kassem (2015) for shear strength estimation of squat walls provides a single closed-form expression, which is more accurate and reliable than other predictive equations available in the design codes and literature.

Hwang et al. (2001) proposed a softened strut-and-tie model for determining the shear strength of squat walls. A similar model for the seismic resistance of beam-column joints has been proposed by Hwang and Lee (1999, 2000). This model was based on the strut-and-tie concept and derived to satisfy equilibrium, compatibility, and constitutive laws of cracked reinforced concrete. Three strut-and-tie load paths (Hwang and Lee 1999, 2000) were proposed to model the force transfer within the squat wall, and they are the diagonal, horizontal, and vertical mechanisms.

Mun and Yang (2016) established a simplified strut and tie model for squat RC shear walls, based on the crack band theory of fracture mechanics for evaluating the lateral load capacity. The load transfer mechanism of concrete was identified by the strut-and-tie action contributed by the web concrete and longitudinal reinforcement of the boundary elements of the walls, whereas that of shear reinforcement was identified by the tie action idealised using a statically indeterminate truss system.

Zhi et al. (2017) developed a three panel strut-and-tie model considering the confinement effect on concrete strength of the boundary element based on ACI 318-14 code and strut-and-tie model of Hwang et al. (2001) and Kassem (2015) to investigate the force transfer mechanism of the specimens. Hwang et al. (2001) and Kassem (2015) proposed a softened strut-and-tie and a closed-form expression, respectively, to predict the shear strength of squat walls based on three strut-and-tie load paths that were diagonal, horizontal and vertical mechanism. They were both applied only to squat walls that the shear strength is sufficiently less than the flexural strength. It is generally recognized that a more complex truss (more-panel) is required with aspect ratio of concrete members increasing to avoid a strut angle less than 25º. Furthermore, in fact, there are no clear boundaries of aspect ratio to distinguish the dominant shear-transfer mechanism of members that are a direct strut and a sectional shear with aspect ratio between 2 and 2.5. It was observed that the simplest strut-and-tie model approach was conservative for shear walls with aspect ratio between approximately 2.35 to 2.5.

In all the past studies, various strut-and-tie model for RC squat shear wall have been developed considering the single wall panel. However, in multistoried buildings the shear wall are connected with the floor slabs at every floor levels, resulting in many such panels. Thus, a detailed study is required for developing the strut-and-tie model of a shear wall connected to floor slabs in a multistoried building.

2.4 COUPLED STRUCTURAL WALLS

In most of the multistoried RC frame-wall buildings, the walls are connected to slabs at the different floor levels. Due to the architectural or other requirements, shear walls may be closely located along

the same frame grid-line. In the first case, the coupling action of slab and shear wall behaviour plays an important role in the overall building response. In the second case, the set of walls is known as beam-coupled shear walls or slab-coupled shear walls if they are joined with a set of beams or slabs at certain levels. The coupled shear wall also provides more openings, which increase the functional flexibility in architecture. Furthermore, by coupling individual flexural walls, the lateral load resisting behavior gets changed significantly. Also, if the floor slabs are rigidly connected to the walls, they serve in effect as connecting beam to produce shear interaction between the two inplane cross walls. In this section past research work on the behaviour of such slab-coupled and beam-coupled walls is reviewed.

When the two laterally loaded shear walls (Figure 2.10) are compared, the overturning moment is resisted at the base by a single moment reaction in case of cantilever wall (Figure 2.10a). However in case of coupled walls, a moment reactions are developed at the base of each wall. In addition, a couple is also formed by the axial forces in each wall segment that is carried across the coupling beam by vertical shear (Figure 2.10b).

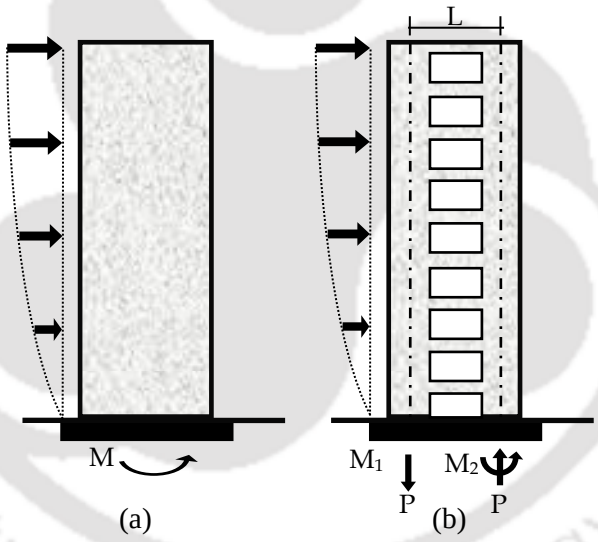

Figure 2.10: Lateral load resisting mechanism of shear walls: (a) cantilever wall and (b) walls coupled by beams (Paulay and Taylor, 1981).

The relative magnitudes of internal moment resistance for beam coupled and slab coupled shear wall are shown in Figure 2.11. The stiff and reinforced coupling beam will develop significant shear force, and as a result, a large axial force will be introduced in the wall. Since the major part of the moment resistance is obtained because of the axial force couple component that mechanism tends to become the major source of energy dissipation during strong earthquake shaking. However, when slab coupling is used, slabs induce relatively small axial forces in the wall because of their flexibility and small potential strengths, the moment demand on the walls (M_1+M_2) increases rapidly (Figure 2.11).

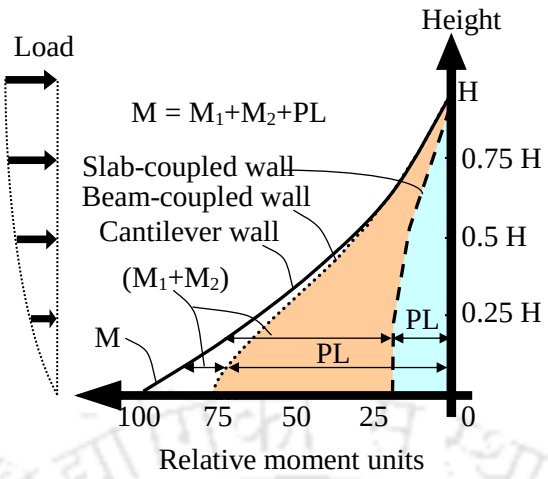

Figure 2.11: Comparison of moment distribution in laterally loaded coupled shear walls with the internal moment in isolated cantilever wall (Paulay and Taylor, 1981).

2.4.1 Beam Coupled Shear Walls

A beam-coupled shear wall is generally formed when the shear wall contains one or more rows of openings along the same vertical panel (Figure 2.10b). During strong earthquake shaking significant inelastic actions can occur in the coupling beams than in the coupled walls. It has been observed that the beam experiences a large number of shear reversals as compared to the walls (Paulay and Priestley, 1992). Coupling beams that contains inadequate shear reinforcement fail in diagonal tension (Figure 2.12a). The diagonal cracks tends to divide a relatively shorter beam into two triangular parts. If the shear force associated with the flexural strength of the beam at the wall face is not transmitted by the vertical stirrups, it will results in only the diagonal failure. However, after only few load reversals, flexural cracks at the critical support section will interconnect and a sudden sliding shear failure tends to occur (Figure 2.12b). Providing diagonal reinforcement in coupling beam results in ductile behaviour with excellent energy dissipating properties (Figure 2.12c). The diagonal bars are either in tension or in compression over the full length, hence the bond problems within the coupling beams do not arise. Such beams can then sustain large deformations imposed on them during the inelastic response of coupled wall (Park and Paulay, 1975). When more slender beams with a span to depth ratio of 3 to 4 are used in coupled shear walls, the possibility of sliding shear failure across the plastic hinge zone may also arise. In such cases it will be more practical to use diagonal bars bent approximately at 45° along both the directions across the plastic hinge zones at both the ends. The overall response of the coupled shear wall structure is primarily determined by the behaviour of the coupling beam provided that the plastic hinge zone at the base of the shear wall is adequately reinforced for lateral stability and ductility (Paulay and Taylor, 1981).

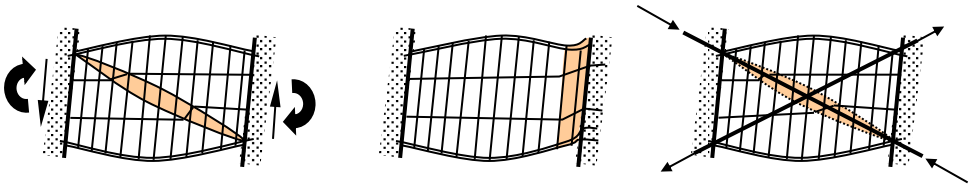

(a) (b) (c)

Figure 2.12: Mechanism of shear resistance in coupling beam: (a) diagonal tension failure, (b) sudden sliding shear failure at beam-wall junction, and (c) diagonal reinforcement in coupling beam (Paulay and Priestly, 1992).

2.4.1.1 Modeling and Analysis

In order to compute the elastic distribution of internal forces and deformations under the influence of code specified lateral forces, it is important to accurately model the wall piers, the coupling beam elements, and the wall-beam connections between them. As discussed in Section 2.3**,** the coupled shear wall can be modeled by an equivalent frame member and also by finite element meshing. In case of equivalent frame model, a rigid link is used to represent the physical width of the wall, and a rigid connection is assumed between the coupling beam and the link (El-Tawil et al., 2010). Finite element model is used to analyse structural walls, particularly flanged walls and walls with irregular geometry. Various finite element models proposed by several researchers have been discussed in Section 2.3.3. Selection of proper mesh size is an important aspect of finite element modeling of RC walls for obtaining proper behaviour.

2.4.1.2 Reinforcement in Coupling Beam

The shear strength of the coupling beam must be greater than the shear force that can be developed when plastic hinges form at its two ends. This demands a limit to be imposed on the tension steel content in such beams. Reinforcement in the coupling beam may consist of parallel reinforcement or full length diagonal reinforcement. Parallel reinforcement needs to be well anchored into the wall. Closely spaced stirrups must be provided over the full length of the beam to confine the concrete and provide better shear strength (Figure 2.13a). Diagonal reinforcement is more efficient as compared to the parallel reinforcement in the coupling beams (Park and Paulay, 1975). The diagonal bars are also well anchored in the wall and restrained over full length to avoid buckling (Figure 2.13b).

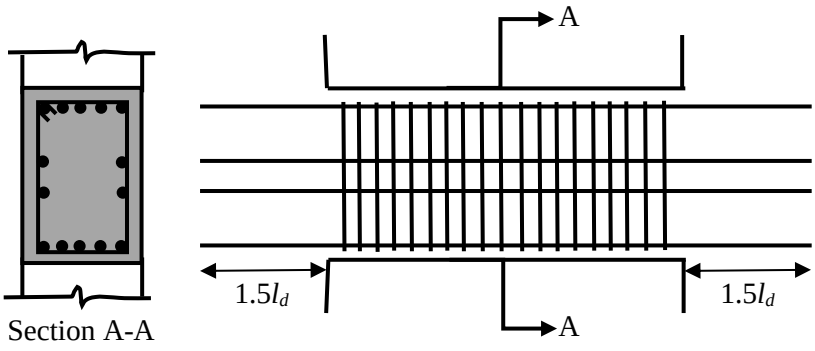

(a)

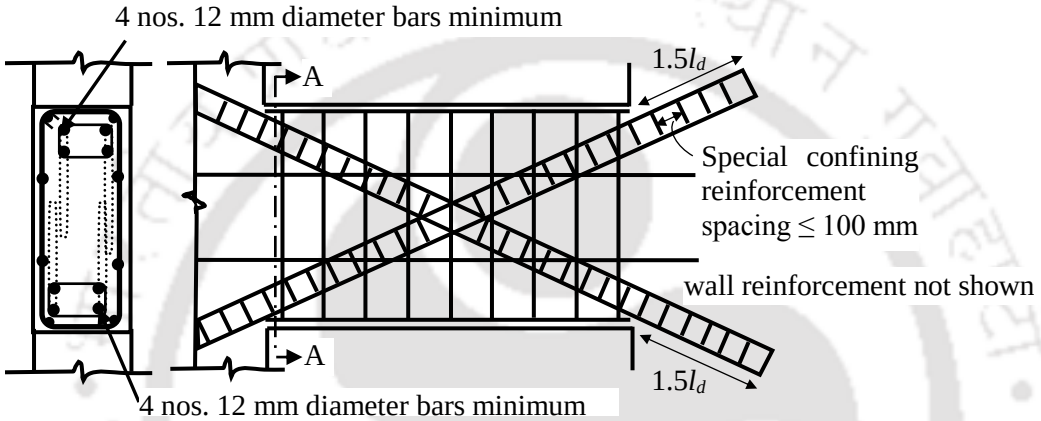

(b)

Figure 2.13: Typical reinforcement details for coupling beam: (a) parallel reinforcement and (b) diagonal reinforcement as per IS: 13920-2016 (Medhekar and Jain, 1993).

2.4.2 Slab Coupling of Shear Walls

For slab-coupled shear walls, the coupling action is mobilized through the response of the connecting floor slab (Figure 2.14a). To investigate the coupling response, it is convenient to study a wall unit with the mechanism of coupling at one floor only. In such systems, the possible failure modes can be: (a) local shear failure of the slab, (b) flexure failure of slab (c) torsional cracking of slab and (d) yielding of reinforcement in slab. During strong earthquake shaking if sufficiently large rotation occurs in the wall, yield line moments develop in the slab (Figure 2.14b), which possibly lead to significant shear transfer across the openings. Transverse bending and consequent torsion also occur in the slab due to the rotation of walls (Figure 2.14c). Shear transfer at and around the leading edges of the wall at the opening may become a critical feature leading to punching shear failure before the yield lines could reach the free edges of the slab. Torsional cracking of the slab and shear distortions around the toe are responsible for the poor hysteretic response of such slab-wall system. Therefore, slab coupling is not a significant source of energy dissipation in ductile

coupled wall-slab system (Paulay and Priestly, 1992; Paulay and Taylor, 1981). RC slab-coupled wall is widely used all over the world because of its easy implementation in highrise buildings, in which the coupling of the cross walls by the floor slabs can lead to an efficient structural system for resisting lateral loads. A few past studies on behaviour of slab-coupled shear walls are reviewed here.

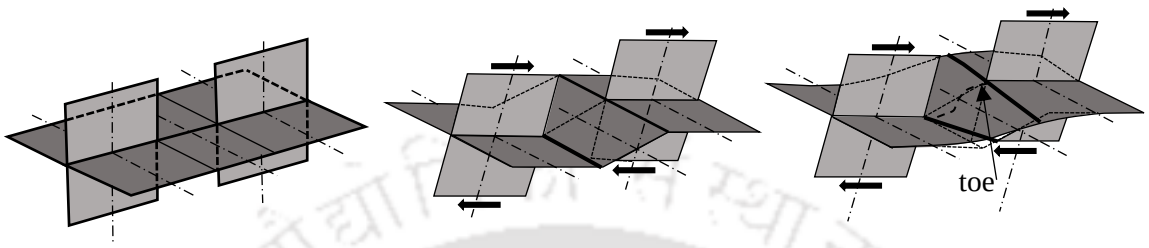

(a) (b) (c)

Figure 2.14: Details of slab-coupled shear walls: (a) typical view of coupling slab, (b) development of yield line moments in slab, and (c) reduced curvature near the edges due to torsional distortion (Paulay and Priestly, 1992).

Experimental studies carried out using various arrangements of longitudinal and transverse slab reinforcement by Paulay and Taylor (1981), suggest that minimum longitudinal reinforcement prescribed by the building design requirement needs to be placed outside the central strip across the doorway (Figure 2.15). Bars enclosed by stirrups ties within a strip width were found to be more effective in developing flexural strength required for coupling two shear walls. Stirrups in slab strip were found to enhance ductility by confining the cracked concrete and by preventing buckling of flexural bars. Transverse bars prevented total punching failure at the wall toes although shear deformation in the elastic range of response was significant. The use of steel section embedded in the slab in the vicinity of wall toes and placed at right angles to the coupled walls proved very effective in controlling punching shear and early damages. The stiffness of the slab during reversed cyclic loading gets reduced significantly with increasing displacement ductility demand. The observed stiffness degradation was more severe in coupling slab as compared to coupling beam and hence the system cannot be considered suitable as a primary source of energy dissipation in slab coupled wall structures.

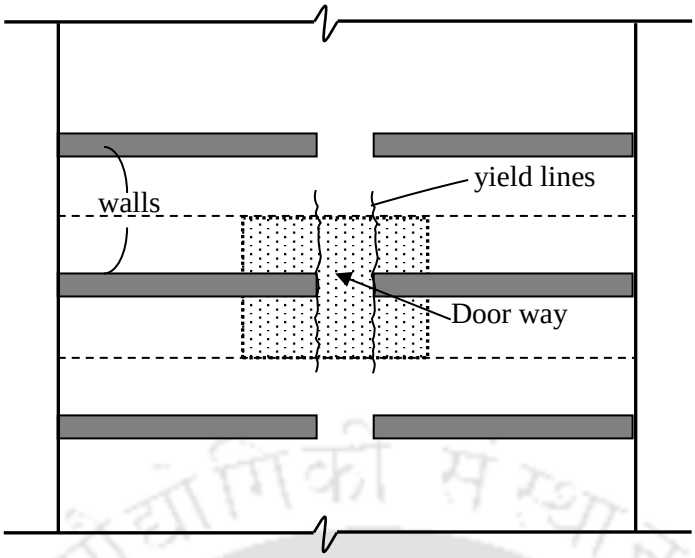

Figure 2.15: Observation of cracks in the plan view of a typical slab-wall coupling system (Paulay and Taylor, 1981).

Numerous studies have been carried out on the coupling action between floor slabs and shear walls to determine the bending stiffness of the slab for the overall structural behaviour. However, very little attention has been given to the corresponding flexural and shear action of the slab. Coull and Chee (1983) carried out finite element analysis of the coupled system to obtain the induced bending moment and shear forces. A design method was proposed based on the estimated shear forces to check against punching shear failure in slabs. In the analysis, the slab panel was divided into an assembly of plate bending elements using a suitable mesh pattern. The mesh size was finer in the region close to the wall than other regions with high stress gradients. A very wide range of simple and higher order elements of triangular and rectangular shapes was investigated and, it was concluded that the most suitable element from the point of view of convergence was the rectangular Adini-Clough-Melosh (ACM) element of plan dimensions a and b and thickness t. The typical element has three degree of freedom namely two rotations and transverse deflection at each node (Figure 2.16). A single comprehensive design curve was derived (Figure 2.17) showing the variation of critical bending moment factors for quick evaluation of the stresses induced in the slab. Based on an assessment of the interactive shear forces between the wall and the slab, a design procedure was proposed for checking against punching shear failure of the slab. Similar design curves were developed for the slab coupled flanged shear walls. T- and L-shaped shear walls were analysed using finite element method to evaluate the critical design bending stresses, subjected to a unit relative wall rotation or vertical displacement. A similar method is proposed for checking against punching shear failure of the slab and design curves have been developed for coupled planar flanged walls-slab systems (Coull and Chee, 1984).

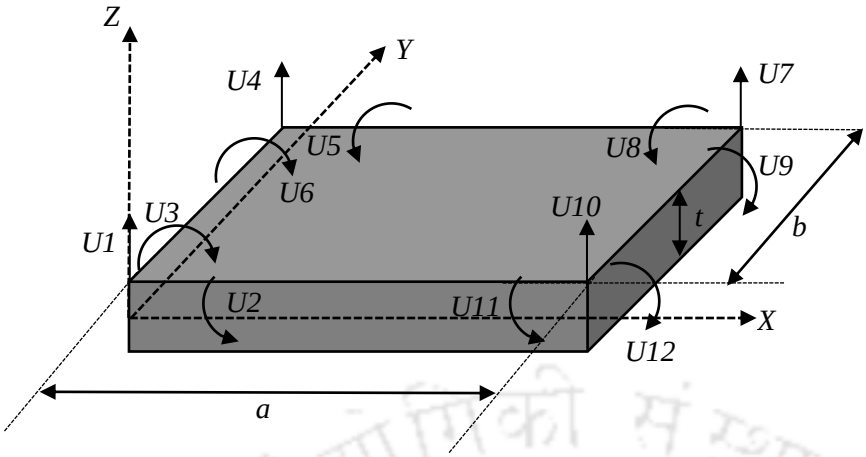

U1, *U4*, *U7* and *U10* are the translational DOFs while *U2*, *U3*, *U5*, *U6*, *U8*, *U9*, *U11* and *U12* are the rotational DOFs

Figure 2.16: Nodal degrees of freedom of ACM element (Onu, 1984).

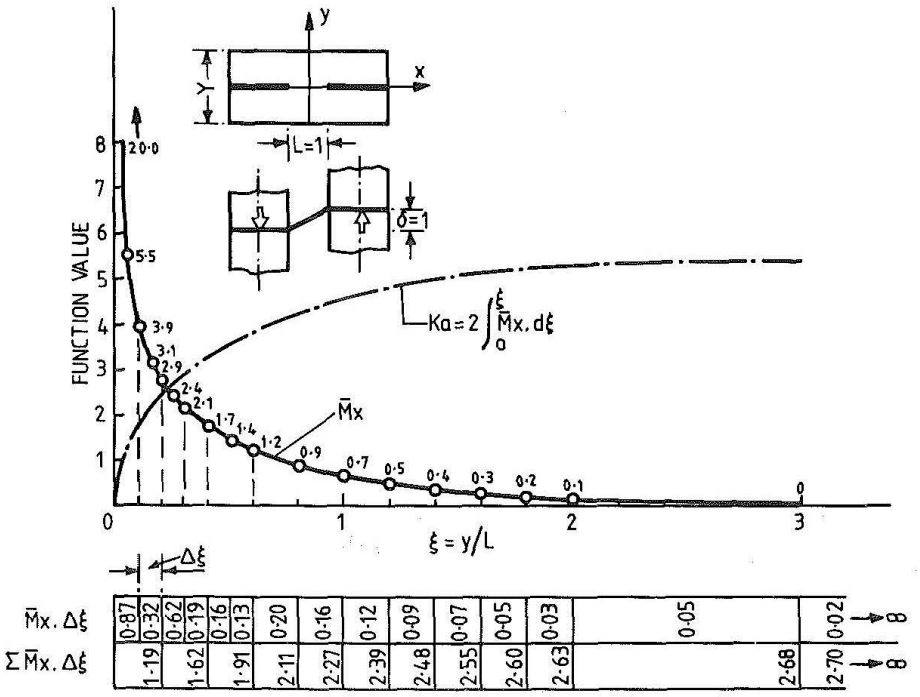

Figure 2.17: Generalized design curve for longitudinal bending moments at critical transverse slab section (Coull and Chee, 1983).

The previous studies were based on linear elastic finite element analysis of uncracked slab section. In another study by Coull and Chee (1990), the influence of a pseudocrack on the coupling slab behaviour was observed. The high stress concentrations around the inner edged of the shear wall led to local cracking of the concrete, along with yielding of reinforcing steel, causing a significant reduction in the coupling stiffness due to the loss of flexural resistance. Cracking is also expected

to cause a redistribution of stresses to other parts of the slab which were still uncracked; this may possibly lead to some compensation for the loss of stiffness at the crack location. The study concluded that the presence of crack across the highly stressed inner end of the wall results in a substantial reduction in the effective coupling stiffness, especially when the wall-opening ratio is very small.

Qadeer and Smith (1969), carried out both theoretical and experimental investigations of the flexural stiffness of the slab against the parallel rotation of pair of in-line walls. Stiffness values, with varying size and spacing of the walls and slab proportions were assigned to cover the wide range of practical possibilities. The experimental results for the stiffness of slabs connecting shear wall validated the accuracy of the analytical studies. The proposed curves for the stiffness of the slab against the rotation of the walls may be used to obtain the effective width or to derive an equivalent flexural rigidity for the connecting slab. The calculated slab stiffness is found to be less than that estimated by empirical method with an angle of dispersion of 45° or effective full width. Also, a fixed angle of dispersion cannot be adopted for calculating the slab stiffness as this arbitrary angle varies with the dimensions of slab and walls.

The floor slabs and shear walls together act as a rigid jointed frame in resisting gravity and lateral loads during earthquake shaking. The vertical shear caused by the lateral loads in the floor slabs, like the gravity loads, are transmitted to the walls. The junction between the slab and wall becomes a critical region due to high stress concentration. Bari (1996) used a 3D nonlinear finite element program to study the strength and stiffness of shear wall-floor slab connection. The program incorporated 20 noded isoparametric brick element with embedded steel. Fifteen specimens were tested to study the effect of shear reinforcement in the slab and various load and geometric parameters that govern the strength of the connection along with comparison of analytical and experimental results. The adopted model predicted ultimate loads to an acceptable level of accuracy. The punching and flexural type of failure were also predicted satisfactorily.

Schwaighofer and Collins (1977) performed experiments to investigate the stiffness, shear strength and flexural strength of coupling slab in RC shear wall-slab system. Under lateral loading, a pair of coupled shear walls underwent relative displacements in the longitudinal direction of the walls (Figure 2.18). The experiment showed that the cracks developed around the coupled edges of the walls at the junction of slab and walls. Before these cracks were visible, the deterioration in the stiffness of slab was noticed. On further increase of the wall displacement, the cracks spread along the walls and new cracks from the corners developed and spread across the entire width of the slab (Figure 2.19). However, in none of the past studies, the inelastic behaviour of wall in presence of coupling slabs has not been investigated.

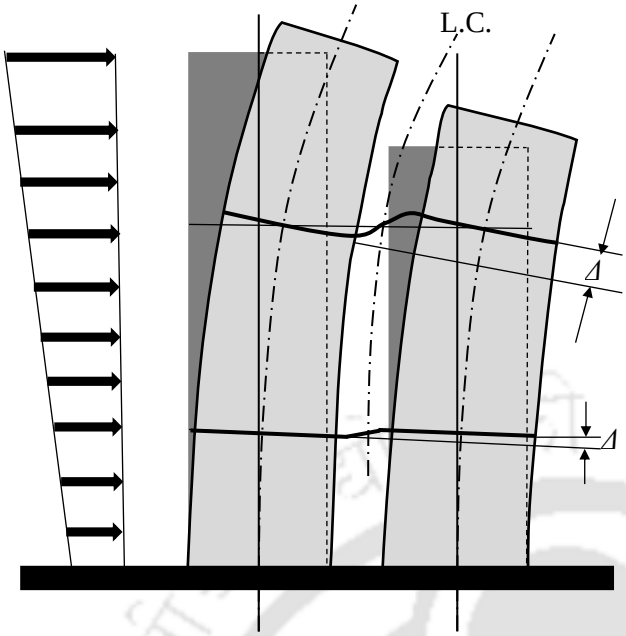

Δ = Relative displacement of floors

L.C. = Line of contraflexure in slab

Figure 2.18: Relative displacements of floors (Schwaighofer and Collins, 1977).

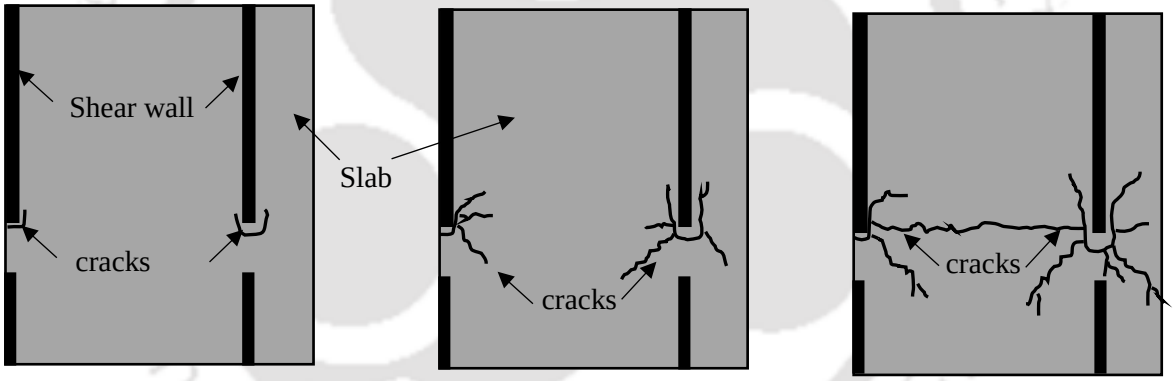

Figure 2.19: Crack patterns at the top of the slab in slab-coupled wall system: (a) first visible crack, (b) initial crack spread back along the wall and (c) flexural crack across the entire width of slab (Schwaighofer and Collins, 1977).

2.5 STRUCTURAL WALL-SLAB JUNCTION

In multistoried RC frame-wall buildings, the structural wall is connected to floor slabs at different levels. Thus, every wall-slab junction plays an important role in the transfer of forces from slab to the wall and down to the foundation at the bottom. During strong earthquake shaking, the junction region is subjected to high stress concentration which may lead to failure in that region and change the force distribution in the wall and other lateral load-resisting elements. To avoid redistribution of forces from walls to other elements not necessarily designed for lateral load resistance, the wall-

slab connection was recommended to be designed considering stress concentration (Pantazopoulou and Imran, 1992). It was observed that the design of slab-wall connection is governed by the same requirements as shear walls, although it is common practice to omit shear design consideration due to the large extent of connection boundary between slabs and walls. A simple plane stress model was used to develop expressions for estimating the nominal shear resistance at the slab-wall junction. The governing code requirements were evaluated based on the experimental evidence and indicated that the existing codal equations are unconservative in case of lightly reinforced slab diaphragms. An expression for the nominal shear resistance of the slab-wall connection region of typical slab was also proposed.

Greeshma and Jaya (2013) carried out experimental and analytical studies of the floor slab-shear wall connection by considering two different reinforcement details, namely (i) conventional joint detailing with the provision of U-shaped hooks connecting shear wall and slab and (ii) extension of slab reinforcement into the shear wall as 90° bent bars at the core region with the provision of shear reinforcement in the slab. Good energy dissipation capacities were observed with the provision of shear reinforcement for an effective width of the slab as compared to the conventional joint reinforcement details. The experimental results were compared with numerical simulation results obtained using the finite element software ANSYS and it was found that the experimental results are in good agreement with the numerical results. Also, the specimens detailed with 90° bent slab bars with slab shear reinforcement exhibited higher ultimate strength as compared to the other specimens. They concluded that the exterior shear wall-slab joint with slab shear reinforcement and 90° bent bars at the joint can be effective in regions with the possibility of moderate to high intensity of earthquake shaking.

In another study, the behaviour of a core wall-slab connection was investigated experimentally under earthquake induced deformation to identify alternative details for improving the performance of that connection under large rotational demands (Klemencic et al., 2006). The main objective was to study the performance of those connections when subjected to gravity load combined with slab-wall rotation consistent with deformation compatibility of building lateral drifts. Two full-scale specimens were constructed and subjected to design gravity loads and increasing lateral deformations. In this study, the slab-wall connection was made through reinforcing dowels placed near the top and bottom of the slab, with mechanical couplers at the slab-wall interface, often supplemented with intermittent shear keys. The test successfully demonstrated that connection details proposed by the researchers achieved the collapse prevention performance objective of 2% interstory drift as required by common building codes.

Rad and Adebar (2009) studied the interaction between tower walls and foundation walls due to

diaphragm action of concrete floor slabs. The concrete slabs and columns are assumed to be part of the gravity load system, not the seismic force resisting system, and the interaction between these two systems is usually ignored by designers for simplicity. The core walls extend from the top of the tower down to the foundation, and are supported near the base by a surrounding structure that may be partially or entirely below grade (Figure 2.20). The foundation walls import significant rigidity to the base structure. Nonlinear response history analysis was carried out to understand the reverse shear phenomenon. Depending on the stiffness of floor diaphragms, and on the shear rigidity and flexural rigidity of the highrise concrete walls, the reverse shear force below the flexural hinge may be much larger than the base shear above the flexural hinge. Nonlinear dynamic analyses indicated that the maximum reverse shear force is proportional to the bending moment capacity of the wall and inversely proportional to the accompanying base shear force. The conclusions from this study were summarized in terms of a complete design procedure that made use of a series of linear static analyses with appropriate reduced effective flexure and shear stiffness to estimate the reverse shear force.

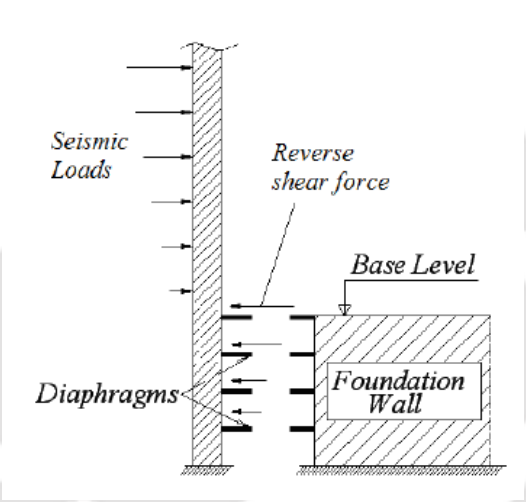

Figure 2.20: Seismic shear force demand below base level (Rad, 2009).

In another study, comparative analyses of experimental and numerical research were carried out for RC connections between the precast slab and monolithic wall and both monolithic slab and wall elements (Zenunović and Folić, 2012). In total six specimens (3 precast and 3 monolithic) were tested under quasi-static loading. Mathematical models were proposed in order to analyse both types of connection, based on the exact method of displacement. Furthermore, the stiffness matrix was modified by introducing the stiffness parameter for the semi-rigid connection. An approximate strut-and-tie model was proposed according to the stress field analysis obtained by FEM was proposed. From the experiments, it was proved that the designed precast connection enable dislocation of joints opening on the outside of the wall and dissipation of seismic energy comparable with similar monolithic connection.

Mercer (2009) examined the nonlinear shear response of walls including the effect of wall-slab system through state of the art nonlinear finite element analysis. The objective of the research was to quantify the shear capacity and response from the wall-slab system. A state-of-the-art finite element analysis was performed studying the behaviour of shear-critical walls. The analysis was carried out by varying the parameters such as horizontal reinforcement ratio, axial load and different slab spacings. The existing nonlinear shear models to describe the wall behaviour were first validated. Then, the failure of the wall without slabs was analysed and the shear behaviour of walls was compared with the behaviour of equivalent membranes. A simple shear model was developed to predict the shear capacity of the wall-slab system as well as the shear strain response of isolated systems. Also, some guidelines were provided for potential future development of a wall-slab system shear model. Although the past studies on wall-slab junction focused on the overall behaviour of the building system including different failure modes, none of the studies investigated in detail the influence of floor slab on wall behaviour and the possible change in the design strategy of the structural wall.

2.6 DESIGN OF STRUCTURAL WALL

Like other structural members, the design forces and moments in a structural wall section are obtained after carrying out structural analysis under design load combinations. The same requirement is mandated in design guidelines of different countries (BIS, 2016a; ACI 318-14, 2014; BS EN 1998-1, 2005). Although, structural walls are expected to incur less damage as compared to RC beams and columns during strong earthquake shaking, proper reinforcement detailing can impart a certain level of ductility in the seismic behaviour of the walls (Paulay and Priestley, 1992). Thus, the structural design codes of different countries prescribe reinforcement detailing for desirable seismic behaviour (BIS, 2016a; ACI 318-14, 2014; BS EN 1998-1, 2005). In the following sub-sections, the salient flexural and shear design provision for RC structural walls are discussed.

2.6.1 Flexure Design

The flexural strength of slender rectangular shear wall section can be derived by using the same assumptions as for reinforced concrete beam (Cardenas and Magura, 1973). A typical isolated shear wall is subjected to bending moments and shear forces due to lateral loads, and to axial compression caused by the gravity. Hence, the strength of the critical section across the wall can be evaluated from the moment – axial force interaction relationship (Park and Paulay, 1975). The vertical reinforcement present in the wall determines the flexural capacity and hence the maximum shear force to which it can be subjected. Two types of flexural failure may take place in the wall section, namely (a) flexural tension failure and (b) flexural compression failure. For walls with enlarged

boundary elements, IS: 13920-2016 recommends calculation of design moment capacity based on superposition of web capacity and couple due to boundary elements. However, guidelines like ACI 318-14 and Eurocode 8 (Part 1) (BS EN 1998-1, 2005) recommends estimation of design capacity using composite section. In the following sub-sections the salient flexural design provisions prescribed by some of the codes are reviewed.

2.6.1.1 Provisions of IS: 13920-2016

The design moment of resistance, M_{uv}, of a shear wall section is calculated in a similar way as prescribed for RC columns in IS: 456-2000. The cracked flexural strength of the wall section should be greater than its uncracked flexural strength. This provision is for those walls which are much larger in cross section than required from strength consideration alone. In walls without boundary elements, vertical reinforcement consisting of at least 4 bars of 12 mm diameter arranged in 2 layers should be provided along the edge of the wall. Concentrated vertical reinforcement near the edges of the wall is more efficient in resisting bending moment. The moment of resistance of slender rectangular shear wall section with uniformly distributed vertical reinforcement is estimated as follows.

(a) For under-reinforced wall section, i.e., $\frac{x_u}{L_w} < \frac{x_u^*}{L_w}$

$$\frac{M_{uv}}{f_{ck}\, t_w\, L_w^2} = \varphi\left[\left(1+\frac{\lambda}{\varphi}\right)\left(\frac{1}{2}-0.416\frac{x_u}{L_w}\right)-\left(\frac{x_u}{L_w}\right)^2\left(0.168+\frac{\beta^2}{3}\right)\right] \tag{2.8}$$

where,

$$\frac{x_u}{L_w}=\frac{\varphi+\alpha}{2\varphi+0.36};\ \frac{x_u^*}{L_w}=\frac{0.0035}{0.0035+0.87\frac{f_y}{E_s}};\ \varphi=\frac{0.87 f_y \rho}{f_{ck}};\ \lambda=\frac{P_u}{f_{ck} t_w L_w}$$

where, ρ is the vertical reinforcement ratio = $A_{st}/t_w L_w$, A_{st} is area of uniformly distributed vertical reinforcement, β is $0.87 f_y/(0.0035 E_s)$, E_s is elastic modulus of steel and P_u is the design axial compression on wall.

(ii) For over-reinforced wall section, i.e., $\frac{x_u^*}{L_w} < \frac{x_u}{L_w} < 1.0$, normalized moment capacity is expressed as,

$$\frac{M_{uv}}{f_{ck}\, t_w\, L_w^2} = \alpha_1\left(\frac{x_u}{L_w}\right) - \alpha_2\left(\frac{x_u}{L_w}\right)^2 - \alpha_3 - \frac{\lambda}{2} \tag{2.9}$$

where, $\alpha_1 = \left[0.36 + \varphi\left(1 - \frac{\beta}{2} - \frac{1}{2\beta}\right)\right]$; $\alpha_2 = \left[0.15 + \frac{\varphi}{2}\left(1 - \beta - \frac{\beta^2}{2} - \frac{1}{3\beta}\right)\right]$; $\alpha_3 = \frac{\varphi}{6\beta}\left[\frac{1}{x_u/L_w} - 3\right]$

The value of x_u/L_w to be used in this equation, should be calculated from the quadratic equation

$\alpha_1\left(\frac{x_u}{L_w}\right)^2 + \alpha_4\left(\frac{x_u}{L_w}\right) - \alpha_5 = 0$, where, $\alpha_4 = \left(\frac{\varphi}{\beta} - \lambda\right)$; and $\alpha_5 = \left(\frac{\varphi}{2\beta}\right)$

These equations were derived, assuming a rectangular wall section of depth L_w and thickness t_w that is subjected to combined uniaxial bending and axial compression. The vertical reinforcement is represented by an equivalent steel plate along the length of the section. The design stress-strain curve assumed for concrete is the same as prescribed in IS: 456-2000 whereas, that for steel is assumed to be bilinear. Although IS: 13920-2016 does not explicitly suggest any equation for wall with enlarged boundary elements, the boundary elements are designed considering the axial force (tension and compression) calculated using the additional design moment apart from the design flexural capacity.

2.6.1.2 Provision of Other Codes

As per the provision of ACI 318-14, the design moment of resistance at a particular section of shear wall can be calculated as:

$$M_u = 0.5 A_{st}\, f_y\, l_w\left(1 + \frac{N_u}{A_{st}\, f_y}\right)\left(1 - \frac{c}{l_w}\right) \tag{2.10}$$

where, M_u is design resisting moment at section, N_u, P_f is the axial load, positive if compression, A_{st} is the total area of vertical reinforcement at section, f_y is the specified yield strength of the vertical reinforcement, L_w is the horizontal length of the wall, ϕ_s is the resistance factor for steel reinforcement and embedded steel anchors (CSA A23.3 Cl.8.4.3) and c is the distance from the extreme compression fiber to neutral axis (Park and Paulay, 1975).

Similar equation for moment of resistance (M_r) was derived for the Canadian Code A23.3-14 as:

$$M_r = 0.5\phi_s f_y A_{st} L_w \left(1 + \frac{P_f}{\phi_s f_y A_{st}}\right)\left(1 - \frac{c}{L_w}\right) \tag{2.11}$$

In general, shear wall subjected to combined axial and flexure can be designed using interaction diagram in a similar manner to columns. For walls connected with floor slabs, the flexural design procedure has not been investigated or discussed separately in any of the past studies.

2.6.2 Shear Design

For seismic shear design of an RC wall section, elastic shear demand is calculated using various code-prescribed load combinations. Subsequently, shear design is compared with design shear resistance to check the safety of wall against possible shear failure. Inelastic shear demand in RC wall is obtained when flexural energy dissipation mechanisms are mobilised at overstrength conditions; this is obtained by applying capacity design principle. In capacity design, potential plastic hinge regions are designed and detailed to achieve the required strength and ductility, and other regions are designed to remain elastic during the formation of plastic hinge. In ductile isolated slender walls, the bottom region is typically detailed for the formation of a single plastic hinge, and in lightly reinforced walls, detailing is done to account for distributed plastic hinge throughout the height of wall. Design codes prescribe design shear strength of concrete τ_c based on diagonal tension failure mode (BIS, 2016a; ACI 318-14, 2014; CSA, 2004).

2.6.2.1 Provisions of IS: 13920-2016

The Indian Ductile Detailing Code IS: 13920-2016 (BIS, 2016a) and the Indian Concrete Code IS: 456-2000 (BIS, 2000) provisions are referred for the earthquake-resistant design of isolated shear walls. For shear design, the critical section for determining design shear force is to be considered at a distance of $0.5\,L_w$ or $0.5\,H_w$, whichever is less from the base of the wall. Once the design shear force at the critical section is estimated from structural analysis, the nominal shear stress is obtained as $\tau_v = V_u / t_w\, d_w$, where, V_u is the factored shear force, t_w is the thickness of the web and d_w is the effective depth of the wall section. The nominal shear stress is checked against the maximum design shear strength ($\tau_{c,\max}$) of concrete to ensure safety against shear compression failure. Based on the area of the tension steel provided in the longitudinal reinforcement, the design shear strength (τ_c) of concrete is obtained as per the tabulated values in IS: 456-2000. The estimated value of τ_c is recommended to be further enhanced in the presence of axial compression at the critical section of the wall. The values of τ_v and τ_c are compared to determine whether minimum shear reinforcement will suffice at the section (if $\tau_v \le \tau_c$) or the shear reinforcement needs to be designed (for $\tau_v > \tau_c$).

For the second case, the area of horizontal shear reinforcement, shear walls shall be provided with reinforcement in the longitudinal and transverse directions in the plane of the wall. The minimum reinforcement ratio shall be 0.0025 of the gross area in each direction. This reinforcement shall be distributed uniformly across the cross section of the wall. The uniform distribution of the shear reinforcement helps to control the width of the inclined cracks. The maximum spacing of reinforcement in either direction shall not exceed the smaller of $L_w/5$, $3t_w$, and 450 mm; where L_w is the horizontal length of the wall, and t_w is the thickness of the wall web. However, the provided horizontal reinforcement should not be less than the prescribed minimum amount of reinforcement as per IS: 13920-2016. The Indian guidelines also suggest that the provided uniformly distributed vertical reinforcement shall not be less than the provided horizontal reinforcement as obtained from flexural design.

2.6.2.2 Provision of ACI 318-14

Shear design provisions of ACI 318-14 consider the behaviour of both slender and squat walls for prescribing the clauses. The nominal shear strength can be calculated as $V_n = V_c + V_s$ where V_c is the nominal shear strength provided by concrete and V_s is the steel shear resistance. The code prescribed that the ideal strength to be provided is related to the required strength by $\phi_r V_n \geq V_u$, where ϕ_r is the strength reduction factor and V_u is the factored shear force at the section. V_n at any horizontal section for shear in plane of wall shall not be taken greater than $0.83\sqrt{f_c'}\, t_w d$, where d shall be taken equal to $0.8l_w$. V_c shall not be taken greater than $0.17\lambda\sqrt{f_c'}\, t_w d$ for walls subject to axial compression, or shall not be taken greater than $0.17\left(1+\frac{0.29N_u}{A_g}\right)\lambda\sqrt{f_c'}\, t_w d$ for wall subject to axial tension, where N_u is the factored shear force, f_c' is the compressive strength of concrete, λ is the modification factor for concrete and A_g is the gross area of concrete section.

Horizontal shear reinforcement shall be provided if V_u exceed $\phi_r V_c$. V_s shall be calculated as $V_s = \frac{A_v f_y d}{s}$ where, A_v is the area of horizontal shear reinforcement with spacing s. Ratio of horizontal shear reinforcement area to gross concrete area of vertical section, ρ_t, shall not be less than 0.0025. The prescribed minimum spacing of horizontal and vertical shear reinforcement is the same as that mentioned in IS: 13920-2016. Ratio of horizontal shear reinforcement area to gross

concrete area of vertical section, ρ_l, shall not be less than the larger of 0.0025 and $\rho_l = 0.0025 + 0.5\left(2.5 - \frac{h_w}{L_w}\right)(\rho_t - 0.0025)$.

For earthquake resistant structures, V_u shall be obtained from the lateral load analysis using the factored load combinations. V_n of structural wall shall not exceed $V_n = A_{cv}\left(\alpha_c \lambda \sqrt{f_c'} + \rho_t f_y\right)$ where $\alpha_c = 0.25$ for $H_w/L_w \le 1.5$, and $\alpha_c = 0.17$ for $H_w/L_w \ge 2$ and varies linearly between 0.25 and 0.17 for H_w/L_w between 1.5 and 2.

2.6.2.3 Provision of Canadian Code A23.3-14

Canadian code has adopted similar provision mentioned in ACI 318-14, slender shear walls are prescribed to be designed against factored axial load, factored moment about one or both axes, and factored shear force. Squat shear walls are prescribed to be designed using strut-and-tie models.

According to A23.3-14, the shear resistance of a shear wall shall be determined by $V_r = V_c + V_s$, where V_c is the concrete shear resistance and V_s is the steel shear resistance. The shear resistance for concrete can be determined as $V_c = \phi_c \lambda \beta \sqrt{f_c'}\, t_w d_v$ where, ϕ_c is the resistance factor for concrete, λ is the factor to account for concrete density, β is the factor accounting for the shear resistance of cracked concrete, and d_v is the effective shear depth of the wall equal to $0.8l_w$. The shear resistance provided by the horizontal reinforcement (V_s) can be determined as $V_s = \phi_s A_h f_y\, d_v \cot\theta / s$ where s is the spacing of horizontal reinforcement, f_y is the yield strength for horizontal reinforcement, ϕ_s is the resistance factor for steel, and $\theta = 35^\circ$ is the angle between the diagonal tension crack and the longitudinal wall axis. Suggested to be considered as 35°. Also, a minimum amount of distributed horizontal reinforcement needs to be provided if $V_f \le V_c$, where V_f is the factored shear force.

2.7 PLASTIC HINGE LENGTH

During strong earthquake shaking, a significant amount of energy gets dissipated at certain sections of a few members in an RC frame-wall buildings. Such localized zone of energy dissipation is known as plastic hinge zone. The performance of each plastic hinge zone determines the member-level response and the global response as it influences the load carrying and deformation capacities of the members. In seismic design of RC members, the length of each plastic hinge (L_p) zone is an

important parameter as sufficient confinement should be provided for the concrete to increase the ductile response of the member. Most of the studies done on plastic hinge length (L_p) in RC elements have focused on length of the member, depth or height of the cross section of the member, yield stress of the tension reinforcement and bar diameter of the tension reinforcement. However, some researchers have also investigated the stress-strain properties of steel reinforcement and the effect of axial compression, which have a significant influence on L_p. In this section, the different analytical expressions of L_p, proposed in past studies for beams, columns and shear wall are reviewed.

2.7.1 Beams and Columns

In case of isolated RC column, the plastic hinges form at the maximum moment region. If L_p is known, the tip displacement of a column can be easily obtained by integrating curvatures. Therefore, accurate assessment of L_p is important in relating section-level response to member-level response of a concrete column. Many researchers (Baker, 1956; Baker and Amarakone, 1964; Mattok, 1964; Mattok, 1967; Corley, 1966) studied L_p to estimate the flexural deformation capacity of RC beams. To estimate the flexural deformation capacity, the plastic rotation capacity (θ_p) and the L_p are used as,

$$\theta_p = \left(\frac{\varepsilon_{cu} - \varepsilon_{ce}}{c} \right) L_p \tag{2.12}$$

where, ε_{cu} is the maximum concrete compressive strain, ε_{ce} is elastic concrete compressive strain and c is distance from extreme compression fiber to neutral axis (Figure 2.21).

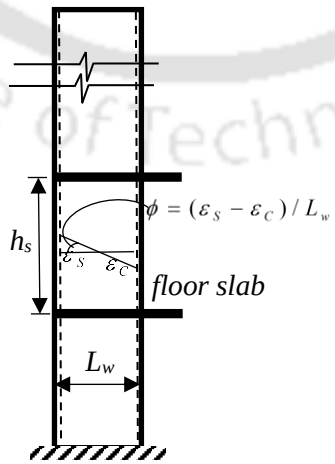

Figure 2.21: Estimation of curvature at any section along the height of wall.

Baker (1956) investigated the plastic deformation of hinges and members in concrete frames. It was proposed that the length of plastic hinge in column is between *0.5h* and *h*, where, *h* is the depth or height of the member. Baker and Amarakone (1964) proposed the following expression to determine the plastic hinge length of members with unconfined concrete as,

$$L_p = k_1 k_2 k_3 \left(\frac{L_s}{d}\right)^{1/4} \tag{2.13}$$

$$k_2 = 1 + 0.5_3 \left(\frac{P}{P_u}\right)^{1/4} \tag{2.14}$$

$$k_3 = 0.9 - \frac{f_{ck} - 13.8}{92} \tag{2.15}$$

where, L_s is the distance from the section of maximum moment to the section of zero moment, k_1 is the factor for the influence of the tension reinforcement (considered as 0.7 for mild steel or 0.9 for cold worked steel). k_2 is the factor for the influence of axial load, k_3 is the factor for the influence of concrete strength, d is the effective depth of the member, P is the axial load, P_u is the axial compressive strength of the member without any bending moment and f_{ck} is the concrete cube strength in MPa.

Sawyer (1964) developed a design methodology for RC frames based on a bilinear moment-curvature relationship. Three assumptions were made to develop the method, namely (a) the maximum moment at any section is equal to the ultimate moment (M_u), (b) the ratio M_y / M_u is taken as 0.85 based on the previous test results obtained for beams, and (c) the spread of plasticity upto a distance of d/4 from the end in which the bending moment is equal to the yield moment (M_y). The plastic hinge length proposed on the basis of the assumption is given by,

$$L_p = 0.25d + 0.075L_s \tag{2.16}$$

Mattock (1964) performed tests on simply supported beams subjected to a concentrated load at the midspan to investigate the effect of confinement of the concrete in compression and the effect of the size of the member in their rotational capacity. 37 beams were tested to investigate how the rational capacity is influenced by the concrete strength, the effective depth, the distance from the section of maximum moment to the point of contraflexure and the amount and yield stress of reinforcement. On the basis of these experiments, the following equation was proposed to calculate the plastic hinge length as,

$$L_p = \frac{d}{2}\left\{1+\left(1.14\sqrt{\frac{L_s}{d}}-1\right)\left[1-(\omega-\omega')\sqrt{\frac{d}{0.411}}\right]\right\} \tag{2.17}$$

where, ω and ω' are the tension and compression reinforcement index respectively.

On the basis of the previously mentioned experiments, the following equation was proposed by Corley (1966) to obtained L_p as,

$$L_p = 0.5d + 0.032\frac{L_s}{\sqrt{d}} \tag{2.18}$$

Based on the previous experiments carried by Mattock (1964) and Corley (1966), the simplified equation proposed by Mattock (1967) was given as,

$$L_p = 0.5d + 0.05L_s \tag{2.19}$$

The ACI-ASCE Committee 428 (1968) proposed lower and upper bounds for the plastic hinge length in beams and frames with the expression as,

$$Min\left[R_\varepsilon\left(\frac{d}{4}+0.03L_sR_m\right), R_\varepsilon d\right] < L_p < R_\varepsilon\left(\frac{d}{2}+0.10L_sR_m\right) \tag{2.20}$$

where, $R_\varepsilon = \dfrac{0.004-\varepsilon_{ce}}{\varepsilon_{cu}-\varepsilon_{ce}}$, $R_m = \dfrac{M_{\max}-M_y}{M_u-M_y}$, R_ε is the strain ratio, R_m is the moment ratio, ε_{ce} is the concrete strain in the extreme compression fiber at yield curvature, ε_{cu} is the concrete strain in the extreme compression fiber at ultimate curvature (neglecting the effects of confinement, loading rate and the strain gradients) and $M_{\max}$ is the maximum moment in the length of the member.

Priestly and Park (1987) performed experiments on concrete bridge columns with different cross-sections subjected to combined axial load and bending to study their strength and ductility. The influence of axial load, the amount and yield strength of the transverse reinforcement and the aspect ratio on the seismic behavior of concrete bridge column was investigated. Based on these test results the expression for the plastic hinge length was proposed as,

$$L_p = 0.08L_s + 6d_b \tag{2.21}$$

The equation was used to compute the plastic hinge length of the columns with different aspect ratios that were tested by other researchers, and the obtained values of L_p were compared. It is

observed that the average value plastic hinge length calculated for all the test was approximately as $0.5h$.

In one experimental study, 14 RC bridge columns with different cross sections were subjected to combined axial load and bending action for assessing the strength and ductility of the columns (Zahn et al., 1986). As the equation of L_p, proposed by Priestly and Park (1987), was valid for RC bridge columns with axial load, the validity of the same equation in presence of axial compression was also checked as part of the study. The test observations showed that the inelastic curvatures spread over a longer portion of the column due to concrete spalling when under large axial compression. Considering the effect of axial load L_p was proposed as,

$$L_p = \left(0.08L_s + 6d_b\right)\left(0.5 + 1.67\frac{P}{f_c^{'}A_g}\right); \quad for \quad \frac{P}{f_c^{'}A_g} < 0.3 \tag{2.22}$$

$$L_p = \left(0.08L_s + 6d_b\right); \quad for \quad \frac{P}{f_c^{'}A_g} \geq 0.3 \tag{2.23}$$

For circular columns with no confinement and one ring of reinforcement, L_p was recommended as,

$$L_p = 0.06L_s + 4.5d_b \tag{2.24}$$

Paulay and Priestly (1992) proposed the following expression to estimate the plastic hinge length.

$$L_p = 0.08L_s + 0.022f_y d_b \geq 0.044f_y d_b \tag{2.25}$$

where, f_y is the yield strength of reinforcement in MPa. The authors indicated that for commonly used beam and column dimensions, Eq. 2.25 gave plastic hinge lengths of approximately as $0.5h$.

Moehle (1992) indicated that the equivalent plastic hinge length in RC columns depends on the section depth, aspect ratio, bar diameter and the axial and shear force. He stated that good agreement with experimental results may be obtained when the plastic hinge length is equal to $0.5h$.

2.7.2 RC Walls

Paulay (1986) presented design procedures for ductile reinforced concrete walls for earthquake resistance. He indicated that the plastic hinge length was primarily a function of the wall length. Based on this, the plastic hinge length id proposed in between $0.5L_w$ and L_w. Wallace and Moehle (1992) presented an analytical procedure to determine the requirement of confined boundaries in

RC wall subjected to earthquake loading. They stated that the plastic hinge length is usually between $0.5L_w$ and L_w. Paulay and Priestly (1993) reported tests on ductile concrete walls of rectangular cross section subjected to seismic loading to study out of plane buckling. In that study, the curvature ductility demand was not underestimated and the plastic hinge length gave a good approximation of the portion of the height of the wall over which out of plane buckling can occur. L_p was proposed as,

$$L_p = 0.2L_w + 0.044H_w, \tag{2.26}$$

where, H_w is the total height of shear wall.

Susani and Der Kiureghian (2001) developed probabilistic displacement capacity and demand models for RC walls, and also derived an expression for the plastic hinge length in the walls, using the earlier test results (Corley, 1996; Mattock, 1967). From the 40 beams tested by these researchers, 29 of them were selected with effective depth greater than 0.5m. That data was used to estimate the plastic hinge length as,

$$\frac{L_p}{d} = \alpha_1 + \alpha_2 \frac{\sqrt{L_s}\, l_s^{3/2}}{d^2} + \xi_L, \tag{2.27}$$

where, l_s is the standard length equal to 1 m, inserted to make the model parameters dimensionless. $\alpha_1 (= 0.427)$ and $\alpha_2 (= 0.077)$ are model parameters and ξ_L is the model error term.

Experiments were carried out by Panagiotakos and Fardis (2001) on RC members (beams, columns and walls) subjected to uniaxial bending, with and without axial loads, to derive expressions for deformation at yield and failure levels, in terms of the geometric and mechanical properties of the menber. Results obtained from 1012 specimens were used to calculate the plastic hinge length as,

$$L_{p,cy} = 0.12L_s + 0.014a_{si}d_b f_y, \text{ for cyclic loading and} \tag{2.28}$$

$$L_{p,mon} = 1.5L_{p,cy} = 0.18L_s + 0.021a_{si}d_b f_y, \text{ for monotonic loading} \tag{2.29}$$

where, $L_{p,cy}$ is the plastic hinge length for cyclic loading, $L_{p,mon}$ is the plastic hinge length for monotonic loading, a_{si} is taken as 1.0 if slippage of longitudinal reinforcement is possible, and taken as zero if there is no possibility of slippage.

Based on the results of nonlinear finite element analyses using a model validated by test results, an expression is proposed by Bohl and Adebar (2011) for L_p as a function of wall length, moment shear ratio, and axial compression. Eq. 2.30 is proposed for estimating the lower-bound plastic hinge length L_p of isolated walls as a function of wall length L_w, bending moment-to-shear force ratio $z = M/V$, and $\frac{P}{f_c^{'} A_g}$ axial compression stress ratio. The ratio $z = M/V$ can either be determined from analysis or estimated as $0.7H_w$ for plastic hinging near the base of a wall, which is primarily due to displacement demand under fundamental mode dominant behaviour. The axial compression force *P* can either be determined from analysis or estimated from the gravity load at the top of the plastic hinge region of the wall. The proposed L_p was given as,

$$L_p = (0.2L_w + 0.05z)\left(1 - 1.5\frac{P}{f_c^{'} A_g}\right) \leq 0.8L_w \tag{2.30}$$

An improved expression for the calculation of L_p for structural walls has been proposed by Kazaz (2013). The model depends on the wall length, the axial load ratio, the wall horizontal web reinforcement ratio, and the shear-span-to-wall-length ratio. The proposed plastic hinge length was found to constitute 40%-50% of the length of the plastic zone, that is, of the region where yielding takes place. It was shown that the equation proposed in that study was more accurate as compared to the relations proposed in other studies. It has been found that the widely used assumption of, $L_p = 0.5L_w$, underestimates the plastic hinge length as the wall length increases and shear effects become more pronounced. The proposed equation of plastic hinge length was given by,

$$L_p = 0.27L_w\left(1 - \frac{P}{A_w f_c^{'}}\right)\left(1 - \frac{f_y \rho_{sh}}{f_c^{'}}\right)\left(\frac{M/V}{L_w}\right) \leq 0.8 \tag{2.31}$$

where, $\frac{P}{A_w f_c^{'}}$ is the wall axial load ratio, and ρ_{sh} is the ratio of vertical web reinforcement of wall. Deriving the plastic hinge length in the form similar to that given by previous researchers lead to the simplified equation of plastic hinge length as,

$$L_p = 0.143L_w + 0.072M/V \tag{2.32}$$

where, M/V is moment-to-shear ratio at the plastic hinge section.

All the past studies on plastic hinge length in RC walls have been carried out on isolated walls without any connected floor slab. The proposed expressions of L_p may change under the influence of floor slab. One of the objective of the present study is to investigate the same.

2.8 DRIFT CRITERIA FOR SHEAR WALL BUILDINGS

In multistoried RC wall-frame buildings, one of the objectives of providing RC wall is to reduce the lateral displacement level of the building by virtue of its large in-plane stiffness.
During strong earthquake shaking, a structural wall is not expected to remain elastic (Wallace and Moehle, 1992) with the possible inelastic actions at the base of the wall. Allowing inelastic deformations tends to reduce the force demand on the wall and provides a fuse to limit actions on other structural elements. In order to exhibit stable, inelastic response, the wall must be specially detailed at critical regions, i.e., special transverse reinforcement must be provided within regions where significant inelastic deformations are expected to be concentrated (Thomsen and Wallace, 2004)

The lateral displacement of a structural system is an important parameter from the seismic design point of view. It has three major implications, namely (a) structural stability, (b) additional seismic demand on structural component due to large deformations and (c) damage to various non-structural components. Introduction of displacement-based design (DBD) led to more realistic consideration of wall deformability in the design method. This is very important in performance-based design of RC wall buildings with the possibility of lateral displacement being used as a performance limit state. In the past, research has been carried out to obtain performance objectives and relate the level of structural damage to parameters like lateral displacements and drift. Seismic assessment of existing structures or design of new structures can be carried out by displacement-based design procedures to ensure that particular deformation-based criteria are met (Priestley et al., 2007).

Within this scope, several investigations have been conducted for the improvement of displacement-based procedures and associated deformation limits. Limit states for displacement-based design and assessment are defined in the form of lateral drift ratios at overall structural level, and section curvatures, rotations and strains at component level. Procedures have been developed to relate the level of damage that is associated with the structural response in terms of displacements (drift ratio) to strain-based limit state (Wallace and Moehle, 1992).

Wallace (1995) developed simplified approaches for symmetrically and unsymmetrical reinforced walls with axial load. In addition, requirements for distribution of flexural strength over the height of the wall and limiting values for shear stress were also suggested. Based on the computed strain

distribution, both detailed and simplified approaches were presented to determine the amount and distribution of required transverse reinforcement. It was also observed that the wall aspect ratio and wall shear stress are important design parameters.

Thomsen and Wallace (2004) carried out experiments on rectangular and T-shaped shear walls to verify the displacement based design approach. A simplified application of displacement-based design was incorporated into ACI 318-99 to evaluate detailing requirements at wall boundaries. Results of the tests indicate that the walls detailed using displacement-based design had lateral drift capacities in excess of 2% of the specimen height, which was greater than that required by design guidelines (which was prescribed as 1.5%).

Kazaz et al. (2012) carried nonlinear static analysis of several wall specimens by varying parameters like wall length, shear-span-to-wall- length ratio, axial load level, the amount of boundary element longitudinal reinforcement, and horizontal web reinforcement. The deformation limits at yield and ultimate damage state for the curvature, rotation and drift ratio were obtained. Expressions and limiting values were proposed for yield and ultimate deformation capacity of structural walls, based on the most influential parameters. The proposed equations closely match the corresponding experimental results.

Carrillo and Alcocer (2012) developed a performance-based backbone model capable of predicting the seismic behavior of RC walls for one- and two-storied housing. The selected tri-linear model was associated with three failure limit namely, (a) diagonal cracking, (b) peak shear strength and (c) ultimate deformation capacity. The model was developed on the basis of the observed response of 39 quasi-static and shake table experiments on RC walls. Iterative nonlinear regression analyses were performed for deriving the semi-empirical equations. Several analytical parametric studies were conducted on structural walls to investigate their deformation and strength properties (Wallace and Moehle, 1992, Priestley and Kowalsky, 1998). The primary interest of these studies has been the global response parameters, such as the drift or plastic rotation (Seneviratna and Krawinkler, 1997) and shear strength (Ghosh and Markevicius, 1991).

All the past studies on deformation limits in RC walls or lateral drifts limits, were carried out on isolated slender walls. None of the studies focused on evaluation of such limits for RC walls connected to floor slabs in a multistoried building.

2.9 GAP AREAS

In the present chapter, past research on modelling global behaviour of beam-coupled and slab-coupled walls, design aspects, estimated plastic hinge length and lateral drift aspects of isolated RC walls have been reviewed. None of the past studies has focused on detailed investigation of the behavior of floor slab and shear wall junction under earthquake shaking. Also, none of the studies consider the effect of floor slabs for the evaluation of plastic hinge length of shear wall and the recommended lateral drift for shear wall buildings does not consider the effect of connected to floor slabs.

2.10 SCOPE OF THE WORK

The scope of the present study is identified as follows:

(a) To develop a simplified model for the shear wall-slab junction region for carrying out nonlinear analysis.

(b) Investigation of tensile and compressive damage patterns in the rectangular shear wall-slab assemblage under lateral loads.

(c) Estimation of plastic hinge length for the rectangular shear wall-slab junction region.

(d) Possible change in seismic design methodology of rectangular RC wall without boundary elements considering the influence of connected floor slab.

Chapter 3
FINITE ELEMENT MODELLING AND VALIDATION

3.0 OVERVIEW

Finite Element Method (FEM) is one of the structural analysis methods for investigating the detailed behaviour of any structural sub-assemblage. To achieve the objectives of the present study, finite element modelling of the entire RC frame-wall building and the wall-slab sub-assemblage is carried out. In this chapter, the modelling details and the associated validation study are discussed.

The basic dimensions and the applied load on the building considered for analysis are discussed in the present study along with the material properties considered. Among the various material modelling techniques proposed for concrete in the past, Concrete Damage Plasticity (CDP) model is discussed in detail in this chapter. Other than the material model used, the choice of solution procedure also affects the accuracy of the solution obtained. At the outset, it is essential to discuss the chosen material parameters. The material properties are validated with the experiments on slab-wall connection carried out by Pantazopoulou and Imran (1992) at the University of Toronto. The specimen used in these experiments is chosen for calibrating the parameters of the CDP model in ABAQUS (ABAQUS, 2011).

3.1 MATERIAL MODELLING

Under low confining pressures, concrete acts in a brittle manner and the main failure mechanisms are cracking in tension and crushing in compression. If the confining pressure is adequately large to prevent the crack, the brittle behavior of concrete gets modified significantly. Two different material models for concrete, namely (a) elasto-plastic and (b) CDP models have been employed during the analysis. The elasto-plastic model is assigned to the beams and columns of the full building, whereas, the CDP model of ABAQUS is chosen for shear wall and slab. The detailed description of this model is presented in the next section. The model assumes that the material is isotropic and requires the compressive and tensile behavior of concrete. It can simulate stiffness degradation with the help of damage parameters, d_t and d_c. Detailed explanation about the damage parameters is provided in the following section. The model also works well under cyclic loads. Stiffness recovery parameters, w_t and w_c are used to consider stiffness recovery under cyclic loads.

3.2 ELASTO-PLASTIC MODEL

For the elasto–plastic model, the same stress–strain curve of concrete is considered for tension and compression regions. The plastic yield strength is given as the ultimate strength of concrete. The material hardening is considered as isotropic.

Most materials that exhibit ductile behavior (large inelastic strains) yield at stress levels that are orders of magnitude less than the elastic modulus of the material, which implies that the relevant stress and strain measures are "true" stress (Cauchy stress) and logarithmic strain (ABAQUS, 2011). Material data for all of these models should, therefore, be given in these measures. If the nominal stress-strain data for a uniaxial test and the material is isotropic, a simple conversion to true stress and logarithmic plastic strain is

$$\sigma_{true} = \sigma_{nom}(1 + \varepsilon_{nom}) \tag{3.1}$$

$$\varepsilon_{\ln}^{pl} = \ln(1 + \varepsilon_{nom}) - \frac{\sigma_{true}}{E} \tag{3.2}$$

where, E is the young's modulus, σ_{true} is the true stress, $\sigma_{nom}$is the nominal stress, ε_{nom} is the nominal strain and $\varepsilon_{\ln}^{pl}$ is the logarithmic plastic strain. Plastic strain values (Eqs. 3.1 and 3.2) are used in defining the hardening behavior. Furthermore, the first data pair refers to onset of plasticity, that is, the plastic strain value must be zero in the first pair. These concepts are applicable when hardening data are defined in a tabular form for plasticity models in ABAQUS/Standard.

3.3 CONCRETE DAMAGE PLASTICITY MODEL

In the past research, several model is developed to study the effect of softening of concrete for different structural members (Hsu and Mo, 1985a; Hsu and Mo, 1985b; Vecchio and Collins, 1981; Vecchio and Collins, 1982). However, in the present study, the CDP model is considers which, uses the concepts of isotropic damaged elasticity in combination with isotropic tensile and compressive plasticity to represent the inelastic behavior of concrete. It provides a general capability for modeling concrete and other quasi-brittle materials in all types of structures. It can be used for plain concrete, even though it is intended primarily for the analysis of RC structures. It can be used with rebar to model concrete reinforcement. It is designed for applications in which concrete is subjected to monotonic, cyclic, and/or dynamic loading under low confining pressures. It consists of the combination of nonassociated multi-hardening plasticity and scalar (isotropic) damaged elasticity to describe the irreversible damage that occurs during the fracturing process. It allows user control of stiffness recovery effects during cyclic load reversals. It can be defined to be sensitive to the rate

of straining. It can be used in conjunction with a viscoplastic regularization of the constitutive equations in ABAQUS/Standard to improve the convergence rate in the softening regime. It requires that the elastic behavior of the material be isotropic and linear.

The plastic-damage model is based on the work by Lubliner et al. (1989) and by Lee and Fenves (1998). The model is a continuum, plasticity-based damage model for concrete. It assumes that the main two failure mechanisms are tensile cracking and compressive crushing of the concrete material. The evolution of the yield (or failure) surface is controlled by two hardening variables, $\tilde{\varepsilon}_t^{pl}$ and $\tilde{\varepsilon}_c^{pl}$, where $\tilde{\varepsilon}_t^{pl}$ and $\tilde{\varepsilon}_c^{pl}$ are tensile and compressive equivalent plastic strains, respectively. These are linked to failure mechanisms under tension and compression loading, respectively. The equivalent plastic strains are obtained by subtracting the elastic strain from the total strain.

3.3.1 Uniaxial tension and compression behaviors

Under uniaxial compression (Figure 3.1a), the response is linear till the initial yield strength, σ_{c0}. In the plastic regime, the response is typically characterized by stress hardening followed by strain softening beyond the ultimate stress, σ_{cu}. Under uniaxial tension (Figure 3.1b) the stress-strain response follows a linear elastic relationship until the value of the failure stress, σ_{t0} is reached. The failure stress corresponds to the onset of micro-cracking in concrete. Beyond the failure stress the formation of micro-cracks is represented macroscopically with a softening stress-strain response, which induces strain localization in concrete.

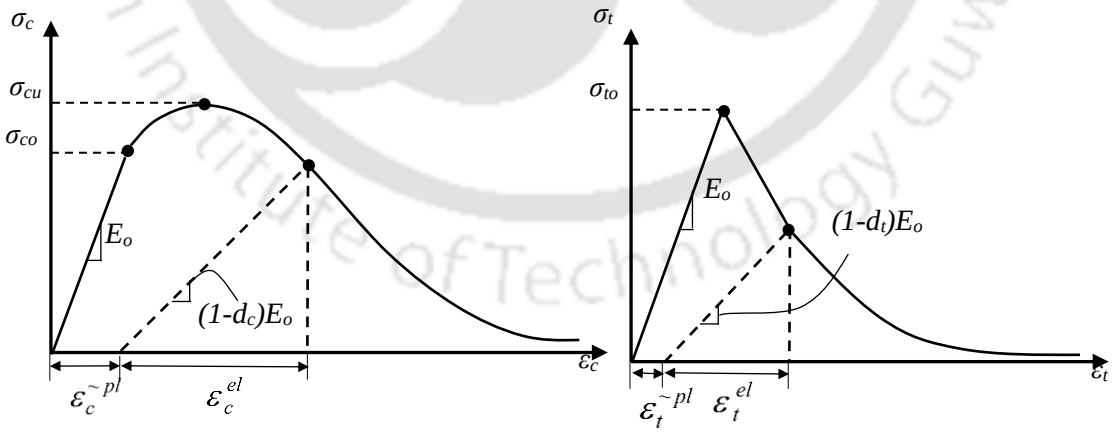

(a) (b)

Figure 3.1: Response of concrete to uniaxial loading: (a) compression and (b) tension.

The uniaxial tensile and compressive response of concrete are characterized by damage plasticity. The stress-strain curves are also converted into stress versus plastic strain curves of the form

$$\sigma_t = \sigma_t\left(\tilde{\varepsilon}_t^{pl}, \dot{\tilde{\varepsilon}}_t^{pl}, T, f_i\right) \tag{3.3}$$

$$\sigma_c = \sigma_c\left(\tilde{\varepsilon}_c^{pl}, \dot{\tilde{\varepsilon}}_c^{pl}, T, f_i\right), \tag{3.4}$$

Where, $\tilde{\varepsilon}_t^{pl}$ and $\tilde{\varepsilon}_c^{pl}$ are the equivalent plastic strains, $\dot{\tilde{\varepsilon}}_t^{pl}$ and $\dot{\tilde{\varepsilon}}_c^{pl}$ the equivalent plastic strain rates, T is the temperature, and f_i are other predefined field variables.

As shown in Figure 3.1, when the concrete specimen is unloaded from any point on the strain softening branch of the stress-strain curves, the unloading response is weakened as characterized by the reduction of stiffness. The degradation of the elastic stiffness is characterized by two damage variables, d_t and d_c which, are assumed to be functions of the plastic strains, temperature, and field variables as,

$$d_t = d_t\left(\tilde{\varepsilon}_t^{pl}, T, f_i\right), \quad 0 \le d_t \le 1, \tag{3.5}$$

$$d_c = d_c\left(\tilde{\varepsilon}_c^{pl}, T, f_i\right), \quad 0 \le d_c \le 1, \tag{3.6}$$

The values of one and zero for the damage variables refer to complete damaged material and no damaged material, respectively. Considering the damaged variables, the stress-strain relationships are formulated as,

$$\sigma_t = (1 - d_t) E_0 \left(\varepsilon_t - \tilde{\varepsilon}_t^{pl}\right), \tag{3.7}$$

$$\sigma_c = (1 - d_c) E_0 \left(\varepsilon_c - \tilde{\varepsilon}_c^{pl}\right). \tag{3.8}$$

The effective tensile and compressive cohesion stresses determine the size of the yield surface and are given as,

$$\bar{\sigma}_t = \frac{\sigma_t}{(1 - d_t)} = E_0 \left(\varepsilon_t - \tilde{\varepsilon}_t^{pl}\right), \tag{3.9}$$

$$\bar{\sigma}_c = \frac{\sigma_c}{(1 - d_c)} = E_0 \left(\varepsilon_c - \tilde{\varepsilon}_c^{pl}\right). \tag{3.10}$$

Under uniaxial conditions the equivalent plastic strain rates are given as $\dot{\tilde{\varepsilon}}_t^{pl} = \dot{\varepsilon}_{11}^{pl}$ for tension, and $\dot{\tilde{\varepsilon}}_c^{pl} = -\dot{\varepsilon}_{11}^{pl}$ for compression, respectively.

3.3.1.1 Strain rate decomposition

In the incremental theory of plasticity, the total strain rate $\dot{\varepsilon}$ is decomposed into an elastic part and a plastic part as,

$$\dot{\varepsilon} = \dot{\varepsilon}^{el} + \dot{\varepsilon}^{pl} \tag{3.11}$$

where, $\dot{\varepsilon}^{el}$ is the elastic part of the strain rate, and $\dot{\varepsilon}^{pl}$ is the plastic strain rate. The plastic strain represents all irreversible deformations including those caused by micro-cracks.

3.3.1.2 Stress-strain relations

The general stress-strain relation is given as,

$$\sigma = (1-d) D_0^{el} \left(\varepsilon - \varepsilon^{pl}\right) = D^{el} \left(\varepsilon - \varepsilon^{pl}\right), \tag{3.12}$$

where, D_0^{el} is the undamaged elastic stiffness of the material and D^{el} represents the degraded elastic stiffness. The damage variable *d* ranges from 0 (no damage) to 1 (complete loss of integrity), the total strain is represented by ε, and the plastic strain by ε^{pl}. According to Malm (2009), in case of proportional loading of concrete structures, where cracking results from uniaxial tensile stress, isotropic models are considered sufficiently accurate. The stiffness degradation is isotropic and characterized by a single degradation variable *d*. In continuum damage mechanics, the stiffness degradation (or damage variable) can be modelled by defining a relation between Cauchy stresses and effective stresses as,

$$\bar{\sigma} = \frac{\sigma}{(1-d)}, \tag{3.13}$$

where, $\bar{\sigma}$ is the effective stress. Substituting Eq. (3.13) into Eq. (3.12) we get,

$$\bar{\sigma} = D_0^{el} \left(\varepsilon - \varepsilon^{pl}\right) \tag{3.14}$$

When damage occurs, the effective stress is a better representative parameter than the Cauchy stress because it is the effective stress area that carries the external loads (ABAQUS, 2011).

Two hardening variables are used to characterize damage states in tension and compression.

$$\tilde{\varepsilon}^{pl} = \begin{bmatrix} \tilde{\varepsilon}_t^{pl} \\ \tilde{\varepsilon}_c^{pl} \end{bmatrix} \tag{3.15}$$

These variables control the evolution of the yield surface and the degradation of the elastic stiffness. The evolution of the hardening variables is given by:

$$\dot{\tilde{\varepsilon}}^{pl} = h\left(\bar{\sigma},\ \tilde{\varepsilon}^{pl}\right)\dot{\varepsilon}^{pl} \tag{3.16}$$

$$\tilde{\varepsilon}_t^{pl} = \int_0^t \dot{\tilde{\varepsilon}}_t^{pl} dt \tag{3.17}$$

$$\tilde{\varepsilon}_c^{pl} = \int_0^t \dot{\tilde{\varepsilon}}_c^{pl} dt \tag{3.18}$$

3.3.1.3 Yield function

The plastic damaged concrete model in ABAQUS make uses of the yield function proposed by Lubliner et al. (1989) and incorporates the modifications proposed by Lee and Fenves (1998) to account for different strength evolutions under tension and compression. The yield function uses two stress invariants of the effective stress tensor namely (a) the effective hydrostatic pressure, $\bar{p}$, and (b) the Mises equivalent effective stress $\bar{q}$. Its evolution is controlled by the hardening variables $\tilde{\varepsilon}_t^{pl}$ and $\tilde{\varepsilon}_c^{pl}$.

The two stress invariants are defined as,

$$\bar{p} = -\frac{1}{3}\bar{\sigma}\, I \tag{3.19}$$

$$\bar{q} = \sqrt{\frac{3}{2}\bar{S}\,\bar{S}} \tag{3.20}$$

where, $\bar{S}$ represents the deviatoric part of the effective stress tensor $\bar{\sigma}$, defined as,

$$\bar{S} = \bar{p}I + \bar{\sigma} \tag{3.21}$$

In terms of effective stresses, the yield function as shown in Figures 3.2 and 3.3 is expressed as:

$$F = \frac{1}{1-\alpha}\left(\bar{q} - 3\alpha\bar{p} + \beta\left(\tilde{\varepsilon}^{pl}\right)\left\langle\hat{\bar{\sigma}}_{\max}\right\rangle - \gamma\left\langle-\hat{\bar{\sigma}}_{\max}\right\rangle\right) - \bar{\sigma}_c\left(\tilde{\varepsilon}_c^{pl}\right) = 0 \tag{3.22}$$

with

$$\alpha = \frac{(\sigma_{b0}/\sigma_{c0})-1}{2(\sigma_{b0}/\sigma_{c0})-1}; \quad 0 \le \alpha \le 0.5, \tag{3.23}$$

$$\beta = \frac{\bar{\sigma}_c(\tilde{\varepsilon}_c^{pl})}{\bar{\sigma}_t(\tilde{\varepsilon}_t^{pl})}(1-\alpha)-(1+\alpha), \tag{3.24}$$

$$\gamma = \frac{3(1-K_c)}{2K_c-1}, \tag{3.25}$$

where, α, β and γ are dimensionless material constants, $\hat{\bar{\sigma}}_{\max}$ is the algebraically maximum principal effective stress, $\bar{\sigma}_t$ and $\bar{\sigma}_c$ are the effective tensile and compressive cohesion stress, σ_{b0} is the initial equibiaxial compressive yield stress, σ_{c0} is the initial uniaxial compressive yield stress. K_c is the ratio of the second stress invariant on the tensile meridian, $[q(TM)]$, to that on the compressive meridian, $[q(CM)]$, at initial yield for any given value of pressure invariant p such that the maximum principal stress is negative: $\hat{\bar{\sigma}}_{\max} < 0$. A value of $K_c = 2/3$ is recommended for concrete (Lubliner et al. 1989).

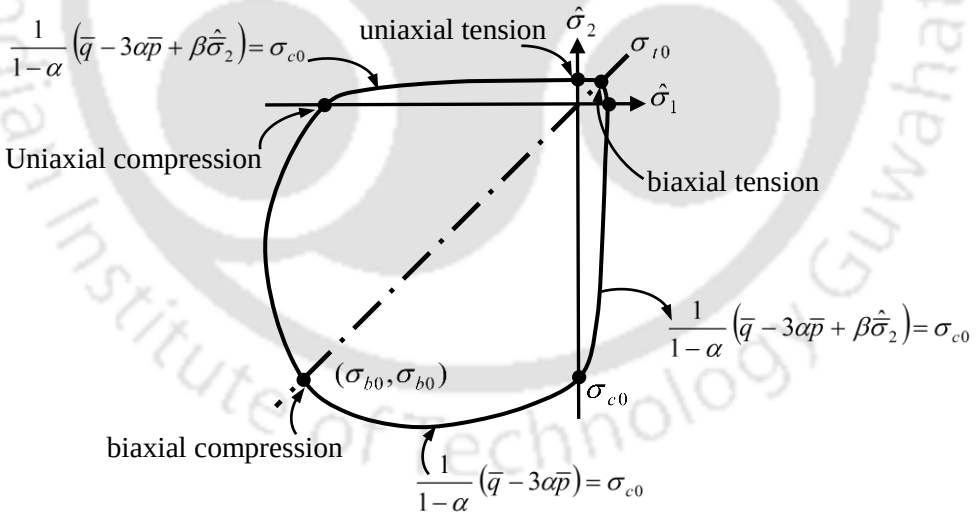

Figure 3.2: Yield surface for concrete in plane stress condition.

The CDP model assumes a non associated plastic flow rule given by,

$$\dot{\varepsilon}^{pl} = \dot{\lambda}\frac{\partial G(\bar{\sigma})}{\partial \bar{\sigma}} \tag{3.26}$$

where, $\dot{\lambda}$ is the nonnegative plastic multiplier. The flow potential G represents the Drucker-Praguer hyperbolic function.

$$G = \sqrt{(e\,\sigma_{to}\,\tan\psi)^2 + \bar{q}^2} - \bar{p}\,\tan\psi\,, \tag{3.27}$$

where, e is a parameter, referred to as the eccentricity, that defines the rate at which the function approaches the asymptote (the flow potential tends to a straight line as the eccentricity tends to zero); σ_{t0} is the uniaxial tensile stress at failure and ψ is the dilatation angle measured in the $p-q$ plane at high confining pressures. The recommended value for the eccentricity is $e=0.1$, which implies that the material has almost the same dilatation angle over a wide range of confining pressure stress values (ABAQUS, 2011).

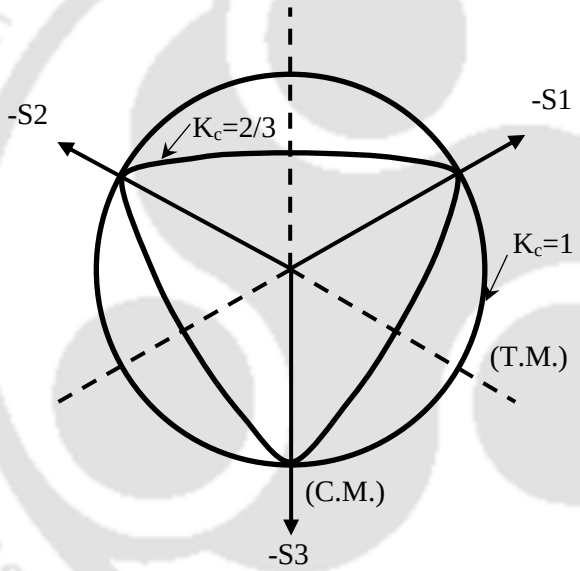

Figure 3.3: Yield surfaces in the deviatoric plane, corresponding to different values of K_c. (ABAQUS, 2011).

3.3.1.4 Uniaxial Cyclic Behaviour

Figure 3.4 shows a uniaxial load cycle of the damaged material. Under uniaxial cyclic loading conditions the degradation mechanisms are quite complex, involving the opening and closing of previously formed micro-crack as well as their interactions. Experimentally, it is observed that there is some recovery of the elastic stiffness as the load changes sign during a uniaxial cyclic test. The stiffness recovery effect, also known as the "unilateral effect," is an important aspect of the concrete behavior under cyclic loading. The effect is usually more pronounced as the load changes from

tension to compression, causing tensile cracks to close, which results in the recovery of the compressive stiffness.

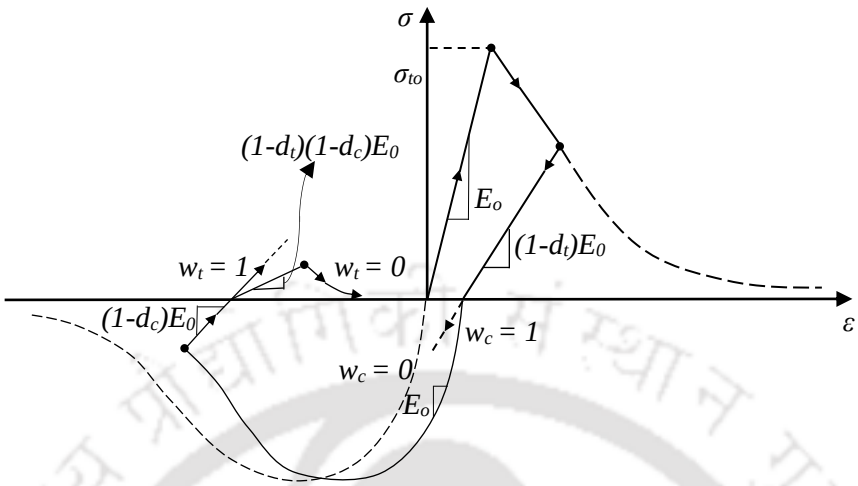

Figure 3.4: Uniaxial load cycle (tension-compression-tension) assuming default values for the stiffness recovery factors: $w_t = 0$ and $w_c = 1$ (ABAQUS, 2011).

The weight factors, w_t and w_c, control the recovery of the tensile and compressive stiffness upon load reversal, respectively. w_c, which results in the recovery of the compressive stiffness, is more important due to the closure of tensile cracks during the transition from tension to compression. The stiffness recovery factors are chosen as the default values: $w_t = 0$ and $w_c = 1$. For the tension stiffening effect, strain option is used for tension stiffening of the concrete, which is more suitable for concrete with reinforcement. The reduction of concrete tensile strength to zero is assumed to occur at 10 times the strain at failure.

The reduction of the elastic modulus is given in terms of a scalar degradation variable *d as*

$$E = (1-d)\,E_0 \tag{3.28}$$

where, E_0 is the initial elasticity modulus of the material. The degradation variable d is a function of the stress state and the uniaxial damage variables d_t and d_c as follows:

$$(1-d) = (1-s_t d_c)(1-s_t d_c), \quad 0 \le s_t, s_c \le 1, \tag{3.29}$$

where, s_t and s_c are functions of the stress state that represents the stiffness recovery for reversal loads, express as:

$$s_t = 1 - w_t r^*(\bar{\sigma}_{11}), \quad 0 \le w_t \le 1 \tag{3.30}$$

$$s_c = 1 - w_c r^*(\bar{\sigma}_{11}), \quad 0 \le w_c \le 1 \tag{3.31}$$

where, w_t and w_c are factors that control the recovery of the tension and compression stiffness upon load reversal, and $r^*(\bar{\sigma}_{11})$ is a function of the tensile $(\bar{\sigma}_{11}) > 0$ and compressive $(\bar{\sigma}_{11}) < 0$ side of the cycle, defined as,

$$r^*(\bar{\sigma}_{11}) = H(\bar{\sigma}_{11}) = \begin{Bmatrix} 1 & if\ \bar{\sigma}_{11} > 0 \\ 0 & if\ \bar{\sigma}_{11} < 0 \end{Bmatrix} \tag{3.32}$$

Figure 3.5 shows the effect of the recovery factors when the load changes from tension to compression. The initial stiffness in compression is fully recovered when $w_c = 1$ and there is no stiffness recovery when $w_c = 0$. Under uniaxial cyclic conditions, the equivalent plastic strains are also generalized as $\tilde{\dot{\varepsilon}}_t^{pl} = r^* \dot{\varepsilon}_{11}^{pl}$ in tension, and $\tilde{\dot{\varepsilon}}_t^{pl} = -\left(1 - r^*\right) \dot{\varepsilon}_{11}^{pl}$ in compression.

In the current study, the dilation angle is assumed as 55°, eccentricity as 0.1, viscosity parameter as 0.01, shape factor (K_C) as 0.667 and stress ratio σ_{b0}/σ_{c0} as 1.16 (Gulec and Whittaker, 2009). Under uniaxial tension, the stress-strain response follows a linear elastic relationship until *the* onset of micro-cracking in concrete (failure stress) (Figure 3.4). Beyond this limit, the micro-cracked concrete is characterized by a softening stress-strain response. Under uniaxial compression, the response is linear till the value of initial yield. In the plastic regime, the response is typically characterized by stress hardening followed by strain softening beyond the ultimate stress. When the concrete specimen is unloaded from any point on the strain softening branch of the stress-strain curve, the unloading response is weakened and the material damage reduces the elastic stiffness.

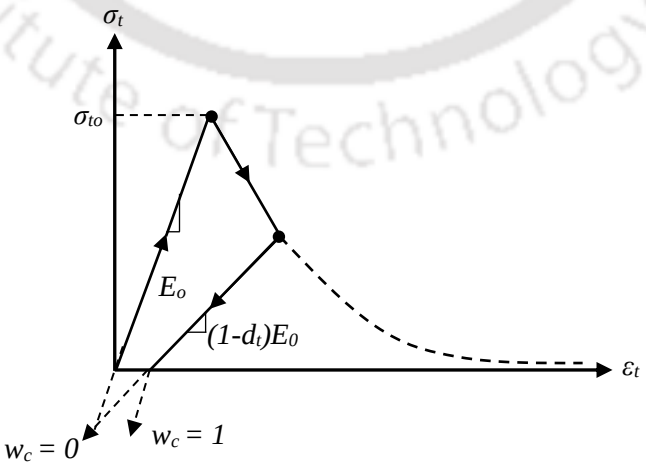

Figure 3.5: Effect of the compression recovery parameter w_c [ABAQUS, 2011].

The degradation of the elastic stiffness is characterized by two damage variables, d_t and d_c as given in Eqs. 3.33 and 3.34, respectively, as proposed by Zheng et al. (2012). The two parameters are expressed as,

$$d_t = 1 - \sqrt{\frac{1}{\left[\alpha_t (x-1)^{1.7} + x\right]}} \qquad x \geq 1, \quad x = \frac{\varepsilon}{\varepsilon_t}, \quad \alpha_t = 0.312 f_t^2 \tag{3.33}$$

$$d_c = 1 - \sqrt{\frac{1}{\left[\alpha_d (x-1)^2 + x\right]}} \qquad x \geq 1, \quad x = \frac{\varepsilon}{\varepsilon_c}, \quad \alpha_t = 0.157 f_c^{0.785} - 0.905 \tag{3.34}$$

where, f_t is the average value of axial tensile strength, f_c the average value of axial compressive strength (taken as 25 MPa in the study), ε the compressive or tensile damaged plasticity strain, ε_c the compressive strain corresponding to f_c (taken as 0.002 in the study) and ε_t the tensile strain corresponding to f_t. The salient material properties of the concrete and reinforcing steel are mentioned in Table 1.

Table 3.1: Material properties for concrete and steel

Material	Density (kg/m^3)	Elastic Modulus (MPa)	Poisson's Ratio	Compressive Strength (MPa)	Tensile Strength (MPa)	Yield Stress (MPa)	Ultimate Stress (MPa)
Concrete	2,500	25,000	0.2	25	3.5	-	-
Steel	7,800	2,00,000	0.3	-	-	415	527

3.3.1.5 Behavior of Concrete and Steel Reinforcement

In the current study, the uniaxial stress-strain curve is considered linearly elastic up to 30% of the maximum compressive strength (Figure 3.6a). Beyond this point, the curvilinear nature extends till the maximum compressive strength, f_c. The post-peak softening behavior of the stress-strain curve, till the crushing failure at an ultimate strain, ε_u, is given by the parabolic expression of Eq. 3.35 as,

$$\sigma_c = f_c \left[2 \frac{\varepsilon}{\varepsilon_0'} \left(1 - \frac{\varepsilon}{2\varepsilon_0'} \right) \right] \tag{3.35}$$

where, ε_0' is the strain related to the peak stress. The modulus of elasticity, E_c and the compressive strength of the concrete are dependent on each other and E_c is considered as $E_c = 5000\sqrt{f_{ck}}$ (BIS, 2000).

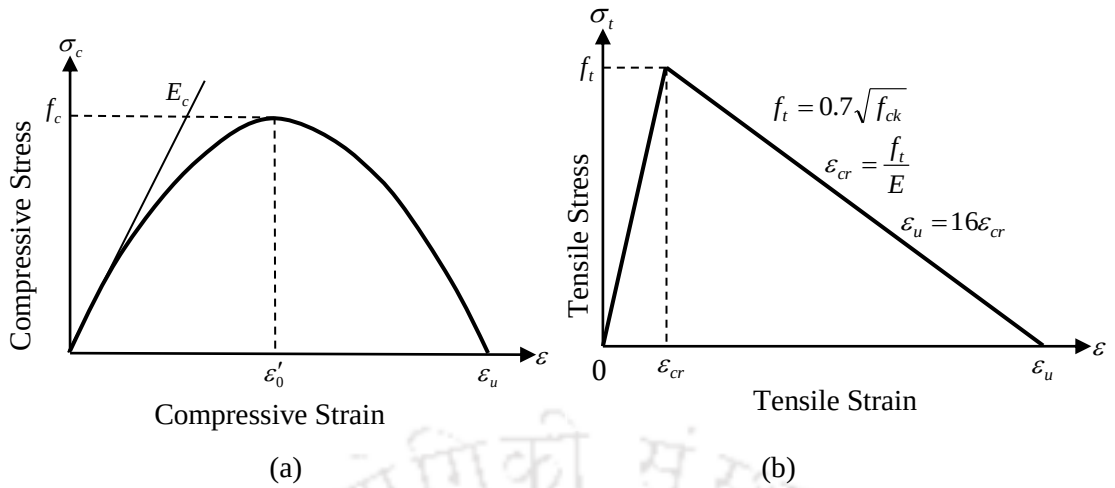

Figure 3.6: Stress-strain profiles for concrete (a) in compression and (b) in tension.

The concrete behaves as a linear elastic material till the uniaxial cracking strength, f_t after which softening behavior is assumed. The softening rate depends on the size of the elements in the crack region. The post-failure behavior for direct straining across cracks is modeled with a tension stiffening option, which is specified by either post-failure stress–strain relation or by applying a fracture energy based cracking criterion. In this study, tension stiffening is defined with an assumed post-failure stress–strain relation (Figure 3.6b). Steel reinforcement is modelled with plasticity model in ABAQUS for both tension and compression (Figures 3.7a and 3.7b). Plastic strain values (Eqs. 3.1 and 3.2) are used in defining the hardening behaviour. Furthermore, the first data pair must correspond with the onset of plasticity that is, the plastic strain value must be zero in the first pair. These concepts are applicable when hardening data are defined in a tabular form for plasticity models in ABAQUS/Standard. The details of the reinforcement used in the analysis are provided in Table 3.1.

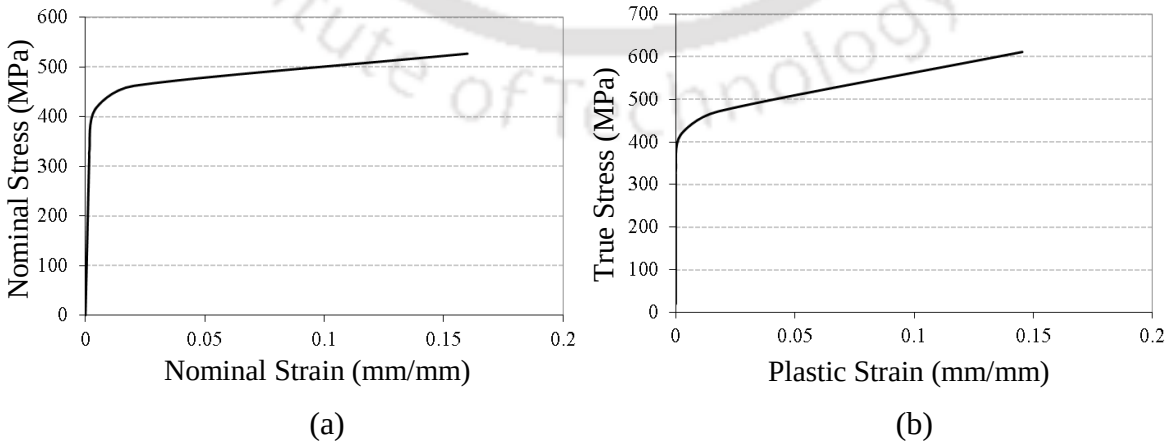

Figure 3.7: Stress-strain relationship for reinforcement: (a) Nominal and (b) Plastic.

3.4 ANALYSIS PROCEDURE

The analysis in ABAQUS is carried out by dividing the problem history into steps. The problem can be divided into different phases such as gravity load, pre-loading, main loading etc., between which the boundary conditions may remain same or change. Such phases are defined as steps, for which the type of analysis to be performed is also specified. ABAQUS offers two techniques to solve the problems, namely ABAQUS/Standard and ABAQUS/Explicit. Both the techniques solve the equilibrium equations using numerical step-by-step procedure at discrete intervals of time Δt apart. ABAQUS/Standard, using Newton Raphson method, employs an implicit integration scheme, where in each time step the stiffness matrix has to be assembled to calculate the displacement. The time increment is chosen such that the solution is accurate within the tolerance limits. Hence, in problems involving nonlinearity, such as nonlinear materials, large deformation, nonlinear boundary conditions, contacts, etc., there may be convergence issues since it requires very small time increments. The storage of the stiffness matrix at each time step also requires large memory to perform the analysis. However, accurate solutions can be obtained using ABAQUS/Standard. The implicit finite element method has been applied effectively to 3D problems for some considerable time. It has the advantage that it can analyse static and quasi-static events easily because it is unconditionally stable with respect to the size of the time increment. Due to its stability, the implicit analysis is considered in this study to carry out analysis.

3.5 VALIDATION

For any detailed finite element study, the material parameters and the modelling methodology need to be validated for judging the consistency, reliability and accuracy of the obtained results. In the past, several analytical and numerical studies have been carried out on the behavior of floor slab in shear wall. However, very few experimental works are available on this topic. A series of experiments for investigation of the behavior of slab-wall connection were carried out by Pantazopoulou and Imran (1992) at the University of Toronto. The specimens studied were the typical slab system of a multistoried structure. The floor system was used as a prototype. The test specimen was a half scaled model of the interior shear wall-slab connection in the prototype structure. In the present study, the experimental specimen (Figure 3.8a) was analysed using ABAQUS and the results are compared with the available experimental results. Figure 3.8b presents the finite element model constructed using ABAQUS. The compressive strengths of the concrete used in the slab and shear wall were 27.6 MPa and 32.5 MPa respectively. The yield strengths of reinforcing bars for slab and shear wall were 410 MPa and 400 MPa respectively.

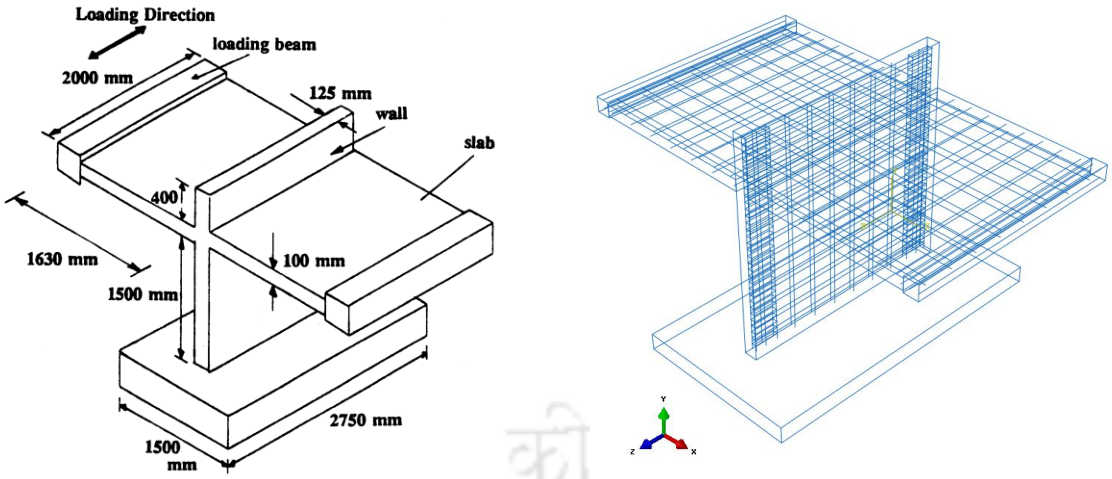

(a) (b)

Figure 3.8: (a) Details of the specimen tested at the University of Toronto and (b) reinforcement details in ABAQUS model.

The details of experimental set up and loading history are mentioned in Pantazopoulous and Imran (1992). The slab and shear wall reinforcement, which consist of 8 mm and 10 mm rebars, are modeled as an elasto-plastic material with isotropic hardening. Shear walls, slabs and loading beams are discretized with eight-noded solid elements with reduced integration option (C3D8R). Two noded linear truss element (T3D2) was used to model the steel reinforcement. The concrete model adopted herein, is a Concrete Damaged Plasticity (CDP) model implemented in ABAQUS. Full bond between concrete and reinforcement is assumed using embedded element constraint. Tie constraint is assigned to the nodes at the shear wall-slab and shear wall-foundation interfaces.

It is observed that for a large range of lateral displacement (till 16.5mm) the pushover curve from finite element analysis matched closely with the experimental lateral force-lateral deformation curve (Figure 3.9a). This indicates simulation of proper boundary conditions and load application in the finite element model. For large displacement, the actual degradation of strength in experiment is not captured in the finite element model. Figure 3.9b represents the comparison of the observed lateral deflection profiles of the shear wall and slab at 0.7% drift with the results of the experimental model. Although the shear wall and slab are planar diaphragm members, they show significantly different behavior. Due to initiation of cracks in slab at early stages of experiment, the displacement is overestimated from finite element analysis results. However, the wall displacements are underestimated from the analysis. The difference in the analytical and experimental result is mainly due to the mesh size considered for the analysis. The mesh size used for discretization is based on the matching of the global behavior (load-displacement curve as shown in Figure 3.9a) of the ABAQUS model with the experimental results. At the same time, the local behavior is significantly sensitive to the mesh size.

Although the trends in the variation of lateral displacement are similar for both ABAQUS model and the experimental results, the difference in the values arises due to the considered discretization. Also, similarity in the crack pattern confirms the selection of appropriate mesh size.

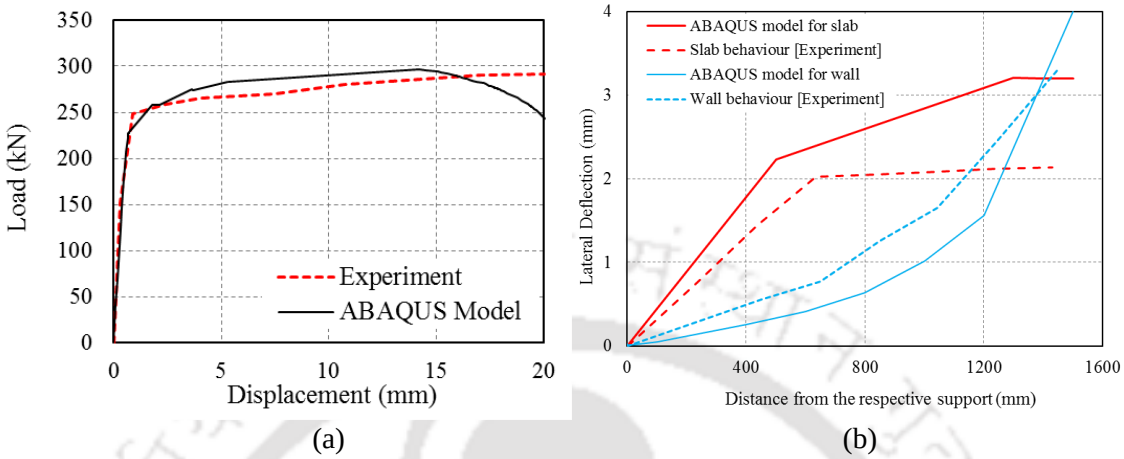

Figure 3.9: Comparison of experimental results with ABAQUS: (a) lateral load - lateral displacement behaviour and (b) lateral deflections of shear wall and slab.

Stresses in the longitudinal reinforcement of slab for two different displacement levels are compared with the finite element simulation results. The stresses are obtained at the face of the shear wall and at the quarter of the span from the shear wall in Figures 3.10a and 3.10b respectively. The stress distributions at the two cross sections are similar and the pattern of the stress distributions match with that of the ABAQUS simulation. However, there is an error of about 25% in the stresses in the longitudinal bar as compared with the experimental result (ABAQUS results are more conservative).

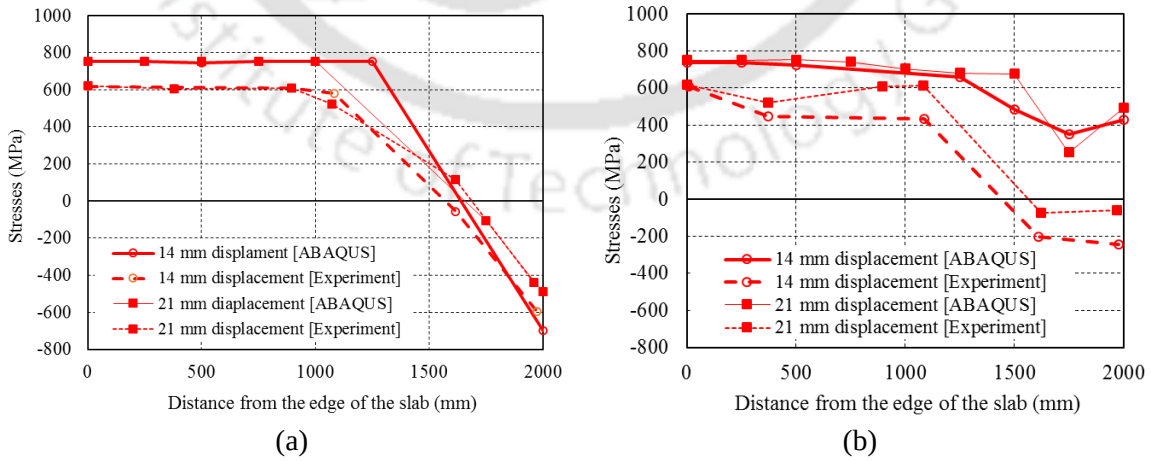

Figure 3.10: Stresses in the longitudinal reinforcement of slab for two different displacement level: (a) stress distribution at the face of the shear wall and (b) stresses located at a quarter of the span from the shear wall.

The cracking patterns from the experimental and the finite element studies are compared in Figures 3.11 and 3.12. Pantazopoulous and Imran (1992) have reported that flexural shear cracks developed in the slab at the junction with the shear wall at 3.5 mm lateral displacement. As the maximum plastic equivalent principal strains from the ABAQUS model give a better representation of the cracks, these strains are shown to represent the cracking patterns in finite element analysis.

The cracking pattern at the shear wall-slab assemblage was observed to be similar to that in the experimental observations (Figures 3.11a, 3.11b, 3.12a and 3.12b). The tensile damage patterns obtained analytically at the junction of the shear wall and slab at 3.5 mm and 21 mm lateral displacement level are presented in Figures 3.11c and 3.12c respectively. The tensile damage pattern represents the crack propagation. It was observed that the cracking started at the junction of the shear wall and slab and propagated in the slab. Damage in the slab was mostly concentrated within the region adjacent to the shear wall. It was observed that the finite element analysis results are in good agreement with the experimental results. All the observations indicate that the simulation of the experimental results could be carried out with reasonable accuracy. Thus, the material modelling parameters of ABAQUS are established for use in further finite element simulations.

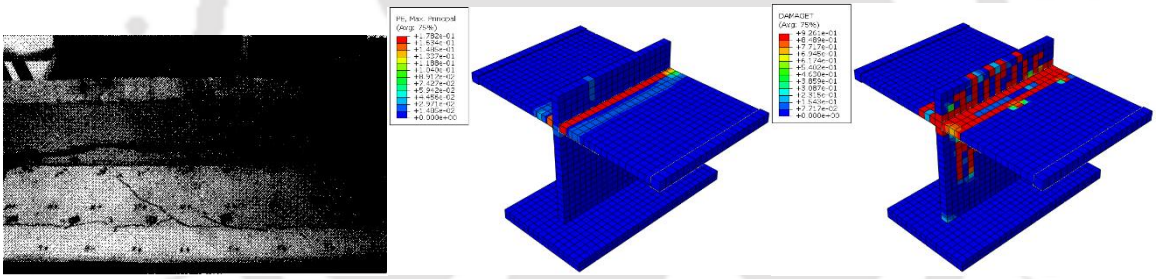

(a) (b) (c)

Figure 3.11: Cracking pattern at 3.5 mm lateral displacement: (a) Experimental results from University of Toronto test; (b) plastic strain pattern and (c) tensile damage pattern from ABAQUS results.

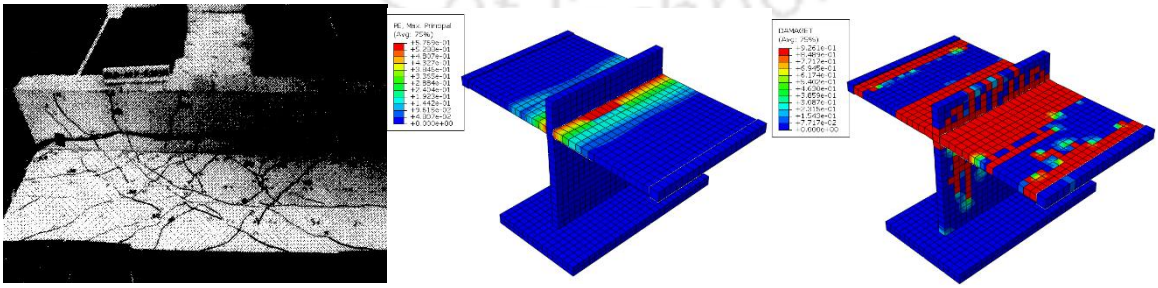

(a) (b) (c)

Figure 3.12: Cracking pattern at 21 mm lateral displacement: (a) Experimental results from University of Toronto test; (b) plastic strain pattern and (c) tensile damage pattern of ABAQUS model.

3.6 FINITE ELEMENT MODELLING

In this section, finite element modelling of RC shear wall frame building is discussed. Firstly, the five storied symmetrical building is modelled using the program SAP2000 (CSI, 2000), to carry out the linear static analysis under the design vertical and lateral loading combinations. Later, nonlinear static analysis of a five storied and a ten storied symmetrical building is carried out using ABAQUS/Standard program. Also, an exterior shear wall-slab assemblage is considered to study the behavior of the junction region under lateral loading. A parametric study has been carried out by varying design parameters such as, axial load, length and storey height of shear wall to study their effect on the behavior of junction region.

3.6.1 Detailing of Shear Wall-Slab Junction

Two RC wall-frame buildings with symmetric plan (Figure 3.13) and assumed to be located in seismic zone V, are modelled using the program SAP2000 in the present study. The two buildings are five and ten-storied high with the total heights as 15 m and 30 m, respectively. The beams and columns are modelled using two-noded frame elements and floor slab and structural walls are modeled using four-noded shell elements. The typical storey height and the shear wall thickness are considered as 3 m and 300 mm, respectively. Both roof and floor slabs have thickness of 120 mm. The total intensity of live load is considered as 3 kN/m^2 and floor finish loading as 1 kN/m^2. Seismic weight at each floor of the building is obtained as the sum of dead and live loads. Reduced live load is considered on roof and floor when combined with earthquake loads as per Indian standard (BIS, 2016b), which recommends using 25% of live load on floor slab (if Live load is less or equal to 3 kN/m^2) and no live load on roof.

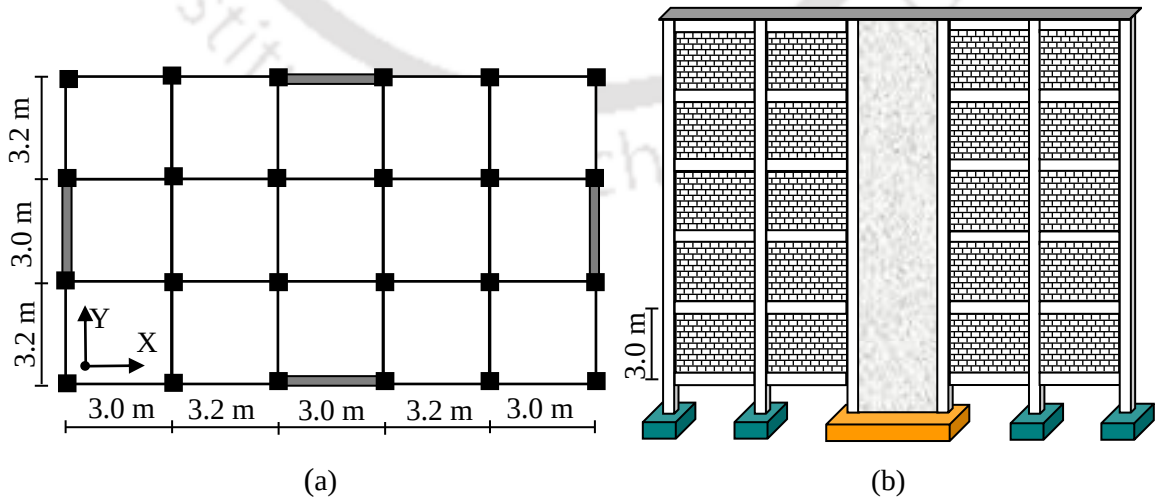

Figure 3.13: Details of buildings considered in the analysis: (a) plan (b) elevation.

Design lateral force at each floor level is calculated as per Indian Seismic Code IS: 1893 (Part 1) (BIS, 2016b). The design vertical loads are obtained considering dead loads of members and code specified live loads on floor slabs. At each floor level, the lateral force in each of the two plan directions (X and Y) is shared equally by the two walls oriented in that particular direction. The walls are designed and detailed against combined vertical and lateral forces as per the relevant Indian Standard (BIS, 2016b).

In the junction region, the longitudinal reinforcement of the slab is extended up to the wall. 8 mm diameter bar spaced at 150 mm in the RC shear wall is provided in two layers along both horizontal and vertical directions. The reinforcement provided in the floor slab is 8 mm diameter bar placed at 300 mm spacing in both directions. The reinforcement details in the shear wall - floor slab junction are shown in Figure 3.14. Both the top and bottom bars of the slab are bent at 90º and extended up and down to the exterior face of the shear wall. The reinforcement ratios in vertical and horizontal directions are the same in case of shear wall.

3.6.2 Methodology

One five storied and another ten storied symmetrical frame shear wall building (FSWB) with or without embedded reinforcement are used for the simulations. To study the detailed behavior of the shear wall - slab junction, an exterior wall-slab assemblage (EWSC) is considered from the five storied building. 8-noded hexahedral (brick) elements (C3D8R) are used for concrete with reduced integration characteristics. 2-noded linear truss elements (T3D2) are used to model reinforcement. The embedded method is adopted to simulate the bond between the concrete and the reinforcement, assuming perfect bond. Two brick elements were used through the thickness of the 120 mm slab with all concrete elements having the same mesh size of 60 mm. Restraints were introduced at the bottom edges of the specimens in the direction of the applied load. The translational and rotational Degrees of Freedom (DoFs) are restrained at the bottom nodes of all the specimens. The outer edges of slabs are supported on rollers in case of EWSC model. The out-of-plane bending of the shear wall and the vertical bending of slab are restrained along the roller supported edges. Generally, a shear wall is designed to resist shear forces and bending moments in its own plane. In the present study, displacement based pushover analysis is carried out in the in-plane direction of the wall to investigate the behavior of slab-wall junction. Hence, the out-of-plane movement of the wall is restrained in the present study. In finite element analysis, the in-plane displacement of the wall-slab assembly does not get mobilized properly in absence of the restraint of vertical displacement. Also, the intention of the study is to investigate the possible damages in the slab and the slab-wall junction due to the in-plane lateral displacement of the wall. The vertical displacement of the slab under the

applied vertical load does not influence the damage of the slab and the slab-wall junction significantly. Thus, the vertical restraint does not affect the slab-wall junction behavior.

Chapter 4 provides the details regarding the geometry and the boundary conditions of the specimens that are used for the simulations. FSWB specimens are analyzed using monotonic nonlinear static analysis in ABAQUS/Standard and ESWC specimen is analyzed using both monotonic nonlinear static and slow cyclic analysis in ABAQUS/Standard. In the monotonic static analysis, a displacement is applied in the plane of the shear wall at the top node of the wall. In case of slow cyclic analysis, the sequence of applied displacements consists of three cycles at each displacement of 2.5, 5, 10, 20, 40, 60, 80, and 100 mm. The displacement is increased with a smooth amplitude curve. Among the constitutive models for simulating the behavior of concrete, the CDP model is used and a detailed description of this model is already furnished earlier in this chapter.

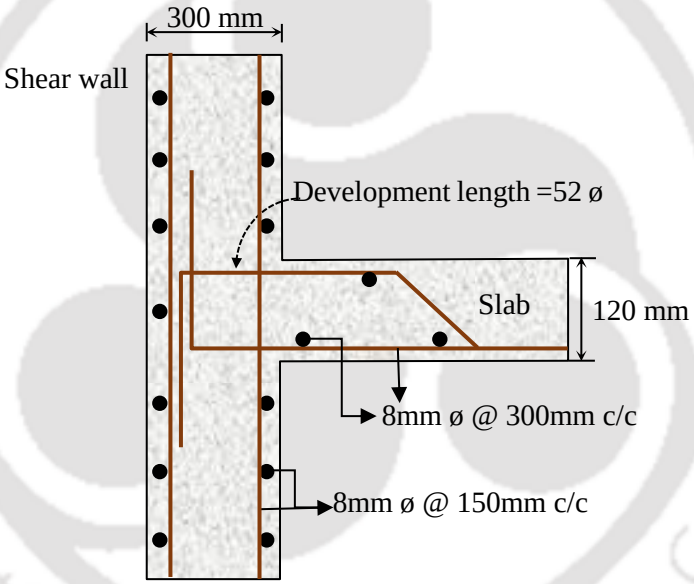

Figure 3.14: Detailing of reinforcement at shear wall - slab junction.

3.6.3 Mesh Convergence Study

In the present study, the FSWB and EWSC models are analysed under combined vertical compression and lateral force at the top of the wall. Mesh convergence study is performed for the EWSC model. Three different mesh sizes (75 mm, 100 mm and 150 mm) are adopted in the analysis of shear wall-floor slab connection in order to investigate the influence of mesh sensitivity on its response. Although there is a marginal difference in the normalized lateral shear capacities for the specimens with 75 mm, 100 mm and 150 mm mesh sizes, the mesh size of 150 mm is adopted in

order to avoid the hourglassing numerical problem and the distortion associated with the C3D8R elements (Genikomsou and Polak, 2015) (Figure 3.15).

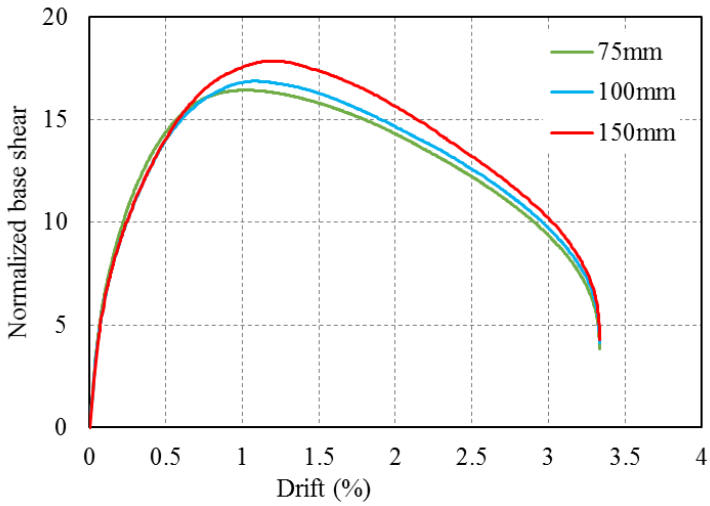

Figure 3.15: Variation of base shear with lateral drift for EWSC specimen with different mesh sizes.

The choice of adopting 150 mm mesh size is based not only on the load-deflection response but also on the comparison with the damage patterns. In the present study, the accuracy of the FE solution is assessed by comparing the tensile damage pattern. It is observed that the propagation of tensile damage does not depend on the mesh size. Similar damage pattern is observed considering different sizes of mesh. Also, the measure of tensile damage is similar considering all the mesh sizes (Figure 3.16). By adopting the mesh size of 150 mm, the number of elements gets reduced and the analysis takes less time to complete than by considering smaller mesh sizes. Since the 150 mm mesh size is not affecting the damage propagation and giving the maximum capacity, for all subsequent analyses, the mesh size of 150 mm is adopted.

3.7 SUMMARY

In this chapter the details of the material parameters used for finite element modelling are discussed. Referring to the past research, the material parameters are selected and the behaviour is validated with the experimental results of Pantazopoulou and Imran (1992). The concrete model adopted herein, is a Concrete Damaged Plasticity (CDP) model implemented in the finite element code, ABAQUS. It is observed that the finite element analysis results are in good agreement with the experimental results. Thus, the material modelling parameters of ABAQUS can be used in further finite element simulations. Mesh convergence study is also carried out with the 150 mm size mesh being adopted for all parametric studies.

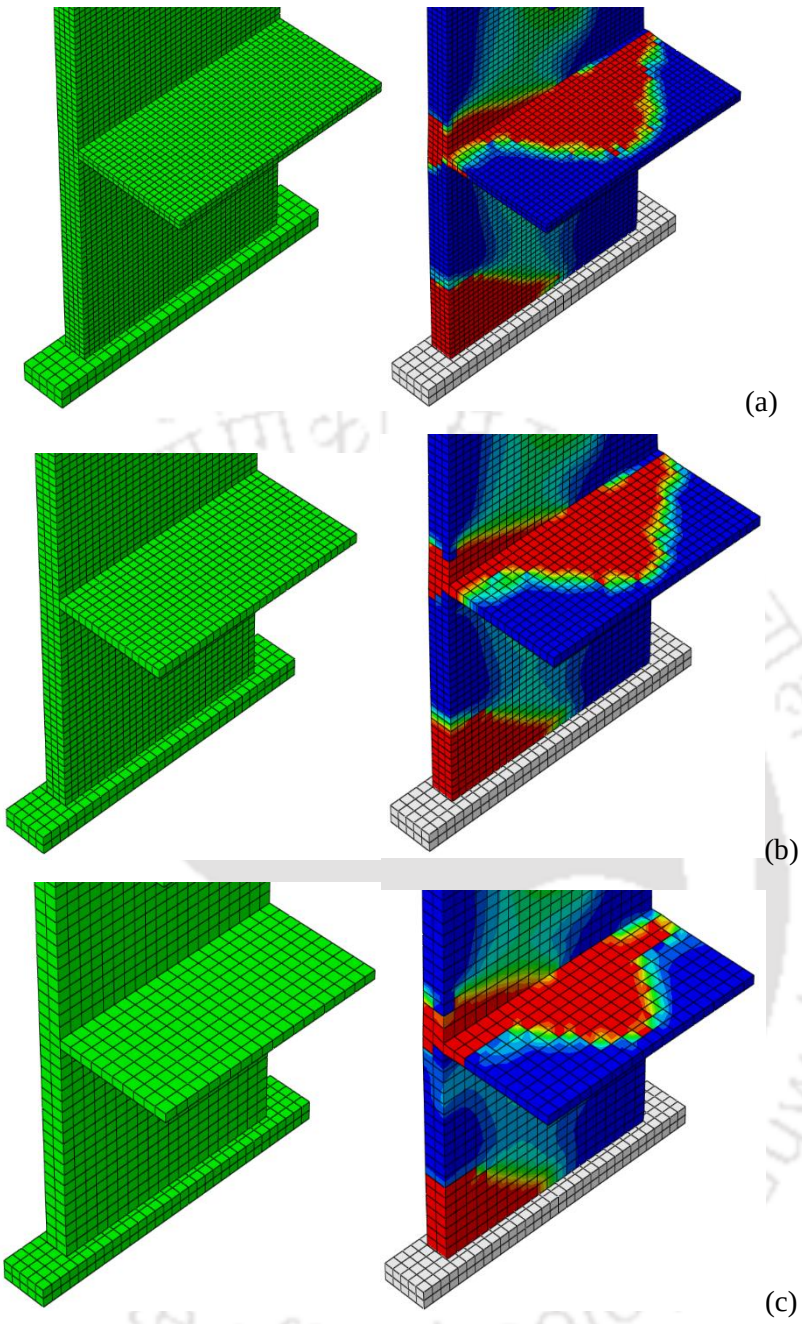

Figure 3.16: Finite element meshing and damage pattern for EWSC model with different mesh sizes: (a) 75 mm (b) 100 mm and (c) 150 mm.

Chapter 4
ASSESSMENT OF TENSILE DAMAGE

4.0 OVERVIEW

RC structural walls play an important role in transfer of forces from floor slabs to the foundation below in a multistoried wall-frame building. To investigate the influence of the presence of slab on the behaviour of slender wall, detailed finite element modelling of a five-storied building and a ten-storied building is carried out using the program ABAQUS/Standard. The models have been subjected to non-linear static analyses to observe the extent of possible damages in wall, slab and their junction region. The influence of vertical and horizontal reinforcement on the damages is also studied. The difference in the behaviour of the wall in each building with the behaviour of isolated slender wall is highlighted. Further, a wall-slab sub-assemblage is also analyzed to stimulate the observed behaviour of the walls in the multistoried buildings. The main intension of the study carried out is to develop a simplified but efficient analytical model. The result of all those analyses are discussed in this chapter.

4.1 DETAILS OF SPECIMENS

A hypothetical wall-frame building is considered to be located in seismic zone V as per Indian Earthquake Code (BIS, 2016b). Using finite element program ABAQUS, the beams, columns, shear walls and slabs are modelled with eight-noded linear hexahedral 3D solid continuum elements with reduced integration (C3D8R). Two noded linear truss element (T3D2) is used to model the steel reinforcement. Figure 4.1 gives details regarding the geometry and the boundary conditions of the specimens that are used for the simulations.

The concrete and reinforcement are modelled using CDP characteristics and elasto-plastic properties respectively. The validated material parameters, used in the previous chapter, are assigned to the models. Considering the variation in concrete material model and presence of reinforcement, four different frame shear wall buildings (FSWB) (Table 4.1) are modelled in the present study. For FSWB1 model, the building is of 10 stories with the storey height as 3 m with no reinforcement embedded in the structural elements. FSWB2 model is similar to FSWB1 except that the building is of 5 stories with the total height of shear wall as 15 m. In both these models, all the structural elements are modelled using CDP concrete model. The FSWB3 model is simulated without reinforcement embedded in the concrete. FSWB4 is similar to FSWB3 except that FSWB4 has

embedded reinforcement in shear wall and in floor slabs. As the study is intended to investigate the behaviour of the slab-wall junction region, linear elastic behaviour of concrete is considered for the beams and the columns in models FSWB3 and FSWB4.

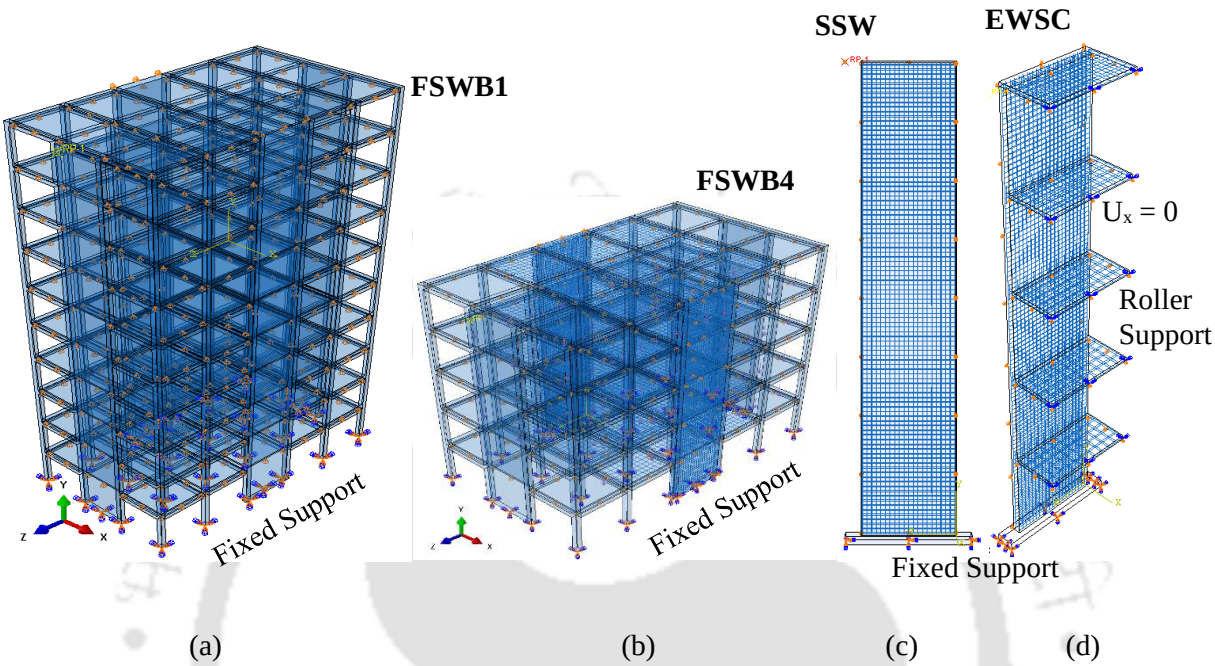

Figure 4.1: Geometry and boundary conditions of specimens used for pushover analysis: (a) ten storied building; (b) five storied building; (c) isolated slender wall and (d) exterior wall-slab assemblage.

Table 4.1: Detail of specimens simulated

Model Configuration	FSWB1	FSWB2	FSWB3	FSWB4	EWSC	SSW
Wall thickness (mm)	300	300	300	300	300	300
Wall length (mm)	3000	3000	3000	3000	3000	3000
Wall height (m)	30	15	15	15	15	15
Vertical bars of wall	-	-	-	8@150	8@150	8@150
Horizontal bars of wall	-	-	-	8@150	8@150	8@150
Slab reinforcement	-	-	-	8@300	8@300	8@300
Slab thickness (mm)	120	120	120	120	120	120
Slab width (mm)	1500	1500	1500	1500	1500	-
Concrete material model	CDP	CDP	CDP for wall and slab only	CDP for wall and slab only	CDP	CDP

Next analyzed specimen is the exterior shear wall-slab connection (EWSC) taken from the five storied FSWB model The intention of analyzing EWSC model is to see whether the wall and slab-wall junction behave in a similar way as observed in the FSWB model. Lastly, one isolated slender

shear wall (SSW) is modelled with embedded vertical and horizontal reinforcement to observe how the behavior changes by the inclusion of the floor slab.

Beams, columns, shear walls and floor slabs are created in individual parts using solid elements in case of FSWB model. Connectivity is checked among the individual modelled parts after assembly. Tie contact technique is utilized to create proper interaction between shear wall and floor slab and also between the beams and columns [ABAQUS, 2011]. Using this technique, embedded nodes are placed at desired locations with the constraints on translational Degrees of Freedom (DoFs) of the embedded element by the host element. The rebars are modelled as the embedded region in concrete using constraints in the interaction module, and making the concrete the host. Thus, rebar elements can only have translations/rotations equal to those of the host elements surrounding them. In this simulation, the embedded technique is used to constrain the two-node truss elements (steel reinforcement) with solid element (shear wall and floor slab) in order to create proper bond between steel and concrete. The translational and rotational DoFs are restrained at the bottom nodes for all the specimens. The outer edges of slabs are supported on rollers in case of EWSC model. The out of plane bending of the shear wall and the vertical bending of slab are restrained along the roller supported edges.

For 15 m height of wall, the allowable lateral displacement for elastic behaviour (BIS, 2016b) is obtained as 60 mm. However, as the study is intended to capture the possible nonlinearities and the associated damage in wall-slab assembly, significantly higher values of lateral displacement have been considered for displacement-controlled nonlinear static analysis. The total target lateral displacements of 500 mm for EWSC and SSW models and 750 mm for all models of five and ten storied frame - shear wall building (FSWB) are applied at the top level in the plane of the wall. Translational restraints are imposed at the bottom nodes of the specimen to simulate the full restraint boundary condition at the wall-footing junction. The gravity loads (both dead and live loads) on slab are assigned as pressure loads on the surface of solid elements. The total intensity of loading on slab including live load and floor finish is considered as 4 kN/m^2.

HYSD Fe415 steel reinforcing bars are used to model the reinforcement in the specimens described in the previous section. The reinforcement is obtained in the wall and slab by considering the design load combinations provided as per Indian seismic code, BIS, 2016b. The detailing of reinforcement in shear wall and continuous floor slabs is done as per Indian Standard, SP: 34– 1987 (BIS, 1987). The detailing of steel reinforcement at the shear wall-slab junction for both EWSC and FSWB models is explained in Chapter 3. A typical reinforcement mesh in the floor slab is shown in Figure 4.2, which is used to simulate FSWB4 model.

The reinforcement is embedded in the slabs panels which are located between grid lines 2 and 5. These slab panels are expected to be influenced by the behaviour of wall-slab junctions for wall A and wall B. The other slab panels are analysed without reinforcing steel embedded in them, as the main intention of the study is to check the behavior at the wall-slab junction region.

4.2 Response of Finite Element Models

The response of nonlinear static analysis of the ten storied frame shear wall building (FSWB1) is compared with the analysis results of one of the five storied frame shear wall building (FSWB2) to understand the behaviour of the wall and the wall-slab junction. Both the models are laterally displaced up to 750 mm. For comparing the behaviour of the different finite element models, tensile damage patterns are extracted. These represent the extent of cracking. Different drift levels are chosen to compare the propagation of tensile damage corresponding to the results obtained at drift levels of model FSWB4, as FSWB4 is the only model with embedded reinforcement among the FSWB models. Figures 4.3 and 4.4 represent the propagation of tensile damage at different drift levels, namely (a) 0.04% (development of first crack at the base of the wall); (b) 0.48% (tension yielding of vertical reinforcement at the bottom of wall); (c) 1.22% (yielding of reinforcement of slab at junction region) and (d) 2.5% for FSWB1 and 5% for FSWB2 (final stage). In both the cases, the damage starts from the base of the shear wall and propagates to the wall-slab junctions at different floor levels. Also, the slab which is connected to the shear wall undergoes maximum damage. At the same drift level, similar damage patterns are observed in the wall panels and wall-slab junctions in the two models. Thus, the height of building does not influence the damage pattern in walls.

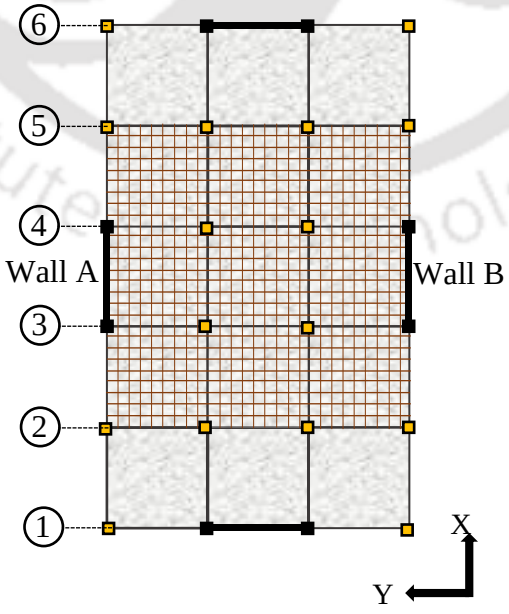

Figure 4.2: Plan of FSWB with reinforcement mesh.

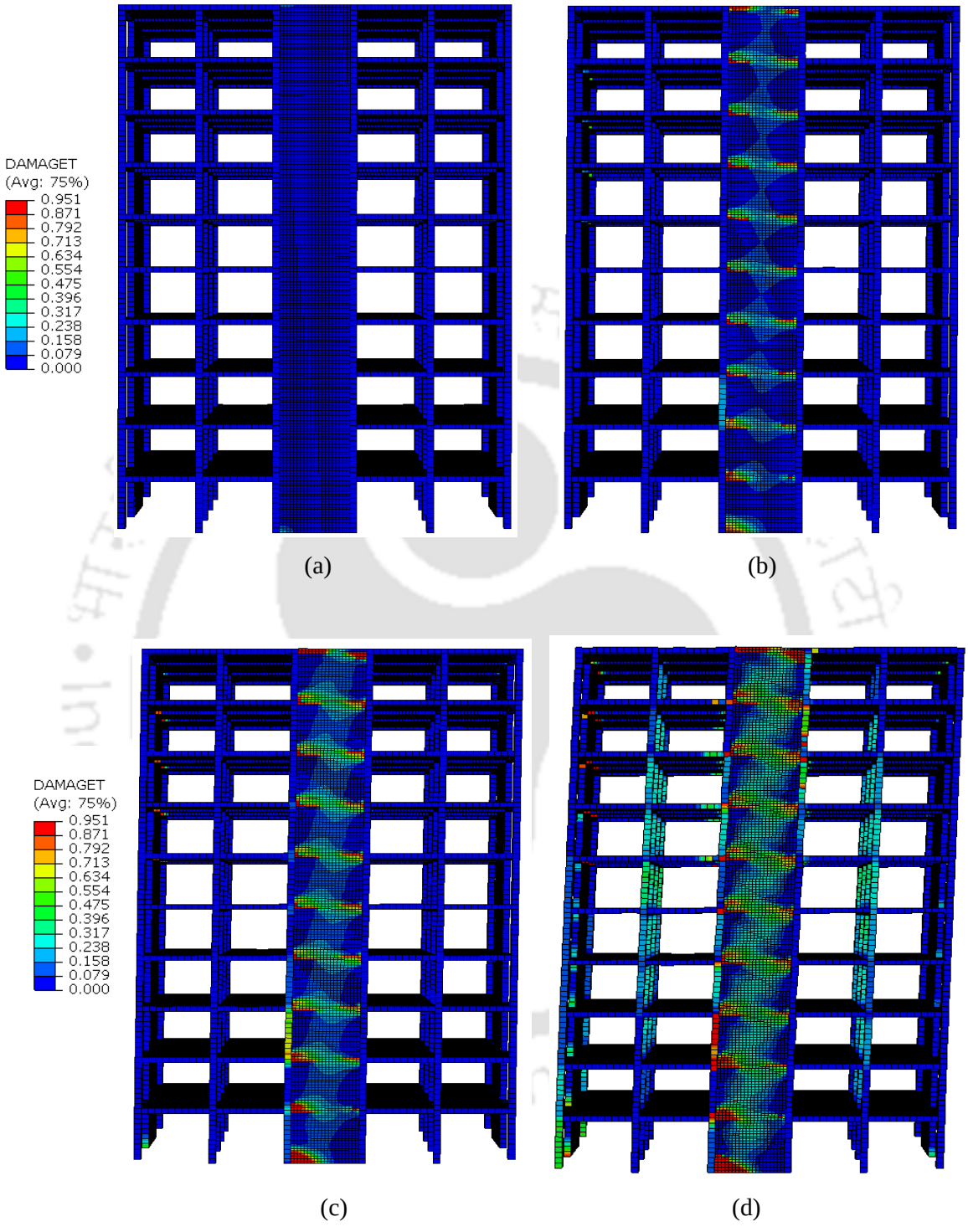

Figure 4.3: Propagation of tensile damage in FSWB1 model at different drift levels: (a) 0.04%, (b) 0.48%, (c) 1.22% and (d) 2.5% (Final stage).

Next, the behaviours of FSWB3 and FSWB4 are compared to see the influence of reinforcement on the tensile damage pattern in wall panels and wall-slab junction. The observed tensile damage patterns for FSWB3 and FSWB4 are the same as observed for FSWB1 and FSWB2 (Figure 4.5). In all the cases, the cracking of concrete started at the base of the shear wall at a lateral drift of 0.04% and propagated up to the wall-slab junction. Subsequently, compressive struts start developing in the wall between the floor slabs. Thus, the slender wall gets partitioned into a number of squat wall panels between the floor slabs for transfer of forces from different floor levels through the wall to the foundation. Also, it is observed that maximum cracks tend to develop in the slab panels connected with walls A and B (Figures 4.6 and 4.7). The floor slab panels not connected with those walls, experience less cracks and very less damage. The intermediate floor slabs exhibit higher levels of tensile damage over a larger area as compared to the roof slab. This is because of more propagation of damage from the corresponding wall-slab junctions due to concentration of higher compressive stress through strut action from the connected upper and lower storey wall panels. At the final stage, similar damage patterns are observed in the intermediate floor slabs. The behavior of FSWB4 model is explained in details in the next section. In the walls located along the perpendicular direction of the applied displacement, strut action is not observed to develop between the floor slabs. However, the junction region shows significantly less damage as compared to the junctions of wall A and B (Figures 4.6 and 4.7).

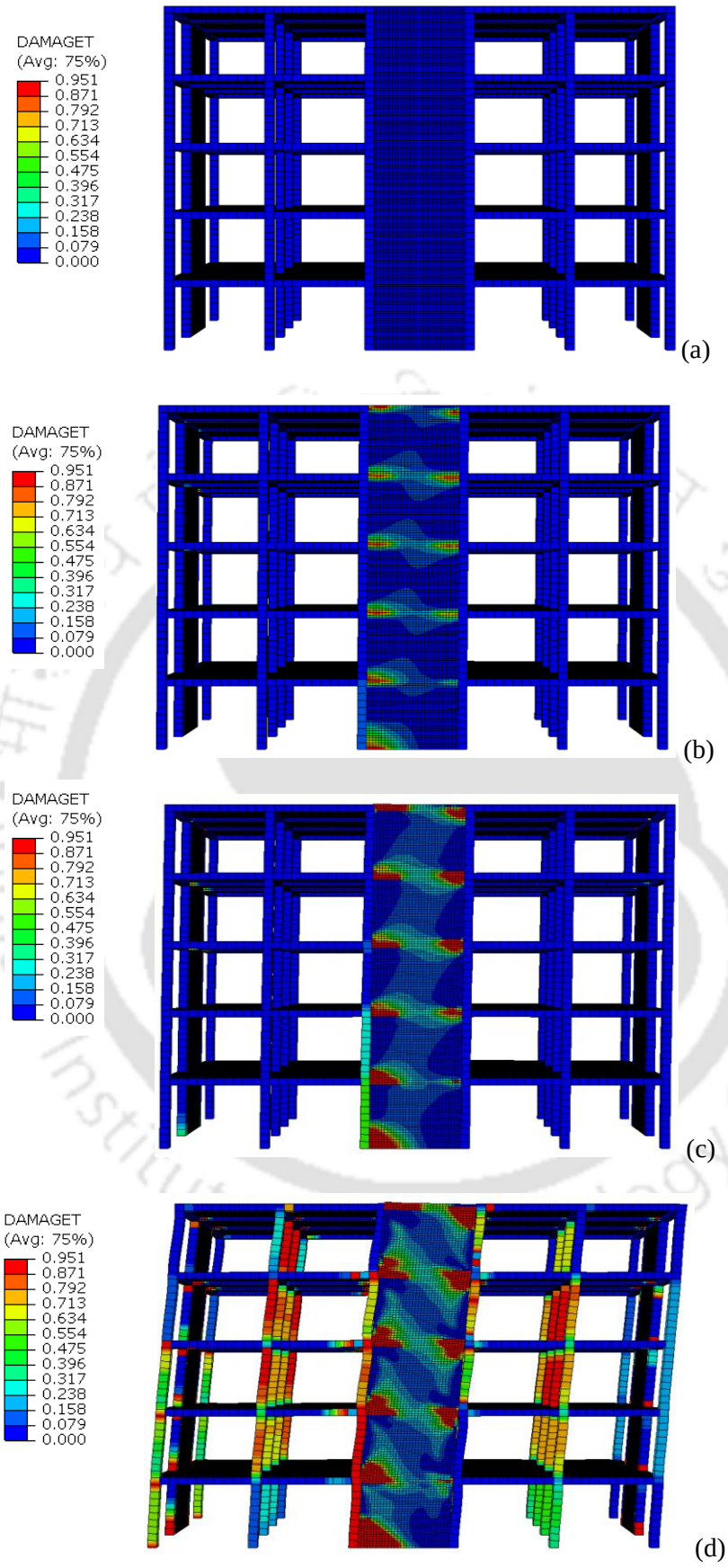

Figure 4.4: Propagation of tensile damage in FSWB2 model at different drift levels: (a) 0.04%, (b) 0.48%, (c) 1.22% and (d) 5% (Final stage).

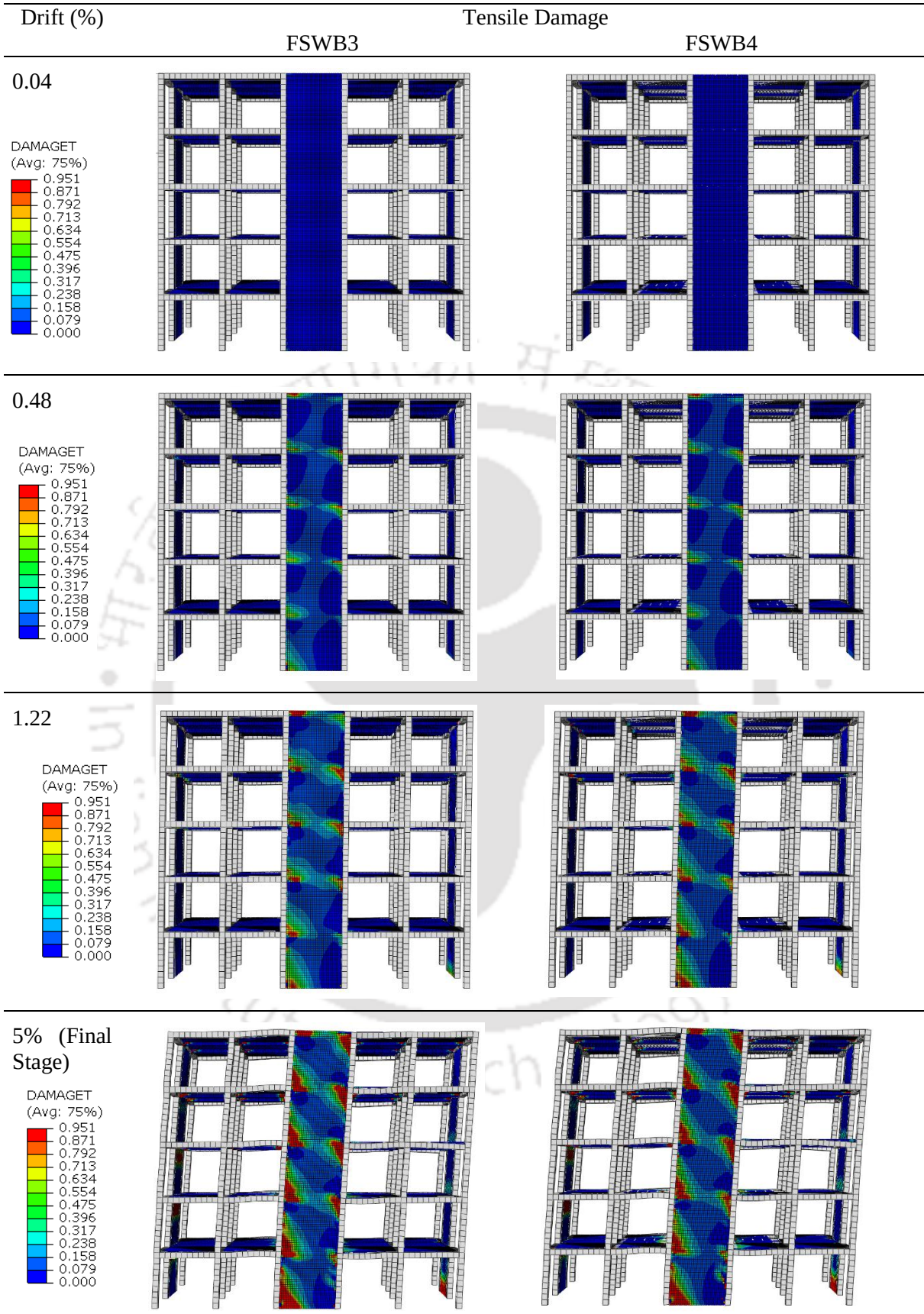

Figure 4.5: Comparison of propagation of tensile damages of FSWB3 and FSWB4 models at different drift levels.

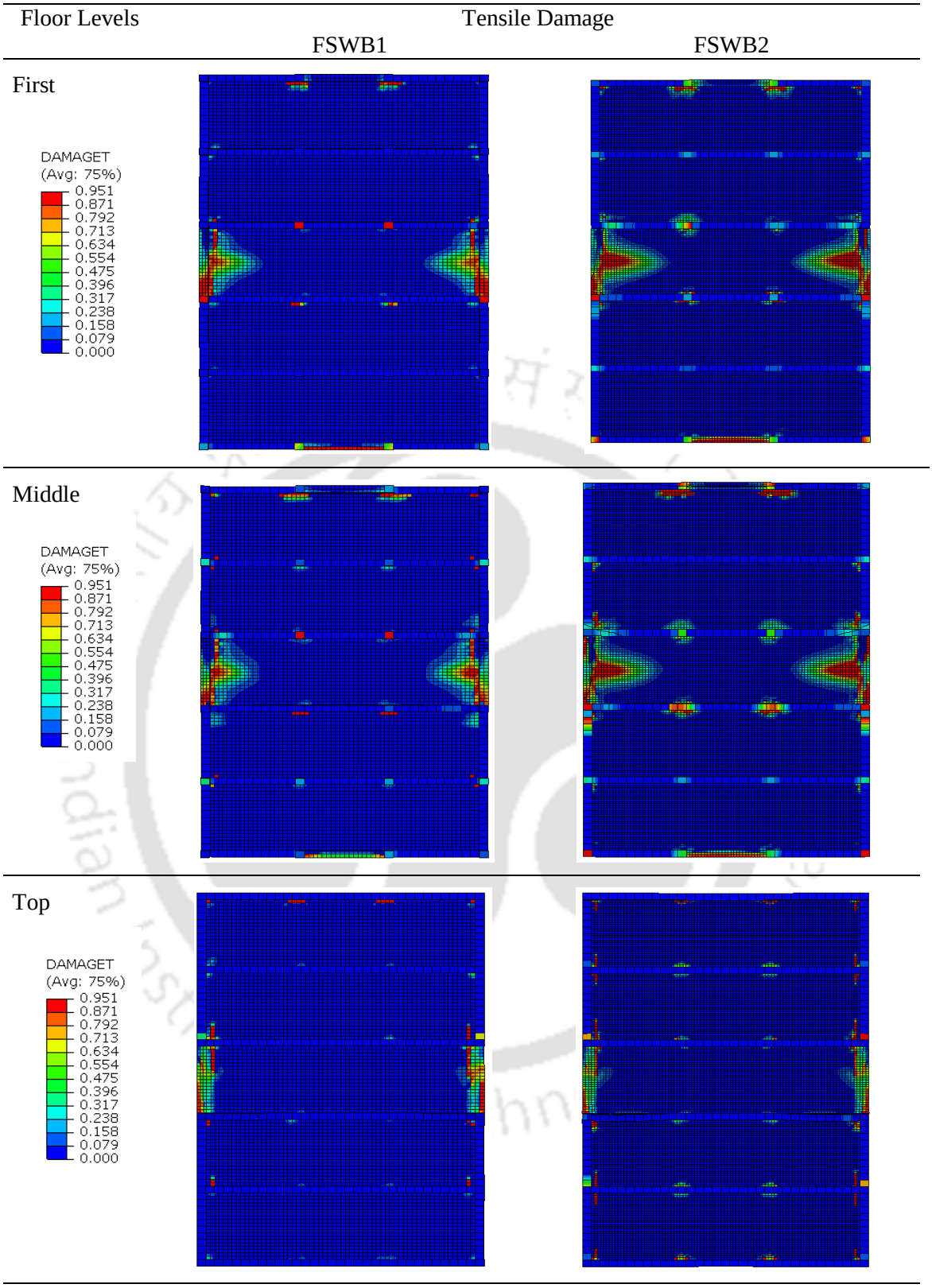

Figure 4.6: Comparison of tensile damage patterns in the slabs at different floor levels of FSWB1 and FSWB2 models at the final drift level.

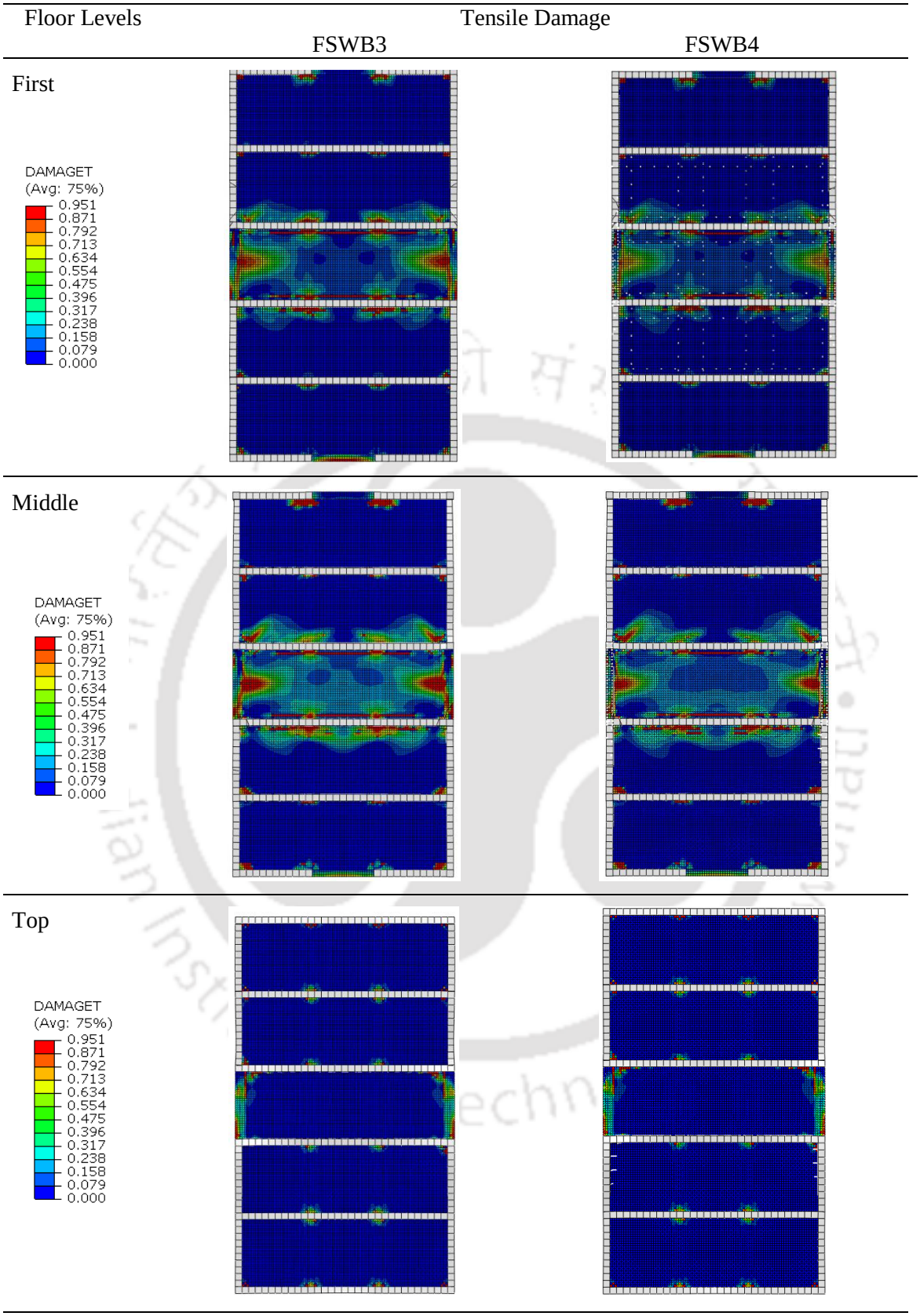

Figure 4.7: Comparison of tensile damage patterns in the slabs at different floor levels of FSWB3 and FSWB4 models for the final drift level.

4.2.1 Behaviour of FSWB4 Model

Nonlinear static analysis of FSWB4 model is carried out along X-direction, and the salient points on the capacity curve are shown in Figure 4.8. The base shear is normalized with respect to the weight of the model and plotted against lateral drift. The peak shear strength of FSWB4 model is reached at a lateral drift of 1.65% along X direction. The propagation of cracks in FSWB4 model is presented in Figure 4.5 at different drift levels. At the lateral drift of 0.03%, the concrete in the slab region near the slab-wall junction at first floor starts cracking. The development of cracks at the bottom of the shear wall starts at a drift of 0.04%. The onset of cracks at first floor level is due to the development of diagonal tension, from strut action, in the squat wall panel between two floor slabs. Tension yielding of vertical bar at the bottom of the wall starts at 0.48% lateral drift. This shows the onset of material nonlinearity well before the code specified elastic drift limit. The peak strength of concrete is reached at a lateral drift of 0.76%. At a drift of 1.22%, the longitudinal reinforcement in the slab near the junction region of floor slab and shear wall starts yielding. The vertical reinforcement at the base of the wall reaches its ultimate strain value at a lateral drift of 3.30%, leading to rupture of vertical bar in tension. The first crushing of concrete occurs at the toe region of the wall at 2.20% lateral drift. This is due to the very high concentration of compressive stress at the toe of the wall under the combined effect of diagonal compression (from the bottom wall panel) and flexural compression. At the slab-wall junctions in the upper floors, the combined effect reduces due to lesser flexural compression.

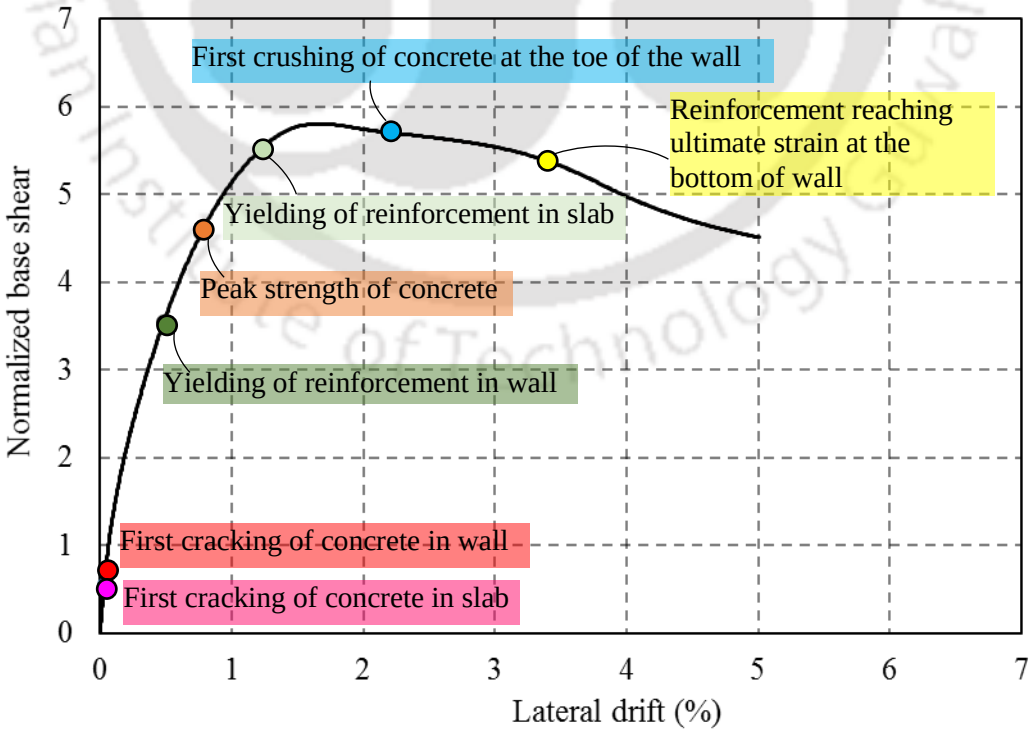

Figure 4.8: Variation of normalised base shear during nonlinear static behaviour of FSWB4 model.

The equivalent plastic strain in concrete at the shear wall - slab junction along the length of the wall signifies the possibility of crushing of concrete. This may lead to the development of a major sliding shear crack across the wall-slab junction in the plane of the wall. The sliding cracks can further result in the formation of compressive strut in wall panel between the floor slabs. Yielding of the slab and wall reinforcement adjacent to the wall-slab junction region, occurs simultaneously. It is observed that the reinforcement in the floor slab, which is connected to the shear wall yields first, while the reinforcement in the unconnected slab remains unyielded. The vertical reinforcement in the shear wall region yields mostly at the slab-wall junction region.

4.2.2 Behaviour of EWSC Model

Displacement controlled nonlinear static analysis is carried out on a five storied exterior shear wall - floor slab assemblage (EWSC model) from FSWB4 model for detailed study of the wall-slab junction region. The target lateral displacement is applied in the plane of the shear wall. Figure 4.9 shows salient point for the global response of the EWSC model. The nature of capacity curve for EWSC model is the same as that obtained for FSWB4 model with expectedly less lateral strength. Figure 4.10 shows the propagation of cracks from the initial cracking with subsequent local crushing of concrete up to the final displacement stage.

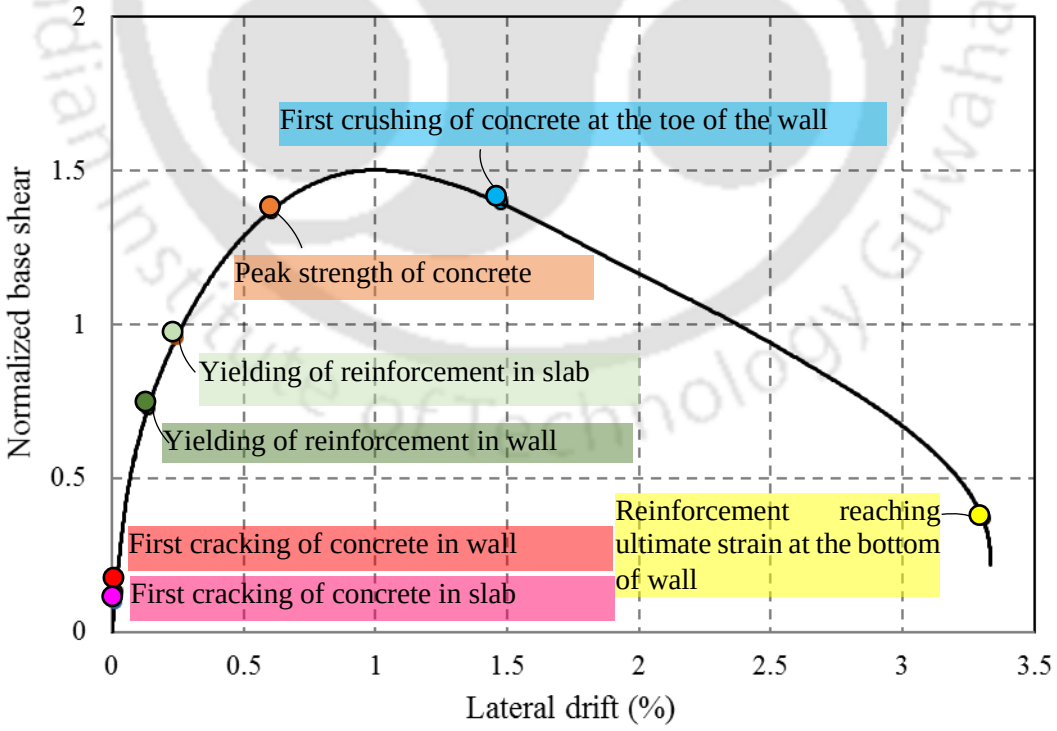

Figure 4.9: Variation of normalised base shear during nonlinear static behaviour of EWSC model.

First cracking starts at the first floor slab at a drift of 0.01%. The cracking of concrete in the shear wall starts at 0.014% drift from the bottom and propagates to the shear wall-slab junction region. The vertical bars on the tension side at the bottom of the wall start yielding at a lateral drift of 0.136%. Also at the same displacement, some of the vertical reinforcement at the first floor shear wall-slab junction region start yielding. The reinforcement in the slab starts yielding at 0.245% drift. Thus significant nonlinear behaviour is observed in wall and slab well before the code specified elastic drift of 0.4%. The crushing of concrete starts in slab-wall junction at a lateral drift of 1.47%.

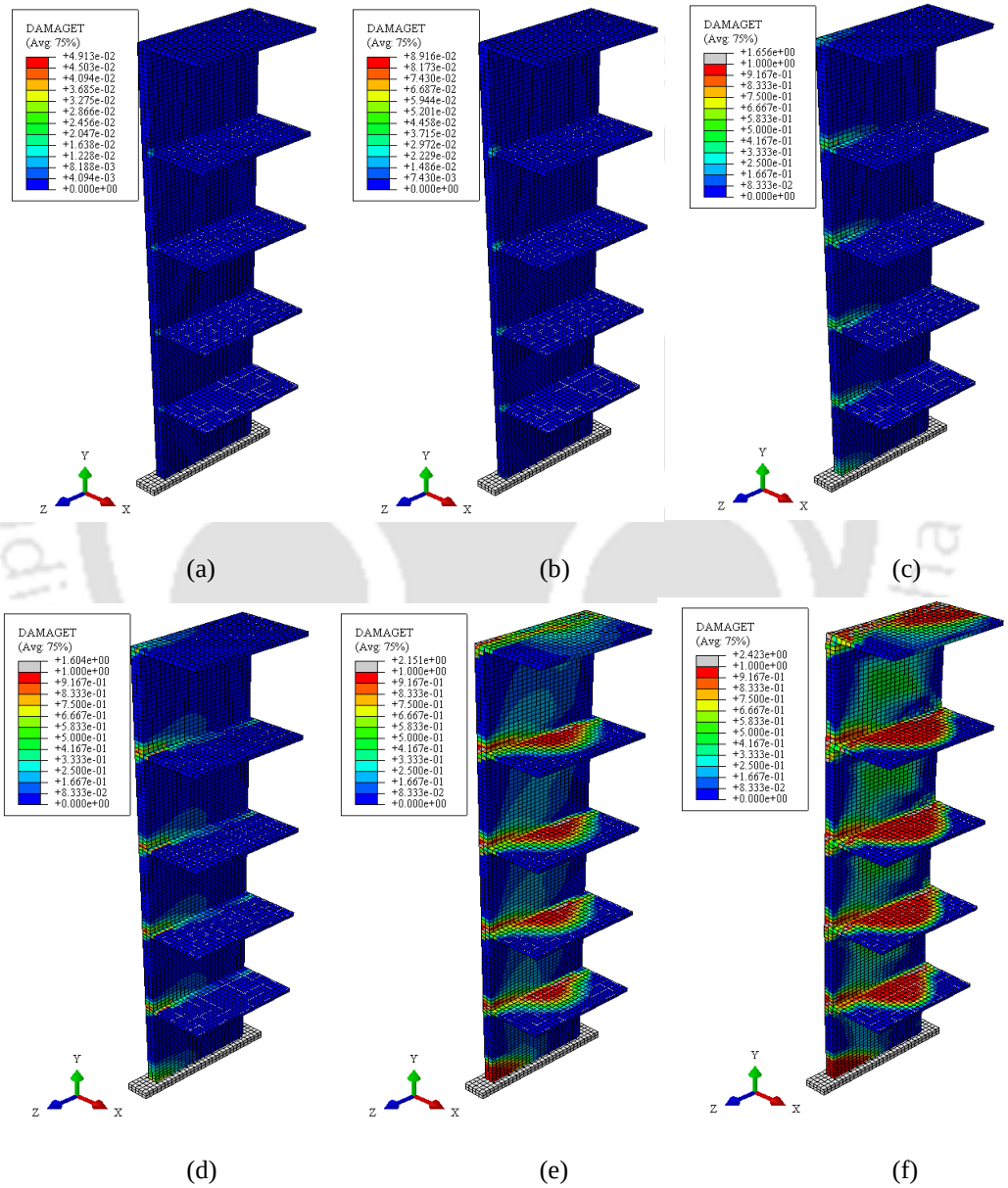

Figure 4.10: Tensile damage pattern for EWSC model at: (a) first cracking in slab, (b) first cracking in wall, (c) yielding of reinforcement in wall, (d) yielding of reinforcement in slab, (e) crushing of core concrete at slab-wall junction and (f) final stage.

Due to the presence of floor slab, a diagonal compressive strut develops in the wall panel between two successive floor slabs. Thus, the wall panels between the floor slabs behave similar to squat walls. The floor slab significantly modifies the behaviour of the slender wall by partitioning it into squat wall panels. The diagonal struts tend to concentrate the damage at the wall-slab junction regions. As the floor slabs provide diaphragm action in actual buildings, EWSC model aims to investigate possible damages in such slab diaphragm. The peak lateral strength of EWSC model is reached at a lateral drift of 1%.

The behavior of the junction between the shear wall and floor slab has been studied by observing the stresses in the steel reinforcement, equivalent plastic strain and tensile damage pattern. Concentration of compressive stresses is observed to be higher at the slab-wall junction as compared to that at the base of the wall. Similar results were observed in the experimental study carried by Ile and Reynouard (2004). Deformation in individual bar at wall-slab junction also leads to concentration of stresses. Stresses in the longitudinal reinforcement of the slab start reaching the yield values from the face of the wall and extend linearly to the edge support. The stresses in the longitudinal reinforcement of shear wall remain constant over the wall panels along the height of the wall except in the junction region. In the shear wall – slab junction region, most of the vertical reinforcing bars are yielded. The maximum tensile damage is observed in the shear wall-slab junction region and spreads diagonally between the two adjacent floor slabs concentrating the stresses at the corners. Flexural shear cracks are formed in the slab at the junction with the shear wall (Pantazopoulou and Imran, 1992). In addition, major cracks develop on the tension side of the slab from the face of the shear wall.

4.2.3 Comparison of FSWB and EWSC Models

The equivalent plastic strain values for FSWB and EWSC model are compared at different displacement level. To compare the behaviour of vertical reinforcement in EWSC and FSWB, the variation of plastic strain value in the reinforcement across the length of wall at the first floor level is shown for 3.33% and 5% lateral drift in FSWB model and 3.33% lateral drift for EWSC model (Figure 4.11a). Comparing the values of equivalent plastic strains for EWSC and FSWB model, it is observed that the strain variation is following similar pattern at 3.33% lateral drift. Also, the strain values are observed to be almost the same in the reinforcement for both the models at that displacement level. Figure 4.11b shows comparison of the variation in the equivalent plastic strain in the top longitudinal reinforcement of floor slab from the face of the wall for EWSC and FSWB models. The tensile strains develop in the reinforcement up to 3.33% drift from the face of the wall. At 3.33% lateral drift, the strain values are observed to be almost similar for both the models.

Based on the same plastic strain values in reinforcement and formation of strut in partitioned wall panels, it can be concluded that EWSC model can be conveniently used for studying the behaviour of wall-slab junction instead of the more detailed FSWB4 model. Use of EWSC model will lead to significant reduction in computational effort. EWSC model is considered in further study to carry out the parametric study by varying the design parameters.

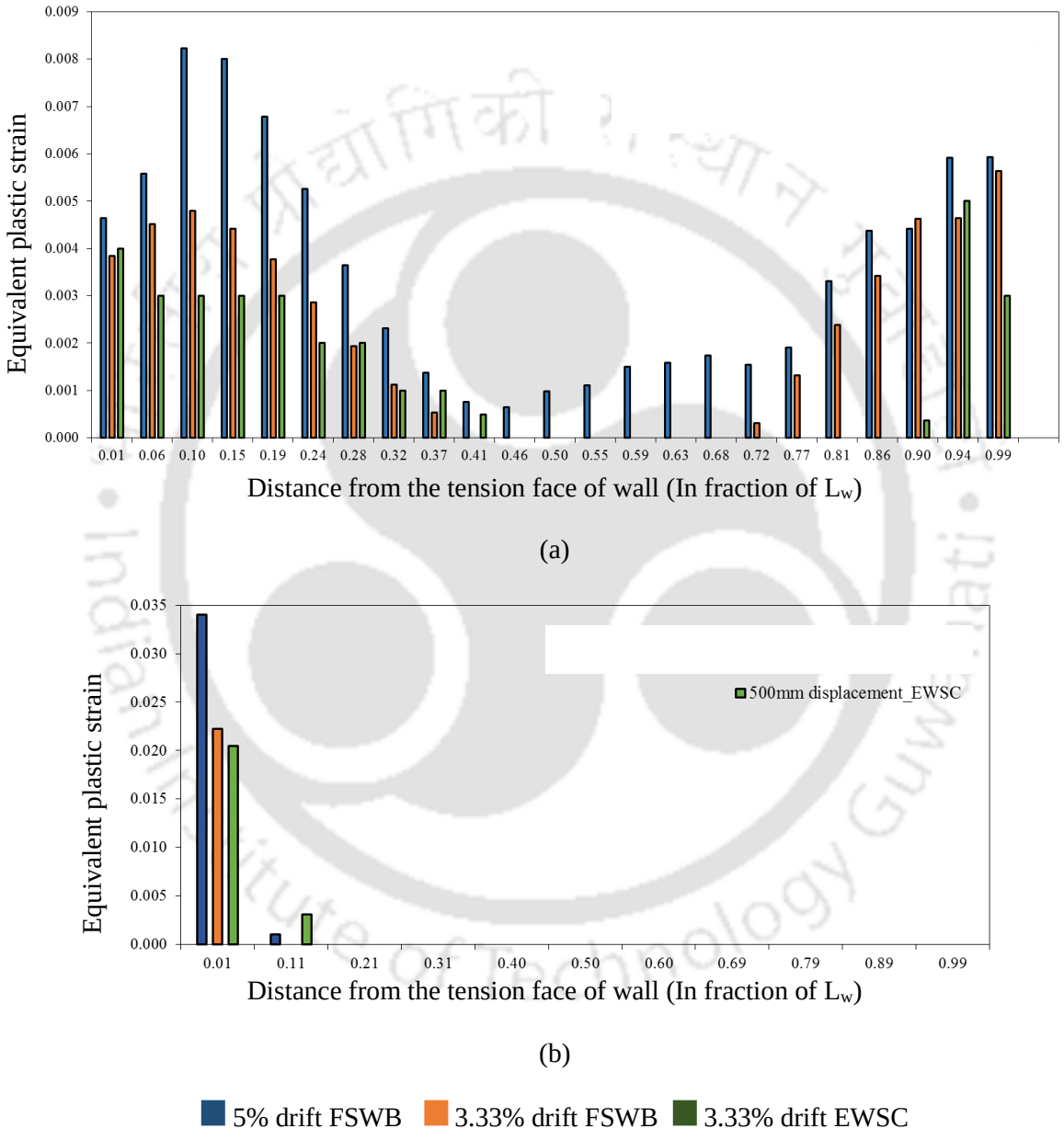

Figure 4.11: Comparison of equivalent plastic strain at first floor level of EWSC and FSWB: (a) in vertical reinforcement of the wall and (b) in longitudinal reinforcement of slab.

4.2.4 Comparison of EWSC and SSW Models

In practice, the shear wall in a multistoried building is analyzed and designed as an isolated slender wall. To investigate the influence of slab on the behaviour of shear wall, the behaviour of SSW model is compared with that of EWSC model. For SSW model, displacement-controlled nonlinear static analysis is carried out with the total target displacement applied at the top level. Although the overall capacity curve has the same trend as that of EWSC model (Figure 4.12), the salient points are discussed. It is observed that after achieving the peak strength, the model exhibits a gradual loss of lateral strength. The peak lateral strength of the entire wall is achieved at a lateral drift of 0.77% whereas, for EWSC model it is at a lateral drift of 1%. First cracking of concrete started at the early drift of 0.05% whereas, in case of EWSC model the cracking of concrete in the shear wall starts at 0.014% drift due to the presence of slab at each floor level. The vertical bar on the tension side of the wall started yielding at a lateral drift of 0.31% at the top. The peak compressive strength of concrete in wall is achieved at 0.66% lateral drift for SSW model. The vertical reinforcement of the wall does not reach its ultimate strain value, thus some reserve capacity remains in reinforcement. The first crushing of concrete occurs at the toe region of the wall when the lateral drift is 1.66% and 1.47% for SSW and EWSC models respectively.

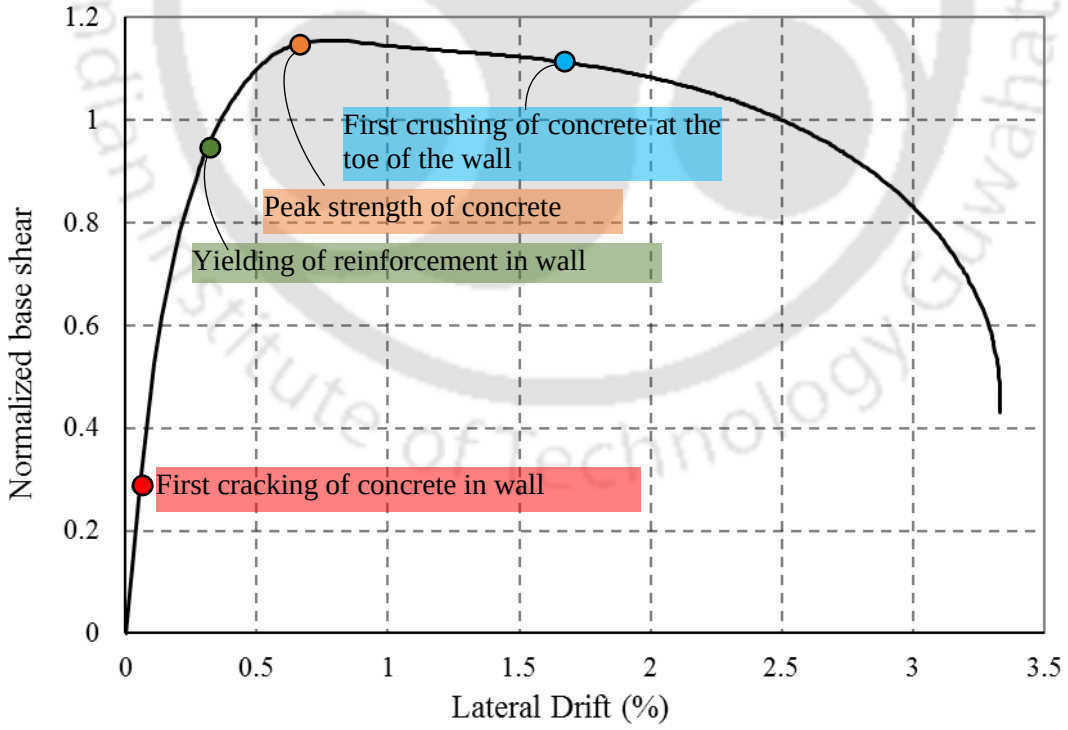

Figure 4.12: Variation of normalised base shear during nonlinear static behaviour of SSW model.

The maximum plastic equivalent principal strains also represent the onset of possible cracks in finite element analysis. The comparison of tensile damage pattern for SSW and EWSC models are shown in Figure 4.13a. The reduction in the lateral strength of the wall is mainly due to compressive crushing of concrete at the toe of the wall. The compressive damage pattern for both SSW and EWSC is shown in the Figure 4.13b. The tensile damage pattern follows the same trend as that of cracking pattern. The face of the shear wall which is under tension experiences the tensile damage first. The damage starts from the base of the wall and propagates vertically upward until the maximum displacement is reached. Longitudinal stresses in horizontal reinforcement are not significant. Figure 4.14 represents the plastic strain in the vertical reinforcement of the wall at the height of 3m from base (first floor level). The equivalent plastic strain value is more in case of SSW model as compared to EWSC, as the isolated shear wall displaces more in flexure. The maximum value is at the tension face and linearly decreasing with increase in distance from the tension face. In case of EWSC model, the equivalent plastic strain is observed at the compression edge also due to the presence of floor slab.

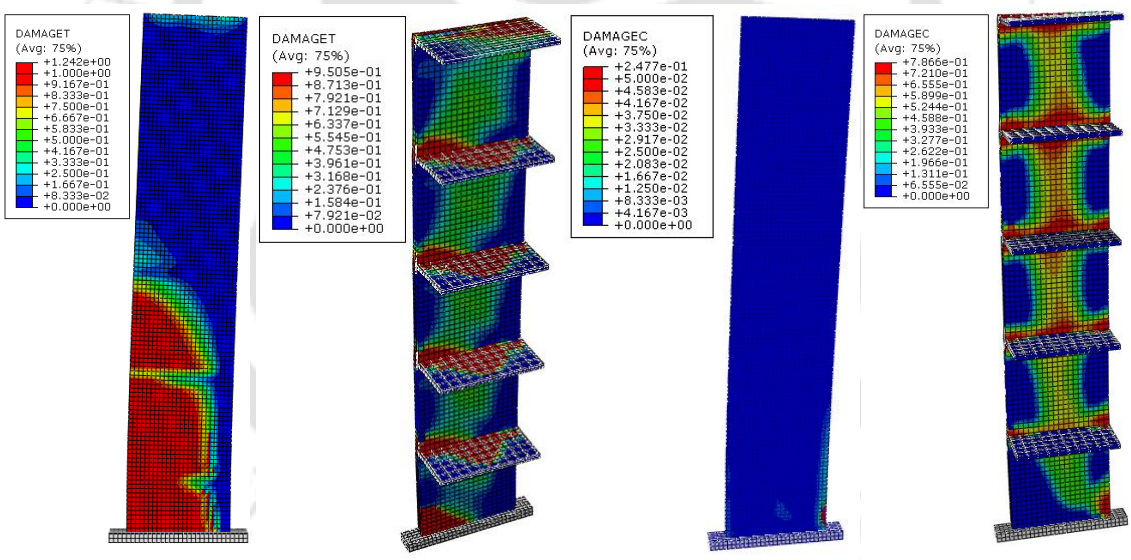

(a) (b)

Figure 4.13: Comparison of response of SSW and EWSC models at maximum drift level: (a) tensile damage pattern and (b) compressive damage pattern.

4.3 SUMMARY AND CONCLUSIONS

In this chapter, the finite element analysis of five different models are carried out to study the behavior of shear wall - floor slab junction. These consists of one ten-storied building, three five-storied building with different characteristics (FSWB models) and one shear wall-slab sub-assemblage (EWSC model). Further, one isolated slender shear wall model (SSW) is also analyzed to study the influence of slab on the behaviour of wall.

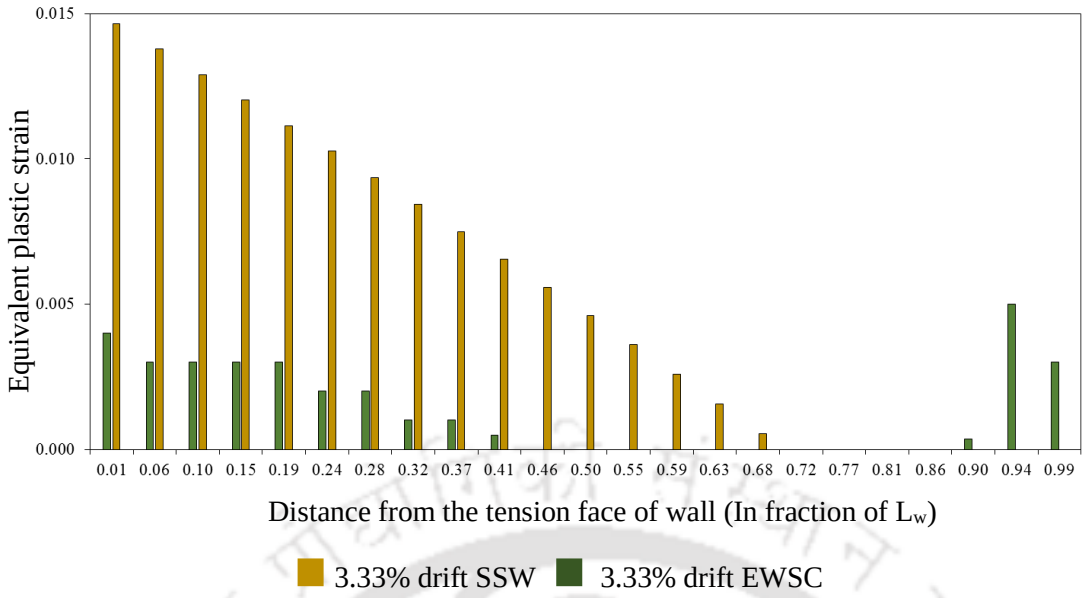

Figure 4.14: Variation of equivalent plastic strain in vertical reinforcement for SSW and EWSC models.

Conventionally, slender shear walls in multistoried buildings are designed in the same way as isolated shear walls. However, due to the presence of slabs, lateral stiffness of wall tends to increase at each slab-wall junction. Thus, the slender wall gets partitioned into a number of smaller panels between successive floor slabs. Each such panel behaves as a squat wall with the formation of diagonal strut between two successive slab-wall junctions. This is observed for both EWSC and FSWB models in the current study. Thus, the design methodology should consider strut formation and associated failure modes for slender walls in multistoried buildings with floor slabs. The strut formation leads to further propagation of damage in the floor slab as observed in EWSC model. Conventionally, beams, columns and structural walls are designed to undergo desired levels of damage during strong earthquake shaking. Floor slabs are not expected to undergo any seismic damage. However, the portion of the floor slab connected to the walls undergoes significant damage at higher levels of lateral displacement (as observed from the behaviour of EWSC and FSWB4 models). Significant damage at slab-wall junction may also lead to formation of sliding shear crack across the wall. Any damage in slab is also difficult to repair as compared to the damages in beam, column or structural wall. Thus, a new design methodology involving prevention or reduction of damage in slab needs to be evolved.

The finite element analysis results confirm that the maximum stress concentration develops at the base of the shear wall (EWSC) first and then propagates to the upper floor level at the junction. Also, the developed tensile damage and the stresses are higher in the portion of the slab connected

to the shear wall. The slab panels not connected to the wall experience less strain and damage. The behaviour of the shear wall slab assemblage (EWSC), with respect to maximum tensile stresses and tensile damage, is in good agreement with the five storied building model (FSWB).

The finite element analysis also shows the formation of maximum stress concentration at the base of the wall for both EWSC and SSW models. Due to the presence of slab, stress concentration propagates to each slab-wall junction sequentially at upper levels in the EWSC model. However, in all FSWB models, stress concentration is formed at first floor slab-wall junction. Although stress concentration is observed to propagate at slab-wall junction in EWSC and in all FSWB models, crushing of concrete occurs first at the toe of the wall for both the models. This is because of extremely large stress concentration at that location due to combination of flexural compression and diagonal compression in bottom panel. This observation also confirms the formation of diagonal strut and partitioning of slender wall into squat wall panels. Thus, an overall seismic design methodology for damage avoidance behaviour of floor slabs in multistoried RC frame-wall building needs to be evolved.

The results of the different analytical studies carried out in this chapter show that the EWSC can be conveniently used as the model to successfully predict the response of the structure. Therefore, further studies will consider only EWSC model to understand the behaviour of wall-slab junction.

Chapter 5
ANALYSIS OF WALL-SLAB ASSEMBLAGE: A PARAMETRIC STUDY

5.1 OVERVIEW

In highly seismic regions, slender reinforced concrete (RC) structural wall is commonly used in high-rise buildings as a primary lateral load resisting element. These walls are very effective in limiting the lateral drift of the building due to their large in-plane stiffness. However, presence of floor slabs influences the behaviour of the shear wall. Also, the current design requirements for RC shear walls do not account for the presence of floor slabs. To understand the behavior of wall-slab junction and to address the shortcomings of the current design requirements, the influence of two parameters, namely (a) aspect ratio and (b) longitudinal reinforcement ratio on the behavior is studied analytically. The present chapter presents the detailed investigation of the influence of floor slab on the behaviour of shear wall. An exterior shear wall - slab assemblage from a multistoried building is considered to carry out nonlinear static analysis.

The ESWC models analyzed in Chapter 4 are considered for carrying out the parametric study and investigate the damage pattern at the wall-slab junction region under in-plane loading. For the different slender shear wall-floor slab specimens, the amount of vertical reinforcement and the wall length are varied. Using finite element analysis of the specimens, stresses and damage patterns are monitored in wall, slab and at the shear wall-slab junction to observe the possible failure modes in both wall and slab. The results highlight the requirement of changes in seismic design methodology of RC wall, slab and wall-slab junction.

5.2 DESCRIPTION OF THE ASSEMBLAGE STUDIED

Considering different aspect ratios and vertical reinforcement ratios of the shear wall, eight different models (Table 5.1) are analyzed in the present study. Two different vertical reinforcement ratios, namely (a) 0.25% and (b) 3% in the shear wall are adopted in the analysis in order to investigate the damage pattern in the floor slab. As tensile damage in the slab may extend beyond the ends of the wall on either sides (Figures 3.11c and 3.12c), floor slabs in all the models except WSC1 and WSC5 have been extended on both sides of the shear wall. It is observed that an extension of slab by a length $L_w/4$ (where L_w is the length of the wall) on either side of the wall, is sufficient to capture the

possible extent of damage in the slab. The specimens WSC1, WSC2, and WSC3 are identical except for the length of the slab and the wall. Similarly, WSC5, WSC6 and WSC7 are identical except the length of the slab and the wall. WSC1 and WSC5, WSC2 and WSC6, WSC3 and WSC7, and WSC4 and WSC8 are identical except for the vertical reinforcement ratio in the wall. WSC4 and WSC8 differ from all other specimen in height. These walls are more slender as compared to the other models. Bars of 8 mm diameter are used at 150 mm spacing as vertical reinforcement in WSC1, WSC2, WSC3 and WSC4. While WSC5, WSC6, WSC7 and WSC8 are reinforced with 28 mm diameter bars at 130 mm spacing in vertical direction, 8 mm diameter bars are used at 150 mm spacing as horizontal reinforcement in all the models. The thickness of wall, thickness of slab and length of slab are considered as 300 mm, 120 mm and 1500 mm, respectively.

Table 5.1: Specifications of the models used in the analysis

Model Configuration	WSC1	WSC2	WSC3	WSC4	WSC5	WSC6	WSC7	WSC8
Wall length (mm)	3000	3000	6000	3000	3000	3000	6000	3000
Wall height (m)	15	15	15	25	15	15	15	25
Vertical reinforcement ratio	0.25%	0.25%	0.25%	0.25%	3%	3%	3%	3%
Vertical bars	8@150	8@150	8@150	8@150	28@130	28@130	28@130	28@130
Horizontal bars	8@150	8@150	8@150	8@150	8@150	8@150	8@150	8@150
Slab length (mm)	3000	4500	9000	5000	3000	4500	9000	5000

Both shear wall and slab are discretized with eight-noded solid elements having reduced integration characteristics (C3D8R). Two noded linear truss element (T3D2) is used to model the steel reinforcement. The rebars are modelled as embedded region in concrete using constraints in the interaction module, and making concrete the host. The analyzed specimens are the exterior shear wall-floor slab connection under lateral loading applied at the top. The entire height of the wall and half width of floor slab, at every floor level, of the five storey frame-shear wall building (Kaushik and Dasgupta, 2013) is considered for simulation. The translational and rotational Degrees of Freedom (DoFs) are restrained at the bottom nodes of the wall for all the specimens. At the end of the slab, all DoFs are restrained except in-plane displacement and rotations θ_x and θ_z. The out-of-plane bending of the shear wall and the vertical bending of slab are restrained. Mesh convergence study is carried out for the WSC1 model. Three different mesh sizes (75 mm, 100 mm and 150 mm) are adopted in the analysis of shear wall-floor slab connection in order to investigate the mess sensitivity of the model. Details of the mesh convergence study is given in Chapter 3. For all subsequent analyses, the mesh size of 150 mm is adopted.

Concrete Damage Plasticity (CDP) model is used to assign concrete properties (as discussed in Chapter 3). The steel reinforcement in wall and slab is modeled using theplasticity model in the

finite element program. The material properties of the M25 grade concrete and HYSD Fe415 steel are shown in Table 3.1. The reinforcement is obtained in the wall and slab by considering the design load combinations as per Indian Standard of earthquake resistant design (BIS, 2016b). The detailing of reinforcement in shear wall and continuous floor slabs is done as per Indian Standard (BIS, 1987). The detailing of steel reinforcement at the shear wall - slab junction is already explained in Chapter 3. For shear walls, the reinforcement is provided along the horizontal and vertical directions in two layers.

Displacement-controlled nonlinear static analyses of the eight models described in Table 5.1 are carried out using Newton-Raphson method. For 15 m height of wall, code specified elastic drift limit (BIS, 2016b) comes out to be 60 mm. However, as the study is intended to capture the possible nonlinearities and the associated damage in wall-slab assembly, significantly higher values of lateral displacement have been considered. The lateral displacement of 500 mm is applied at one of the top node in the plane of the shear wall (Figures 5.1a and 5.1b). Along with the target lateral displacement of 500 mm, a triangular variation of displacement distribution is considered along the height of the wall (Figure 5.1c). It is observed that the pattern of displacement distribution along the height of the walls does not affect the nonlinear response of the slab-wall assemblage significantly. The gravity loads (both dead and live loads) on slab are assigned as pressure loads on the surface of the solid elements. The behavior of the junction between the shear wall and floor slab has been studied by observing the stresses in the steel reinforcement, plastic strain, minimum principal stress, tensile damage and compressive damage patterns.

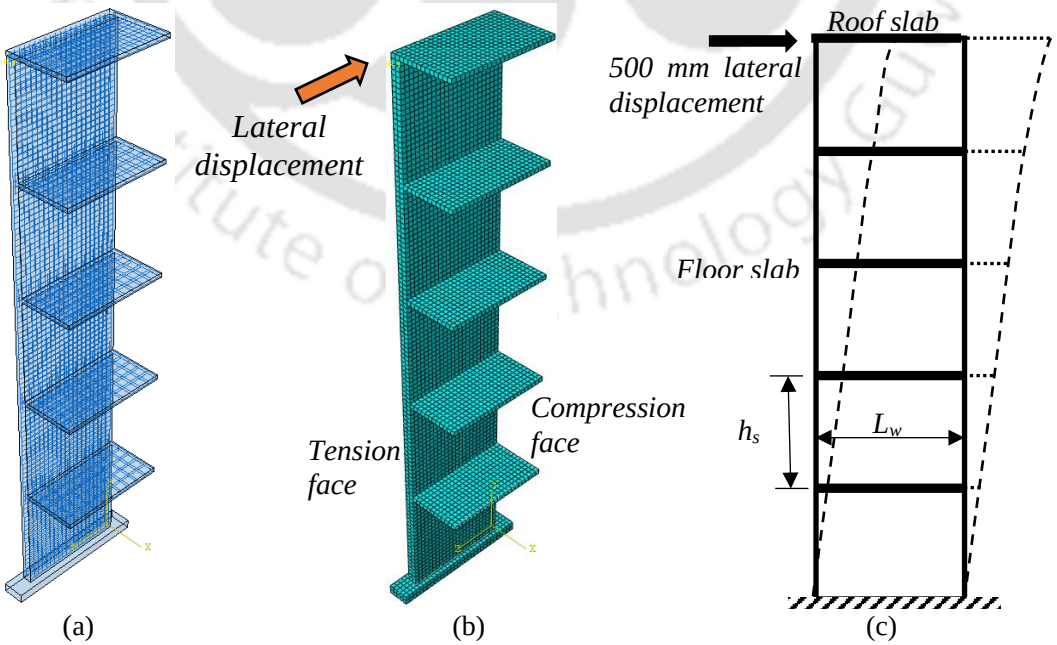

Figure 5.1: Finite element model of WSC1 specimen: (a) steel reinforcement, (b) applied lateral displacement and (c) triangular variation of displacement.

5.3 RESPONSE OF SHEAR WALL - SLAB ASSEMBLAGE

The response of shear wall-slab assemblage for displacement controlled nonlinear static analysis is presented in this section.

5.3.1 Shear Force - Drift Relationship

For all the models, the variation of base shear capacity (normalized with respect to self-weight) with lateral drift is obtained by carrying out nonlinear static analyses (Figure 5.2) and the results are summarized in Table 5.2. A few salient points are also indicated on the capacity curves of the respective models. The failure modes such as: (a) yielding of vertical reinforcement in wall, (b) yielding of reinforcement in slab, and (c) crusing of concrete have been studied. For WSC1, the model with vertical reinforcement ratio of 0.25% in shear wall, the first cracking of concrete occurs in the slab near the junction region at a drift of 0.02%. The cracking of shear wall starts at the bottom tension face at a lateral drift of 0.05%. Yielding of vertical reinforcement at the bottom tension face of shear wall occurs at a drift of 0.13%. The reinforcement in the slab at the junction region yields at a drift of 0.2% and the maximum lateral load capacity is reached at a drift of 1.19% (Figure 5.2a).

Table 5.2: Comparison of salient points for shear force - drift relationship of different models

Model	Maximum normalized base shear	First cracking of concrete in wall		First cracking of concrete in slab		Yielding of vertical reinforcement in wall		Yielding of reinforcement in slab	
		Drift (%)	Normalized shear	Drift (%)	Normalized shear	Drift (%)	Normalized shear	Drift (%)	Normal-ized shear
WSC1	17.85	0.053	4.18	0.028	2.32	0.130	7.26	0.205	9.21
WSC2	16.85	0.061	4.16	0.029	2.17	0.131	6.79	0.197	8.42
WSC3	21.41	0.061	5.57	0.029	3.07	0.094	7.25	0.155	9.44
WSC4	5.90	0.060	1.61	0.017	0.60	0.318	4.17	0.140	2.68
WSC5	26.39	0.053	5.50	0.028	3.00	0.221	12.43	0.460	17.87
WSC6	25.15	0.105	7.66	0.029	2.80	0.211	11.35	0.401	15.70
WSC7	27.11	0.121	8.67	0.054	5.29	0.191	11.23	0.191	11.23
WSC8	8.38	0.039	1.30	0.017	0.65	0.563	6.76	0.215	4.04

In case of WSC2 model, the floor slabs have been extended on both sides from the face of the shear wall in order to study the spread of damage in the slab along the length of the wall. The maximum lateral load capacity is reached at a drift of 1.22% (Figure 5.2b). The maximum lateral load capacity of WSC2 gets decreased approximately by 7% as compared to WSC1 because of spreading of more damage in the floor slab region. Yielding of vertical reinforcement in the shear wall and horizontal reinforcement in slab takes place at the same drift level as that of WSC1. The cracking patterns in the shear wall and floor slab are observed to be similar to those of WSC1.

WSC5 is similar to WSC1 except for the amount of vertical reinforcement ratio in the shear wall. The maximum load carrying capacity of WSC5 is more as compared to WSC1 due to the higher amount of vertical reinforcement in the shear wall. At a drift of 1.38%, WSC5 reaches its maximum lateral load capacity (Figure 5.2a). The first cracking of concrete in shear wall and floor slab of WSC5 takes place at a drift level same as that for WSC1. In case of WSC5, the vertical reinforcement of shear wall yielded before the yielding of the slab reinforcement at a drift of 0.22%.

The difference in the models WSC6 and WSC2 is the amount of vertical reinforcement present in the shear wall. WSC6 is analysed using 3% vertical reinforcement ratio in the shear wall. At a drift of 1.35%, it reaches its maximum lateral strength. It is observed that the development of first crack in WSC6 takes place at the slab region near the junction of shear wall and slab. The first crack in the floor slab occurs at a drift of 0.02% and that in shear wall at 0.1% drift (Figure 5.2b). The yielding of vertical reinforcement in shear wall occurs at a drift ratio of 0.2%. The reinforcement of the slab in the junction region gets yielded at a drift ratio of 0.4%.

For WSC3, the length of shear wall is increased to twice as that of WSC2. The shear wall behaves more like a squat wall in between the floor slabs. WSC7 is similar to WSC3 except for the amount of vertical reinforcement in the shear wall. Both WSC3 and WSC7 reach their maximum strength at drift levels of 0.99% and 1.06%, respectively (Figure 5.2c). The vertical reinforcement in the shear wall and the horizontal reinforcement in the slab at the junction region starts yielding at the same drift level as that of WSC2. But the lateral load capacities at those drift levels are more than those of WSC2. As the entire wall behaves like an assembly of squat wall panels, the flexural deflections for models WSC3 and WSC6 are less as compared to other models, resulting in the higher maximum lateral load capacity.

The structural parameters of WSC4 and WSC8 are similar to those of WSC2 and WSC6, respectively. The only difference in these models is the height of the slender shear wall. WSC4 and WSC8 are modeled with 0.25% and 3% vertical reinforcement ratios in shear wall, respectively. The maximum lateral strength occurs for WSC4 and WSC8 at a drift of 0.92% and 1.28%, respectively (Figure 5.2d). There is a reduction in the maximum load capacity of these models because of the slenderness of the wall as compared to the other models. Due to the flexural mode of behaviour in slender wall, yielding and crushing of concrete occur earlier than occurrence of those failure modes in a squat wall. In case of squat walls, crushing of concrete under diagonal compression occurs later. Also, in these models, yielding of reinforcement in the slab takes place before the yielding of wall reinforcement. The first cracking of concrete in slab occurs at a very less drift ratio of 0.01%, and at the same drift level, slab reinforcement also gets yielded in both the models. The vertical reinforcement in shear wall at wall-slab junction yields at 0.31% for WSC4

and 0.56% for WSC8 model. The vertical steel of shear wall in WSC8 yields at a higher drift compared to WSC4 due to higher amount of steel. At the wall-slab junction region, the combined effect of in-plane moment of wall and the slab moment cause the yielding of the slab steel first in the tension face of the junction. On the compression face of the junction, the reinforcement in slab region does not yield in tension due to the counteractive nature of the in-plane moment.

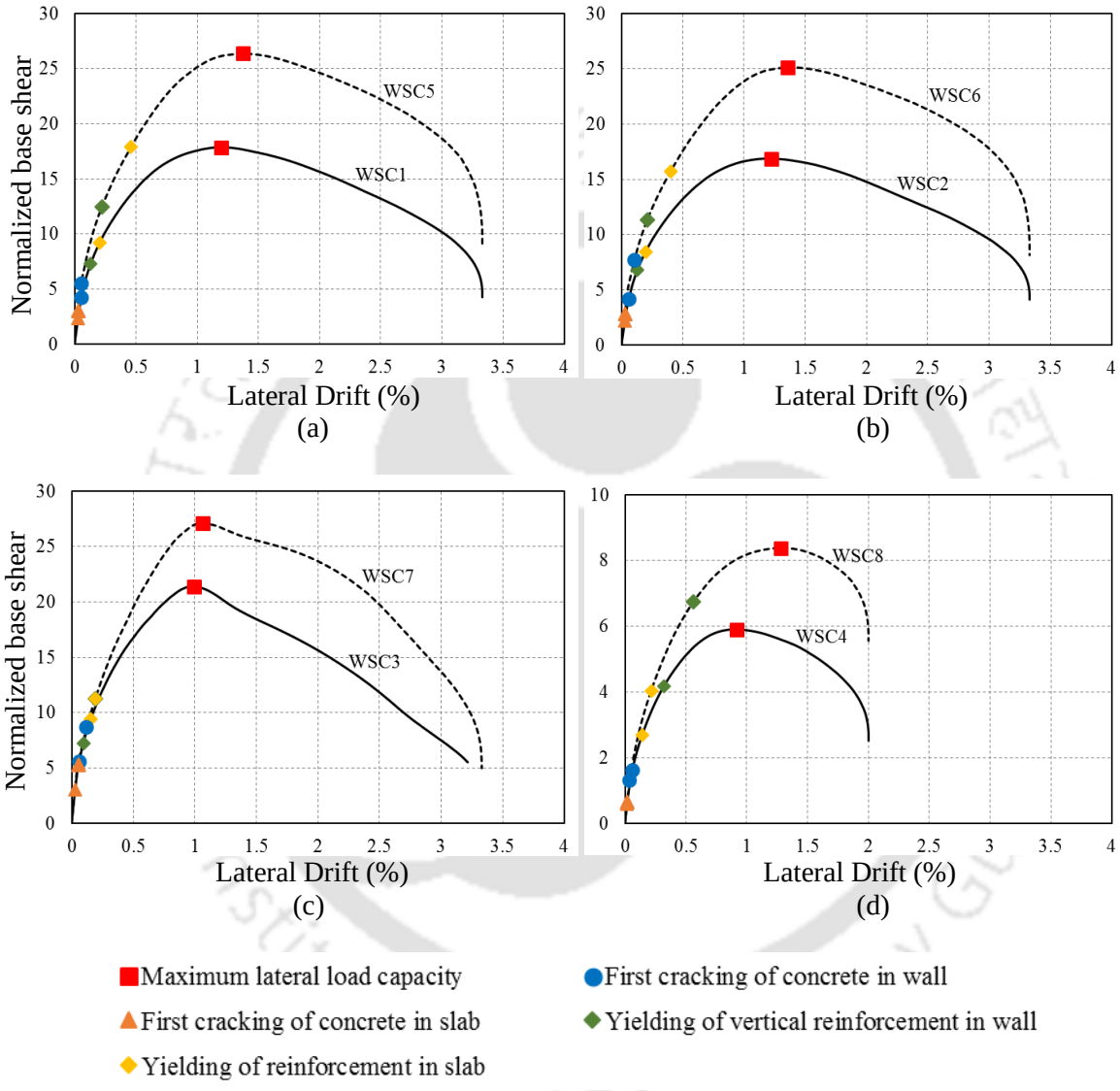

Figure 5.2: Comparison of lateral shear force-drift variation for different wall-slab models: (a) WSC1 and WSC5; (b) WSC2 and WSC6; (c) WSC3 and WSC7; (d) WSC4 and WSC8.

5.3.2 Minimum Principal Stress

Figure 5.3 shows the variation of minimum principal stresses in the shear wall at adrift level of 3.33%, normalized with respect to the characteristic compressive strength of concrete, along the

height (H_w) of wall panel, varying from $0.2H_w$ to the full height of the wall panel. The principal stresses at the tension and compression faces of the wall are more as compared to the values in the middle of the wall. Due to this stress development, the damage is concentrated more at the tension and compression faces. The stresses in the concrete are more due to the high vertical reinforcement ratio in the shear wall. The nearly uniform variation of stresses in the middle of the wall shows the extent of strut formation. Due to the same length of shear wall in models WSC1, WSC2, WSC5 and WSC6, the minimum principal stress have similar pattern at the tension and compression faces (Figures 5.3a and 5.3b). Due to the similar stresses, the lateral load capacity for all the four models are almost similar (Figures 5.2a and 5.2b). For models WSC3 and WSC7, due to the increase in the length of the shear wall, uniform variation of the stresses is observed along the length of the wall and the values are less compared with the other models (Figures 5.3c), due to which, the strut action is not dominant in this case. Due to the large stresses in the models WSC4 and WSC8 (Figure 5.3d), the lateral capacity gets reduced as observed in Figure 5.2d. At a height H_w from the wall-slab junction, i.e., at the bottom of the next upper floor slab-wall junction, the higher stress values reflect the tendency of strut formation. Concrete at those locations fails earlier as compared to the models with squat wall panels.

5.3.3 Propagation of Crack and Damage

The variation of equivalent plastic strain in slab concrete with respect to the lateral drift is obtained at different locations along the wall-slab junction (Figure 5.4). Since the maximum equivalent plastic strain reflects the trend of crack formation, the tendency of crack formation in slab concrete in the different models is also obtained.

For WSC1, WSC2, WSC5 and WSC6 models (Figures 5.4a and 5.4b), almost similar cracking patterns are observed due to the same aspect ratios of the wall panels. The plastic strain values for 3% vertical reinforcement ratio are less as compared to the values obtained for 0.25% steel ratio, leading to less cracking in the junction region. The vertical reinforcement at the tension face of the shear wall starts yielding first resulting in the high plastic strain concentration.

It is observed that the plastic strain value reduces with increasing distance from the tension face of the wall. The web portion of the shear wall experiences less strain and the strain increases in small amount at the compression face. The plastic strain values increase with the drift as the cracks start propagating from the tension face of the shear wall. Cracking of concrete starts at the base of the shear wall and propagates up to the wall-slab junction. Due to the presence of the floor slab, a diagonal strut develops in the wall panel between two successive floor slabs, thus, the slender wall gets partitioned into a number of squat wall panels between the floor slabs.

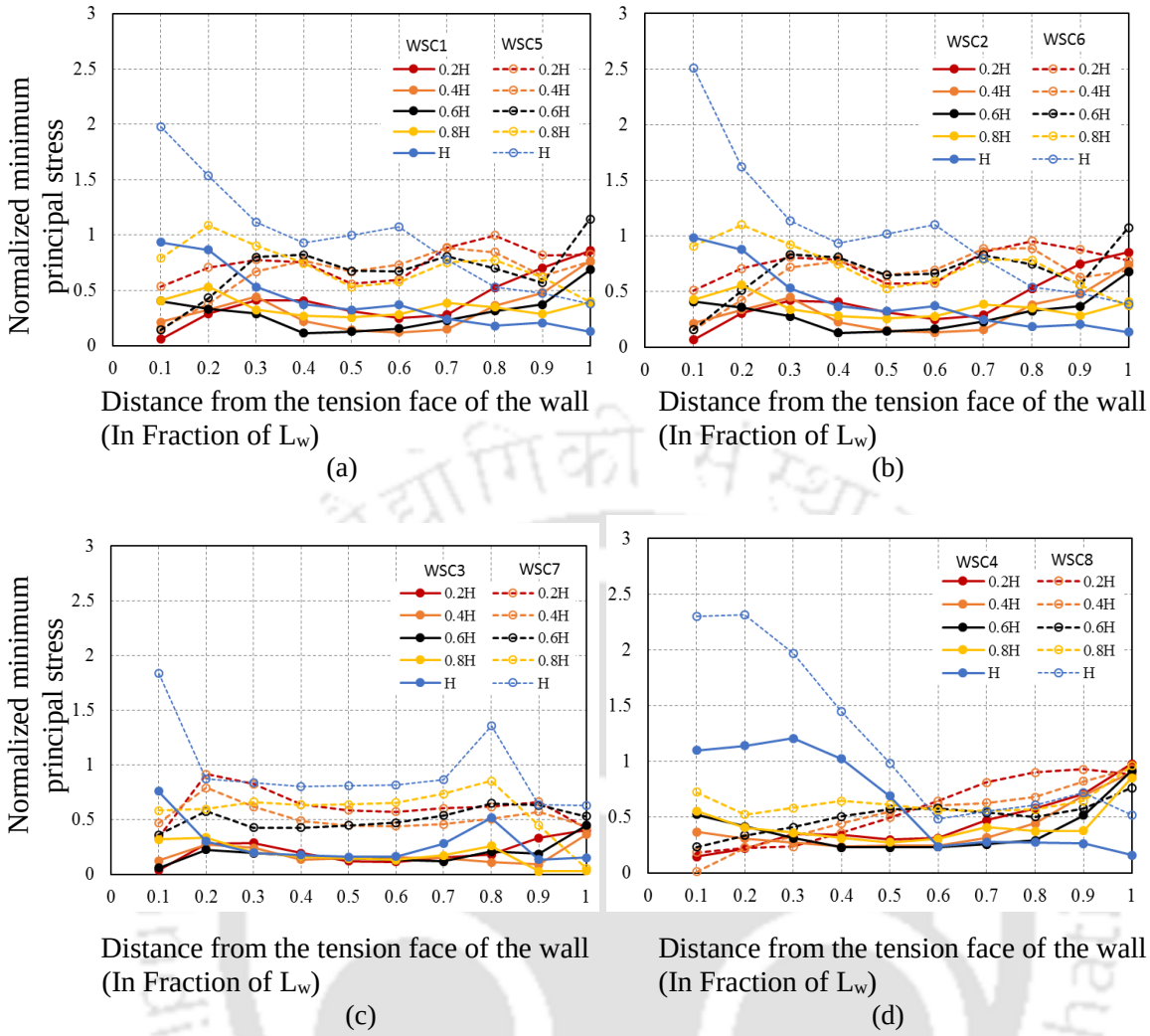

Figure 5.3: Variation of minimum principal stress in shear wall: (a) WSC1 and WSC5; (b) WSC2 and WSC6; (c) WSC3 and WSC7; (d) WSC4 and WSC8.

For WSC3 and WSC7 (Figure 5.4c) models, squat wall behaviour is observed due to the low aspect ratio of those specimens. Maximum cracking is observed in the floor slab at the two ends of the wall-slab junction region. In this case also, the strut action spreads over a large region in the wall panel due to lower aspect ratio. Since the length of the shear wall is more, cracks do not propagate till the middle of the slab for low drift ratios. Though plastic strain values in the middle portion of the slab increase after 0.75% drift, the maximum values are observed at the two ends of the wall-slab junction.

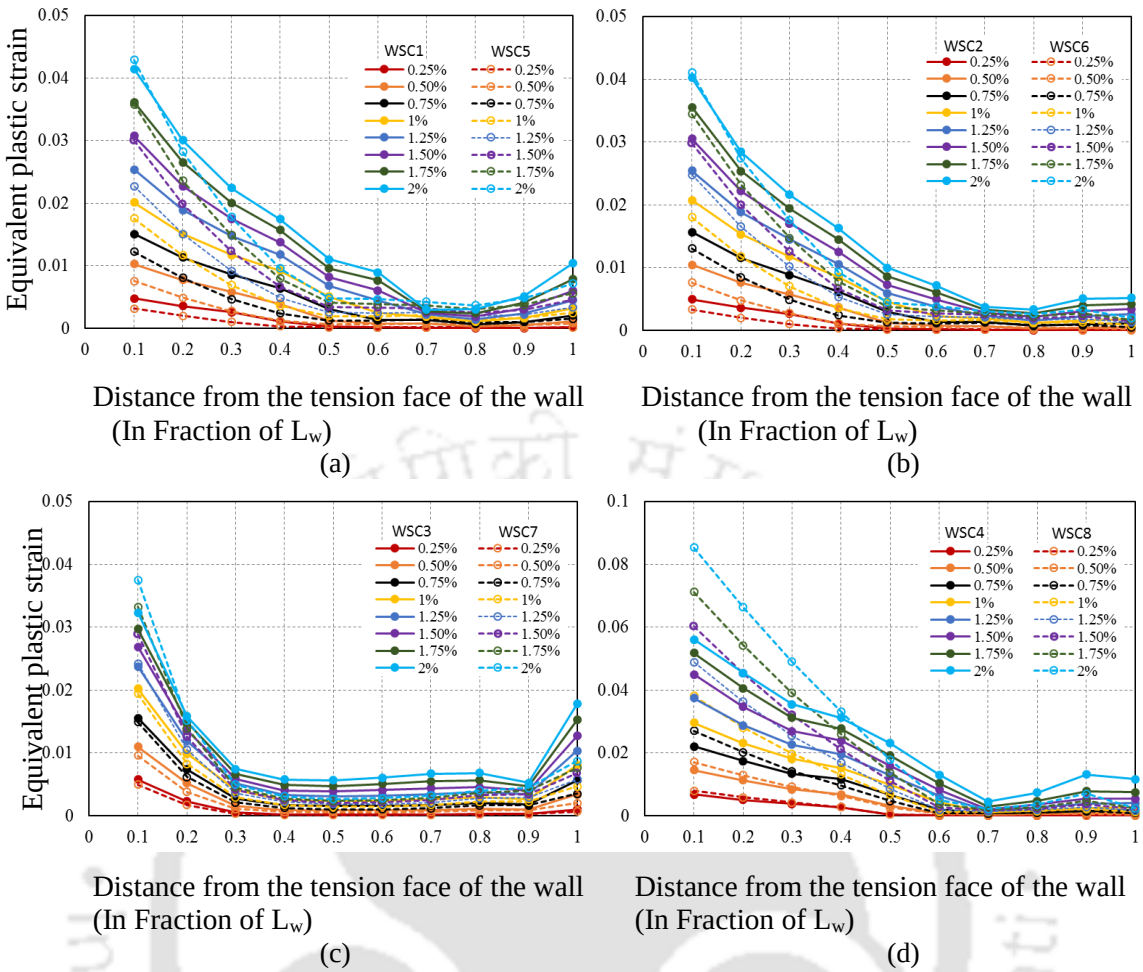

Figure 5.4: Comparison of equivalent plastic strain in slab along the length of shear wall: (a) WSC1 and WSC5; (b) WSC2 and WSC6; (c) WSC3 and WSC7; (d) WSC4 and WSC8.

For WSC4 and WSC8 (Figure 5.4d), the plastic strain values are maximum as compared to the other models leading to a large number of cracks at the tension face of the wall and also in the floor slab. It is concluded that the aspect ratio and the reinforcement ratio significantly affect the damage propagation and the load carrying capacity. Specimen with lower reinforcement ratio tends to develop more cracks in the junction region. After a drift level of 0.5%, the equivalent plastic strain in concrete at the shear wall-slab junction along the length of the wall exceeds the crushing strain of concrete (0.01). This may lead to the development of a major sliding shear crack across the wall-slab junction in the plane of the wall. The sliding cracks can further result in the formation of compressive strut in wall panel between the floor slabs.

Higher values of compressive stresses are observed at the wall-slab junction as compared to those observed at the base of the wall. Similar results were observed in the experimental study carried by Ile and Reynouard (2004). Deformation of individual bar at wall-slab junction also leads to

concentration of stresses. Stresses in the longitudinal reinforcement of the slab reach the yield values starting from the face of the wall and extend linearly to the edge support. In the shear wall-slab junction region, most of the vertical reinforcing bars get yielded. The maximum tensile damage is observed in the shear wall-slab junction region and spreads diagonally between two consecutive floor slabs concentrating the stresses at the corners. Flexural shear cracks are formed in the slab at the connection with the shear wall (Pantazopoulou and Imran, 1992). In addition, major cracks develop in the slab at the tension face of the wall-slab junction.

Figures 5.5 and 5.6 show the propagation of cracks from the initial cracking to the crushing of concrete up to the final displacement. The cracks in the shear wall start from the bottom and propagate to the shear wall-slab junction region. However, at wall-slab junction, first cracking starts at the first floor slab and then in the shear wall. The vertical bars on the tension side at the bottom of the wall start yielding for all the models. Also at the same displacement level, some of the vertical bars at the first floor shear wall-slab junction region start yielding. Since the yielding of reinforcement in the shear wall and floor slab starts at a very low drift ratio, significant nonlinear behavior is observed in wall and slab well before the code specified elastic drift of 0.4% (BIS, 2016b). The crushing of concrete is observed to initiate in wall-slab junction at a lateral drift of 1.47% for WSC1 and WSC2 and at 1.6% for WSC5 respectively. Due to the presence of floor slab, a diagonal compressive strut develops in the wall panel between two successive floor slabs similar to squat wall behaviour. Thus, the floor slab significantly modifies the behavior of the slender wall by partitioning it into squat wall panels.

Comparing WSC1, WSC2 and WSC5 models at different drift ratios, it is observed that with higher reinforcement in WSC5, the patterns of cracking and tensile damage are completely different as compared to the other two models. The damage does not spread significantly in the floor slab for WSC5, whereas, in case of WSC1 and WSC2, diagonal struts tend to concentrate the damage at the wall-slab junction regions along with considerable propagation of damage in the slab panel (Figure 5.5). These models are compared since the length of the wall is same in all of them.

Lateral drift (%)	Tensile damage pattern		
	WSC1	WSC2	WSC5
0.5	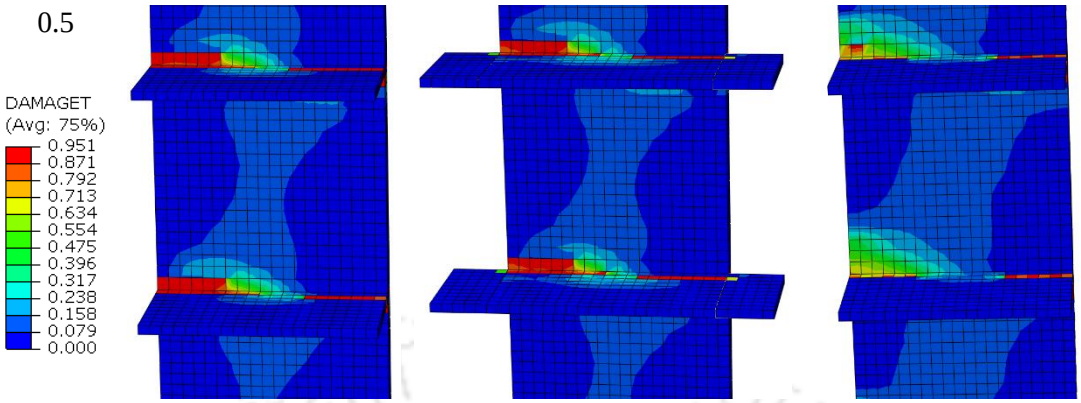		
1.0	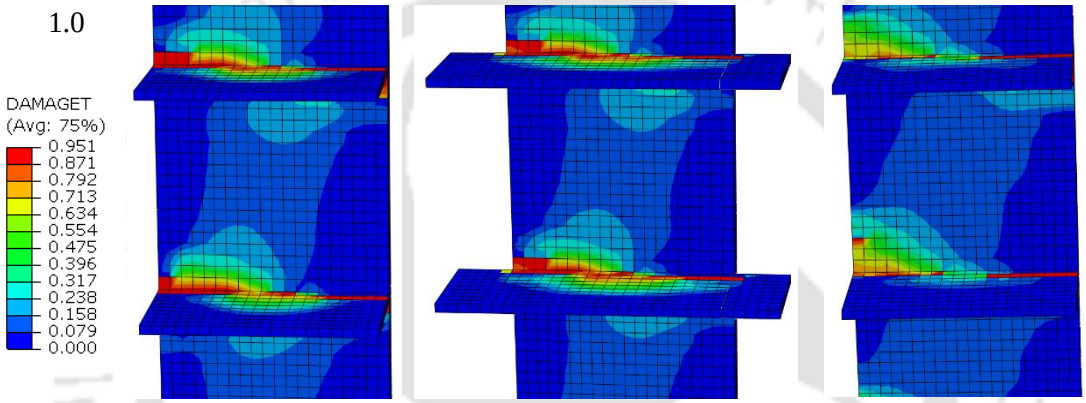		
1.5	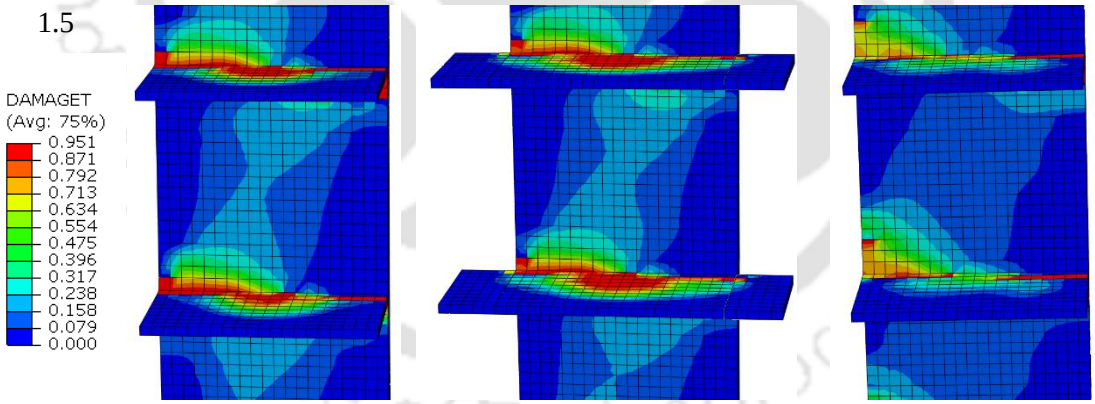		
2.0	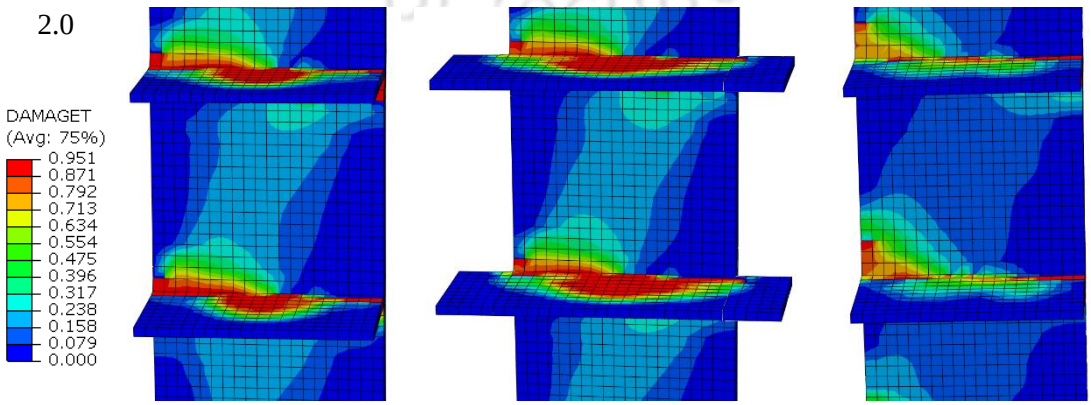		

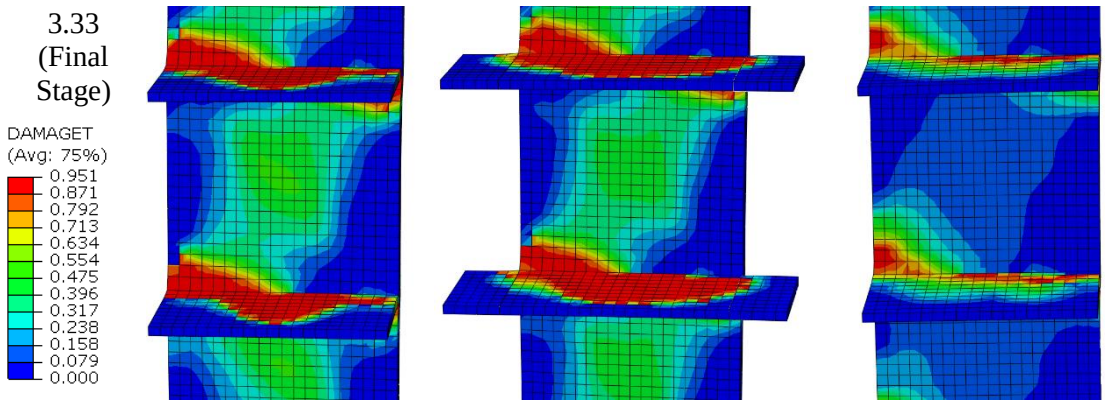

Figure 5.5: Variation of tensile damage with lateral drift level in WSC1, WSC2 and WSC5 models.

Comparing the pattern in WSC2, WSC3 and WSC4 models, it is observed that the formation of strut is more prominent in case of WSC2. All these models are compared as they are having the same reinforcement ratio but different aspect ratios. WSC3 model is more squat and WSC4 model is more slender than WSC2 model. Comparing the propagation of damage in the slab and the wall at different drift levels, it is observed that the maximum level of damage is attained faster in case of slender wall model (WSC4). Less damage propagation is observed in squat wall model (WSC3). It is observed that the slab reinforcement connected to the shear wall, along the length of wall, yields first, while the reinforcement in the extended slab region remains unyielded. The vertical reinforcement in the wall yields mostly at the wall-slab junction region.

Also, it is observed from the cracking pattern and tensile damage pattern that maximum cracks are developed in the slab panels connected with shear wall. The extended part of floor slab panels, not connected with shear wall, experiences less cracks and very less damage. Conventionally, slender shear wall in multi-storied buildings is designed in the same way as an isolated shear wall. However, due to the presence of slabs, lateral stiffness of wall tends to increase at each wall-slab junction. Thus, the slender wall gets partitioned into a number of smaller panels between successive floor slabs. Each such panel behaves as a squat wall with the formation of diagonal strut between two successive wall-slab junctions as observed for WSC1 and WSC2 models. Thus, the design methodology for slender walls in multistoried buildings with floor slabs need to consider strut formation and the associated failure modes in the partition wall panels.

Lateral drift (%)	Tensile damage pattern		
	WSC2	WSC3	WSC4
0.5	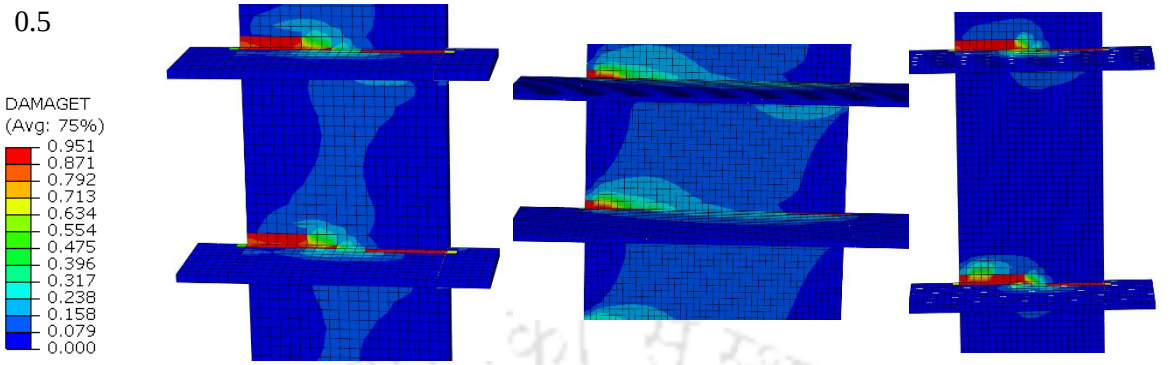		
1.0	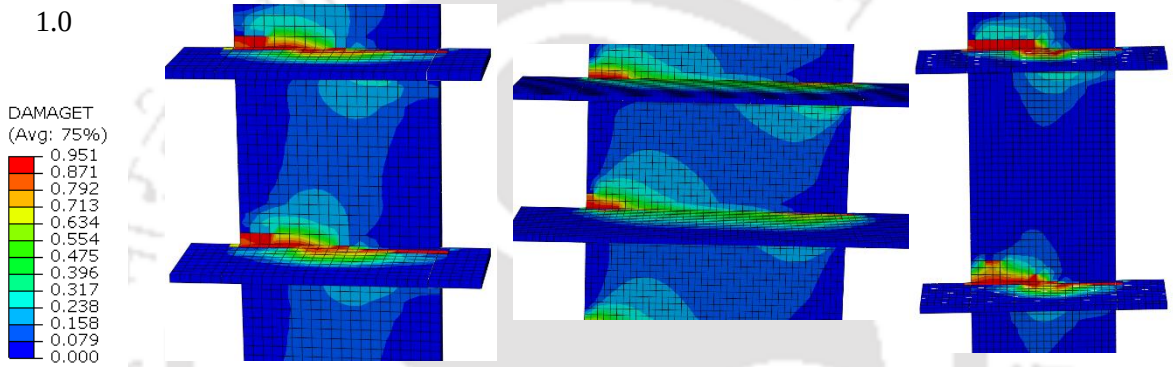		
1.5	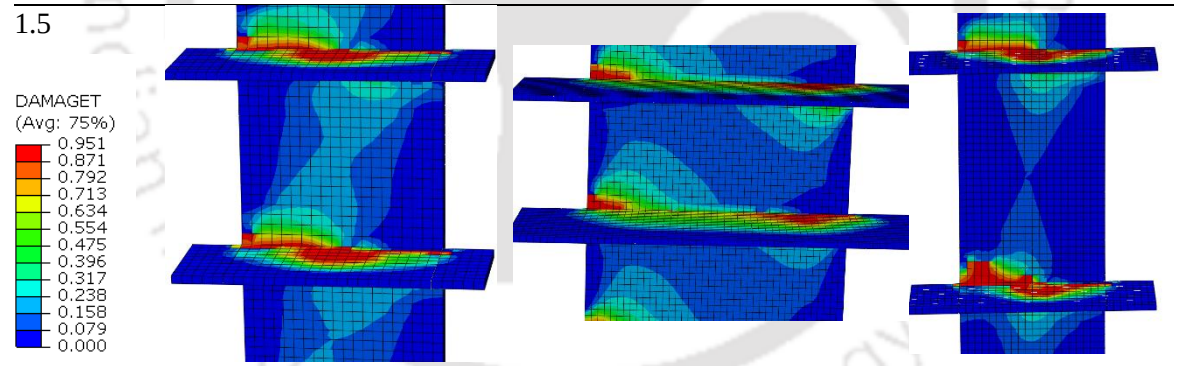		
2.0	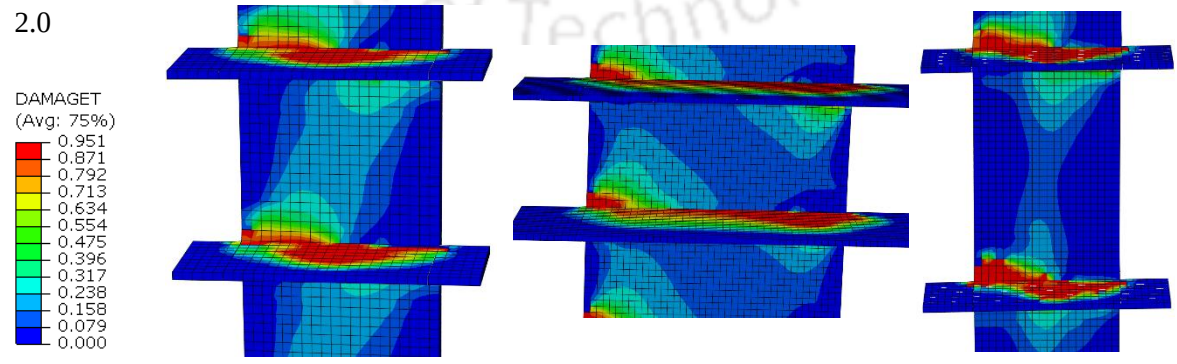		

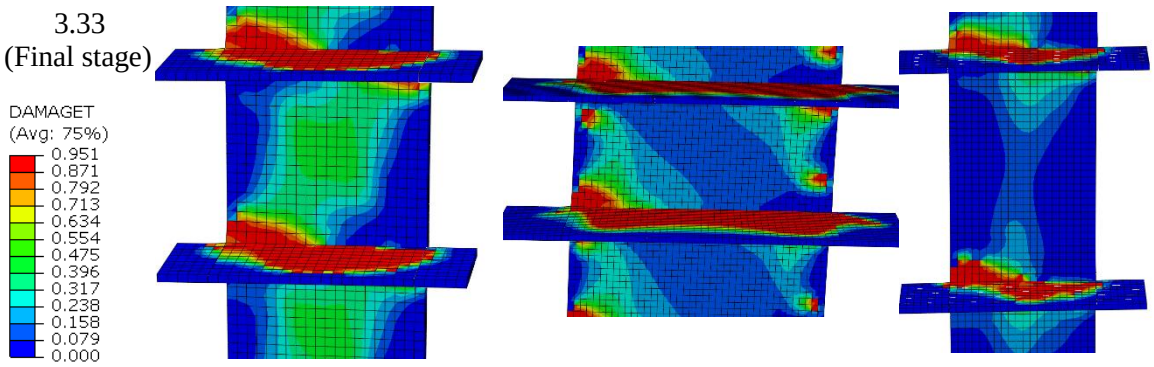

Figure 5.6: Variation of tensile damage with lateral drift level in WSC2, WSC3 and WSC4 models.

5.3.4 Tensile and Compressive Damages

In order to find the effect of aspect ratio and vertical reinforcement of shear wall on the damage pattern at shear wall - slab junction region, the variation of tensile damage in slab with drift ratio is obtained at different distances from the face of the wall (Figure 5.7). For all the cases, the tensile damage starts at the base of shear wall and then it forms at the shear wall-slab junction. For WSC1 and WSC2 models (Figures 5.7a and 5.7b), similar behavior is observed with the tensile damage reaching the maximum value below 0.5% drift. The only difference is that the tensile damage spreads beyond the face of the shear wall (towards the extended slab) in case of WSC2 model, whereas, the spread of damage is lesser in case of WSC1 model. For WSC5 and WSC6, the behaviors are similar to WSC1 and WSC2 models respectively, however, the damage in the floor slab is less as compared to WSC1 and WSC2 models. Maximum damage does not reach the middle of the slab even at high drift ratios. Maximum damage in the shear wall is concentrated at the tension face and to some extent at the compressive face.

WSC3 and WSC7 models (Figure 5.7c) show less damage as compared to the previously described models. The maximum damage occurs in the slab at the tension face. As the distance increases from the tension face, it is observed that the damage in the slab does not reach the maximum damage value even at high drift ratios. Thus, by increasing the length of the shear wall and the percentage of steel in shear wall, damage in the floor slab can be avoided. Since the floor slab is experiencing less damage, the load carrying capacity is maximum in this case. Due to higher aspect ratios of WSC4 and WSC8 models, the shear wall is slender as compared to other models. They experience maximum damage at a low drift ratio, hence the load carrying capacity is less in these cases. Thus, increasing the percentage of vertical reinforcement in the shear wall leads to reduced damage in the floor slab connected to it. The code specified minimum vertical reinforcement in shear walls needs to relooked at and possibly modified accordingly.

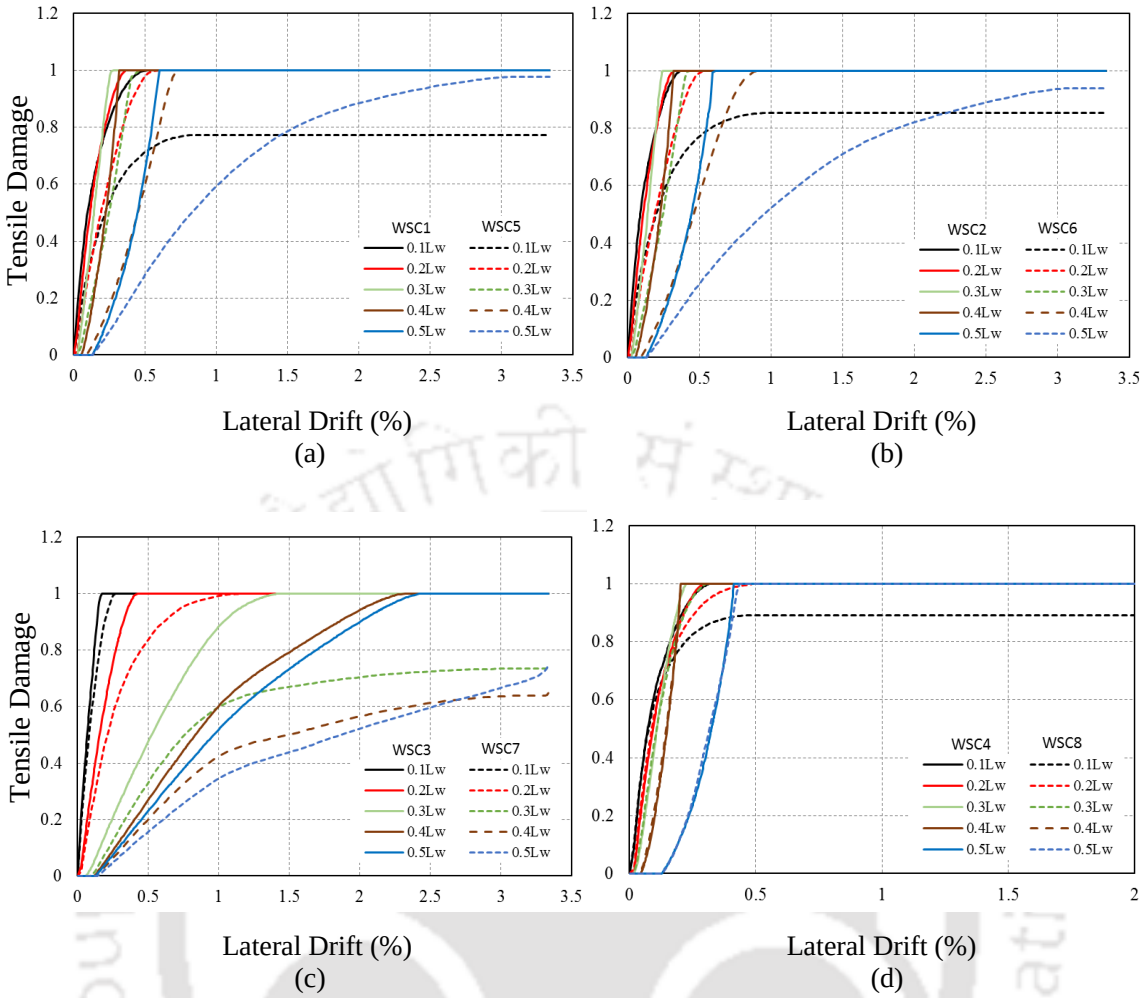

Figure 5.7: Variation of tensile damage in slab along the length of shear wall: (a) WSC1 and WSC5; (b) WSC2 and WSC6; (c) WSC3 and WSC7; (d) WSC4 and WSC8.

The maximum tensile damage is observed in the shear wall-slab junction region and spreads diagonally between the two floor slabs concentrating the stresses at the corners. In previous experiments flexural shear cracks were observed to form in the slab at the connection with the shear wall (Pantazopoulou and Imran, 1992). In addition, major cracks develop on the tension side of the slab from the face of the shear wall. Although floor slabs are not expected to undergo any damage during earthquake shaking, the portion of the floor slab connected to the wall undergoes significant damage at higher levels of lateral drift. The tensile damage starts propagating into the slab from the junction region. Figure 5.8 shows the propagation of cracks from the face of the wall into the slab. For models WSC1, WSC2, WSC3 and WSC4 with less reinforcement ratios, the cracks propagate across the full width of the slab to maximum damage. For WSC5, WSC6, WSC7 and WSC8 models, the maximum tensile damage is attained at a distance of one fourth width of the slab from the face of the wall. From Figure 5.8, it is clear that increasing the minimum percentage of steel in the shear wall may lead to lesser damage in the floor slabs.

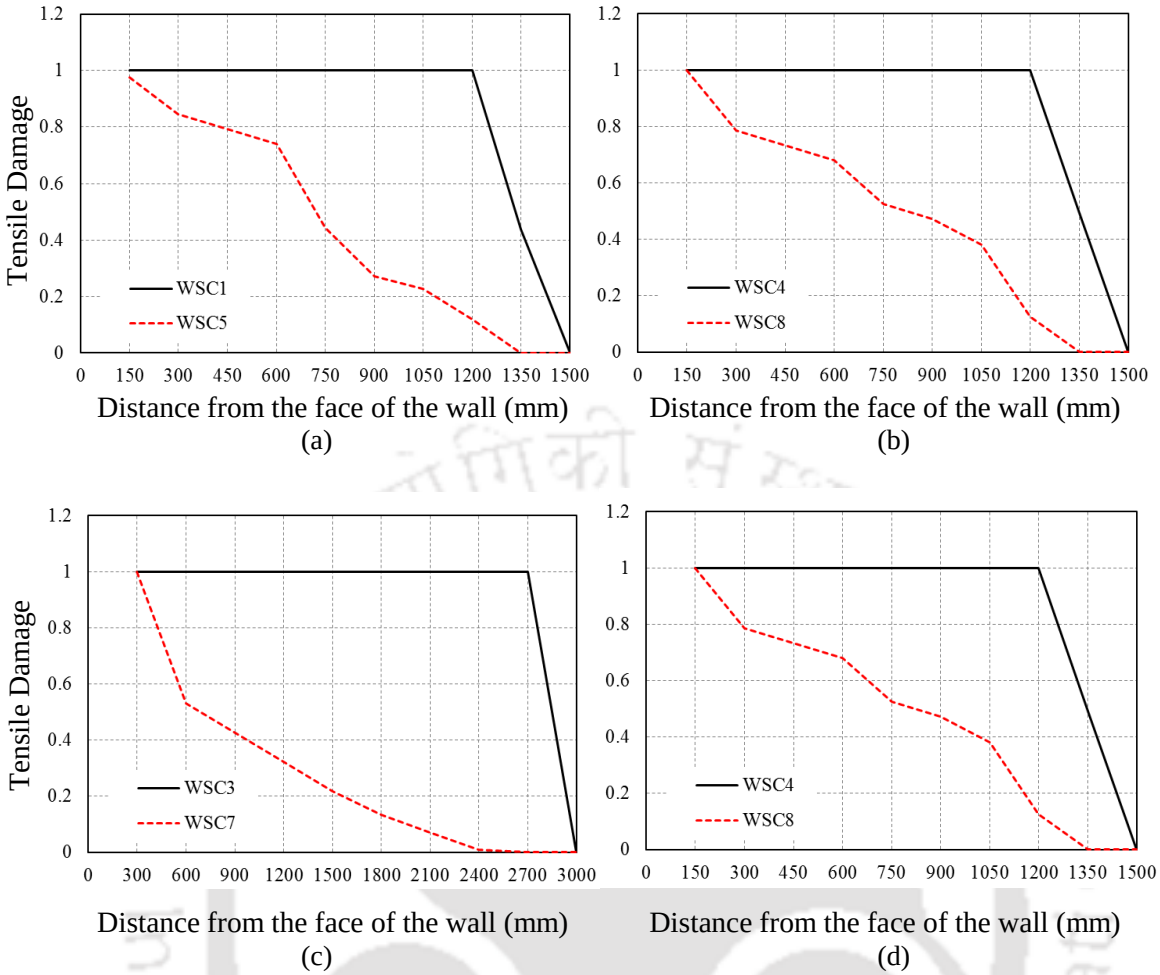

Figure 5.8: Variation of tensile damage in slab with distance from the face of shear wall: (a) WSC1 and WSC5; (b) WSC2 and WSC6; (c) WSC3 and WSC7; (d) WSC4 and WSC8.

The compressive stresses in concrete lead to the development of compressive damage. The major compressive damage is observed in the slab at a distance of one fourth length of slab from the tension face of the shear wall. Also some damage is observed on the compressive face. Figure 5.9 explains the pattern of compressive damage in slab at the junction region for all the models. For all the models except WSC3 and WSC7, the compressive damage starts at a higher drift value. Due to the low aspect ratio of the wall for those specimens, higher compressive stresses in concrete develop at the junction of shear wall and floor slab reflecting behavior of wall panel like squat wall. The damage is concentrated mostly near the tension and compression faces of the wall and gets reduced with increase in distance from the face of the wall. The compressive damage starts at very high drift ratios when concrete is over-reinforced at the compressive face of the shear wall. The tensile damage is more dominating for all the models, as the reinforcement at the bottom of the shear wall reaches its yield limit first. Then, the reinforcement in the slab at the junction region starts yielding, due to which more tensile damage is observed at the shear wall-slab junction.

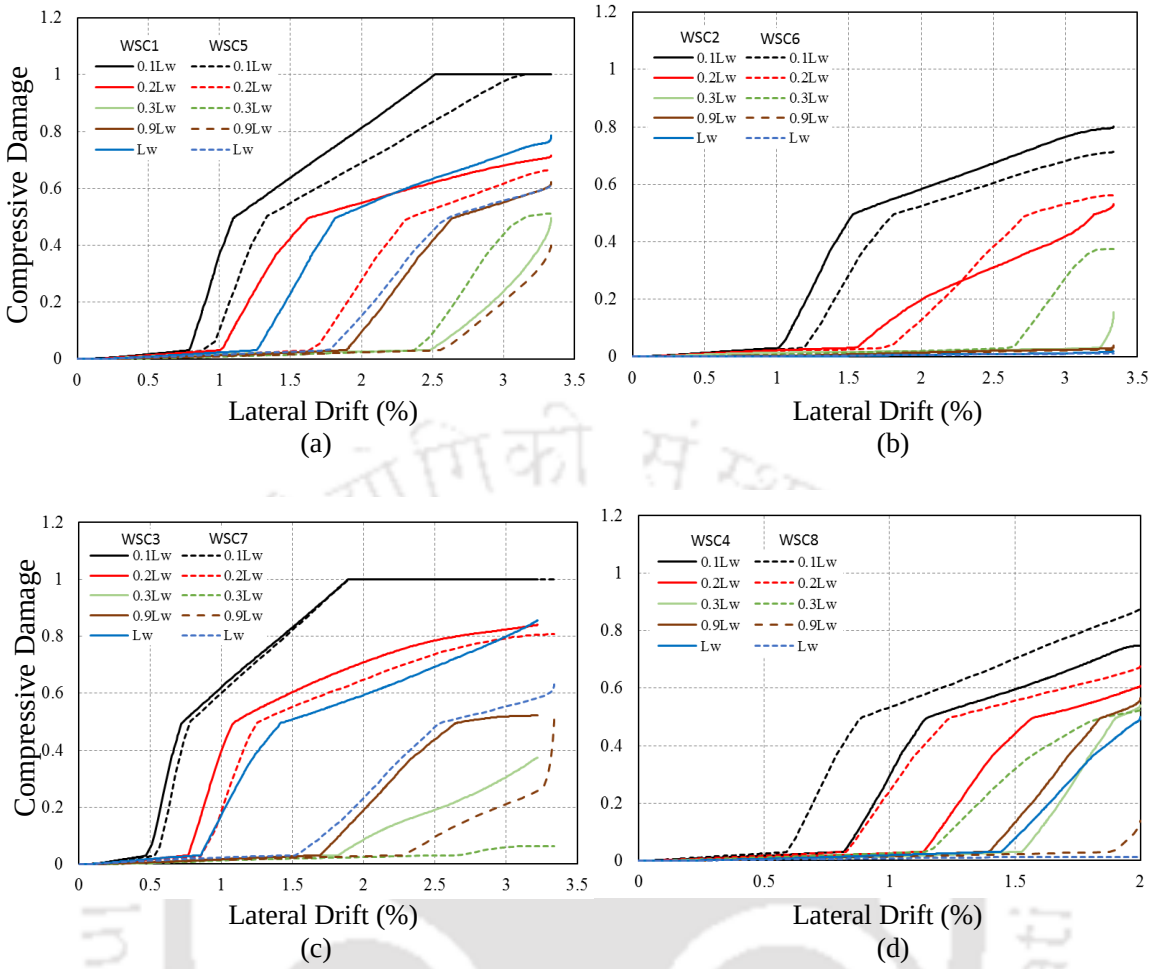

Figure 5.9: Variation of compressive damage in slab along the length of shear wall. (a) WSC1 and WSC5; (b) WSC2 and WSC6; (c) WSC3 and WSC7; (d) WSC4 and WSC8.

5.4 DISCUSSION OF RESULTS

In this chapter, result of nonlinear static analysis of wall-slab assemblage carried out using CDP model, which are used to predict the behavior of shear wall - floor slab junction are discussed. In particular, eight different shear wall-slab assemblages with different aspect ratios and vertical reinforcement ratios are analyzed for obtaining the influence of parametric variation on wall-slab junction behaviour. The CDP model has been first calibrated using experimental results of Pantazopoulou and Imran (1992). After validation with the experimental results, simulation of eight different models is performed in ABAQUS/Standard using IMPLICIT method to study the seismic damage pattern of the shear wall-slab assemblages. The findings of the study are summarized in the following paragraphs:

1) WSC1 and WSC2 models show similar behaviour in terms of lateral load carrying capacity. The maximum lateral load capacities of WSC5 and WSC6 models are higher than those of WSC1 and WSC2 models. The maximum lateral load capacities depend on the vertical

reinforcement ratio in the wall and the aspect ratio. WSC3 and WSC7 models have larger lateral load capacities as compared to all other models. On the other hand, WSC4 and WSC8 models have the lowest capacities. The analytical results show that lower aspect ratio of wall panel between two successive floor slabs results in higher load carrying capacity of the specimen.

2) Equivalent plastic strain distribution in the slab along the length of the wall shows maximum equivalent plastic strain values for WSC4 and WSC8 models leading to a large number of cracks at the tension face of the wall. Models with lower reinforcement ratios (WSC1, WSC2, WSC3 and WSC4) tend to develop more cracks at the junction region. After a lateral drift level of about 0.5%, the strain value exceeds the crushing strain of concrete leading to major sliding cracks. Compressive strut in the wall panel starts developing between the floor slabs due to the formation of cracks at the tension and the compression faces of the wall.
3) The study shows that the tensile and compressive damage in the slab depend on the aspect ratio and the amount of vertical reinforcement ratio in the wall. It is observed that higher aspect ratio and lower reinforcement ratio result in maximum damage at lower drift values.
4) Considering the tensile damage at the junction region, it is observed that the maximum stress concentration develops at the base of the shear wall first and then forms at the upper floor level slab-wall junction. Also, the developed tensile damage and the stresses are more in the portion of the slab connected to the shear wall along its length. The slab panels not connected to the wall experience less strain and damage. Conventionally, slender shear wall in multistoried buildings are designed in the same way as isolated shear walls. However, due to the presence of slabs, lateral stiffness of wall tends to increase at each wall-slab junction. Thus, the slender wall gets partitioned into a number of smaller panels between successive floor slabs. Each such panel behaves as a squat wall with the formation of diagonal strut between two successive wall-slab junctions as observed in WSC1 and WSC2 models. Thus, the design methodology should consider strut formation and associated failure modes for slender walls in multistoried buildings with floor slabs.
5) Conventionally, beams, columns and structural walls are designed to undergo desired levels of damage during strong earthquake shaking. Floor slabs are not expected to undergo any seismic damage. However, in the present study it is observed that the portion of the floor slab connected to the walls undergoes significant damage even at moderate levels of lateral drift. Significant damage at wall-slab junction may also lead to formation of sliding shear crack across the wall. Any damage in slab is also difficult to repair as compared to the damages in beam, column or structural wall. Thus, a new design methodology involving prevention or reduction of damage in slab needs to be evolved.

Chapter 6
PLASTIC HINGE LENGTH IN RC SHEAR WALL CONNECTED WITH FLOOR SLABS

6.0 OVERVIEW

In multistoried RC wall-frame buildings, shear walls play an important role in the seismic behaviour of such buildings. At every floor level in such building, the walls are generally connected to the floor slabs. In the previous chapters, it was observed that the floor slabs tend to partition the slender wall into panels with mobilized squat wall behaviour. Also, the concentration of tensile and compressive damages at the wall-slab junctions indicates development of material nonlinearity at certain locations along the height of wall. This is in contrast to the conventional isolated slender wall behaviour with a single region of inelastic behaviour. Past studies have mainly focused on isolated slender wall specimens with the zone of predominantly inelastic behaviour, i.e., the plastic hinge zone developed at the base of the wall under seismic actions. However, the regions of nonlinearity and inelastic action in a wall connected with floor slabs have not been investigated in any past study. In the present study, displacement-based nonlinear static analysis is carried out, under monotonic as well as cyclic modes, to investigate the plastic hinge region in shear wall - floor slab assemblages. To obtain the plastic hinge length (L_p), a parametric study is carried out by varying axial compression on wall and wall panel aspect ratio. It is observed that unlike the concentration of inelasticity at the base of a wall without slabs, the curvature demand increases significantly at the wall-slab junction, leading to the development of nonlinearity and damage at those locations. Based on curvature distribution and variation of tensile damage along the height of the wall, closed form expressions for estimation of plastic hinge length are proposed for shear wall with slabs connected at every floor level.

6.1 PLASTIC HINGE LENGTH

In multistoried RC frame buildings, typical material nonlinearity is observed in beams and columns during strong earthquake shaking. Along with beams and columns, similar nonlinear behaviour may get mobilized in shear walls for RC frame-wall buildings. The development of material nonlinearity along with possible tensile damages takes place in the plastic hinge region of each member. The extent of the plastic hinge zone is expressed in terms of plastic hinge length (L_p). In isolated slender shear wall specimen, maximum nonlinearity and the plastic hinge zone develop at the base of the

wall. Also it is assumed that the maximum curvature at the bottom of the wall is uniform over the plastic hinge length which is considered within the range of $0.5L_w$ to L_w, where L_w is the wall length. All the past studies on estimation of L_p in shear wall specimens have been carried out on isolated slender wall specimens.

6.1.1 Parameters required for estimation of L_p

Plastic hinges are expected to form at the regions of maximum bending moment demand in RC members. Traditionally, the concept of plastic hinge is discussed in the context of cantilever RC members in which the tip displacement can be easily obtained by integrating curvature with a known L_p value. Therefore, accurate assessment of L_p is important in relating section-level response to member-level response. The L_p depends on many factors such as: 1) level of axial force, 2) gradient of bending moment, 3) level of shear stress in the plastic hinge region, 4) mechanical properties of longitudinal and transverse reinforcement, 5) compressive strength of concrete, and 6) level of confinement in the potential hinge region. In the past, researchers (Baker, 1956; Baker and Amarakone, 1964; Mattock, 1964; Mattock, 1967 and Corley, 1966) studied L_p to estimate the flexural deformation capacity of reinforced concrete beams. To estimate the flexural deformation capacity, the plastic rotation capacity is obtained as,

$$\theta_p = \frac{\varepsilon_{cu} - \varepsilon_{ce}}{c} \times L_p \tag{6.1}$$

where, ε_{cu} is the maximum concrete compressive strain, ε_{ce} is elastic concrete compressive strain and c is distance from extreme compression fiber to neutral axis. In a cantilever column, the plastic hinge length is defined as the equivalent length over which the inelastic curvature is considered to be constant (Park and Paulay, 1975). By elastoplastic idealization of the actual moment-curvature (M-ϕ) response, the yield curvature (ϕ_y) and the ultimate curvature (ϕ_u) are estimated (Figures 6.1a and 6.1b). The assumption of constant inelastic curvature over a length L_p (Figures 6.1c and 6.1d) leads to the expression of total flexural displacement at the tip of the column (Δ_{tip}) as,

$$\Delta_{tip} = \Delta_y + \Delta_p = \frac{\phi_y L_s^{\,2}}{3} + \left(\phi - \phi_y\right) L_p \left(L_s - 0.5L_p\right) \tag{6.2}$$

where, Δ_y is the yield displacement, Δ_p is the plastic displacement and L_s is the distance from critical section to point of contraflexure. The term $\left(\phi - \phi_y\right) L_p$ in Eq. (6.2) refers to the plastic rotation and is based on the assumption that the plastic curvature is lumped in the center of the equivalent plastic hinge length. The terms ϕ and ϕ_y represents the total and yield curvature, respectively, at the base of the shear wall.

By further simplifying Eq. (6.2), Park and Paulay (1975) obtained the relationship between curvature and displacement ductilities as,

$$\mu_{\Delta} = 1 + 3(\mu_{\phi} - 1)\frac{L_p}{L_s}\left(1 - 0.5\frac{L_p}{L_s}\right) \tag{6.3}$$

Equations (6.2) and (6.3) have been commonly used to estimate the L_p of concrete columns. It is interesting to note that the curvature profile along the column is often related to the tip displacement rather than flexural displacement (Park and Priestley, 1982; Priestley and Park, 1987; Paulay and Priestley, 1992; Sheikh and Khoury, 1993; Sheikh et al., 1994 and Bayrak and Sheikh, 1998). Plastic hinge analysis is based on the assumption of an elasto-plastic behaviour and an equivalent plastic hinge length. The elastoplastic idealization of actual M-ϕ curve depends on the type of RC element, Figure 6.2 shows the difference between the equivalent yield curvature for a column and for a shear wall (Adebar and Ibrahim, 2002).

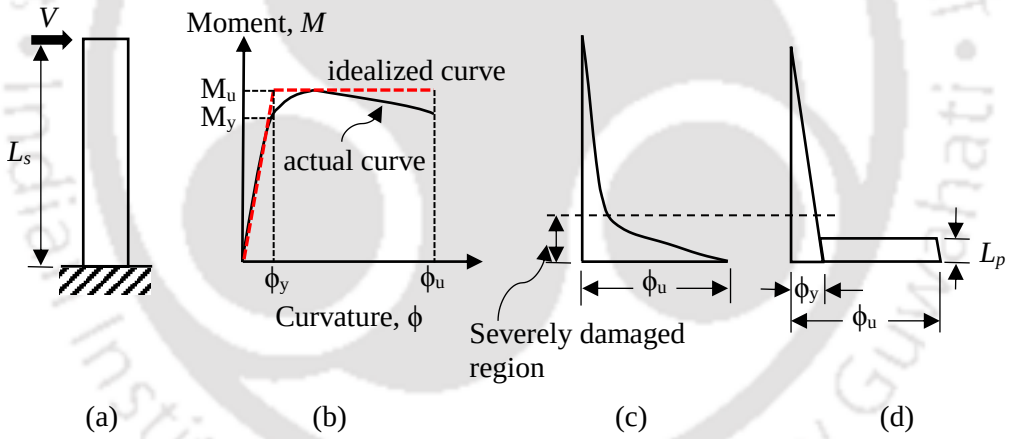

Figure 6.1: Definition of plastic hinge length: (a) Cantilever wall, (b) Moment-curvature curve, (c) curvature of maximum response and (d) equivalent curvature (Park and Paulay, 1975).

6.1.2 Previous Work on Plastic Hinge Length

The following section describes the models developed by various researchers to determine the plastic hinge length for various kinds of concrete elements.

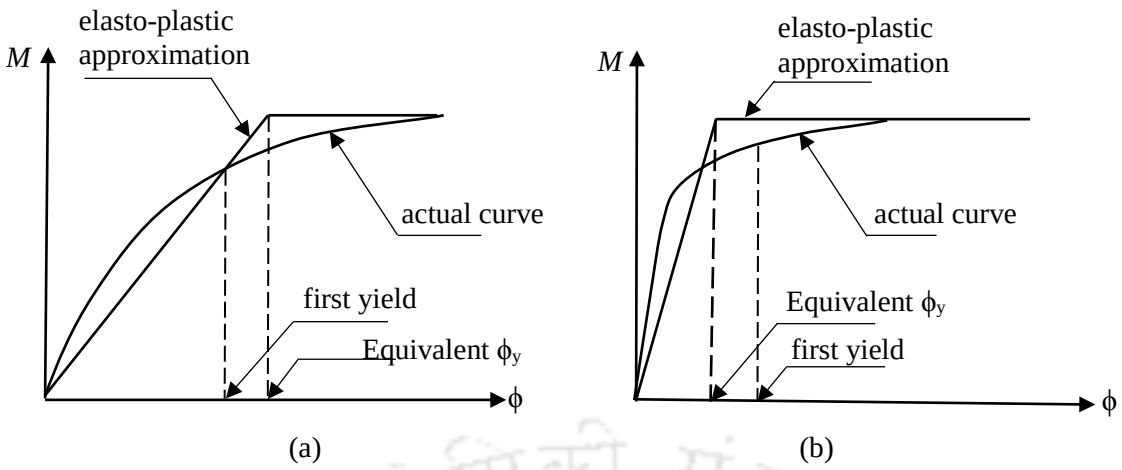

Figure 6.2: Bending moment-curvature relationship for: (a) column and (b) shear wall.

6.1.2.1 Beams and Columns

In the past studies on RC beams and columns, several researchers have proposed the estimation of L_p using different parameters. Chan (1955) suggested that the plastic hinge length is equal to the distance over which the flexural reinforcement yields in beam. Based on the tests carried out on 94 beam and column, Baker (1956) proposed that the plastic hinge length in columns lies between *0.5h* and *h*, where *h* is the column dimension perpendicular to the axis of bending. Baker and Amarakone (1964) proposed an expression for L_p, observing that the structural elements with cold-worked reinforcement have longer plastic hinge zone than the mild steel reinforcement. Sawyer (1964) developed a design methodology for RC frames based on a bilinear moment-curvature relationship. Here, assumption was made that the ratio of yield to maximum moment is 0.85 and the estimate of L_p proposed by Chan (1955) was modified as *0.15* times shear span. It was also assumed that plasticity would spread over a length of *d/4*, and an equation for plastic hinge length was proposed in terms of effective flexural depth and shear span. Mattock (1964) and Corley (1966) conducted experiments on several beams and proposed a similar equation as that of Sawyer (1964) and observed that L_p increases with effective depth *d* and shear span to depth ratio, while it decreases with the quantity of flexural tension reinforcement ratio. Mattock (1967) proposed similar equation of plastic hinge length for beams by varying the coefficients of effective depth and shear span.

6.1.2.2 Shear Walls

Paulay (1986) proposed the expected variation of plastic hinge length in ductile RC walls in the range of $0.5L_w$ to L_w. The same limit was proposed by Wallace and Moehle (1992) considering the confined boundaries in RC walls subjected to earthquake loading. Paulay and Uzumeri (1975)

modified the equation of L_p proposed by Sawyer (1964) to apply for shear walls by assuming effective depth as $0.8L_w$ and lever arm for flexural action, z as H_w with the proposed equation as,

$$L_p = 0.8\alpha_l L_w + \beta_h H_w \tag{6.4}$$

where, H_w is the height of wall. α_l and β_h are dimensionless parameters on length and height of wall, respectively. Paulay and Priestley (1992) reported tests on ductile concrete walls of rectangular cross section subjected to seismic loading to study out-of-plane buckling and recommended the parametric values as α_l =0.25 and β_h =0.044 respectively. Sasani and Der Kiureghian (2001) reexamined the plastic hinge length proposed by Corley (1966) and Mattock (1967) and proposed a new plastic hinge length as,

$$L_p = 0.43\,d + 0.077\sqrt{L_s}\,/d\,, \tag{6.5}$$

Panagiotakos and Fardis (2001) carried out experiments on more than 1000 reinforced concrete members (out of which 61 were shear walls), subjected to uniaxial bending, with and without axial loads, to estimate flexural deformation in terms of the member geometric and mechanical properties. The proposed plastic hinge length is as follows.

$$L_{p,cy} = 0.12L + 0.014 d_b f_y \text{ for cyclic loading, and} \tag{6.6}$$

$$L_{p,mon} = 1.5 L_{p,cy} \text{ for monotonic loading,} \tag{6.7}$$

where, d_b is the diameter of bar in meters, f_y is the yield strength of reinforcement in MPa, $L_{p,cy}$ is the plastic hinge length for cyclic loading in meters and $L_{p,mon}$ is the plastic hinge length for monotonic loading in meters.

Bohl and Adebar (2011) have conducted analyses on a range of isolated walls with different wall lengths, maximum bending moment-shear force ratios, axial compression levels, axial tension levels, and shear stress levels. The results were used to develop a simple expression for L_p as,

$$L_p = \left(0.2L_w + 0.05L_s\right)\left(1 - 1.5\frac{P}{f_c^{'}A_g}\right) \le 0.8L_w\,, \tag{6.8}$$

where, $f_c^{'}$ is the cylinder compression strength of concrete, A_g is the gross area of wall cross section and P is the axial load.

Kazaz (2013) proposed an expression for plastic hinge length for cantilever structural walls depending on wall length, axial force ratio $\left(P/A_g f_c^{'}\right)$, horizontal reinforcement ratio in web of wall, and shear span-to-wall length ratio. The proposed equation of L_p is given by,

$$L_p = 0.27L_w\left(1-\frac{P}{A_g f_c^{'}}\right)\left(1-\frac{f_y\rho_{sh}}{f_c^{'}}\right)\left(\frac{M/V}{L_w}\right)\leq 0.8, \tag{6.9}$$

where, M/V is the shear span and ρ_{sh} is horizontal reinforcement ratio in web of wall.

Mun and Yang (2015) have formulated the L_p as a function of longitudinal tensile reinforcement ratio in the boundary element, vertical shear reinforcement ratio in the web and axial force ratio. Takahashi et al. (2013) carried out experiments on different shear wall specimens by varying wall length, wall thickness, detailing of reinforcement, and axial force to predict the flexural drift capacity, with the extent of plastic hinge zone considered as 2.5 times that of the wall thickness.

In isolated slender shear walls, plastic hinge is expected to form at the base of the wall under lateral loading, with the restriction of plastic rotation in the hinge zone within an acceptable limit. The conventional seismic design based on a single plastic hinge at the bottom of the wall is not applicable for walls in multistoried buildings (Munir and Warnitchai, 2012). It was suggested that plastic hinges may form at several selected locations along the wall height and not just at the base of the shear wall. The deformation of the first storey controls the compatibility forces transferred therein, which to a large extent account for the increase in the base shear demand on the short wall relative to single walls. In another similar study, a second plastic hinge was introduced at the mid-height of the shear wall to allow for more realistic spread of plasticity over the height of the first storey (Beyer et al., 2014).

Several other expressions have been proposed by researchers based on analytical and experimental work on isolated slender shear walls. However, the development of nonlinearity and the possible plastic hinge region in RC wall in presence of floor slabs, have not been investigated in the past studies. In the present study, nonlinear static analysis is carried out on an exterior shear wall-slab assemblage for investigating the plastic hinge length at the junction of shear wall and floor slab with reference to the variation of curvature and tensile damages. The presence of floor slab tends to partition the wall into a number of panels between the successive floors. A parametric study considering the length (L_w), as well as the aspect ratio of wall panel and axial load ratio is carried out and expressions for plastic hinge length at the wall-slab junction are proposed towards the end of the chapter.

6.2 MODELLING AND ANALYSIS DETAILS

A five storey RC frame-wall building located in highest Seismic Zone in India is considered in the present study (BIS, 2016b) (Figure 3.13). From that building, an exterior shear wall - slab assemblage (Figure 4.1d) is considered for investigation of plastic hinge length near the wall-slab junction region (Kaushik and Dasgupta, 2013). The modelling details, using ABAQUS program, are mentioned in Chapter 3. The assemblage is modelled using solid elements with reinforcement embedded in the shear wall and floor slab region. The thickness of shear wall and slab are 300 mm and 120 mm, respectively. Two layers of vertical and horizontal reinforcement are provided in the shear wall; 8 mm diameter bars are spaced at 150 mm vertically and horizontally. In slabs, 8 mm bars are used at top and bottom at a spacing of 300 mm. For all the cases, the shear walls and floor slabs are modeled using Concrete Damaged Plasticity (CDP) properties as discussed in Chapter 3. The assemblage analyzed in the current study has a characteristic concrete compressive strength of 25 MPa. The tensile strength of concrete is assigned as 3.5 MPa. The stress-strain characteristics of concrete in compression and tension are shown in Figures 3.6a and 3.6b, respectively. The elastic modulus of concrete is taken as 25,000 MPa. Steel reinforcement is modelled with the material property assigned using plasticity model in ABAQUS. The yield stress, ultimate stress and the modulus of elasticity of steel are considered as 415 MPa, 527 MPa and 2,00,000 MPa, respectively. The gravity loads (both dead and live loads) on slab are assigned as pressure loads on the surface of solid elements. The total intensity of loading on slab including live load and floor finish is considered as 4 kN/m^2. The floor slabs are tied to the shear wall at the floor levels using tie constraint. The translational and rotational Degrees of Freedom (DoFs) are restrained at the bottom nodes of the wall. As the present study intends to investigate the nonlinear behaviour for in-plane analysis of wall, the outer edges of slabs are supported on rollers, and the out-of-plane bending of the shear wall is prevented. The details of mesh convergence study are mentioned in Chapter 3.

For the parametric study, the length of the wall is considered as 3 m, 4 m, 5 m, 6.7 m and 10 m respectively. The height of the wall in between the floors (storey height, h_s) is kept constant as 5 m. To investigate the influence of axial compression on the plastic hinge region in the wall-slab assemblage, three different force levels of $10\%A_gf_c$, $40\%A_gf_c$ and $70\%A_gf_c$ are considered and they are applied on the top surface of the wall.

Displacement based nonlinear static analyses are performed under monotonic as well as cyclic modes with varying axial load and length of wall. The gravity loads on the slab are kept constant during each analysis. For cyclic loading, the specimen is subjected to three cycles of applied displacement levels of 2.5 mm, 5.0 mm, 10.0 mm, 20.0 mm, 40.0 mm, 60.0 mm, 80.0 mm and 100.0 mm respectively (Figure 6.3a). It is observed that the general trend of force-displacement response

for different ratios of axial force on the assemblage is similar for both cyclic and monotonic analysis case when compared separately. Also, the extent of tensile damage at the junction region at the maximum drift level is similar for different axial load levels. Hence, the possible plastic hinge length in wall-slab junction region is not sensitive to the level of axial compression applied on the top surface of the wall. Thus, all further analyses (monotonic and cyclic) for different lengths of wall are carried out for axial compression of $10\%A_g f_c$. In case of monotonic pushover analysis, first the assemblage is displaced up to a lateral displacement of 500 mm to study the maximum spread of damage in the floor slabs. During actual earthquake shaking, the displacement demand on frame-wall building may not reach that level. Thus, for the same lateral displacement in monotonic and cyclic analyses, the results are presented for the behaviour upto 100 mm lateral displacement.

6.3 Results of Nonlinear Analysis

During cyclic nonlinear static analysis, the peak lateral strength of slab-wall assemblage expectedly increases with reduction in aspect ratio of wall panel (Figures 6.3b - 6.3f). The wall panel with the lowest aspect ratio also exhibits the maximum degradation in lateral strength as reflected from the backbone curves. This is due to the crushing of concrete at the junction region and developing inelasticity at a low drift. As cracking of concrete is not explicitly modelled, the typical pinching characteristics of the force-displacement loop is not observed.

The variation of concrete strain at first floor wall-slab junction shows similar trends at different drift ratios (Figures 6.4a - 6.4e). One of the salient observations is that the strain profiles remain almost the same under the three different axial compression levels ($10\%A_g f_c$, $40\%A_g f_c$ and $70\%A_g f_c$), unlike slender isolated wall in which the influence of axial compression on strain profile in wall cross-section is significant. Due to the similarity of the strain profile of different axial compression levels, the plastic hinge length also remains approximately the same for all the three cases. Similar results were also observed in case of estimated L_p for RC columns in a previous study (Park et al, 1982). As the axial compression on wall is not observed to affect the stress-strain response of the wall-slab specimen, a compression of $10\%A_g f_c$ along with low reinforcement ratio of 0.25% are considered for further analyses.

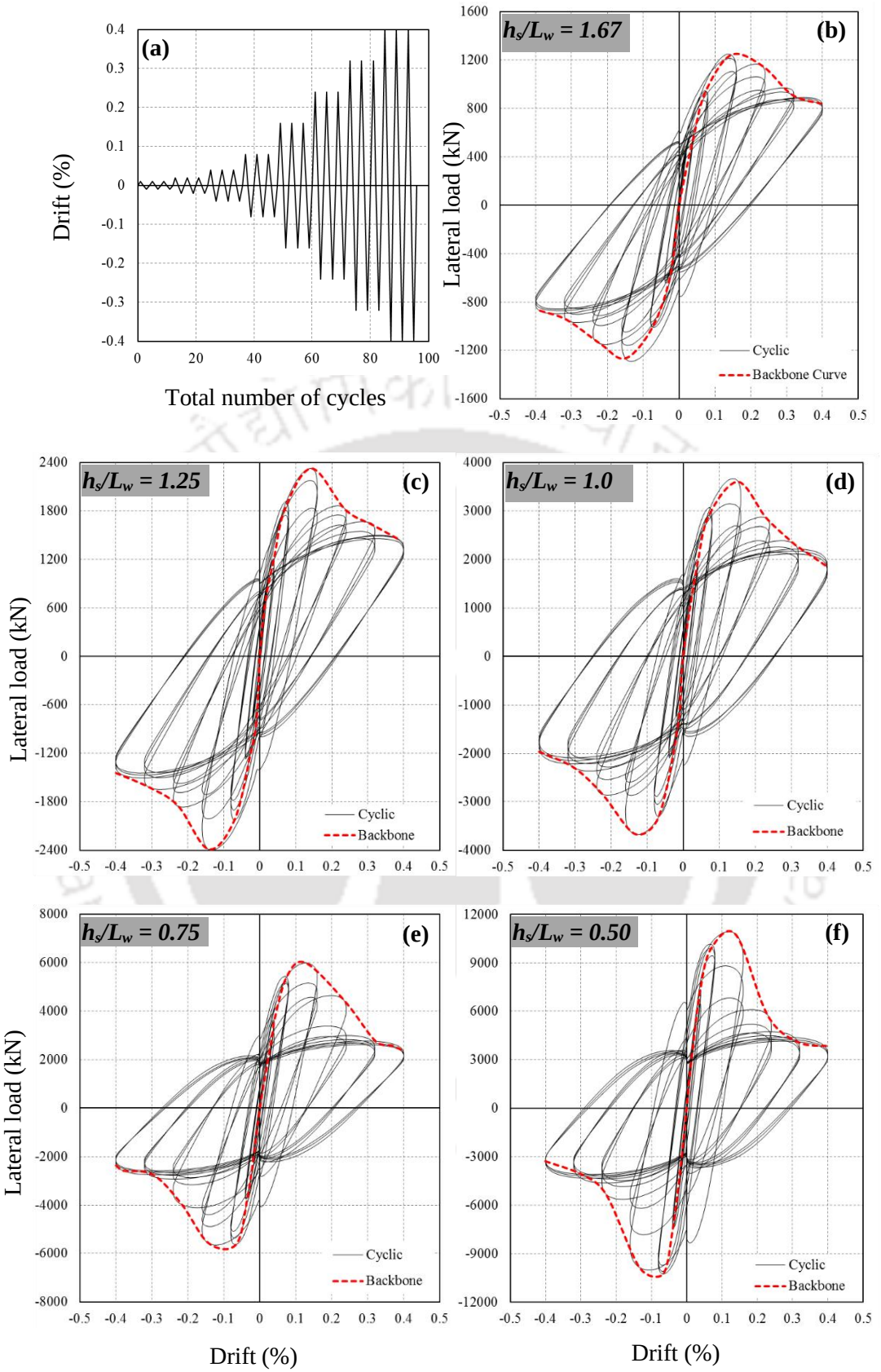

Figure 6.3: Behaviour of wall-slab assemblage under cyclic loading with different panel aspect ratios: (a) Variation of drift level with loading cycles, (b) for aspect ratio 1.67, (c) for aspect ratio 1.25, (d) for aspect ratio 1.0, (e) for aspect ratio 0.75 and (f) for aspect ratio 0.5.

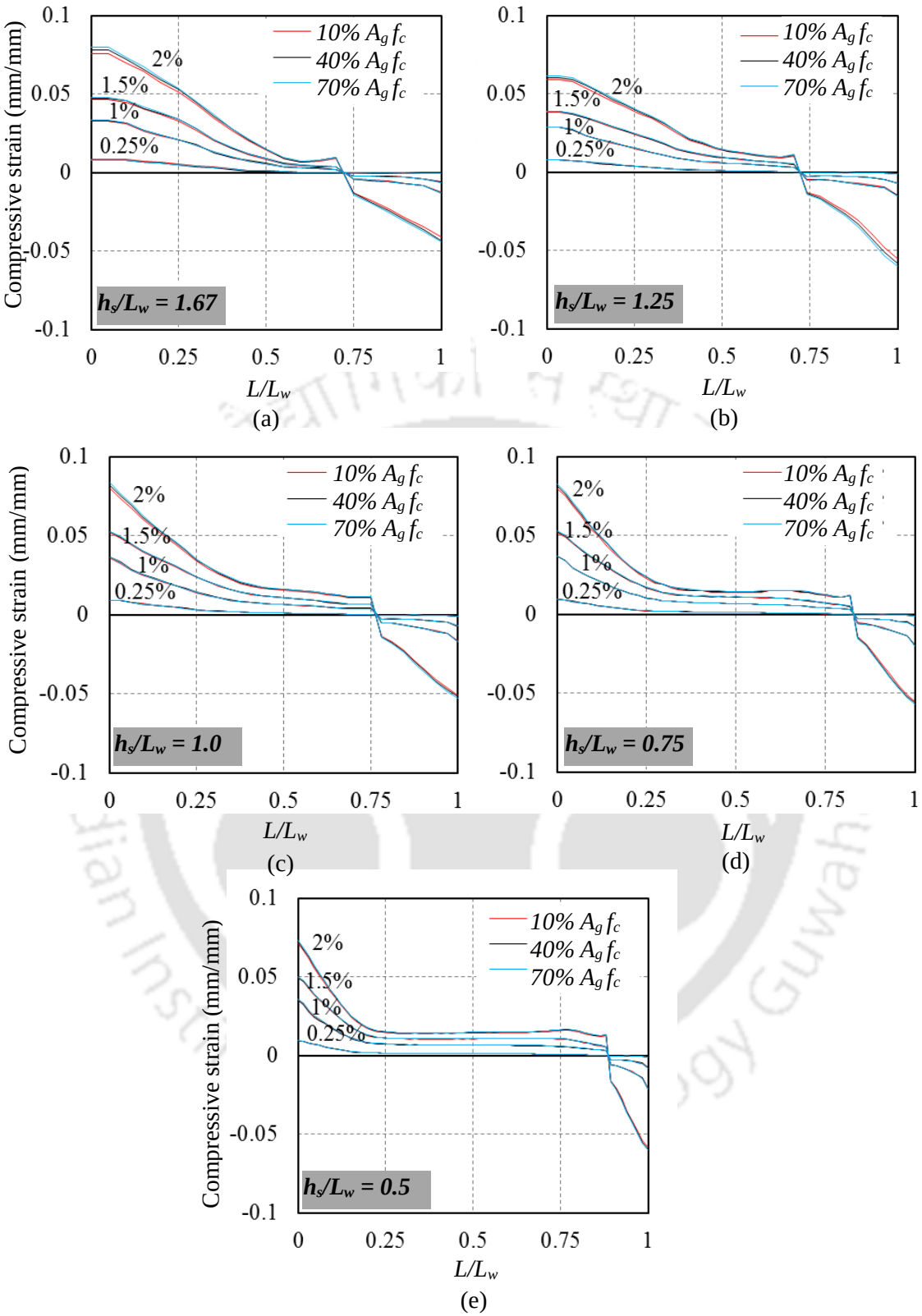

Figure 6.4: Variation of strain in concrete at first floor level along the length of wall in wall-slab junction under different axial compression levels and aspect ratios: (a) for aspect ratio of 1.67, (b) for aspect ratio of 1.25, (c) for aspect ratio of 1.0, (d) for aspect ratio of 0.75 and (e) for aspect ratio of 0.5.

Although the maximum compressive strain in concrete is observed to be the same for the 2% drift level, the maximum tensile strain tends to increase with reduced aspect ratio of wall panel. This is due to the increase in the diagonal tension from the bottom wall panel with mobilization of more squat wall behaviour. Extensive cracking is expected towards the edge of the wall in the wall-slab junction region at the mentioned drift level. For all the drifts levels in the specimen, the strain profile crosses the zero strain point at the same location. Similar trend was also observed for the strain variation along the web of an isolated slender wall in past studies (Thomson and Wallace, 1995). However, the zero-strain point shifts towards the tension side of the wall with reducing panel aspect ratio (Figures 6.4a - 6.4e). Thus, the compression region reduces with increased wall length. The variation of longitudinal stress in the vertical reinforcement on the tension and the compression faces of the wall is shown in Figure 6.5. It is observed that the vertical bar at the wall- slab junction region reaches the yield strength level while the bar over the remaining height of the wall panel remains unyielded.

The floor slabs tend to partition the entire wall into different squat panels, and the strut-and-tie actions lead to concentration tensile and compressive strains in wall-slab junction at every floor level. These further cause yielding of vertical bars only at the junction region and not throughout the height of the wall panel. This highlights a significant deviation from the behaviour of vertical reinforcement in isolated slender shear walls in which the bars yield over a zone at the bottom of the wall during flexural deformations. Similar behaviour is observed for the stress distribution of longitudinal steel in wall panel with increased aspect ratio which tends to make the wall panel more slender. The zone of yielding on the compression face reinforcement towards the bottom of the wall tends to increase with the aspect ratio of wall panels. The curvature is obtained based on the strains obtained at the tension and compressive faces of the wall for maximum drift level (Figure 6.6). The curvature is calculated as,

$$\phi = (\varepsilon_S - \varepsilon_C) / L_w \tag{6.10}$$

where, ϕ is the curvature, ε_s is the strain on tensile face, ε_c is the strain on compressive face and L_w is the length of wall (Kazaz, 2013). The same procedure is adopted for obtaining the curvature profiles along the height of the wall for both monotonic and cyclic loadings. Unlike isolated slender wall section having maximum curvature at the bottom of the wall (Bohl and Adebar, 2011), the slab-wall junction at every floor level is subjected to large curvature as observed in the wall panels on the different aspect ratios (Figures 6.7a - 6.7d). With increasing distance from the wall-slab junction, the curvature reduces sharply to a very small value along the storey height.

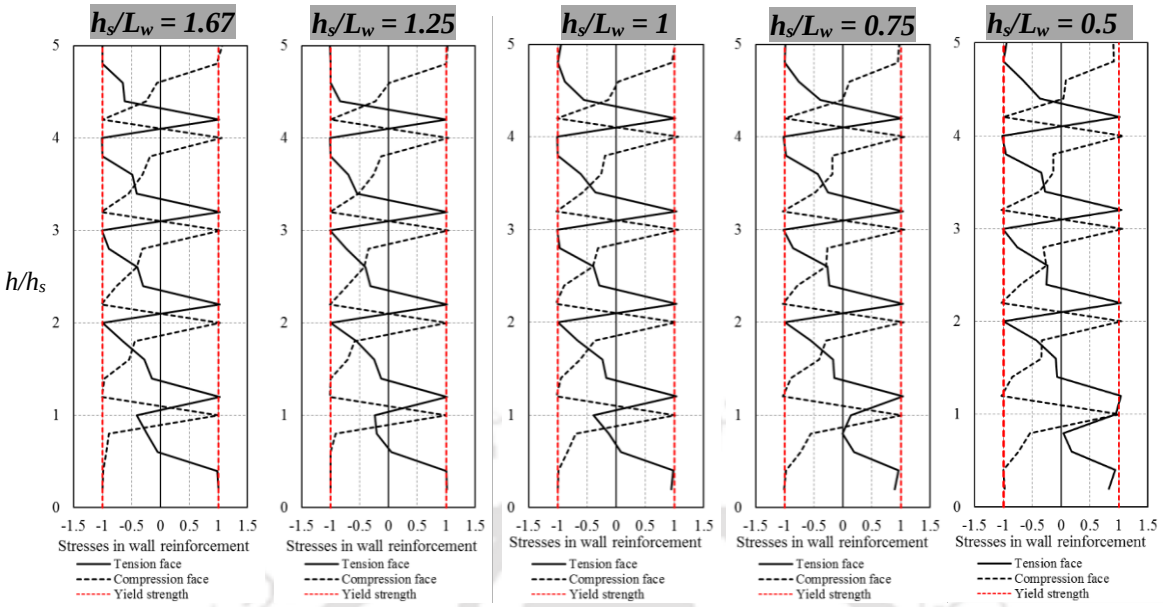

(a) (b) (c) (d) (e)

Figure 6.5: Comparison of stresses (normalized with yield stress) in vertical reinforcement of wall for different wall panel at 2% drift ratio: (a) for aspect ratio of 1.67, (b) for aspect ratio of 1.25, (c) for aspect ratio of 1.0, (d) for aspect ratio of 0.75 and (e) for aspect ratio of 0.5.

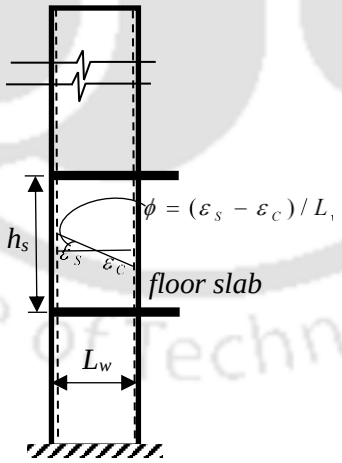

Figure 6.6: Estimation of curvature at any section along the height of wall.

A similar trend is observed for tensile damage in wall in which maximum damages are observed in wall-slab junction region (Figures 6.8a - 6.8d). The tensile damage gets initiated at the base of the wall. However, it does not propagate along the height of the wall but tends to increase at the wall-

slab junction at every floor level. This is due to the partitioning of the wall into a number of panels and the consequent strut and tie action. This is observed for all the specimens with different wall panel aspect ratios. However, along the height of each wall panel, insignificant damages are observed.

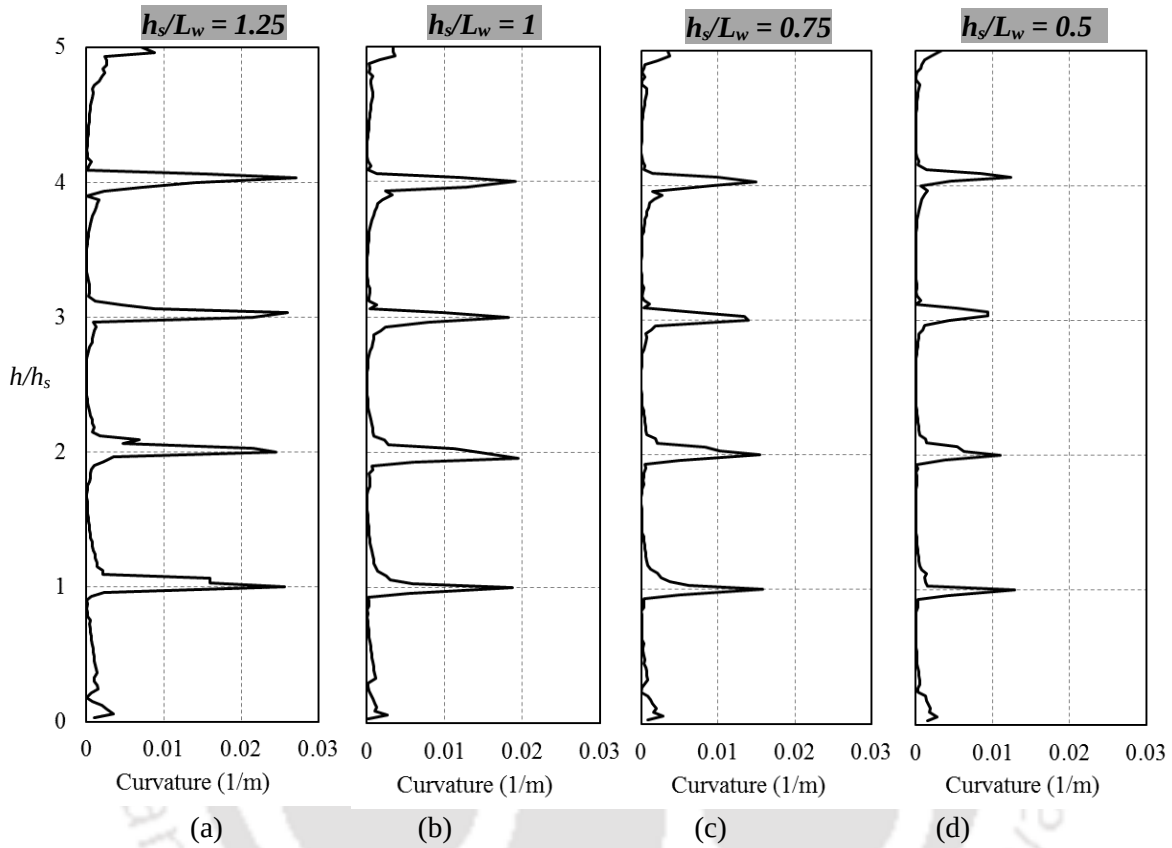

Figure 6.7: Variation of curvature for different aspect ratios of wall panels at final drift level: (a) for aspect ratio of 1.25, (b) for aspect ratio of 1.0, (c) for aspect ratio of 0.75 and (d) for aspect ratio of 0.5.

Conventionally, plastic hinge length in an RC member refers to the distance from the member end in which maximum nonlinearity is expected to occur in steel or concrete or both the materials under flexural behaviour. The flexural deformations are related to the curvature at a particular section, and the plastic hinge length is expressed in terms of curvature and other parameters. Thus, in the plastic hinge zone, maximum tensile and compressive damages occur due to the nonlinear behaviour of the materials. In the present study, the presence of floor slab tends to reduce the flexural deformations along the height of the wall. However, in each wall panel between two successive floor slabs, tensile and compressive damages accumulate at the wall-slab junction region. So, along with curvature and

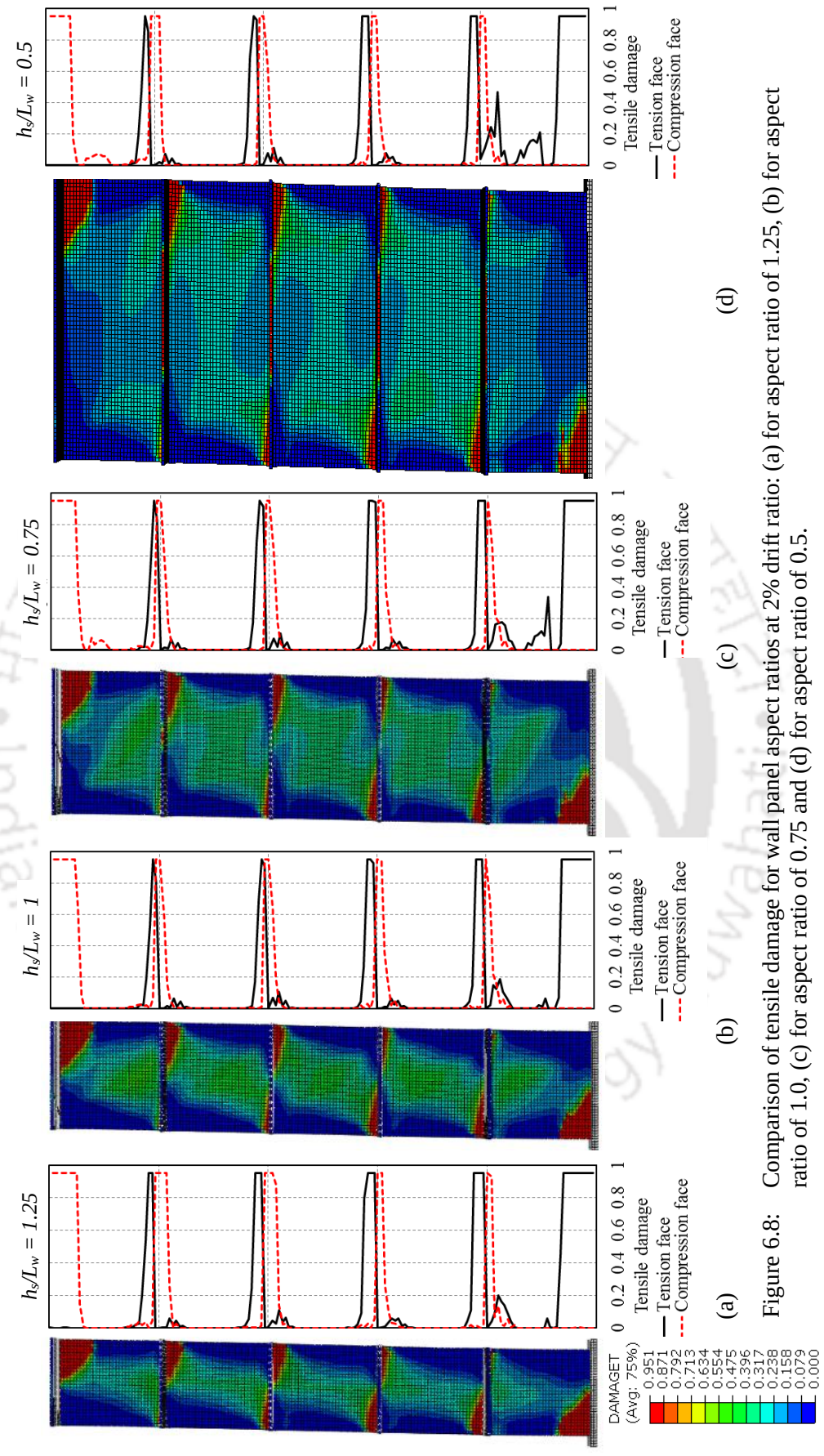

Figure 6.8: Comparison of tensile damage for wall panel aspect ratios at 2% drift ratio: (a) for aspect ratio of 1.25, (b) for aspect ratio of 1.0, (c) for aspect ratio of 0.75 and (d) for aspect ratio of 0.5.

compressive strain in concrete, tensile damage zone is also used to estimate the extent of the plastic hinge region at every wall-slab junction in the present study. For the specimens with wall panel aspect ratios of 1.67, 1.25, 1.0, 0.75 and 0.5, the possible plastic hinge regions are obtained by observing the variation of the mentioned parameters in the wall cross-section (Figures 6.9a - 6.9d). All the parameters show similar distribution across the height of the wall with higher values at each wall-slab junction. By observing the distance over which each of these parameters reduces to zero on each side of the wall-slab junction, the possible extent of plastic hinge region is obtained.

6.3.1 Plastic Hinge Length

Based on the tensile damage at wall-slab junction region, possible extent of plastic hinge region are identified for different wall panel aspect ratios (Figures 6.10 and 6.11) during monotonic and cyclic analyses. Although conventionally inelastic curvature is directly used for expressing the plastic hinge length (L_p), the extent of tensile damage is also considered as a useful indicator for the present study. In case of monotonic pushover analysis, the curvature profile considering the strains at the extreme tension and compressive faces of the shear wall is obtained at the maximum damage level. The curvature profile for cyclic loading is obtained at the maximum lateral load capacity of the shear wall. The variation in stress in the vertical reinforcement over the height of the wall and possible yielding of reinforcement at the wall-slab junction region are related to the maximum tensile damage at the wall-slab junction region. Although the observed maximum curvature reduces with increase in wall panel aspect ratio, the spread of tensile damage also decreases with the spreading out of strut-and-tie action in squat wall panels. This is observed for both monotonic and cyclic displacement-controlled nonlinear static analyses. It is observed that the spread of plasticity at the junction region reduces with an increase in the length of wall. Since the effect of axial compression is not contributing to the tensile damage and the compressive strains at the wall-slab junction region, the aspect ratio is considered as the key parameter affecting the extent of the zone showing inelastic behaviour.

For both monotonic pushover and cyclic pushover analyses, the identified L_p, normalized with respect to the length of the wall, is observed to increase with the wall panel aspect ratio (h_s/L_w) (Figure 6.12). Considering L_p to be linearly varying with storey height and length of shear wall panel, the normalized plastic hinge length at the wall-slab junction is obtained using regression analysis and is expressed as,

$$\frac{L_{p,cyclic}}{L_w} = 0.0546\left(\frac{h_s}{L_w}\right) + 0.0174 \text{ for cyclic loading, and} \qquad (6.12)$$

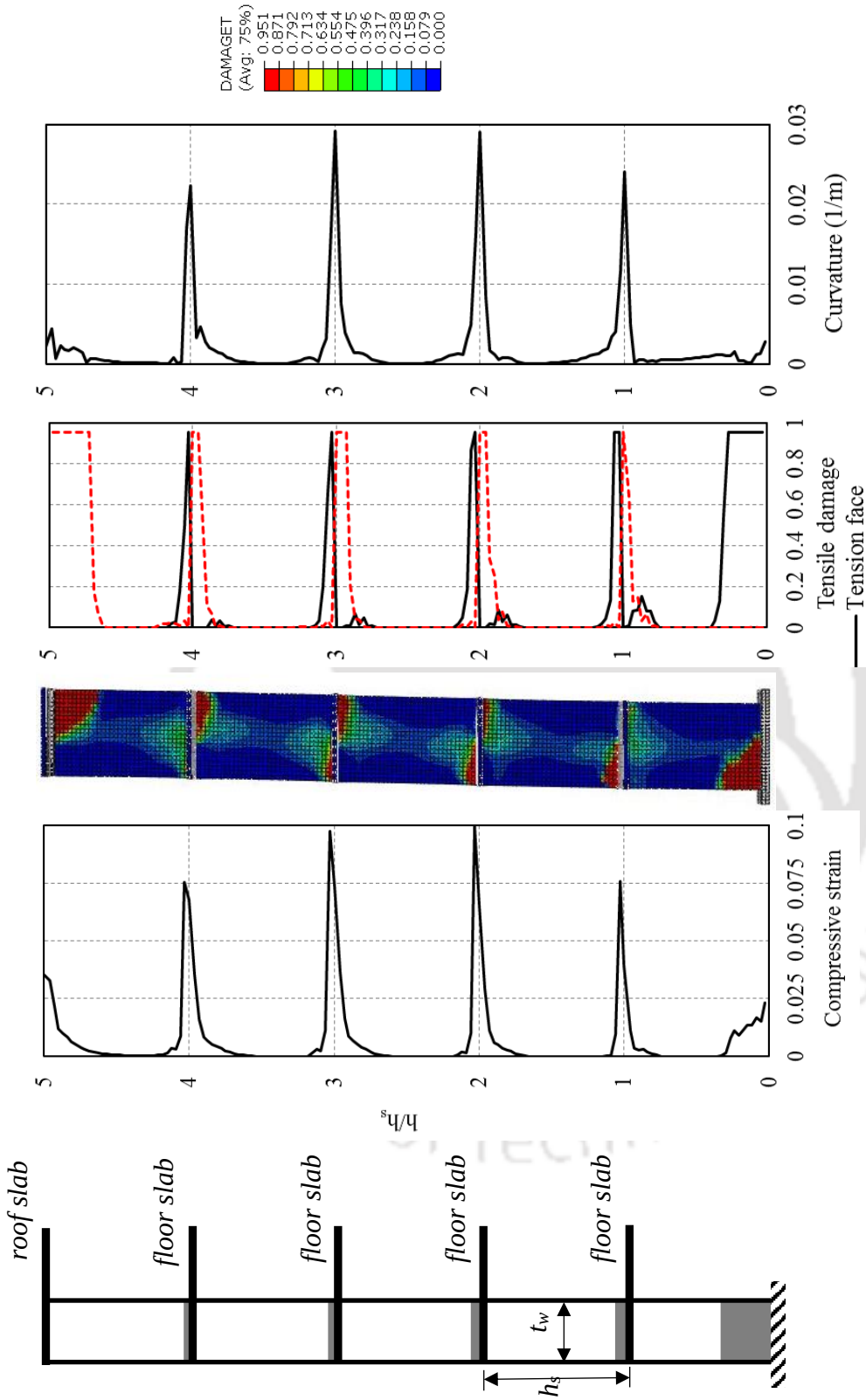

Figure 6.9: Observation of plastic hinge region in specimen with wall panel aspect ratio of 1.67: (a) typical wall-slab assemblage, (b) variation in compressive strain, (c) tensile damge pattern, (d) variation in tensile damage and (e) variation in curvature profile.

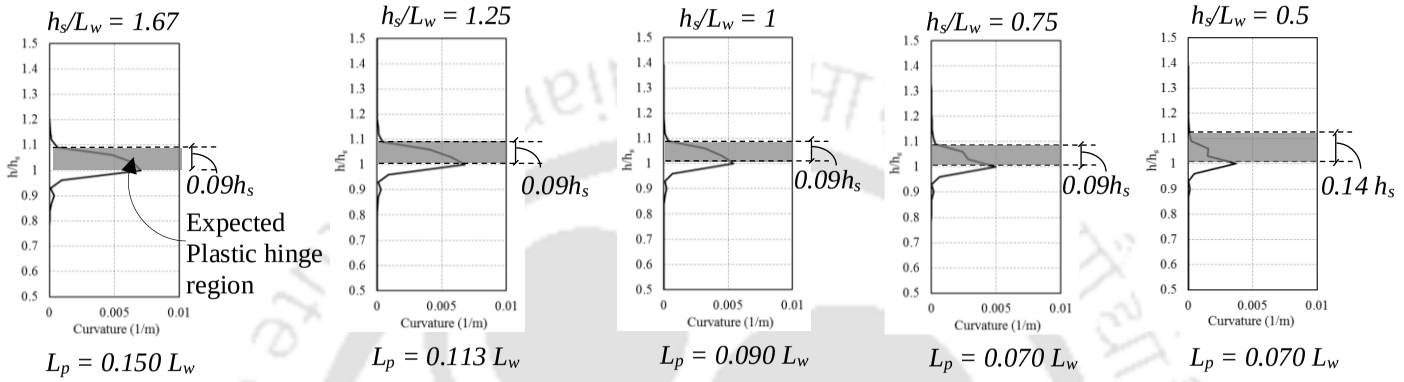

Figure 6.110:Comparison of possible plastic hinge length (L_p) for wall panels with different aspect ratios under monotonic nonlinear static analysis: (a) for aspect ratio of 1.67, (b) for aspect ratio of 1.25, (c) for aspect ratio of 1.0, (d) for aspect ratio of 0.75 and (e) for aspect ratio of 0.5.

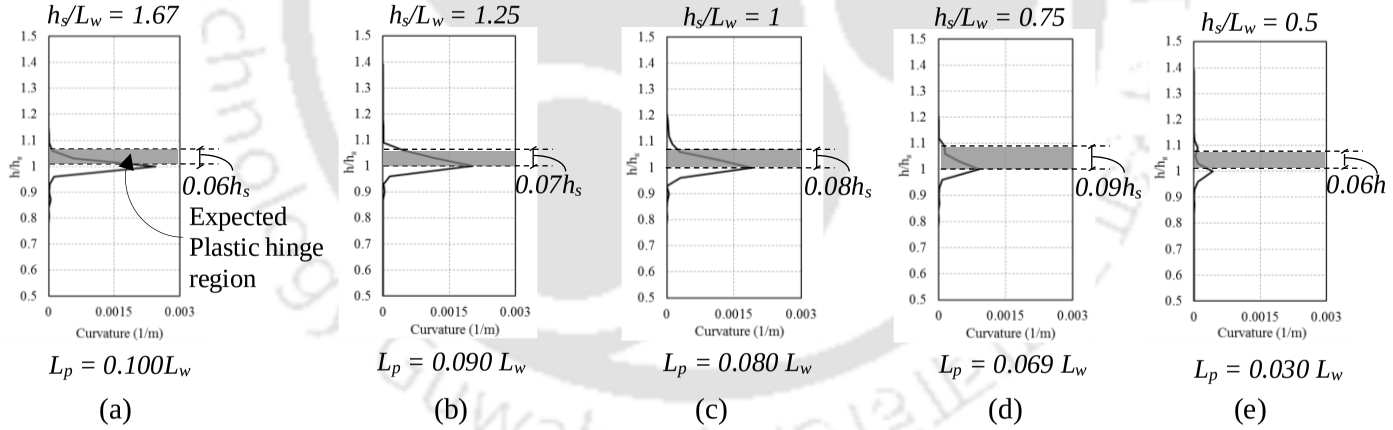

Figure 6.11: Comparison of possible plastic hinge length (L_p) for wall panels with different aspect ratios under cyclic nonlinear static analysis: (a) for aspect ratio of 1.67, (b) for aspect ratio of 1.25, (c) for aspect ratio of 1.0, (d) for aspect ratio of 0.75 and (e) for aspect ratio of 0.5.

$$\frac{L_{p,monotonic}}{L_w} = 0.0728\left(\frac{h_s}{L_w}\right) + 0.0234 \text{ for monotonic loading.} \quad (6.13)$$

From Eqs. (6.12) and (6.13), it is observed that $L_{p,monotonic} \approx 1.34 L_{p,cyclic}$. To examine the accuracy of the proposed Eqs. (6.12) and (6.13), the plastic hinge length (L_p) at the wall-slab junction is estimated for five different lengths of shear wall and compared with the calculated values of L_p proposed in the various past studies on RC walls (Table 6.1). In the past studies, it is mentioned that inelastic behaviour is observed mostly at the bottom of the isolated slender shear wall. However, the presence of slabs at every floor level in a multistoried building leads to inelastic behaviour at the wall-slab junction in addition to the inelastic behaviour at the base of the wall. The estimates of L_p, as per Eqs. (6.12) and (6.13), are obtained considering the possible zones of inelastic behaviour along the height of the wall and at wall-slab junction.

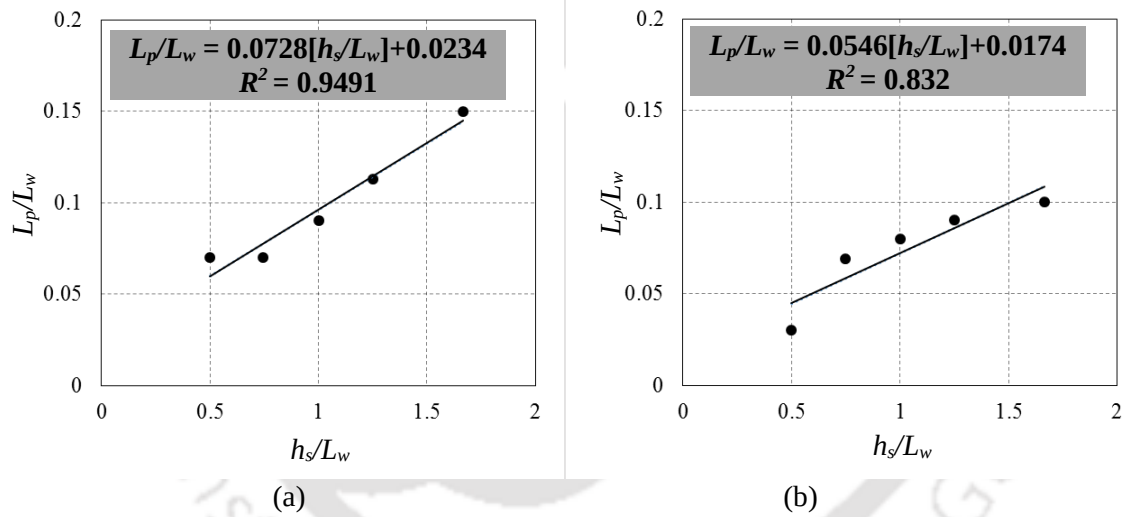

Figure 6.12: Variation of normalized plastic hinge length with wall-panel aspect ratio for: (a) monotonic and (b) cyclic analysis cases.

Among the past studies, Panagiotakos and Fardis (2001) have proposed expressions for plastic hinge length under monotonic and cyclic loadings. Closed form equations were developed for the ultimate deformation capacity and for the deformation at yielding of RC members in terms of their geometric and mechanical characteristics. The database used for the study comprised of 1012 tests (mainly cyclic loading) of RC members in uniaxial bending, with or without axial compression. Out of these specimens, 61 specimens are walls with a rectangular, barbelled, or T-section. On comparing the estimated plastic hinge lengths under monotonic and cyclic loadings, it is observed that the analytical estimates using the equations of Panagiotakos and Fardis (2001) are slightly lesser than

the estimated values as per the proposed equation (Table 6.1). However, the proposed expressions are applicable only for the plastic hinge region adjacent to the wall-slab junction region. Between the two parameters, h_s and L_w, more weightage is given on h_s which reflects the increase in plastic hinge length with more slender wall panel.

Table 6.1: Comparison of plastic hinge length for different lengths of shear wall

Model		L_w = 3 m	L_w = 4 m	L_w = 5 m	L_w = 6.7 m	L_w = 10 m
Baker and Amarakone (1964)		0.49 L_w	0.46 L_w	0.43 L_w	0.40 L_w	0.36 L_w
Sawyer (1964)		0.26 L_w	0.25 L_w	0.24 L_w	0.23 L_w	0.22 L_w
Mattock (1964)		0.47 L_w	0.40 L_w	0.36 L_w	0.31 L_w	0.25 L_w
Corley (1966)		0.42 L_w	0.41 L_w	0.41 L_w	0.41 L_w	0.40 L_w
Mattock (1967)		0.44 L_w	0.43 L_w	0.43 L_w	0.42 L_w	0.41 L_w
Priestly and Park (1987)		0.08 L_w	0.06 L_w	0.05 L_w	0.04 L_w	0.02 L_w
Paulay and Priestly (1992)		0.09 L_w	0.07 L_w	0.05 L_w	0.04 L_w	0.03 L_w
Paulay and Priestly (1993)		0.24 L_w	0.23 L_w	0.22 L_w	0.22 L_w	0.21 L_w
Sasani and Der Kiureghian (2001)		0.36 L_w	0.35 L_w	0.35 L_w	0.34 L_w	0.34 L_w
Panagiotakos and Fardis (2001)	**Cyclic analysis**	**0.10 L_w**	**0.08 L_w**	**0.06 L_w**	**0.04 L_w**	**0.03 L_w**
	Monotonic analysis	**0.15 L_w**	**0.09 L_w**	**0.09 L_w**	**0.07 L_w**	**0.05 L_w**
Bohl and Adebar (2011)		0.24 L_w	0.22 L_w	0.21 L_w	0.20 L_w	0.19 L_w
Kazaz (2013)		0.16 L_w	0.17 L_w	0.18 L_w	0.19 L_w	0.20 L_w
Kazaz (2013)		0.20 L_w	0.19 L_w	0.18 L_w	0.17 L_w	0.16 L_w
Present study	**Cyclic analysis**	**0.11 L_w**	**0.07 L_w**	**0.07 L_w**	**0.06 L_w**	**0.04 L_w**
	Monotonic analysis	**0.14 L_w**	**0.10 L_w**	**0.10 L_w**	**0.08 L_w**	**0.06 L_w**

6.4 CONCLUSIONS

In case of highrise buildings, typically a shear wall is usually connected with the slabs at every floor level. Thus, the analytical estimates of plastic hinge length, proposed in earlier studies without considering the effect of floor slabs, will not be applicable. In the present study, an expression is proposed for estimation of possible plastic hinge length at the junction of shear wall and floor slab. The expression is developed by observing variation in tensile damage pattern and curvature along the height of the wall during monotonic and cyclic nonlinear analyses under constant axial load. Due to the mobilization of the strut-and-tie mechanism in each partitioned wall panel, the

concentration of tensile damage at each floor level plays an important role in identifying the extent of plastic hinge region. The amount of vertical steel in wall is not observed to influence the plastic hinge length at the wall-slab junction region. The reinforcement did not reach the ultimate stress in any of the analysis. The proposed expression needs to be further validated through detailed experimental studies on RC wall-slab junction regions.

Chapter 7
DRIFT CRITERIA FOR RC SHEAR WALL BUILDINGS

7.0 OVERVIEW

The lateral displacement of a structural system is an important parameter from the seismic design point of view. It has three major implications, namely (a) structural stability, (b) additional seismic demand on structural component due to large deformations and (c) damage to various non-structural components. Incorporation of desirable lateral displacement limits in the seismic design methodology has led to the proposition of displacement-based structural design. In the conventional seismic design, limits of lateral drift have been prescribed in the design guidelines of a few countries, e.g., prescription of design elastic lateral drift limit of 0.4% by the Indian Standard IS:1893 (Part 1) (BIS, 2016b). However, direct prescription of inelastic drift limit for desirable seismic behaviour of building is absent in the design guidelines of different countries.

In case of buildings with ductile RC moment-resisting frames, the lateral displacements tends to become large with the increase in the height of the building. Thus, beyond a certain height of such buildings, provision of RC structural wall in the building become necessary. By virtue of its large lateral stiffness, the structural wall tends to reduce the overall displacement of the building during strong earthquake shaking through the floor slab-frame-wall interaction. Although, past studies have been conducted on ultimate drift capacity of lightly reinforced shear wall with low aspect ratio (Duffey et al., 1994), similar investigations on slender shear walls have not prescribed any limiting drifts. As observed in the earlier chapters, the wall-slab junction region in multistoried RC wall-frame buildings tends to incur damage even during static lateral loading. Similar damages in the upper stories of RC wall-frame buildings have been observed during 2010 Chile earthquake. Thus, to prevent extensive damage in the wall-slab junction and subsequent propagated damage in the floor slab, lateral drift limits for slender structural walls need to be prescribed. The present chapter provides details on the investigation of lateral drift limits for a wall-slab assemblage isolated from a multistoried frame-wall building.

Different codes employ different load and material factors (or strength reduction factors) for the design of members, and hence the actual provided strength in different codes may not follow the same pattern as the design base shear. Further, the drift may govern the design in many cases,

resulting in further discrepancies in the actual provided strength. Various codes differ not only in the limits on interstory drift, but also in the estimation procedure. In ASCE 7 (2010), elastic displacement at a floor level is calculated and amplified by a deflection amplification factor depending on the type of building. Limits are provided on amplified interstory drifts, representing the inelastic deformations in the building. Eurocode 8 (BS EN 1998-1, 2005) presents limits on the elastic displacements amplified directly by the behavior factor. NZS 1170.5 (2004) requires the elastic displacements to be multiplied by the structural ductility factor and drift modification factor in order to obtain inelastic displacements. The drift modification factor accounts for higher mode effects and depends on the height of the building. The Indian standard, IS 1893 (Part 1), provides the drift control limits directly on the elastic displacement at the design load, without any amplification for ductility demand. The code limits the drift at design load (i.e., the elastic drift at reduced load), and not the total drift. This has serious implications towards the performance of the buildings designed as per the code.

ASCE 7 (2010) limits story drift according to occupancy category and allows up to 2.5% drift for ordinary multistory RC frame buildings. According to Eurocode 8 (BS EN 1998-1, 2005), the allowable story drift depends on the type of non-structural elements, and for multistory RC framed buildings, the allowable drift is 1% for buildings having brittle non-structural elements, 1.5% for buildings having ductile non-structural elements, and 2% for buildings having non-structural elements or without non-structural elements. NZS 1170.5 allows a story drift of 2.5% for all types of buildings, irrespective of material and occupancy class. IS 1893 limits the interstory drift to 0.4% at the design load level, which renders it dependent on the ductility class of the building (Haldar and Singh 2009). This is also crucial for the development of future versions of seismic codes based on displacement-based design methodology (Khose, et al., 2012). The limits and estimation procedure for permissible drift are necessary considering the nonlinear behaviour of the buildings designed as per the codes.

In the past studies on response of RC shear walls (Wallace and Moehle 1992, Priestley and Kowalsky 1998, Derecho et al. 1978), the structural parameters considered were, (a) ratio of wall cross-sectional area to floor-plan area, (b) fundamental period, (c) shape of the structural wall cross-section, (d) aspect ratio (h_s/L_w) and configuration in the plan, (e) axial load (P/f_cA_w), (f) length, (g) amount of web reinforcement, (h) normalized shear stress, (i) percentage of the longitudinal reinforcement (ρ_b) and (j) confinement of compression zone concrete. In the present study, out of the above mentioned parameters, aspect ratio of wall panel, length of the structural wall axial load and the amount of longitudinal steel are varied as the salient parameters and nonlinear static analysis is carried out. The results of nonlinear static analyses are used to define the lateral drift limit of structural walls. The lateral drift values at maximum damage state for different locations are

presented and a limiting range of lateral drift is recommended to avoid damage at the wall-slab junction region.

7.1 MODELLING DETAILS AND PARAMETERS

An exterior wall-slab assemblage (similar to the specimen mentioned in previous Chapter) of a hypothetical five storied RC frame-wall building (Kaushik and Dasgupta, 2013) is considered for investigation of the drift requirement. The building is assumed to be located in Seismic Zone V as per the Indian Earthquake code (BIS, 2016b) (Figure 3.13a). Considering the variation in wall thickness, slab thickness and wall panel aspect ratio, twelve different models (Table 7.1) are analyzed using finite element program with the material properties and the boundary conditions similar to those of EWSC model.

Table 7.1: Dimensional and reinforcement details of the models used in the analysis for lateral drift criteria

Model Configuration	Wall			Slab				
	Thickness (mm)	Length (mm)	Height (mm)	Longitudinal reinforcement	Transverse reinforcement	Thickness (mm)	Width (mm)	Length (mm)
WSM_TW1	200	3000	15	8@300	8@300	120	1500	3000
WSM_TW2	300	3000	15	8@300	8@300	120	1500	3000
WSM_TW3	400	3000	15	8@300	8@300	120	1500	3000
WSM_TS1	300	3000	15	8@300	8@300	100	1500	3000
WSM_TS2	300	3000	15	8@300	8@300	120	1500	3000
WSM_TS3	300	3000	15	8@150	8@150	200	1500	3000
WSM_TS4	300	3000	15	8@150	8@150	250	1500	3000
WSM_AR1	300	3000	10	8@300	8@300	120	1500	3000
WSM_AR2	300	3000	15	8@300	8@300	120	1500	3000
WSM_AR3	300	3000	25	8@300	8@300	120	1500	3000
WSM_AR4	300	5000	25	8@300	8@300	120	1500	5000
WSM_AR5	300	10000	25	8@300	8@300	120	1500	10000

The elements and the method of modelling are also considered to be the same as the EWSC model. WSM_TW2, WSM_TS2 and WSM_AR2 models are similar to EWSC model in geometry and the provided amount of vertical steel. The models WSM_TW1, WSM_TW2 and WSM_TW3 are identical except the thickness of wall, which is considered as 200 mm, 300 mm and 400 mm, respectively for the three models. In slabs, the longitudinal and transverse reinforcement are provided using 8 mm diameter bars at spacing of 300 mm. Similarly, WSM_TS1, WSM_TS2, WSM_TS3 and WSM_TS4 are identical except the thickness of slab. The thickness of slab is varied and considered as 100 mm, 120 mm, 200 mm and 250 mm, respectively, for WSM_TS1, WSM_TS2, WSM_TS3 and WSM_TS4. For WSM_TS1 and WSM_TS2 models, bars of 8 mm diameter are used at spacing of 300 mm as longitudinal and transverse reinforcement in slab. The slabs of WSM_TS3 and WSM_TS4 are reinforced with 8 mm diameter bars at a spacing of 150

mm. WSM_AR1, WSM_AR2 and WSM_AR3 are identical except the height of shear wall panel between the floor slabs. The height of shear wall panel between the floor slabs is considered as 2 m, 3 m and 5 m for WSM_AR1, WSM_AR2 and WSM_AR3 models respectively. Also, models WSM_AR3, WSM_AR4 and WSM_AR5 are identical except the length of wall. The length of wall is varied as 3 m, 5 m and 10 m, respectively, for these models. Bars of 8 mm diameter are used at 150 mm spacing as vertical reinforcement and horizontal reinforcement in shear wall for all the models in two rows. The maximum damage is observed mainly at three locations, namely (a) at the base of the shear wall, (b) in wall at the wall-slab junction and (c) in slab at the wall-slab junction. The drift levels corresponding to the maximum damages at the mentioned locations are also noted.

7.2 Analysis Details

Displacement based nonlinear static analyses are performed under monotonic loading with no axial load for the mentioned slab-wall assemblages. The gravity loads (both dead and live loads) on slab are assigned as pressure loads on the surface of the solid elements. These loads on the slab are kept constant during each analysis. The target lateral displacement of 500 mm is applied at the top node in the plane of the shear wall with a triangular variation of displacement distribution across the floor levels along the height of the wall (Figure 5.1c). The inelastic drift limit is proposed by carrying out parametric study, first by varying the thickness of shear wall, secondly by varying the thickness of floor slab and lastly by varying the aspect ratio of shear wall panel.

The compressive and tensile stress-strain characteristics of concrete (as discussed in Chapter 3) are assigned using Concrete Damage Plasticity (CDP) model. The steel reinforcement in wall and slab is modeled using plasticity model of ABAQUS program. The concrete members is modelled using 8 noded solid elements with reduced integration (C3D8R) and reinforcement embedded in the shear wall and floor slab regions. The steel reinforcement of the assemblage is modelled with 2 noded truss element (T3D2). The reinforcement is obtained in the wall and slab by considering the design load combinations as per Indian Standard of earthquake resistant design (BIS, 2016b). The detailing of reinforcement in shear wall and continuous floor slabs is done as per Indian Standard (BIS, 1987) and already explained in Chapter 3. The material properties of the M25 grade concrete and HYSD Fe415 steel are given in Table 3.1.

7.3 Evaluation of Results and Proposed Drift Limits

In the previous chapter, it was mentioned that the possible regions of inelastic behaviour are located at the base of the wall and the slab-wall junctions at each floor level. Thus, in the present study, the tensile damage is monitored at those locations for developing lateral drift criteria for frame-wall

buildings with rectangular walls (Figure 7.1). At any location in an RC member, the tensile damage gets initiated through cracking of concrete and finally leads to yielding of reinforcement in tension and crushing of concrete. In the behaviour of shear walls controlled by flexure, the tensile strain in the extreme layer of steel is observed to reach 0.003 at the yield level. In members with more than one layer of reinforcement on the tension side, all the layers do not yield simultaneously. The global behaviour of the assemblage i.e., the variation of lateral shear capacity with lateral displacement) gets influenced by yielding of reinforcement at a single or multiple locations.

In the present study, the percentage drift at first floor level is presented instead of roof level drift of the wall-slab assemblage because the drift obtained at the roof level is not a meaningful measure to investigate the deformation capacity of structural walls (Seneviratna and Krawinkler, 1997). Additionally, the base stories are the most critical regions when the deformability of the cantilevered walls is considered.

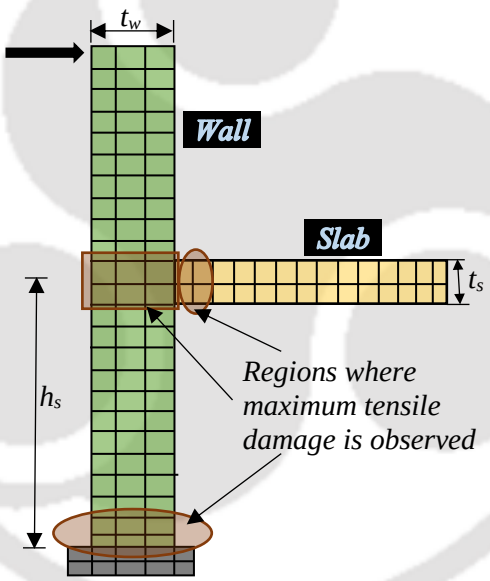

Figure 7.1: Location of regions where maximum tensile damage is observed.

7.3.1 Variation of wall thickness

For variation of wall thickness (200 mm, 300 mm and 400 mm), the models WSM_TW1, WSM_TW2 and WSM_TW3 are analysed and the tensile damage is observed at the different locations as mentioned in Figure 7.1. The different lateral drift levels for the maximum damage states at the different locations are shown in Figure 7.2.

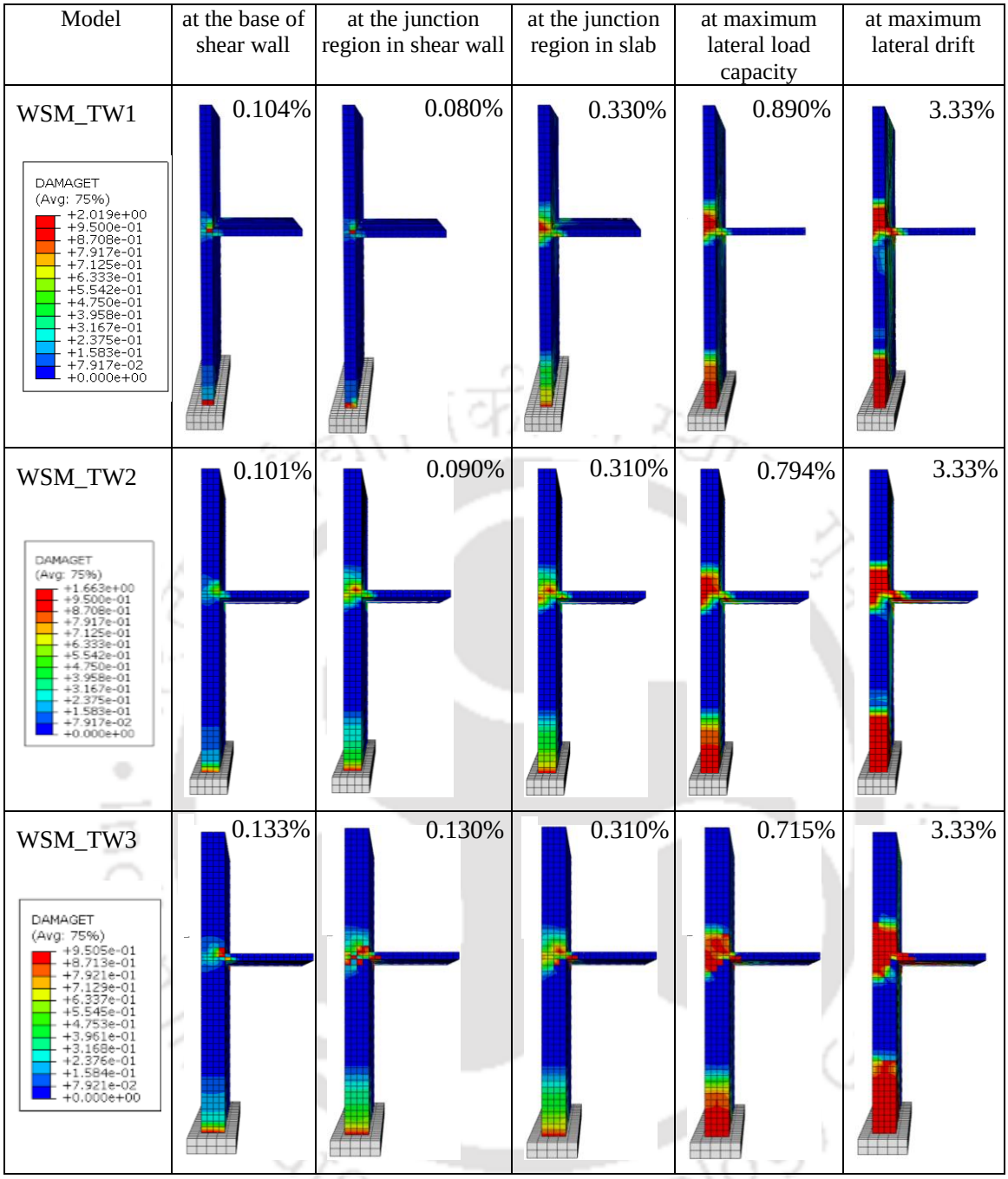

Figure 7.2: Comparison of tensile damage at different drift levels with variation in thickness of shear wall.

Also, the tensile damage pattern is compared at peak lateral shear strength and the drift capacity noted. The drift capacity at the peak shear strength is directly obtained from the pushover curve of each model. As per the current provisions of the Indian Earthquake Code (BIS, 2016b), RC buildings are expected to show linear elastic behaviour till the lateral drift limit of 0.4%. However, for all the studied models, nonlinearity in concrete starts at much lower drift levels. Also, yielding of vertical reinforcement in wall is observed at lower or comparable drift levels. Thus, the existing codal

prescription needs to be relooked at for RC wall-frame buildings considering the realistic behaviour. Figure 7.3 shows the variation of lateral drift level at the attainment of maximum damage at different locations of the assemblage for different thickness of shear wall. It is observed that the percentage drift at maximum damage level for shear wall at its base is 0.10% when the wall thickness is considered as 200 mm, while it gets increased to 0.133% for 400 mm thickness of wall. Also, the percentage lateral drift at maximum damage level for shear wall at the junction region increases with the increase in wall thickness, for example, from 0.08% for 200 mm wall thickness to 0.13% for 400 mm thick wall. The percentage of drift varied from 0.08% to 0.13% in shear wall considering the maximum damages at the base of the shear wall and at the wall-slab junction region. The tensile damage in the slab reaches its maximum value at a higher drift as compared to the drift at which the maximum damage is attained in the shear wall. Hence, the drift limit is proposed considering the maximum damage occurring at a particular drift in the shear wall. Also, at the base of the shear wall it is observed that the drift capacity is minimum when the thickness of shear wall is less (200 mm). The finite element analysis results confirm that the maximum stress concentration develops at the base of the shear wall first and then at the wall-slab junctions of the upper floor levels. Also, the developed tensile damage and the stresses are higher in the portion of the slab connected to the shear walls which are oriented in the direction of the applied displacement. The observed damage in the shear wall at the wall-slab junction reaches its maximum value at lower drift as compared to other locations in the assemblage.

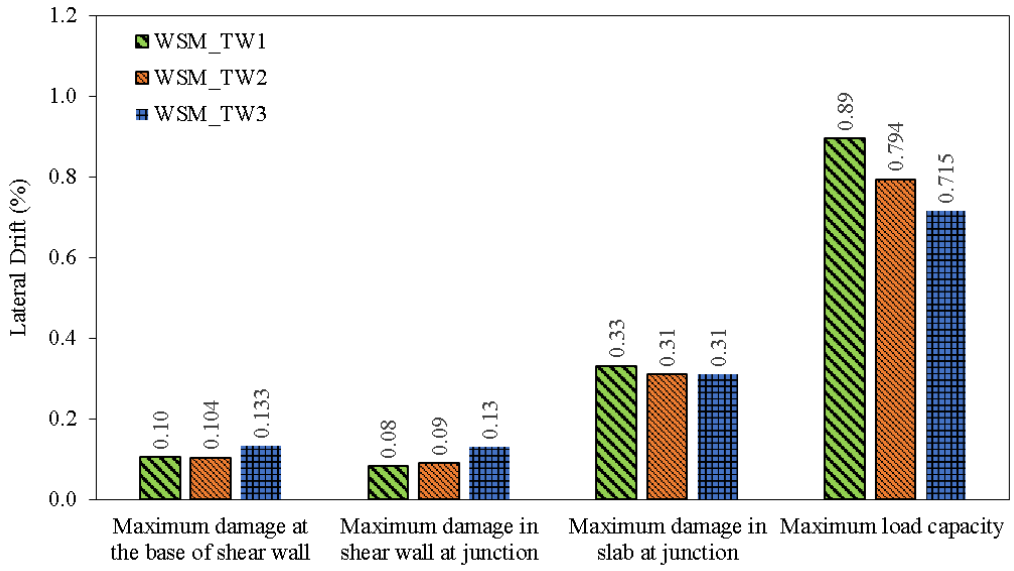

Figure 7.3: Variation of lateral drift levels with respect to maximum damage at different locations of the assemblage for different thickness of shear wall.

Considering three different thickness of shear wall, the variation of tensile damage from zero to maximum at three different locations of the assemblage is obtained (Figure 7.4). Figure 7.4a

compares the damage variation for shear wall of 200 mm thickness. The shear wall in the junction region reaches the maximum damage value first at a very low drift. The damage in the slab reaches the maximum value at a higher drift as compared to the wall. Similar trend is observed when the thickness of shear wall is increased to 300 mm and 400 mm, respectively (Figures 7.4b and 7.4c). Figures 7.4d, 7.4e, and 7.4f show the details of damage pattern at very low drift level for 200 mm, 300 mm, and 400 mm thick walls, respectively. It is observed that in all the cases, the wall experiences inelastic behaviour (maximum damage level) at a drift level between 0.08% and 0.13%. However, IS 1893 (Part 1) (BIS, 2016b) provides the elastic drift limit of 0.4% without considering the inelastic displacement.

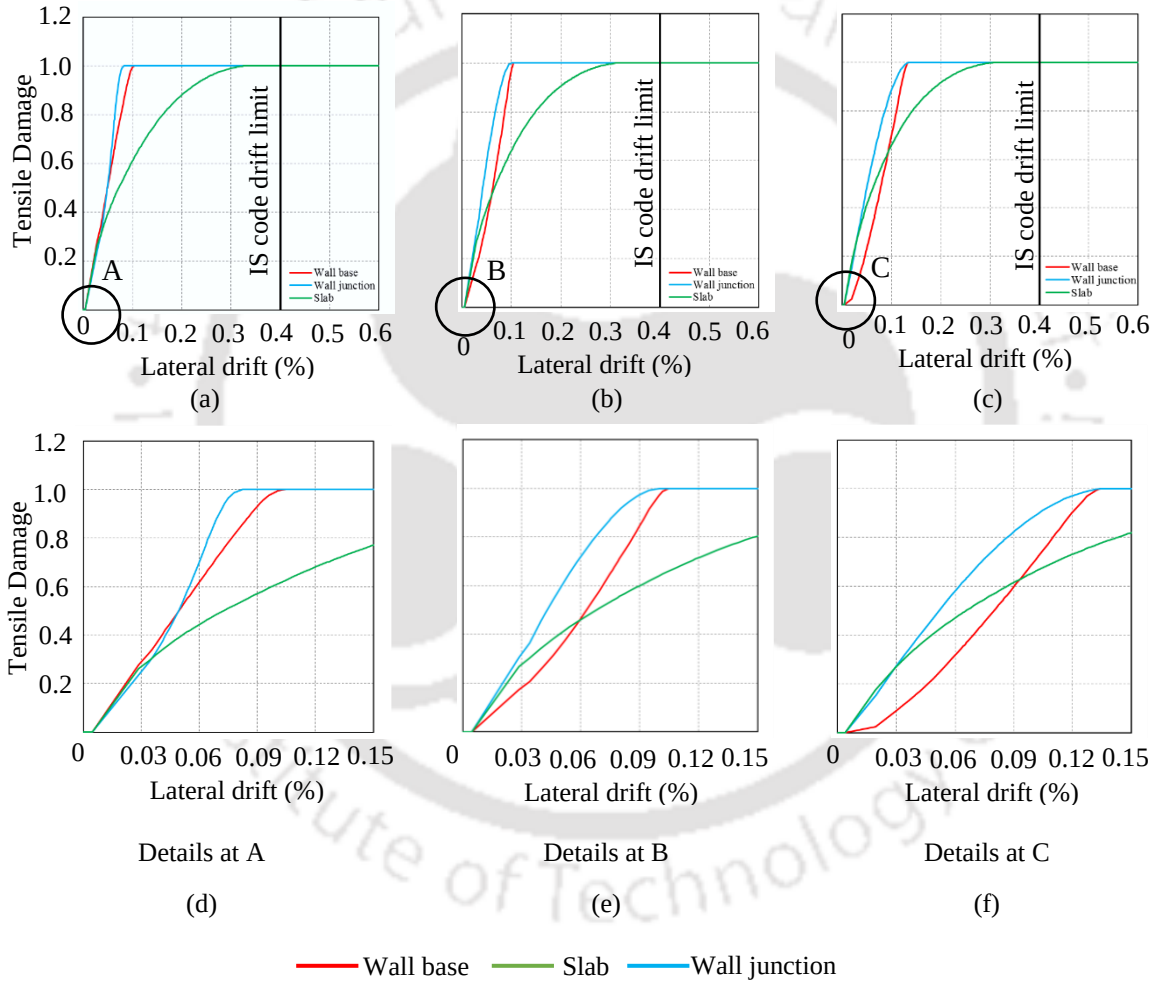

Figure 7.4: Variation of tensile damage at different locations of wall-slab assemblage with the thickness of shear wall; (a) 200 mm, (b) 300 mm and (c) 400 mm, (d) details at A, (e) details at B and (f) details at C.

During pushover analysis, no damage is observed in the wall or slab up to a drift level of around 0.005%. Afterwards, cracks start developing at the base of the shear wall and in the slab at the wall-slab junction region. With increase in the thickness of wall, the tensile damage tends to reduce at

the base of the wall. Maximum variation in the lateral drift level is observed in the shear wall at the junction region. With an increase in the thickness of wall, the maximum damage at the wall-slab junction is reached at a higher lateral drift level. Not much variation is observed in the lateral drift level for maximum damage in the wall at the base and in the slab at the junction region.

7.3.2 Variation of slab thickness

During earthquake shaking, lateral forces are generated at floor level and then transferred through the shear wall to the foundation. Thus, the wall-slab junction becomes a critical region due to high stress concentration. In the present section, the variation of lateral drift level for maximum tensile damages in wall and slab is observed by considering four different thickness of floor slab in the assemblage. Figure 7.5 shows the variation in the lateral drift levels at three different locations of the assemblage.

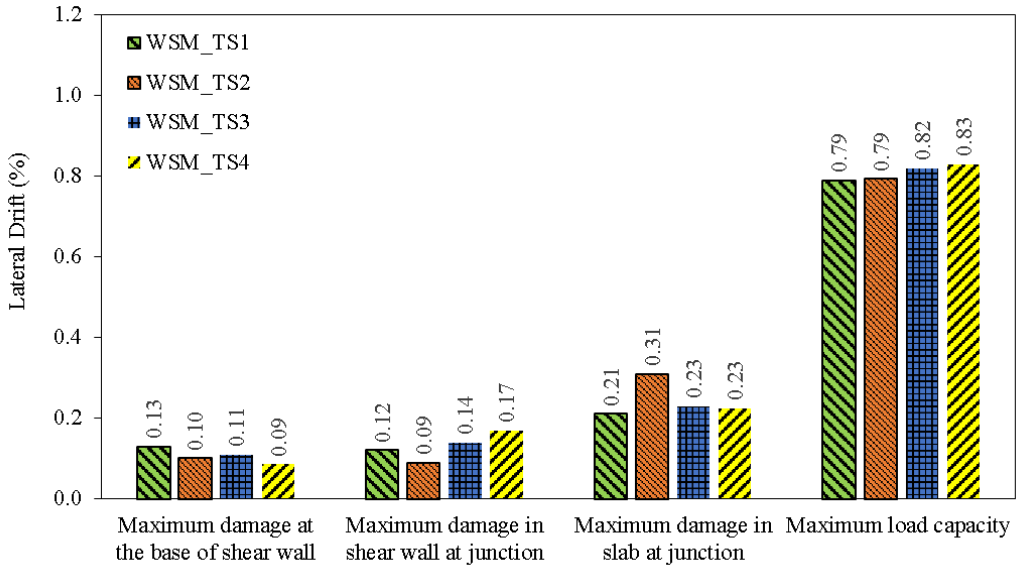

Figure 7.5: Variation of drift levels with respect to maximum damage at different location of the assemblage for different thickness of floor slab.

With the increase in the thickness of the slab, the value of observed drift for maximum damage at the base of the shear wall decreases. Due to increase in the thickness of wall, there is an increase in the lateral load at each floor level, which transfers more force to the shear wall leading to more damage at the base of the shear wall. The tensile damage at the base of the shear wall reaches its maximum value first when the thickness of slab is on the higher side. At the base of the shear wall, the damage reaches its maximum value at different drift levels varying between 0.09% and 0.13% for different thickness of slab. The various drift levels observed considering the maximum tensile damage reaching first at the shear wall in the junction region are 0.12%, 0.09%, 0.14% and 0.17%

(varies between 0.09% and 0.17%) for the models with 100 mm, 120mm, 200 mm and 250 mm thickness of slab, respectively. Figure 7.6 shows the tensile damage reaching its maximum value at different locations of the assemblage. The drift capacity is observed at these locations for maximum damage. As discussed in previous chapters, the shear wall gets partitioned due to the presence of floor slab. Due to the formation of struts between the floor slabs, the cracking get distributed at the slab-wall junctions along the height of the shear wall instead of concentration of inelasticity at the base of an isolated slender shear wall without connected floor slabs. In the slab region, the tensile damage reaches its maximum value at a higher drift level as compared to the drift level causing the same level of damage in shear wall at the junction region. The nonlinearity starts in the shear wall first at a very low drift level which is less than the elastic lateral drift limit recommended by the Indian Seismic Code.

Figure 7.7 explains the variation of tensile damage at the base of the shear wall, in the wall at the slab-wall junction and in the floor slab at the slab-wall junction region. Although the assemblage is displaced up to a lateral drift of 3.33%, but for better comparison, the damage pattern is represented till the lateral drift level of 0.6%. Upto a lateral drift of 0.6%, the elements at the mentioned three locations reaches the maximum damage level. As discussed in the previous section, similar behaviour is observed by varying the thickness of the slab. The shear wall at the wall-slab junction reaches the maximum damage level first and then the same is obtained at other locations. The intensity of damage is more for higher thickness of slab. From Figure 7.7d, it is observed that with an increase in the thickness of wall, the maximum damage reaches the maximum value at the base of the wall first then other locations. Higher thickness of floor slab increases the shear capacity and lateral drift level of the assemblage. With an increase in the thickness of slab, the drift level for maximum damage at the base of the shear wall decreases. The drift level reaching the maximum damage varies between 0.09% and 0.17%.

7.3.3 Variation of aspect ratio of wall panel

From the previous two sections, it is observed that the inelastic behaviour of the wall-slab assemblages started at a very low drift level and the tensile damage reaches it maximum value between drift levels of 0.08% and 0.17% considering the variation in the thickness of wall and slab. In this section, the influence of wall-panel aspect ratio on the attainment of tensile damages is investigated and the lateral drift levels for maximum damages at three different locations of the wall-slab assemblage are presented. As the floor slabs tend to partition the structural wall into a number of panels, the aspect ratio of each panel tends to affect the local behaviour in the vicinity of each wall-slab junction. In this study, walls of 3 m, 5 m, and 10 m in length (L_w) and

Model	at the base of shear wall	at the junction region in wall	at the junction region in slab	at maximum lateral load capacity	at maximum lateral drift
WSM_TS1 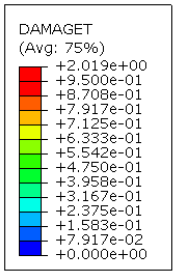	0.13% 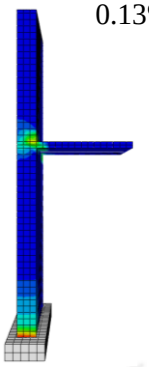	0.12% 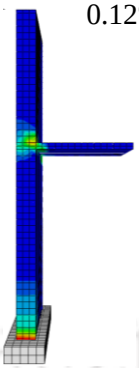	0.21% 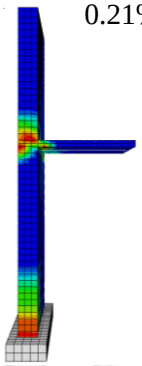	0.79% 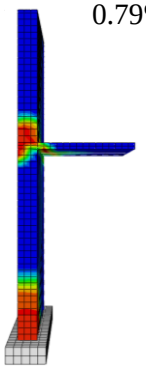	3.33% 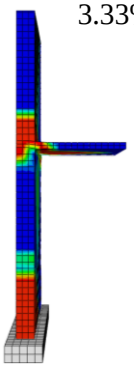
WSM_TS2 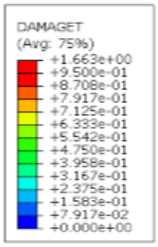	0.10% 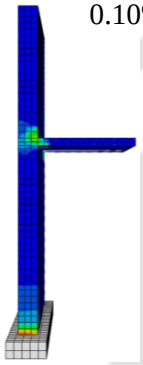	0.09% 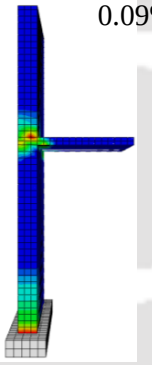	0.31% 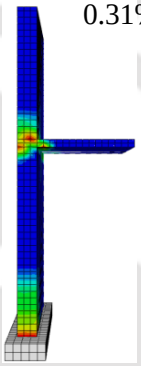	0.79% 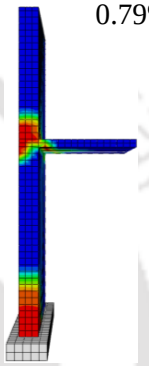	3.33% 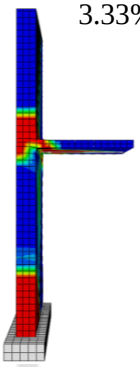
WSM_TS3 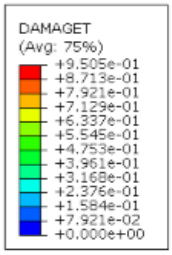	0.11% 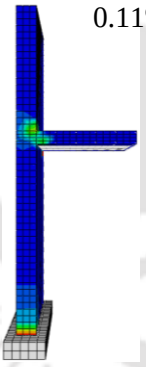	0.14% 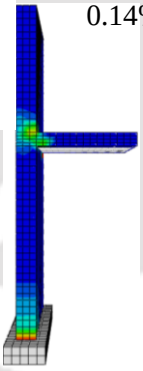	0.23% 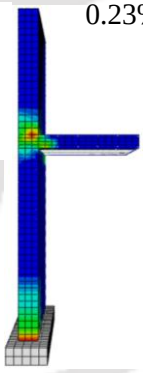	0.82% 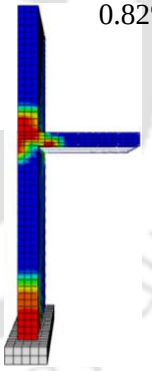	3.33% 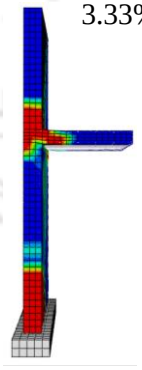
WSM_TS4 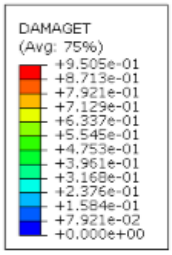	0.09% 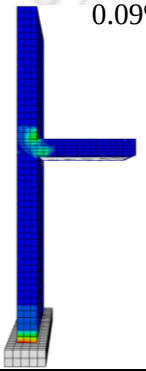	0.17% 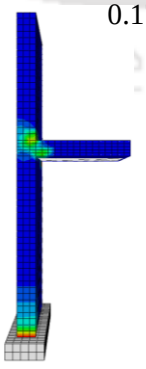	0.23% 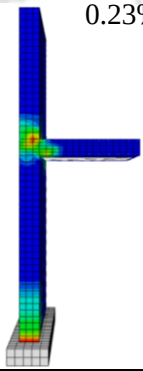	0.83% 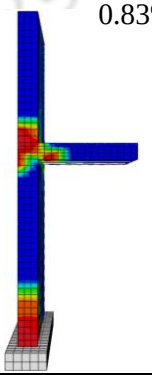	3.33% 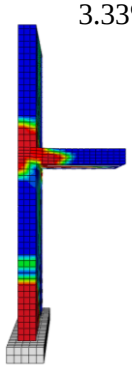

Figure 7.6: Comparison of tensile damage at different drift levels with variation in slab thickness.

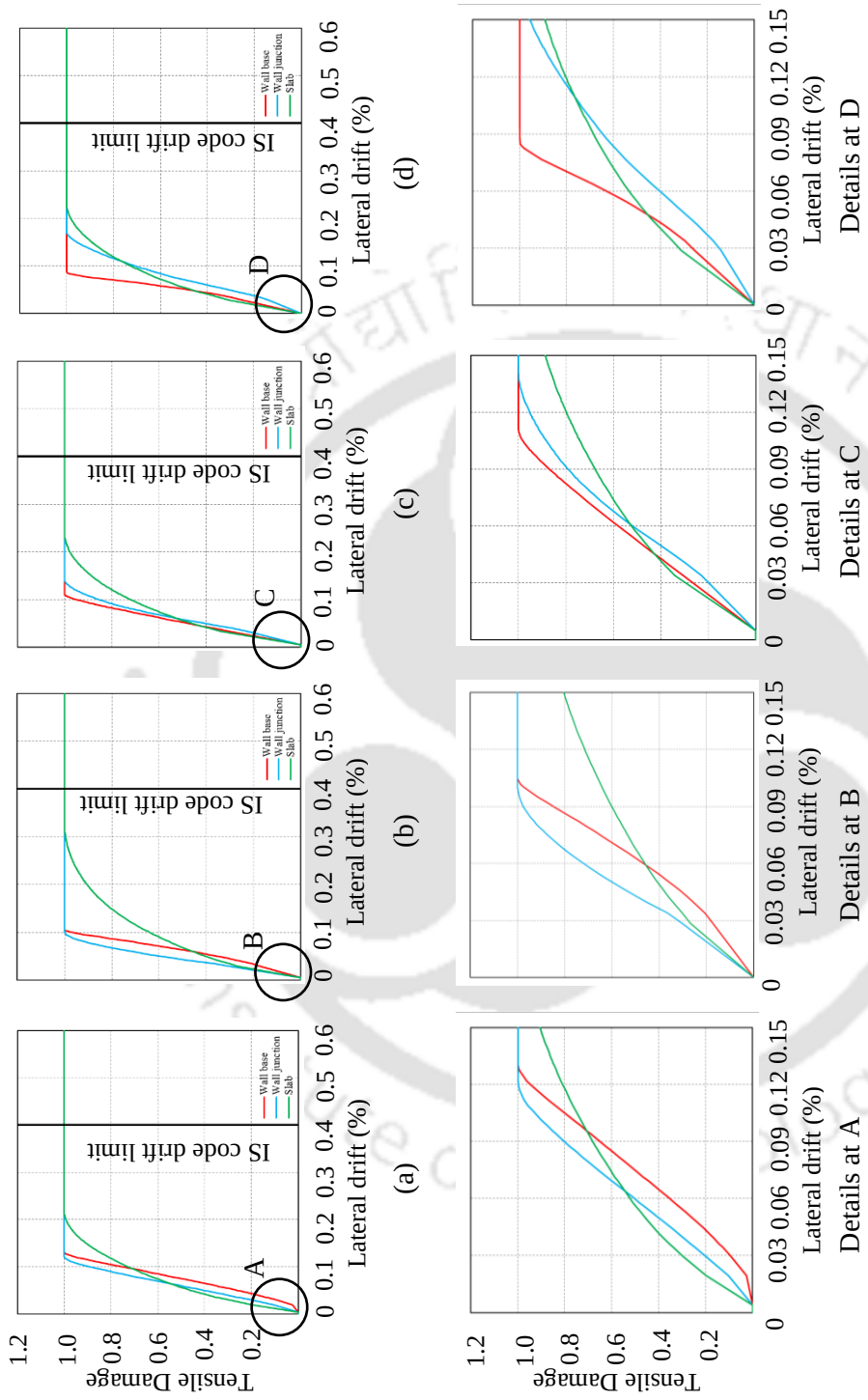

Figure 7.7: Variation of tensile damage at different locations of wall-slab assemblage by varying the thickness of floor slab; (a) 100 mm, (b) 120 mm, (c) 200 mm, (d) 250 mm, (e) details at A, (f) details at B, (g) details at C and (h) details at D.

2 m, 3 m, and 5 m, in effective panel height (h_s) between the floor slab are analyzed. Each pair of wall length and effective panel height corresponds to different wall panel aspect ratios (h_s/L_w), namely (a) 0.5, (b) 0.67, (c) 1 and (d) 1.25. Although not considered as an independent parameter in earlier studies, wall length appears to be an important parameter affecting response of shear walls. As shown in the following sections, for the walls that have the same aspect ratio but different wall lengths (WSM_AR2 and WSM_AR4) the deformation characteristics can be quite different. Variation of lateral drift levels with respect to maximum damage at different locations of the assemblage for different wall panel aspect ratio is shown in Figure 7.8. The drift level considering the maximum damage at the base of the base of the shear wall varies between 0.1% and 0.18%, while it varies between 0.08% and 0.11% in the wall at the junction region of the assemblage.

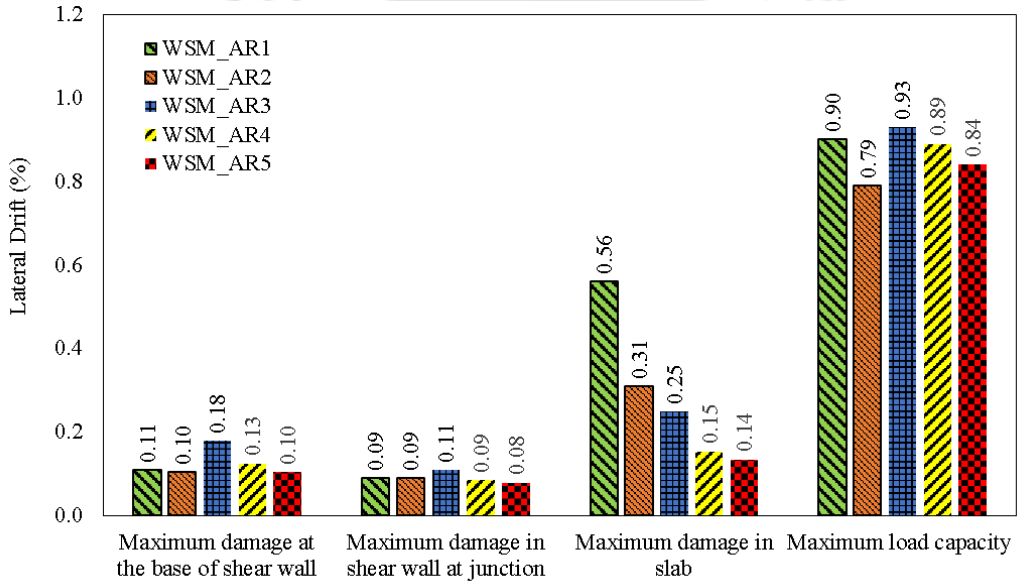

Figure 7.8: Variation of drift levels with respect to maximum damage at different locations of the assemblage for different wall panel aspect ratio.

For all the five models, the tensile damage starts at the base of the shear wall but reaches its maximum value in the shear wall at the junction region (Figure 7.9). For the maximum damage, the observed drift level is less for the shear wall at the junction region as compared to the drift level at the base of the wall. For the slab at the junction region, the maximum tensile damage depends on the length of the shear wall panel. Models WSM_AR1, WSM_AR2, and WSM_AR3 have the same length of wall as 3 m but the aspect ratio varies due to different heights of wall panel between the floors. Since the model WSM_AR1 is squat in nature, the observed drift level is more as compared to other models. As the wall length increases, the lateral drift of the shear wall gets reduced. For models WSM_AR3, WSM_AR4 and WSM_AR5, the lengths of shear wall are 3 m, 5 m and 10 m,

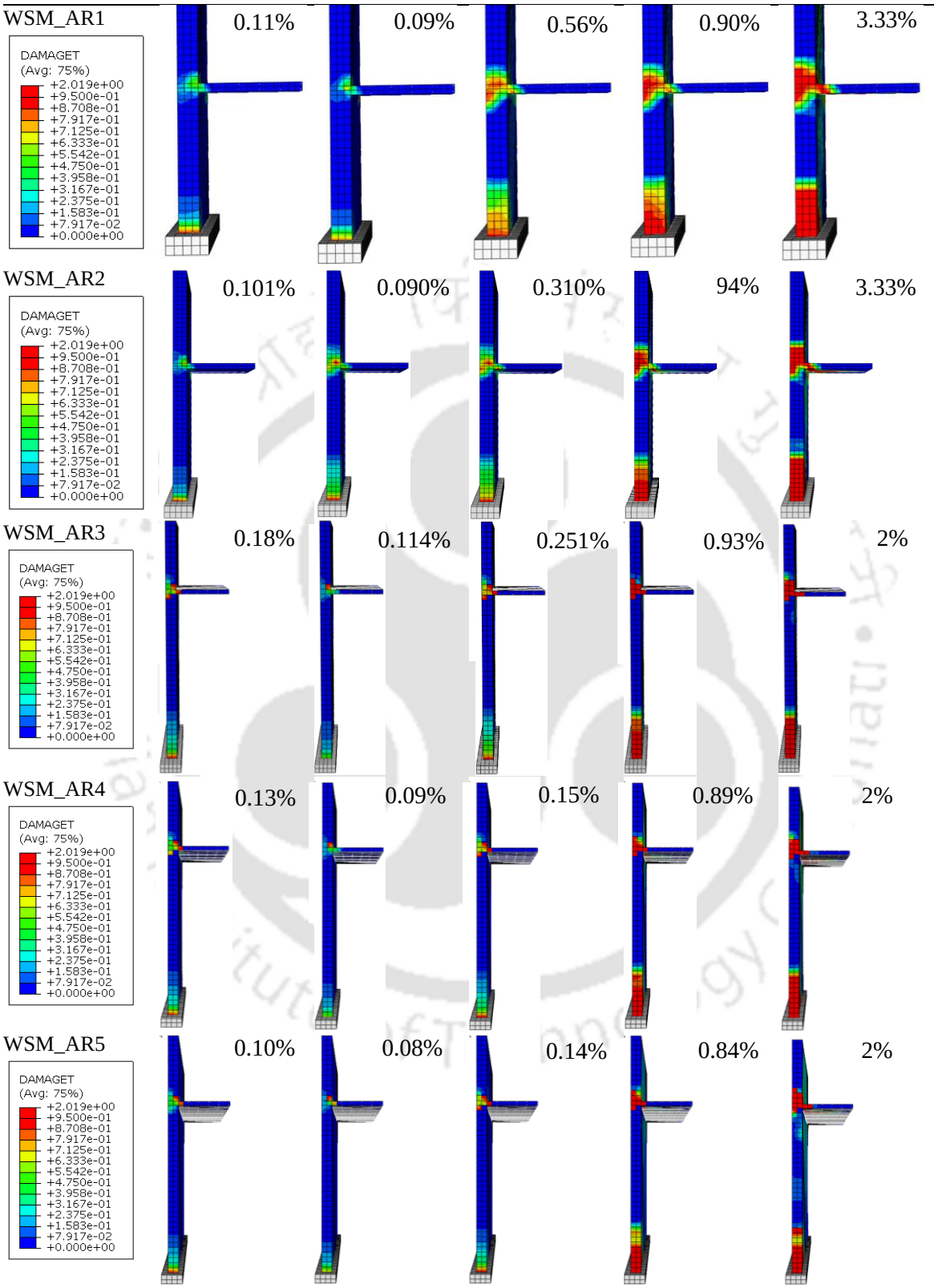

Figure 7.9: Comparison of tensile damage at different drift levels with variation in aspect ratio of wall panel.

respectively, and the lateral drifts observed from the maximum damage in the slab are 0.25%, 0.15%, and 0.14%, respectively. The lateral shear capacity is achieved at almost same drift level for all models.

From Figures 7.10a, 7.10b, and 7.10c, it is observed that the maximum damage is achieved at very low drift level at the base and junction region of shear wall, while the slab at the junction region shows the maximum damage at the higher drift ratio. This is because the length of the wall is same for the three models (WSM_AR1, WSM_AR2 and WSM_AR3). As the length of the wall is increased the drift ratio for maximum damage gets reduced (Figures 7.10d and 7.10e). At the lower drift ratio, cracks start developing at the base of the shear wall first and then in the junction region; thus, no significant damage level is observed (Figures 7.10f, 7.10g, and 7.10h). The cracks in the slab region develop at a very high drift level as compared to that for shear wall. The wall length is found to be the most significant parameter affecting the drift level of the structure. As the length of the shear wall is increased for models WSM_AR4 and WSM_AR5, it is observed the cracks in the slab region start at a lower drift and also the tensile damage reaches its maximum value at lower drift ratio (Figures 7.10i and 7.10j). The drift level varies between 0.08% and 0.18% for the observed maximum tensile damage at the two locations of the shear wall, i.e. at the base and the wall-slab junction region.

7.4 PROPOSED DRIFT LIMITS

Chilean code limits the lateral interstorey displacements resulting from the design forces to 0.2% of the storey height. From the studies carried out on buildings damaged during Chile Earthquake of March 3, 1985, it is observed that most of the multistoried buildings have experienced the maximum interstorey drift between 0.05% to 0.07%, which is much less than the allowable 0.2% (Riddle, 1992). Cassis and Bonelli (1992) carried out studies on four different buildings under three different ground motion records and observed that the drift ratios vary between 0.33% and 0.77%. The Chilean code imposes 0.2% lateral drift limit that results in elastic design, whereas, the building guidelines of USA and Turkey impose a drift limit of 2%. Such wide variations in prescribed lateral drift limits in design practices deserve a limitation for the interstorey drift and performance of tall buildings particularly with RC walls. Based on the records obtained from the 2011 Tohoku earthquake, many buildings reached an average drift ratio of 0.5% to 1% (Celebi and Okawa, 2014).

Although the Indian seismic code (BIS, 2016b) recommends the design elastic lateral drift level for buildings as 0.4%, it is observed that inelastic behaviour gets initiated at different locations in the wall-slab assemblage well before the recommended elastic drift level. From the parametric study carried out with variation in the thickness of wall, thickness of slab and the aspect ratio of wall

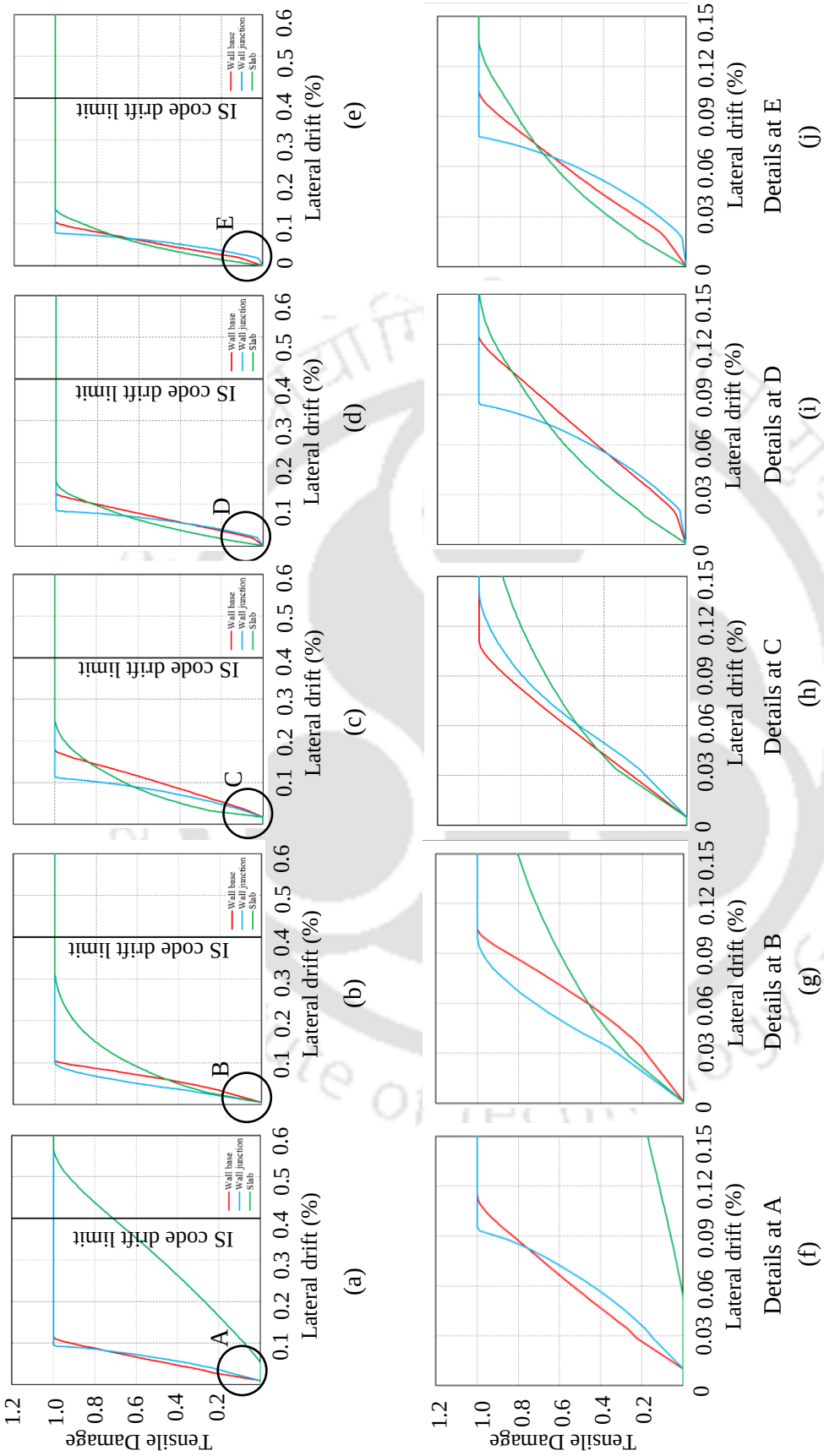

Figure 7.10: Variation of tensile damage at different locations of wall-slab assemblage with aspect ratio of shear wall panel; (a) 0.67, (b) 1 (h_s= 3 m) (c) 1.67, (d) 1 (h_s = 5 m), (e) 0.5, (f) details at A, (g) details at B, (h) details at C, (i) details at D, and (j) details at E.

panel, it is observed that the maximum damage at a lateral drift level in most of the cases is between 0.08% and 0.15%. Based on the parametric study, it is recommended that for RC frame-wall buildings with floor slab-wall junction, the lateral drift should be limited between 0.08% and 0.15% to prevent significant damage in slab at the wall-slab junction region. As the proposed drift limit is purely based on the parametric study involving numerical simulation, an experimental validation is required to propose a single value of the lateral drift limit for the multistoried RC wall-frame buildings displaced under lateral loads. As the level of damage in slab and wall depends significantly on the wall panel aspect ratio, the recommended length of wall should not exceed 3 m along with minimum wall panel aspect ratio of 1.0. With reducing wall panel aspect ratio, the strut action in the wall tends to maximize the tensile damage in the wall-slab junction region, thus increasing possibility of damage in the connected slab. Based on the present study, the following steps are recommended for the design of shear wall to avoid damage at the wall-slab junction region:

Step (i): The buildings should be analysed under design load combination and the maximum lateral drift should be estimated.

Step (ii): If the observed lateral drift is less than the recommended lateral drift (maximum damage in wall at junction region) then the design is acceptable.

Step (iii): Otherwise redesign the members so that the possible lateral drift level gets reduced below the recommended lateral drift (satisfying the recommended length of the wall and wall panel aspect ratio limits).

7.5 CONCLUSIONS

In this chapter, nonlinear static analyses of twelve different wall-slab assemblages are carried out by varying the thickness of shear wall, thickness of floor slab and aspect ratio of shear wall panel. Based on the observed tensile damage at wall-slab junction region, a lateral drift limit between 0.08% and 0.15% is recommended to avoid the possibility of damage propagation in the floor slab under seismic action. The recommended length of wall is 3 m along with minimum wall panel aspect ratio of 1.0. Finally a drift based design procedure for shear wall with connected floor slabs is proposed for implementation. The result obtained is based on a parametric study involving numerical simulation, thus an experimental verification is required to propose a single lateral drift limit for RC wall-frame buildings.

Chapter 8
SUMMARY AND CONCLUSIONS

8.1 OVERVIEW

In the present study, the behaviour and the possible failure modes of an RC wall connected with floor slabs in a typical RC frame-wall buildings, have been investigated. Displacement controlled nonlinear static analysis has been carried out on wall-slab assemblage by varying salient structural parameters. In this chapter, the summary of the study, the salient conclusions drawn and the possible future scope of work have been discussed.

8.2 SUMMARY

The study can be summarized into the following parts:

- *Finite element modelling and material validation*: To achieve the objectives of the present study, finite element modelling of the multistoried building and a wall-slab assemblage is carried out. Also material model (CDP) used for the analysis is validated with an experimental study from the past research.

- *Development of numerical model*: To investigate the influence of floor slab on the behaviour of shear wall, a simplified and efficient numerical model is developed. The model is subjected to nonlinear static analysis to observe the extent of damage at the shear wall-floor slab junction region. Six different models are considered for the analysis, tensile damage patterns for all the models are observed and based on the observed behaviour, the numerical model of wall-slab assemblage is refined for further analysis.

- *Assessment of tensile damage*: By varying the aspect ratio of the shear wall panel and vertical reinforcement ratio in the wall, parametric study is carried out for the shear wall-slab assemblage. Considering different lengths of shear wall, the influence of floor slab on the behaviour of shear wall is studied. The tensile damage in the slab may extend beyond the ends of the wall on the either side, hence the floor slabs in some models are extended beyond the length of the shear wall. The behavior of the junction between the shear wall and floor slab has been studied by observing the stresses in the steel reinforcement, plastic strain, minimum principal stress, tensile damage and compressive damage patterns.

- *Calculation of plastic hinge length at RC wall-slab junction*: As compared to an isolated slender wall, the region of nonlinearity and inelastic actions in a shear wall will differ when connected with the floor slab at every floor level. In the present study, displacement based nonlinear static analysis of the wall-slab assemblage is carried out considering in both monotonic and cyclic modes. The axial compression on wall and the wall panel aspect ratio is varied to propose a close form equations for plastic hinge length of the shear wall when connected with the floor slab.

- *Lateral drift limit for shear wall connected with floor slab*: To investigate the lateral drift limit of the shear wall, parametric study of the wall-slab assemblage is performed. The primary variables are the aspect ratio of the wall panel, thickness of shear wall and thickness of floor slab. The axial load ratio, the amount of horizontal and vertical web reinforcement are kept same for all the models. A limited range of lateral drift is proposed to minimize the damage in slab and wall-slab junction of RC frame-wall buildings.

8.3 CONCLUSIONS

The following salient conclusions are drawn from the study:

1. Under lateral loadings, the slender wall of a shear wall-floor slab system gets partitioned into a number of smaller panels between successive floor slabs. Each such panel behaves as a squat wall with the formation of diagonal strut between two successive slab-wall junctions. Thus, the design methodology should consider strut formation and associated failure modes for slender walls in multistoried buildings with floor slabs. The strut formation leads to further propagation of damage in the floor slab.

2. The portion of the floor slab connected to the walls undergoes significant damage at higher levels of lateral displacement. Significant damage at slab-wall junction may also lead to formation of sliding shear crack across the wall. Thus, a new design methodology involving prevention or reduction of damage in slab needs to be evolved.

3. The finite element analysis results confirm that the maximum stress concentration develops at the base of the shear wall (EWSC) first and then move to the upper floor level at the junction. Also, the developed tensile damage and the stresses are higher in the portion of the slab connected to the shear walls which are oriented in the direction of the lateral loadings.

4. As per the current provision of the Indian earthquake code IS: 1893 (Part-1)-2016, RC buildings are expected to show linear elastic behaviour till the lateral drift limit of 0.4%. However, for all the studied models, nonlinearity in concrete in wall-slab junction starts at much lower drift

levels. Also, yielding of vertical reinforcement in wall is observed at lower or comparable drift levels. Thus, the existing codal prescription needs to be relooked at for RC wall buildings.

5. The tensile and compressive damages in the slab depend on the aspect ratio of the wall panel and the amount of vertical reinforcement in the wall. It is observed that higher aspect ratio and lower reinforcement ratio resulted in maximum damage at lower values of lateral drift.

6. The plastic hinge length for wall-slab junction region increases with the wall panel aspect ratio. A relation between plastic hinge length with monotonic and cyclic loading is developed, which is $L_{p,monotonic} \approx 1.34 L_{p,cyclic}$

7. A lateral drift limit between 0.08% - 0.15% is recommended to avoid the damage at the junction region of shear wall and floor slab during earthquake shaking, and implementation of drift based design of rectangular shear wall is recommended. Also, recommended length of wall should not exceed 3 m along with minimum wall panel aspect ratio of 1.0.

8.4 RECOMMENDATIONS SCOPE FOR FUTURE WORK

Based on the present study, limitations of the study and future extension of this work are discussed. In the present study, parametric studies are carried out to study the behaviour of isolated wall-slab assemblage; however the global response of RC wall-frame multistoried building need to be investigated in light of the proposed design methodology. Present study of wall-slab assemblage does not involve nonlinear analysis under ground motions, and this aspect can be further explored. Experimental studies need to be carried out to validate the proposed equations for plastic hinge length in shear wall connected with floor slabs. Also, the proposed lateral drift criteria for shear wall buildings in the present study needs experimental verifications.

REFERENCES

ABAQUS. (2011). "*ABAQUS analysis user's manual*." Hibbitt, Karlsson, and Sorenson, Pawtucket, R.I.

ACI. (2014). "*Building code requirements for structural concrete*." American Concrete Institute, ACI 318–14, Farmington Hills, MI.

ACI-ASCE Committee 428. (1968). "Progress report on code clauses for limit design." ACI Journal, 65(9), 713–715.

Adebar, P., and Ibrahim, A. M. M. (2002). "Simple nonlinear flexural stiffness model for concrete structural walls." *Earthquake Spectra*, 18(3), 407–426.

ASCE 7-10. (2010). "*Minimum design loads for buildings and other structures*." American Society of Civil Engineers, Virginia, USA.

ASCE-ACI Committee 445. (1998). "Recent Approaches to Shear Design of Structural Concrete." *Journal of Structural Engineering*, ASCE, 124, 1375–1417.

Baker, A. L. L. (1956). "The ultimate load theory applied to the design of reinforced and prestressed concrete frames." *Concrete Publication Limited*, London.

Baker, A. L. L., and Amarakone, A. M. N. (1964). "Inelastic hyperstatic frame analysis." Flexural Mechanics of Reinforced Concrete, SP-12, *American Concrete Institute*, Farmington Hills, MI, 85–142.

Bari, M. S. (1987). "*Design of shear wall connection using shear reinforcement*." Ph.D. Thesis, University of Glasgow.

Bari, M. S. (1996). "Nonlinear finite element study of shear wall-floor slab connections." *Journal of Civil Engineering*. The Institution of Engineers, Bangladesh, CE 24(2), 137–145.

Bayrak, O., and Sheikh, S. (1998). "Confinement reinforcement design considerations for ductile HSC columns." *Journal of Structural Engineering*, ASCE, 124(9), 999–1010.

Belletti B., Damoni, C., and Gasperi, A. (2013). "Modeling approaches suitable for pushover analyses of RC structural wall buildings," *Engineering Structures*, 57(12), 327–338.

Beyer K., Simonini S., Constantin R., and Rutenberg, A. (2014). "Seismic shear distribution among interconnected cantilever walls of different lengths." *Earthquake Engineering and Structural Dynamics*, 43, 1423–1441.

Bignell, J. L., LaFave, J. M., and Hawkins, N. M. (2005), "Seismic vulnerability assessment of wall pier supported highway bridges using nonlinear pushover analyses." *Engineering Structures*, 27(14), 2044–2063.

Bohl, A., and Adebar, P. (2011). "Plastic hinge length in high rise concrete shear walls." *ACI Structural Journal*, 108(2), 148–157.

BS EN 1998-1 (2005). "*Eurocode 8: Design for Structures for Earthquake Resistance, Part 1: General Rules, Seismic Actions and Rules for Buildings*." European Committee for Standardization (CEN), Brussels, Belgium.

Bureau of Indian Standards (BIS) (1987). "*Handbook of concrete reinforcement and detailing.*" *SP: 34*, New Delhi, India.

Bureau of Indian Standards (BIS) (2000). "*Indian standard plain and reinforced concrete – code of practice*." IS 456, Bureau of Indian Standards, New Delhi.

Bureau of Indian Standards (BIS) (2016a). "*Indian standard code of practice for ductile detailing of reinforced concrete structures subjected to seismic forces*, IS 13920, Bureau of Indian Standards, New Delhi.

Bureau of Indian Standards (BIS) (2016b). "*Indian Standard Criteria for Earthquake Resistant Design of Structures. Part 1: General Provisions for all structures and specific provisions for buildings.*" IS 1893, New Delhi, India.

Cardenas, A. E., and Magura, D. D. (1973). "Strength of high rise shear walls-rectangular cross sections." *ACI Special Publication* 36, *Response of Multistorey Concrete Structures to Lateral Forces*, 119–150.

Carrillo, J., and Alcocer, S. M. (2012). "Backbone model for performance-based seismic design of RC walls for low-rise housing." *Earthquake Spectra*, 28(3), 943–964.

Cassis, J. H., and Bonelli, P. (1992). "Lessons learned from the March 3, 1985 Chile earthquake and related research." *Proceeding of the Tenth World Conference on Earthquake Engineering*, Balkema, Rotterdam.

Celebi, M., and Okawa, I. (2014). "Drift issues of tall buildings during the March 11, 2011 M9.0 Tohoku earthquake, Japan – Implications." *Tenth U.S. National Conference on Earthquake Engineering: Frontiers of Earthquake Engineering*, Anchorage, Alaska.

Chan, W. W. L. (1955). "The ultimate strength and deformation of plastic hinges in reinforced concrete frameworks." *Magazine of Concrete Research*, 7(21), 121–132.

Colotti, V. (1993). "Shear behavior of RC structural walls." *Journal of Structural Engineering*, ASCE, 119(3), 728–746.

Corley, W. G. (1966). "Rotational capacity of reinforced concrete beams." *Journal of Structural Engineering*, ASCE, 92(5), 121–146.

Coull, A., and Chee, W. (1986). "Stiffening of structural cores by floor slabs." *Journal of Structural Engineering*, ASCE, 112 (5), 977–994.

Coull, A., and Chee, W. Y. (1983). "Design of floor slabs coupling shear walls." *Journal of Structural Engineering*, ASCE, 109 (1), 109–125.

Coull, A., and Chee, W. Y. (1984). "Stresses in slab coupling flanged shear walls." *Journal of Structural Engineering*, ASCE, 110 (1), 105–119.

Coull, A., and Chee, W. Y. (1990). "Cracked coupling slabs in shear wall buildings." *Journal of Structural Engineering*, ASCE, 116 (6), 1744–1748.

Coull, A., and Wong, Y. C. (1985). "Effect of local elastic wall deformations on the interaction between floor slabs and flanged shear walls". *Journal of Building and Environment*, 20, 169–179.

CSA A23.3-14, (2014). "*Design of concrete structures*." Canadian Standards Association, Rexdale, Ontario.

Dasgupta, K. (2008). "*Improvement in Geometric Design of Reinforced Concrete Shear Walls to resist Earthquake Effects*." Doctor of Philosophy Thesis, Indian Institute of Technology Kanpur, Kanpur.

Derecho, A. T., Ghosh, S. K., Iqbal, M., Freskakis, G. N., and Fintel, M. (1978). "Structural walls in earthquake resistant buildings–Dynamic analyses of isolated structural walls–Development of Design Procedure–Design Force Levels." *Report to the National Science Foundation*, RANN, under Grant No. ENV74-14766, Portland Cement Association, Skokie, IL.

Duffey, T., Goldman, A., and Farrar, C. (1994). "Shear wall ultimate drift limits." *Earthquake Spectra*, 10(4), 655–674.

EERI (1996). "Northridge earthquake reconnaissance report." Volume 2, *Earthquake Spectra*, Supplement C to Volume 11, Earthquake Engineering Research Institute, USA.

Elnashai, A. S., Pilakoutas, K., and Ambraseys, N. N. (1990). "Experimental behaviour of reinforced concrete walls under earthquake loading." *Earthquake Engineering and Structural Dynamics*, 19, 389–407.

El-Tawil, S., Harries, K. A., Fortney, P. J, Shahrooz, B. M., and Kurama, Y. (2010). "Seismic Design of Hybrid Coupled Wall Systems: State of the Art." *Journal of Structural Engineering*, ASCE, 136(7), 755–769.

Fahjan, Y. M., Kubin, J., and Tan, M. T. (2010). "Nonlinear analysis methods for reinforced concrete buildings with shear walls." *Proceedings of 14th European Conference on Earthquake Engineering*.

Fajfar, P., and Fischinger, M. (1990). "Mathematical modeling of RC structural walls for nonlinear seismic analysis." *Proceedings of the European Conference on Structural Dynamics*, Bochum, Germany, 471–478.

Fischinger, M., Vidic, T., and Fajfar, P. (1991). "Evaluation of the inelastic response of a RC building with a structural wall designed according to Eurocode 8." *Proceedings, International Conference on Buildings with Load Bearing Concrete Walls in Seismic Zones*, Paris, France, 487–498.

Fischinger, M., Vidic, T., and Fajfar, P. (1992). "Nonlinear seismic analysis of structural walls using the multiple-vertical-line-element model." *In H. Krawinkler, and P. Fajfar (eds.): Nonlinear Seismic Analysis of RC Buildings*, Elsevier Science Publishers Ltd. London and New York, 191–202.

Fischinger, M., Vidic, T., Selih, J., Fajfar, P., Zhang, H. Y. and Damjanic, F. B. (1990). "Validation of a macroscopic model for cyclic response prediction of RC walls." *In N. B. Bicanic, and H. Mang (eds.): Computer Aided Analysis and Design of Concrete Structures* (2). Pineridge Press. Swansea, United Kingdom, 1131–1142.

Genikomsou, A. S., and Polak, M, A. (2015). "Finite element analysis of punching shear of concrete slabs using damaged plasticity model in ABAQUS." *Engineering Structures*, 98, 38–48.

Ghosh, S. K., and Markevicius, V. P. (1991). "Design of earthquake resistant shear walls to prevent shear failure." *The International Workshop on Concrete Shear in Earthquake*, Houston, Elsevier Science Publishers, Inc., London.

Greeshma, S., and Jaya, K. P. (2013). "Effect of slab shear reinforcement on the performance of shear wall-floor slab connection," *Journal of Performance of Constructed Facilities*, ASCE, 27 (4), 391–401.

Gulec, C. K., and Whittaker, A. S. (2009). "Performance-Based Assessment and Design of Squat Reinforced Concrete Shear Walls." *MCEER Technical Report-09-0010*, MCEER, Buffalo.

Haldar, P., and Singh, Y. (2009). "Seismic performance and vulnerability of Indian code designed RC frame buildings." *ISET Journal of Earthquake Technology*, 46(1), 29–45.

Henriques, J., Simoes da Silva, L., and Valente, I. B. (2013). "Numerical modeling of composite beam to reinforced concrete wall joints part I: global behavior." *Engineering Structures*, 52, 734–746.

Hsu, T. T. C., and Mo, Y. L. (1985a). "Softening of Concrete in Torsional Members - Design Recommendations." *ACI Structural Journal*, 82(4), 1985, 443-452.

Hsu, T. T. C., and Mo, Y. L. (1985b). "Softening of Concrete in Torsional Members - Theory and Tests." *ACI Structural Journal*, 82(3), 1985, 290-303.

Hwang, S. J., and Lee, H. J. (1999). ''Analytical model for predicting shear strengths of exterior reinforced concrete beam-column joints for seismic resistance.'' *ACI Structural Journal*, 96(5), 846–857.

Hwang, S. J., and Lee, H. J. (2000). ''Analytical model for predicting shear strengths of interior reinforced concrete beam-column joints for seismic resistance.'' *ACI Structural Journal*, 97(1), 35–44.

Hwang, S. J., and Lee, H. J. (2002). "Strength prediction for discontinuity regions by softened strut-and-tie model." *Journal of Structural Engineering*, ASCE, 128(12), 1519–26.

Hwang, S. J., Fang, W. H., Lee, H. J., and Yu, H. W. (2001). "Analytical model for predicting shear strength of squat walls." *Journal of Structural Engineering*, ASCE, 127(1), 43–50.

Ile, N., and Reynouard, J. (2004). "Seismic behaviour of R/C walls subjected to multidirectional seismic loading." *Thirteenth World Conference on Earthquake Engineering*, Vancouver, Canada.

Kabeyasawa, T., Shiohara, H., Otani, S., and Aoyama, H. (1983). "Analysis of the full-scale seven-storey reinforced concrete test structure," *Journal of the Faculty of Engineering*, University of Tokyo, 37(2), 431–478.

Kassem, W. (2015). "Shear strength of squat walls: A strut-and-tie model and closed-form design formula." *Engineering Structures*, 84, 430–438.

Kaushik, S., and Dasgupta, K. (2013). "Seismic behavior of slab-structural wall junction in RC building." *Conference on Structural Engineering and Mechanics*. NIT Rourkela, India, Paper No. 054.

Kazaz, I. (2013). "Analytical study on plastic hinge length of structural walls." *Journal of Structural Engineering*, ASCE, 139(11), 1938–1950.

Kazaz, I., Gulkan, P., and Yakut, A. (2012). "Deformation limits for structural walls with confined boundaries." *Earthquake Spectra*, 28(3), 1019–1046.

Khatri, D., and Anderson, J. C. (1995). "Analysis of reinforced concrete shear wall components using the ADINA nonlinear concrete model." *Computers & Structures*, 56 (2/3), 485–504.

Khose, V. N., Singh, Y., and Lang, D. H. (2012). "A comparative study of design base shear for RC buildings in selected seismic design codes." *Earthquake Spectra*, 28(3), 1047–1070.

Kim, H. S., Lee, D. G., and Kim, C. K. (2005). "Efficient three-dimensional seismic analysis of a high-rise building structure with shear walls." *Engineering Structures*, 27(6), 963–976.

Klemencic, R., Fry, J. A., Hurtado, G., and Moehle, J. P. (2006). "Performance of post-tensioned slab-core walls connections." *PTI Journal* 4(2), 7–23.

Kwak, H. G., and Kim, D. Y. (2004). "Material nonlinear analysis of RC shear walls subject to cyclic loadings." *Engineering Structures*, 26, 1423–1436.

Kwan, A. K. H., and He, X. G. (2001). "Finite element analysis of effect of concrete confinement on behavior of shear walls." *Computers & Structures*, 79, 1799–1810.

Lee, D.G. (1987). "*An efficient element for analysis of frames with shear walls*." ICES88.

Lee, J., and Fenves, G. L. (1998). "Plastic-damage model for cyclic loading of reinforced concrete structures." *Journal of Engineering Mechanics*, ASCE, 124 (8), 892–900.

Lubliner, J., Oliver, J., Oller, S., and Onate, E. (1989). "A plastic-damage model for concrete." *International Journal of Solids and Structures*, 25(3), 299–326.

MacGregor, J. C. and Wight, J. K. (2005). "*Reinforced concrete mechanics and design*." Pearson Prentice Hall, New Jersy.

Mahmood, M. (1984). "*Strength and Stiffness of Shear Wall Floor Slab Connection*." Ph.D. Thesis, University of Glasgow.

Malm, R. (2009). "*Predicting shear type cracks initiation and growth in concrete with nonlinear finite elements methods*." PhD Thesis, Royal Institute of Technology, Division of Structural Design and Bridges, Stockholm, Sweden.

Massone, L. M., Orakcal, K., and Wallace, J. W. (2009). "Modeling of squat structural walls controlled by shear." *ACI Structural Journal*, 106(5), 646–655.

Mattock, A. H. (1964). "Rotational capacity of hinging region in reinforced concrete beams." *Proceedings of the International Symposium of the Flexural Mechanics of the Reinforced Concrete*, ASCE-ACI, Miami.

Mattock, A. H. (1967). "Discussion on rotational capacity of reinforced concrete beams." *Journal of Structural Engineering*, ASCE, 93(2), 519–522.

Medhekar, M. S., and Jain, S. K. (1993). "Seismic behaviour, design, and detailing of RC shear walls, part I: Behaviour and strength." *The Indian Concrete Journal*, 67(7), 311–318.

Mercer, S. (2009). "*Nonlinear shear response of cantilever reinforced concrete shear walls with floor slabs*." Master Thesis, University of British Columbia, Vancover.

Moehle J. P. (1992). "Displacement-based design of RC structures subjected to earthquakes." *Earthquake Spectra*, 8(3), 403–428.

Mulas, M. G., Coronelli, D., and Martinelli, L. (2007). "Multi-scale modeling approach for the pushover analysis of existing RC shear walls - part I: model formulation." *Earthquake Engineering and Structural Dynamics*, 36, 1169–1187.

Mun, J. H., and Yang, K. H. (2015). "Plastic hinge length of reinforced concrete slender shear walls." *Magazine of Concrete Research*, ICE Virtual Library, 67(8), 414–429.

Mun, J. H., and Yang, K. H. (2016). "Load capacity of squat RC shear walls by strut-and-tie model." *Institution of Civil Engineers*, ICE Virtual Library, 68(24), 1265–1277.

Munir, A., and Warnitchai, P. (2012). "The cause of unproportionately large higher mode contributions in the inelastic seismic responses of high-rise core-wall buildings." *Earthquake Engineering and Structural Dynamics*, 41, 2195–2214.

NZS 1170.5. (2004). "*Structural design actions Part 5: Earthquake actions-New Zealand*." Standards New Zealand, Wellington 6020.

Onu, G. (1984). "Inclusion of shear effect in the ACM element." *Computers and Structures*, 18(3), 459–464.

Orakcal, K., and Wallace, J. W. (2006). "Flexural modeling of reinforced concrete walls - experimental verification." *ACI Structural Journal*, 103(2), 196–206.

Orakcal, K., Massone, L. M., and Wallace, J. W. (2006). "Analytical modeling of reinforced concrete walls for predicting flexural and coupled–shear-flexural responses." *PEER Technical Report*, University of California, Berkeley.

Panagiotakos, T. B., and Fardis, M. N. (2001). "Deformation of reinforced concrete members at yielding and ultimate." *ACI Structural Journal*, 98(2), 135–148.

Pantazopoulou, S., and Imran, I. (1992). "Slab-wall connections under lateral forces". *ACI Structural Journal*, 89(5), 515–527.

Park, R., and Paulay, T., (1975). "*Reinforced Concrete Structures*." John Wiley and Sons, Inc., New York.

Park, R., Priestley, M. J. N., and Gill, W. D. (1982). "Ductility of square-confined concrete columns." *Journal of Structural Division*, ASCE, 108(ST4), 929–950.

Paulay, T. (1986). "Design of ductile reinforced concrete structural walls for earthquake resistance." *Earthquake Spectra*, 2(4), 783–823.

Paulay, T., and Priestley, M. J. N. (1992). "*Seismic design of reinforced concrete and masonry buildings*." John Wiley and Sons Inc., New York.

Paulay, T., and Priestley, M. J. N. (1993). "Stability of ductile structural walls." *ACI Structural Journal*, 90(4), 385–392.

Paulay, T., and Taylor, R. G. (1981). "Slab coupling of earthquake-resisting shear walls." *ACI Structural Journal*, 78(2), 130–140.

Paulay, T., and Uzumeri, S. M. (1975). "A critical review of the seismic design provisions for ductile shear walls of the Canadian code." *Canadian Journal of Civil Engineering*, 2, 592–601.

Paulay, T., Priestley, M. J. N., and Synge, A. J. (1982). "Ductility in Earthquake Resisting Squat Shear walls." *ACI Structural Journal*, 79(4), 257–269.

Priestley, M. J. N., and Kowalsky, M. J. (1998). "Aspects of drift and ductility capacity of rectangular cantilever structural walls." *Bulletin of the New Zealand National Society for Earthquake Engineering*, 31(2), 73–85.

Priestley, M. J. N., and Park, R. (1987). "Strength and ductility of concrete bridge columns under seismic loading." *ACI Structural Journal*, 84(1), 61–76.

Priestley, M. J. N., Calvi, G. M., and Kowalsky, M. J. (2007). "*Displacement-based seismic design of structures*." IUSS Press, Pavia, Italy.

Qadeer, A., and Smith, B. S. (1969). "The bending stiffness of slabs connecting shear walls." *ACI Structural Journal*, 66(6), 464–473.

Rad, B., and Adebar, P. (2009). "Seismic design of high-rise concrete walls: reverse shear due to diaphragms below flexural hinge." *Journal of Structural Engineering*, ASCE, 135(8), 916–924.

Rad, R. B. (2009). "*Seismic shear demand in high-rise concrete walls*." Ph.D. thesis, Dept. of Civil Engineering, Univ. of British Columbia, Vancouver, B.C., Canada.

Riddell, R. (1992). "Performance of R/C buildings in the 1985 Chile earthquake." *Proceedings of Tenth World Conference on Earthquake Engineering*, Balkema, Rotterdam.

Sasani, M., and Der Kiureghian, A. (2001). "Seismic fragility of RC structural walls: Displacement Approach." *Journal of Structural Engineering*, ASCE, 127(2), 219–228.

Sawyer, H. A. (1964). "Design of concrete frames for two failure stages." *Proceedings of the International Symposium of the Flexural Mechanics of the Reinforced Concrete*, ASCE-ACI, Miami.

Schlaich, J., and Schafer, K. (1993). "The design of structural concrete." *Proceedings of the IABSE Workshop*, New Delhi, India.

Schwaighofer, J., and Collins, M. P. (1977). "Experimental study of the behavior of reinforced concrete coupling slabs." *ACI Structural Journal*, 74(3), 123–127.

Seneviratna, G. D. P. K., and Krawinkler, H. (1997). "Evaluation of inelastic MDOF effects for seismic design." Report No. 120, The John A. Blume Earthquake Engineering Center, Stanford University, Stanford, CA.

Sheikh, S. A., and Khoury, S. S. (1993). "Confined concrete columns with stubs." *ACI Structural Journal*, 90(4), 414–431.

Sheikh, S. A., Shah, D. V., and Khoury, S. S. (1994). "Confinement of high-strength concrete columns." *ACI Structural Journal*, 91(1), 100–111.

Sherstobitoff, J., Cajiao, P., and Adebar, P. (2012). "Repair of an 18-story shear wall building damaged in the 2010 Chile earthquake." *Earthquake Spectra*, 28(S1), S335–S348.

Smith, B. S., and Coull, A. (2011). "*Tall Building Structures: Analysis and Design*." Wiley India Pvt. Ltd., New Delhi.

Takahashi, S., Yoshida, K., Ichinose, T., Sanada, Y., Matsumoto, K., Fukuyama, H. and Suwada, H. (2013), "Flexural drift capacity of reinforced concrete wall with limited confinement." *ACI Structural Journal*, 110(1), 95–104.

Thomsen, J. H., and Wallace, J. W. (2004). "Displacement-based design of slender concrete structural walls: experimental verification." *Journal of Structural Engineering*, ASCE, 130(4), 618–630.

Vecchio, F., and Collins, M. P. (1981), "Stress-Strain Characteristics of Reinforced Concrete in Pure Shear," Final Report, IABSE Colloquium on Advanced Mechanics of Reinforced Concrete (Delft), *International Association for Bridge and Structural Engineering*, Zurich, 211-225.

Vecchio, F., and Collins, M. P. (1982), "The Response of Reinforced Concrete to In-Plane Shear and Normal Stresses," Publication No. 82-03, Department of Civil Engineering, University of Toronto.

Vulcano, A., Bertero, V. V., and Colotti, V. (1988). "Analytical modeling of RC structural walls." *Proceedings of 9th World Conference on Earthquake Engineering*, 6, 41–46.

Wallace, J. W., (1995). "Seismic Design of RC structural walls. Part I: New code format." *Journal of Structural Engineering*, ASCE, 121(1), 75–87.

Wallace, J. W., and Moehle, J. P. (1992). "Ductility and detailing requirements of bearing wall buildings." *Journal of Structural Engineering*, ASCE, 118(6), 1625–1644.

Zenunović, D., and Folić, R. (2012). "Models for behaviour analysis of monolithic wall and precast or monolithic floor slab connections." *Engineering Structures*, 40, 466–478.

Zheng, N., Zhou, J., Yin, Y., Han, J., and Ji, S. (2012). "Non-linear time history response analysis of low masonry structure with tie-columns." *Fifteenth World Conference on Earthquake Engineering*, Lisboa.

Zhi, Q., Guo, Z., Xiao, Q., Yuan, F., and Song, J. (2017). "Quasi-static test and strut-and-tie modeling of precast concrete shear walls with grouted lap-spliced connections." *Construction and Building Materials*, 150(30), 190–203.

Zienkiewicz, O. C., and Cheung, Y. K. (1964). "The finite element method for analysis of elastic isotropic and orthotropic slabs." *Proceedings of the Institution of Civil Engineers*, 28, 471–488.

LIST OF PUBLICATIONS

REFEREED INTERNATIONAL JOURNALS

Kaushik, S., and Dasgupta, K. (2016). "Seismic damage in slab-structural wall junction in RC building." *Procedia Engineering*, Elsevier Publication, 144, 1332 – 1339, 2016.

Kaushik, S., and Dasgupta, K. "Seismic behaviour of slab-structural wall junction of RC building". *Earthquake Engineering and Engineering Vibration*, Springer Publication, (Accepted for Publication).

Kaushik, S., and Dasgupta, K. "Plastic hinge length in RC shear wall connected with floor slabs." *Engineering Structures* (Under Review).

Kaushik, S., and Dasgupta, K. "Nonlinear static behaviour of RC shear wall-floor slab junction of multistoried building."(To be re-communicated).

INTERNATIONAL CONFERENCES

Kaushik, S., and Dasgupta, K. (2017). "Time history analysis of shear wall-floor slab assemblage". *13th International Conference on Vibration Problems (ICOVP), Indian Institute of Technology Guwahati*, Guwahati, India, Paper No. 184

Kaushik, S., and Dasgupta, K. (2016). "Seismic behaviour of RC slab-shear wall assemblage using non-linear static and dynamic analyses". *Structural Engineering Convention, Indian Institute of Technology Madras*, Chennai, India. Paper No. 594.

Kaushik, S., and Dasgupta, K. (2015). "Seismic damage in slab-structural wall junction in RC building". *12th International Conference on Vibration Problems (ICOVP), Indian Institute of Technology Guwahati*, Guwahati, India, Paper No. O0170.

Kaushik, S., and Dasgupta, K. (2013). "Seismic behavior of slab-structural wall junction in RC building". *Conference on Structural Engineering and Mechanics*. NIT Rourkela, India, Paper No. 054.